PREDICTION OF BRAIN TARGET SITE CONCENTRATIONS ON THE BASIS OF CSF PK

IMPACT OF MECHANISMS OF BLOOD-TO-BRAIN TRANSPORT AND WITHIN BRAIN DISTRIBUTION

JOOST WESTERHOUT

PREDICTION OF BRAIN TARGET SITE CONCENTRATIONS ON THE BASIS OF CSF PK

IMPACT OF MECHANISMS OF BLOOD-TO-BRAIN TRANSPORT AND WITHIN BRAIN DISTRIBUTION

PREDICTION OF BRAIN TARGET SITE CONCENTRATIONS ON THE BASIS OF CSF PK

IMPACT OF MECHANISMS OF BLOOD-TO-BRAIN TRANSPORT AND WITHIN BRAIN DISTRIBUTION

Proefschrift

ter verkrijging van

de graad van Doctor aan de Universiteit Leiden

op gezag van Rector Magnificus prof. mr. C.J.J.M. Stolker,

volgens besluit van het College voor Promoties

te verdedigen op 6 maart 2014

klokke 13:45 uur

door

Joost Westerhout

geboren te IJsselstein
in 1982

Promotiecommissie

Promotor:	Prof. dr. M. Danhof
Co-promotor:	Dr. E.C.M. de Lange
Overige leden:	Prof. dr. M. Hammarlund-Udenaes, Uppsala University
	Dr. J.H. Proost, Rijksuniversiteit Groningen
	Prof. dr. P.H. van der Graaf
	Prof. dr. A.P. IJzerman
	Prof. dr. J.M.A. van Gerven
	Prof. dr. T. Hankemeier

If you can believe in something great,
you can achieve something great

- Katheryn E. Hudson -

Aan allen die mij dierbaar zijn

The research presented in this thesis was performed within the framework of project T5-105 of the Dutch Top Institute Pharma at the Division of Pharmacology of the Leiden Academic Centre for Drug Research (LACDR), Leiden University, the Netherlands.

Financial support for the printing of this thesis was provided by:
Leiden Academic Centre for Drug Research (LACDR)
The Netherlands Organization for Applied Scientific Research (TNO)

Printed by Ipskamp Drukkers, Enschede

Table of Contents

Section I

Background and Introduction

Chapter 1

Preclinical prediction of human brain target site concentrations: Considerations in extrapolating to the clinical setting

J. Westerhout, M. Danhof, E.C.M. de Lange

J. Pharm. Sci. 2011; 100(9): 3577-3593

ABSTRACT

The development of drugs for central nervous system (CNS) disorders has encountered high failure rates. In part, this has been due to the sole focus on blood-brain barrier (BBB) permeability of drugs, without taking into account all other processes that determine drug concentrations at the brain target site. This review deals with an overview of the processes that determine the drug distribution into and within the CNS, followed by a description of *in vivo* techniques that can be used to provide information on CNS drug distribution. A plea follows for the need for more mechanistic understanding of the mechanisms involved in brain target site distribution, and the condition-dependent contributions of these mechanisms to ultimate drug effect. As future direction, such can be achieved by performing integrative cross-compare designed studies, in which mechanisms are systematically influenced (e.g. inhibition of an efflux transporter, or induction of pathological state). With the use of advanced mathematical modeling procedures we may dissect contributions of individual mechanisms in animals as links to the human situation.

INTRODUCTION

Central nervous system (CNS) disorders like Alzheimer's disease, Parkinson's disease, multiple sclerosis, epilepsy, schizophrenia, migraine, insomnia, depression, and attention-deficit hyperactivity disorder are currently estimated to affect hundreds of millions of people worldwide (World Health Organization, 2007). While established treatments are currently available for most of these disorders, significant unmet medical needs still remain, as currently available drugs are treating symptoms rather than curing the disease (Business Insights, 2010). Therefore, novel treatments or drugs with a different mechanism of action are needed.

In these days, the CNS sector is struggling as the average cost of getting a drug onto the market is ever increasing and now approaching US$1 billion, whereas there is an expected decline in income due to pricing pressure from generics (Business Insights, 2010). Moreover, many potentially therapeutic compounds fail during development because early drug discovery programs are often using the wrong parameters for estimating CNS exposure (Hammarlund-Udenaes *et al.,* 2008).

It is often said that many CNS drug candidates fail because they do not reach the CNS target due to lack of blood-brain barrier (BBB) permeability. Indeed, the BBB effectively isolates the brain from the blood by the presence of tight junction proteins, connecting the endothelial cells of the brain vessels. In addition, specific metabolizing enzymes and efflux pumps, such as P-glycoprotein (P-gp), are located within the endothelial cells, which may actively remove drugs from the brain. It is therefore true that the BBB can play a major role in limiting the delivery of systemically administered drugs to the CNS. However, this is not the sole reason for the high failure rate in CNS drug development. For a proper CNS effect, the unbound drug should have the ability to access the relevant target site within the CNS. Apart from BBB permeability, this also depends upon other factors, such as plasma pharmacokinetics (PK) and within-brain distribution. These factors are controlled by many mechanisms. Each mechanism has its particular influence by its specific rate and extent, and thereby plays a more or less important role in having the drug in the *right place*, at the *right time*, and at the *right concentration*. Moreover, influences of variables like genetics, gender, age, environmental and pathological conditions

have generally been neglected. It is therefore not surprising that most CNS drug candidates finally fail during development.

As the driving force of CNS drug action is the concentration-time profile at the brain target site, it is important for pharmaceutical companies to have effective, cost-efficient tools to measure and predict human brain target site exposure before proceeding to more expensive clinical trials.

For many (potential) CNS drugs, brain target site concentrations are closely linked, or may even be equal, to unbound drug concentrations in the brain extracellular fluid ($brain_{ECF}$) (De Lange *et al.,* 2000; Hammarlund-Udenaes, 2009). However, the possibility of direct measurement of $brain_{ECF}$ concentrations is highly limited in the clinical phase of drug development. Therefore, unbound drug concentrations in human cerebrospinal fluid (CSF) are used as a surrogate for human $brain_{ECF}$ concentrations. However, the usefulness of CSF concentrations as a predictor of brain target site concentrations can be questioned, as a generally applicable relationship between CSF concentrations and $brain_{ECF}$ concentrations does not exist due to qualitative and quantitative differences in processes that govern the PK at these sites (De Lange and Danhof, 2002; Lin, 2008; Shen *et al.,* 2004).

FACTORS THAT GOVERN THE PHARMACOKINETICS IN THE BRAIN

Drug distribution into the brain is governed by many processes, including plasma PK, plasma protein binding, passive and active transport across the BBB or blood-CSF barrier (BCSFB), and once within the brain, bulk flow, diffusion, and passive and active extra-intracellular exchange.

Plasma pharmacokinetics and protein binding

Once drugs are in the systemic circulation, they can bind to different proteins that are present in plasma. Of the many plasma proteins that can interact with drugs, the most important ones are human serum albumin, α_1-acid glycoprotein, and lipoproteins (Peletier *et al.,* 2009). Acidic and neutral drugs are usually bound more extensively to albumin, whereas basic drugs are usually bound

more extensively to α_1-acid glycoprotein and lipoproteins (Peletier *et al.,* 2009). As protein-bound drugs cannot cross the BBB or BCSFB, unbound plasma concentrations, rather than total plasma concentrations, are considered to be the main determinant for the rate and extent of drug entry into the brain (Mayer *et al.,* 1959). However, it must be noted that information about the level of protein binding by itself is not sufficient for predicting drug distribution into the brain (Pardridge, 1995). As the association and dissociation of drugs to plasma proteins is a dynamic process, it indicates that extensively protein-bound drugs can still enter the brain in sufficient amounts, provided that the rate of dissociation and permeability of the BBB and BCSFB is high enough (Mandula *et al.,* 2006; Morgan and Huang, 1993; Tanaka and Mizojiri, 1999). This implicates that information on the kinetics of plasma protein binding is also essential for accurate prediction of the rate and extent of drug entry into the brain.

Transport across the blood-brain barriers

The barriers between blood and brain are the BBB and the BCSFB. These barriers have many similarities but also important differences, as will be discussed below.

The blood-brain barrier - The BBB is formed by the brain capillary endothelial cells, which are interconnected by tight junction proteins that restrict paracellular diffusion of small hydrophilic molecules from blood to the brain. In addition to these tight junctions, numerous active transport systems are present at the BBB that protect the brain from neurotoxic substances, but also help to maintain the homeostasis of the brain by influx of essential substrates such as electrolytes, nucleosides, amino acids, and glucose. These processes are regulated by interactions with adjacent pericytes, astrocytes, and neuronal cells (Abbott *et al.,* 2006; Bernacki *et al.,* 2008; Davson and Oldendorf, 1967). However, in certain specialized regions in the brain, comprising the choroid plexuses and the circumventricular organs, the capillary endothelial cells are fenestrated and therefore highly permeable (Abbott, 2004). Thus, compounds can cross the capillary walls more or less freely in these specialized regions, but may be restricted in entering the rest of the brain by the BCSFB.

The blood-cerebrospinal fluid barrier - The BCSFB is located at the choroid plexuses in the lateral, third and fourth ventricles of the brain, which are responsible for the production of CSF. The barrier function of the BCSFB is provided by the tight junctions between the epithelial cells of the choroid plexus at the apical site, which contacts the CSF. Like the BBB, several different active transport systems are located at the BCSFB to limit the entrance into the brain of compounds that can easily permeate the choroid plexus' capillaries (Davson and Oldendorf, 1967; Wolburg and Paulus, 2010).

BBB versus BCSFB - It has been assumed that the surface area of the BBB in humans, which is estimated to be ~20 m^2 (Pardridge, 2002), is at least a hundred-fold larger than that of the BCSFB, which is reported to be only 0.2 m^2 (Dohrmann, 1970). This implicates that the BCSFB only plays a minor role in the control of the brain environment (Hammarlund-Udenaes *et al.,* 2008; Lee and Bendayan, 2004; Lee *et al.,* 2001; Roberts *et al.,* 2008). However, this calculation ignores the large surface area provided by the apical microvilli on the epithelial cells. When taking these into account, the total surface area of all choroid plexuses in the rat is estimated to be ~75 cm^2 (Keep and Jones, 1990a). This is only two-fold smaller than the surface area of the BBB, which is estimated to be ~150 cm^2 (Gjedde, 1981; Keep and Jones, 1990b). This implicates that the BCSFB plays a more important role in drug transport between blood and brain than originally assumed. However, because the BBB and BCSFB are anatomically and physiologically different, their relative contributions in the exchange of compounds between blood and brain does not necessarily correspond to the ratio of their respective surfaces. BCSFB transport will (initially) influence the periventricular spaces and tissues, while BBB transport will more affect the total brain.

Active transport across the BBB and BCSFB can be either by carrier-mediated (facilitated) transport, or ATP-dependent transport. Facilitated transport across the BBB and BCSFB is carried out by members of the solute carrier (SLC) family, which include organic cation transporters (OCT), carnitine/organic cation transporters (OCTN), organic anion transporters (OAT), organic anion-transporting polypeptide (OATP), and glucose transporter (GLUT). The different ATP-dependent transport systems at the BBB and BCSFB are all members of the ATP-binding cassette (ABC) transporter

superfamily and include P-gp, breast cancer resistance protein (BCRP), and the multidrug resistance-associated protein (MRP) family (Graff and Pollack, 2004). The direction of flux and subcellular localization of the different transporter systems at the human BBB and BCSFB are depicted in figure 1. Due to inconsistencies in the literature, the direction of flux and subcellular localization of the different transporters are classified as either 'known', 'likely', or 'unknown'. However, it can be concluded that there are some differences between the BBB and BCSFB.

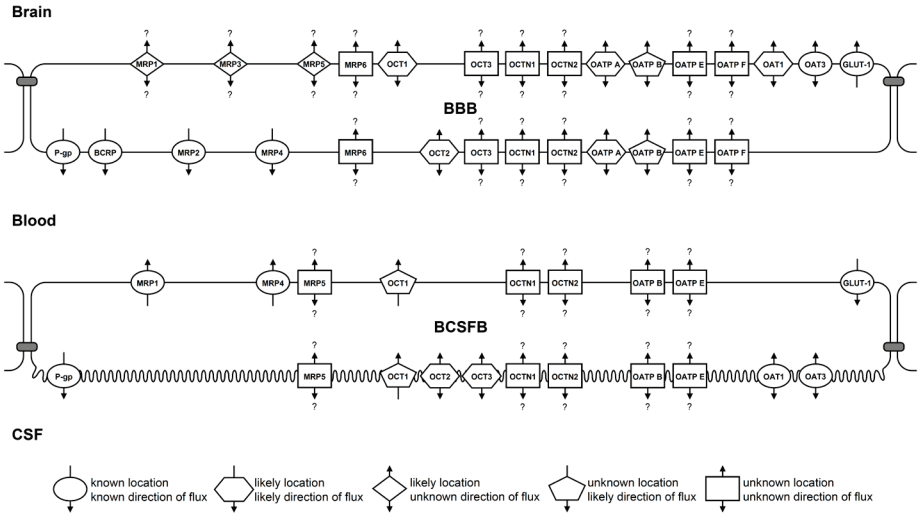

Figure 1. Cartoon of the different active transport systems that are located on the human BBB and BCSFB

It has been well established that P-gp functions as an efflux transporter at the BBB (Schinkel, 1999). However, there has been some evidence that P-gp functions as an influx transporter at the BCSFB (Kassem *et al.,* 2007; Rao *et al.,* 1999). However, previous work by Gazzin and colleagues has indicated that P-gp levels at the BBB are over 200-fold higher than at the BCSFB (Gazzin *et al.* 2008). In contrast, MRP1 has a much higher expression at the choroid plexuses compared to the brain microvessels. This indicates that there are major differences in the mechanisms by which the BBB and BCSFB protect the brain, which could result in significant differences between concentrations at the brain target site and in CSF (Gazzin *et al.*, 2008).

Altogether, this indicates that the impact of active transport on the predictability of brain target site concentrations from CSF concentrations needs to be considered and further investigated.

Enzymatic activity

Several drug metabolizing enzymes, like cytochromes P-450, monoamine oxidases, and UDP-glucuronosyltransferases, have been found at different extracellular and intracellular sites in the brain (Ghersi-Egea *et al.,* 1993; Ghersi-Egea *et al.,* 1994). The activities of some drug-metabolizing enzymes appeared to be several times higher in the small brain microvessels and choroid plexus epithelial cells compared to the cortical parenchymal cells. Thus, the BBB and BCSFB also form an enzymatic barrier to limit the exposure of the brain to drugs (Ghersi-Egea *et al.,* 1993; Ghersi-Egea *et al.,* 1994).

The metabolism that takes place within the brain could result in the conversion of molecules and/or prodrugs to pharmacologically active metabolites. This needs to be taken into account as well during drug development.

Brain$_{ECF}$ bulk flow and CSF turnover

In rats, approximately 80% of the CSF is generated by the choroid plexuses of the lateral, third and fourth ventricles, whereas the remaining 20% comes directly from the brain$_{ECF}$ (Cserr, 1965). In humans, the contribution of brain$_{ECF}$ is estimated to be about 50% (Kimelberg, 2004). After formation, CSF flows from the lateral ventricle through the third and into the fourth ventricle via the aqueduct of Sylvius. CSF then leaves the brain to enter the basal cisterns and subarachnoid spaces, where it is absorbed in the venous system (figure 2) (Miyan *et al.,* 2003; Proescholdt *et al.,* 2000; Segal, 1993).

In humans, CSF is produced at a rate of about 0.4 ml/min (Nilsson *et al.,* 1992). With a total CSF volume of approximately 140 ml (Kohn *et al.,* 1991), this indicates that the total volume of CSF is replaced every 6 hours. In rats, the relative rate of CSF turnover is much higher. With a rate of production of 2.2 µl/min (Cserr, 1965), and a total CSF volume of 250 µl (Bass and Lundborg,

Figure 2. Schematic representation of the CSF flow path

1973), this indicates that the total volume of CSF in the rat is replaced every 2 hours.

It is often stated that drugs equilibrate readily between $brain_{ECF}$ and CSF as the ependymal epithelium that separates $brain_{ECF}$ from CSF does not present a significant barrier to drug movement (Lee *et al.,* 2001). However, compounds do not only diffuse from $brain_{ECF}$ into CSF. It has been shown that there is also bulk flow of $brain_{ECF}$ (Abbott, 2004; Cserr *et al.,* 1981). Due to the bulk flow of $brain_{ECF}$ to CSF, the transport of drugs from $brain_{ECF}$ into CSF is more efficient than the diffusion of drugs from CSF into the $brain_{ECF}$. As a result, the continual drainage of CSF can act as a 'sink' for brain tissue, indicating an active elimination from the brain.

In humans, the rate of $brain_{ECF}$ production is estimated to be 0.15-0.2 ml/min (Begley, 2000; Kimelberg 2004) which is calculated from the estimation that 50% of the CSF production comes from $brain_{ECF}$. With a total $brain_{ECF}$ volume of approximately 240 ml (Begley, 2000), this indicates the total $brain_{ECF}$ volume is replaced every 20-27 hours. At a rate of 0.2-0.5 µl/min in rat brain (Abbott, 2004; Cserr *et al.,* 1981), the rate of $brain_{ECF}$ production is about 10-20% of that of CSF, which corresponds well to the 20% of CSF production from $brain_{ECF}$

(Cserr, 1965). With a total $brain_{ECF}$ volume of 290 µl (Cserr *et al.,* 1981), this indicates that the total $brain_{ECF}$ volume in rats is replaced every 10-24 hours.

It has been suggested that the source of the $brain_{ECF}$ is from a combination of ions and water that come from the bloodstream and from CSF that flows back into the brain along perivascular channels from the ventral surface in the subarachnoid space (Abbott, 2004). This indicates that there is a fraction of CSF that takes a longer route from its site of origin in the choroid plexuses back into the systemic circulation. This also indicates that drug concentrations in $brain_{ECF}$ and CSF are only in part directly related.

Extra-intracellular exchange

Once a drug is in the $brain_{ECF}$ or CSF, it can bind to brain tissue or distribute into brain cells, depending on its physicochemical properties. Hydrophilic drugs are more likely to remain dissolved in the $brain_{ECF}$ and CSF, whereas lipophilic drugs are more likely to bind to brain tissue, or distribute into brain cells (De Lange and Danhof, 2002). However, active transport between $brain_{ECF}$ and the cell is possible as well (Lee *et al.,* 2001). The effect of $brain_{ECF}$-parenchymal exchange has been clearly demonstrated by the study on valproate by Scism *et al.* (2000). Co-administration of probenecid increased the intracellular concentrations without affecting $brain_{ECF}$ concentrations, indicating the presence of a probenecid-sensitive efflux transporter at the brain parenchymal cells.

While most CNS drug targets are facing the $brain_{ECF}$, intracellular targets also exist (Lee *et al.,* 2001). This has to be considered when aiming to determine brain target site concentrations. For targets like membrane receptors, extracellular enzymes, and transporters, $brain_{ECF}$ concentrations may provide the most useful information (De Lange and Danhof, 2002).

TECHNIQUES

In the preclinical setting there are several *in vitro*, *ex vivo* and *in vivo* techniques that provide information on brain target site exposure. Such information can be either direct or indirect, on bound or unbound concentrations, with or without

temporal resolution, and with or without spatial resolution (De Lange *et al.,* 1997; Hammarlund-Udenaes *et al.,* 2009).

A typical parameter that is often used to describe the level of brain exposure is the brain-to-plasma partition coefficient (K_p), which is defined as the ratio of the total drug concentration in the brain versus the total drug concentration in plasma. To compensate for differences in plasma protein binding, as that may restrict brain entry, the total brain-to-unbound plasma partition coefficient ($K_{p,u}$) can be calculated. However, as it is pharmacologically more relevant to use unbound brain target site concentrations rather than total brain concentrations, the unbound brain-to-unbound plasma partition coefficient ($K_{p,uu}$) is considered to be a better parameter for brain target site exposure (Gupta *et al.*, 2006).

All the processes discussed in the previous section affect the rate and/or extent of drug distribution to the brain, being two distinct parameters (Hammarlund-Udenaes *et al.,* 2008). The rate of transport into the brain is dependent on the speed at which a drug molecule can pass the BBB and BCSFB. This is often expressed as permeability (distance/time) or clearance (volume/time). The rate of transport across the BBB and BCSFB is often limited to the permeability rate of the BBB and BCSFB, which is dependent on their condition-dependent characteristics and the physicochemical properties of the drugs. As classical paradigm, BBB and BCSFB transport is governed by lipophilicity. Indeed, if passive transport (diffusion) is the only transport mechanism involved, small lipophilic drugs cross the BBB and BCSFB more readily than large hydrophilic drugs (De Lange and Danhof, 2002; Levin, 1980). For highly permeable compounds, however, the rate of transport across the BBB and BCSFB is limited by the cerebral blood flow (Dagenais *et al.,* 2000). Furthermore, active transport processes into or out of the brain may increase or reduce the permeability rate.

The extent of drug distribution to the brain can be calculated as the ratio of unbound drug concentrations in the brain compared to unbound drug concentrations in plasma at steady state, or by the ratio of unbound AUC in brain relative to unbound AUC in plasma. For compounds that freely diffuse into and out of the brain, thus irrespective of what time that may take, this ratio should be equal to 1. If the ratio is < 1, this indicates that elimination processes (bulk flow, metabolism, active transport out of the brain) play an additional role. For a ratio > 1, active transport into the brain occurs, but may also be the

consequence of tissue binding. Alternatively, if ionization plays a role, ratios < or > 1 may as well result from pH differences between one site and another.

Generally, the extent of drug distribution into the brain is considered of most importance in relation to brain target site exposure. This means that drug discovery and development studies have focused on measuring drug concentrations in brain and plasma under (assumed) steady-state conditions. However, for drugs with a desired rapid onset of action (e.g. analgesics or anesthetics), the rate of entry into the brain is also relevant. Finally, it may be questioned whether fluctuations in brain concentrations, due to fluctuations in plasma concentrations following multiple dosing regimens, may have an impact on the pharmacodynamics (PD) of the drug.

This all implies the need for mechanistic investigations on the contribution of the different processes that govern the brain target site exposure. The techniques that are used to provide information on CNS drug distribution, in the perspective of extrapolation to the clinical setting and prediction of the effect, are discussed below.

Brain perfusion technique

Mayer and colleagues were one of the first to study the rate and extent of drug penetration into the brain (Mayer *et al.,* 1959). During the experiments, plasma concentrations were maintained at steady state by a bolus dose, followed by a constant rate infusion. By measuring brain homogenate concentrations at certain time points, distribution ratios could be calculated. Based on the time needed to reach a distribution ratio of 1, compounds were classified as having a fast (<5 min), intermediate (1.5-2 h), and very slow (>3 h) rate of entry.

Over time, this technique has been adapted so the initial rate of drug transport into the brain could be studied in more detail. Among the adapted techniques are the indicator diffusion technique (Crone, 1965), the brain uptake index technique (Oldendorf, 1970), the intravenous injection technique (Ohno *et al.,* 1978), and the in situ brain perfusion technique (Takasato *et al.,* 1984). In short, radiotracer quantities of a test substance and a diffusible reference such as $^{3}H_2O$ and/or a non-diffusible reference such as [^{14}C]inulin are injected intracarotidly or intravenously and the animal is decapitated 5-30 s later. Total

brain concentrations of the test substance and reference are then compared to concentrations in the injected solution or plasma.

These techniques are very suitable to study the rate and extent of exposure of the brain to the radioactivity, reflecting the compound of interest. However, the radioactivity potentially also includes metabolites. The major disadvantage of the different brain perfusion techniques is that they all use brain homogenate, so they cannot distinguish between intracellular space (ICS), $brain_{ECF}$ or CSF, and bound or unbound concentrations (Liu *et al.,* 2009). Modifications to the in situ brain perfusion technique have allowed distinguishing between accumulation in brain endothelial cells and uptake into brain parenchyma (Preston *et al.,* 1995), as well as uptake into the choroid plexus (Deane *et al.,* 2004). However, none of the brain perfusion techniques can distinguish between the different routes of entry to the brain, which could be by crossing the BBB or BCSFB. Furthermore, it is expensive and time-consuming to synthesize radioactively labeled drugs, making this technique less suited for early drug discovery (Liu and Jia, 2007). Alternatively, non-labeled compounds can be used as well. However, this requires the development of adequate analytical methods, which is evenly time consuming.

Brain homogenate free fraction method

Different methods have been developed to be able to distinguish between unbound and bound concentrations. Lin and colleagues used an equilibrium dialysis setup to determine the unbound fractions in plasma and brain homogenate (Lin *et al.,* 1982). Using the equilibrium dialysis setup, calculation of unbound brain concentrations from total brain concentrations improves the prediction of receptor occupancy compared to the use of just total brain concentrations (Watson *et al.,* 2009). Kalvass and Maurer (2002) adapted the equilibrium dialysis technique to a 96-wells plate that allowed for more high throughput screening. When the fraction unbound in plasma and brain is known, the $K_{p,uu}$ can be calculated from the K_p. Also, the unbound volume of distribution in the brain, which relates the total brain concentration to the unbound $brain_{ECF}$ concentration, can be determined (Fridén *et al.*, 2007).

Even though the brain homogenate free fraction method allows for higher throughput screening during early drug discovery compared to the brain

perfusion technique, the disadvantages remain of using brain homogenate. Because the brain tissue is homogenized, cell structures are destroyed and binding sites that are normally not accessible to a drug *in vivo* may be unmasked (Fridén *et al.,* 2007; Liu *et al.,* 2009). This could result in an erroneous estimation of the unbound fraction in brain tissue. As an alternative, the brain slice technique was developed.

Brain slice technique

The brain slice technique was developed by Newman *et al.* (1991). However, it was Kakee *et al.* (1996) that first applied the brain slice technique to determine unbound drug concentrations in brain tissue. In short, a section of a drug-naïve brain is cut into 300 μm slices, which are then incubated at 37°C in buffer containing the drug. After a certain time, assuming a steady state between buffer and brain slice ECF, the slices are homogenized and drug concentrations in the homogenate and buffer analyzed. In contrast to the brain homogenization method, the cellular structure of the brain tissue remains intact with the brain slice technique, thus it allows to distinguish between intracellular and extracellular as well as bound and unbound concentrations (Fridén *et al.,* 2009a).

Kakee *et al.* (1996) applied the brain slice technique to determine the unbound volume of distribution, which they used for the calculation of the brain efflux clearance rather than brain target site exposure. Fridén and colleagues compared the brain slice technique to the brain homogenate free fraction method in their ability to predict unbound volumes of distribution, as determined by the intracerebral microdialysis technique (see below). They concluded that the brain slice technique was better than the brain homogenate free fraction method for predicting unbound volumes of distribution (Fridén *et al.,* 2007).

All in all, the brain slice technique appears to be better than the brain homogenate free fraction method for the prediction of unbound brain target site concentrations. However, as the brain slice technique is more labor intensive and lower throughput compared to the brain homogenate free fraction method, the latter is still preferred during early CNS drug discovery (Read and Braggio, 2010). Even though recent developments have improved the throughput of the

brain slice technique (Fridén *et al.,* 2009a), it remains to be seen if the brain slice technique will replace the brain homogenate free fraction method during early CNS drug discovery.

CSF sampling

Back in 1959, Mayer and colleagues already recognized that the unbound plasma concentrations, rather than total plasma concentrations, are the main determinant for the rate and extent of drug entry into the brain, as protein-bound drugs cannot cross the BBB or BCSFB (Mayer *et al.,* 1959). However, due to the lack of suitable methods, it took nearly 25 years to acknowledge that the free drug hypothesis is also applicable for pharmacological activity at the brain target site. Danhof and Levy (1984) were one of the first to suggest the use of unbound CSF concentrations rather than total brain concentrations for relating pharmacological activity. They showed that, for phenobarbital, not plasma, nor total brain, but CSF concentrations were constant at the onset of anesthesia (the minimal effective concentration).

The most common method for collecting a CSF sample from humans is by a lumbar puncture (Hill *et al.,* 1999). However, for continuous CSF sampling, a cannula could also be implanted in the lumbar region (Bruce and Oldfield, 1988). In animals, CSF can be obtained relatively easy by a single puncture or the implantation of a cannula in the lateral ventricle or cisterna magna (Bouman and van Wimersma Greidanus, 1979; Cserr, 1965; Cserr, 1971; Nielsen *et al.,* 1980; van Bree *et al.,* 1989). Also, a few examples in literature exist on a lumbar puncture taken from in rats (De La Calle and Paíno, 2002; Wang *et al.,* 2005). As a concentration gradient could exist along the CSF flow path due to its high flow, the location of CSF sampling is very important for interpretation of data and extrapolation to the clinical setting (Summerfield and Jeffrey, 2006).

Mayer and colleagues combined the brain perfusion technique with CSF sampling from the cisterna magna in rabbits to compare the rate and extent of drug penetration between CSF and specific areas of the brain (Mayer *et al.,* 1959). They concluded that these parameters are determined by the lipophilicity of the compound. However, small differences in the rate of entry between CSF and the brain were observed for antipyrine and barbital, whereas their extent of brain entry was similar. Also, differences in both the rate and extent of

penetration of salicylic acid between CSF and brain were observed (Mayer *et al.,* 1959). As salicylic acid is known to be transported by an organic anion transport system (Lorenzo and Spector, 1973), the difference in the rate and extent of penetration may in part result from differences in the activity of such transport systems at the BBB and BCSFB. However, the difference in the rate and extent of penetration may also in part result from differences in physiology between the BBB and BCSFB.

Kalvass and Maurer (2002), Maurer *et al.* (2005), Liu *et al.* (2006), and Fridén *et al.* (2009b), all used single time point CSF samples from the cisterna magna of rats or mice in combination with the brain perfusion technique to compare steady state CSF concentrations to steady state unbound brain concentrations of over one hundred structurally diverse compounds. They all concluded that steady state CSF concentrations were comparable to steady state unbound brain concentrations within a 3-fold error range for compounds that freely diffuse across the BBB and BCSFB. Liu *et al.* (2009) also applied CSF sampling from the cisterna magna of rats in combination with the intracerebral microdialysis technique and showed that steady state CSF concentrations predicted steady state unbound brain concentrations very well within the 3-fold error range for the selected compounds, which also include some P-gp substrates. Possibly, CSF and $brain_{ECF}$ concentrations have had the time to reach equilibrium at steady state. However, for compounds with differences between CSF and $brain_{ECF}$ concentrations beyond the 3-fold error range, qualitative and quantitative differences in transporter activity between BBB and BCSFB may play a role.

The use of CSF as a surrogate for unbound brain target site concentrations has been discussed previously by De Lange and Danhof (2002), Shen *et al.* (2004), and Lin (2008). In short, they concluded that the use of CSF offers one significant advantage over other methods, in that this fluid is accessible both in animals as well as in humans, and provides information on the unbound concentration. However, CSF sampling generally lacks the possibility to obtain concentration-time profiles, at least in humans, whereas in animals, taking a CSF sample significantly affects the CSF volume, of which the impact is not yet known (De Lange *et al.,* 1997).

Intracerebral microdialysis

The intracerebral microdialysis technique is an *in vivo* technique that permits monitoring of local concentrations of drugs and metabolites by implantation of a microdialysis probe in a specific site in the brain (De Lange *et al.,* 1994; Morrison *et al.,* 1991; Nicolaysen *et al.,* 1988; Sabol and Freed, 1988; Ståhle *et al.,* 1991; Terasaki *et al.,* 1991; Wang *et al.,* 1995; Wong *et al.,* 1992). The probe contains a semipermeable membrane that is continuously perfused with a physiological solution that matches the ionic composition of the (extracellular) fluid surrounding the probe. Small enough molecules that are able to pass the membrane will diffuse into or out of the perfusate, down their concentration gradients. The solution that exits the probe, the dialysate, is then collected for analysis. However, because of the continuous flow of the perfusing solution, the concentration in the dialysate will be different from that in the surrounding fluid. The term 'concentration recovery' is used to describe this relationship and should always be determined for quantification of microdialysis data (De Lange *et al.,* 2000).

The microdialysis technique has a number of advantages: (1) Sampling can be performed continuously without fluid loss. (2) High resolution concentration-time profiles can be obtained from distinct brain regions in freely moving individual animals. (3) This reduces the number of animals needed for PK investigations. (4) The samples obtained are protein free. (5) *Ex vivo* analysis of the dialysate samples permits measurement of drug concentrations by any suitable analytical technique. However, the microdialysis also has its disadvantages: (1) The microdialysis technique is labor intensive, expensive, and low throughput. (2) Due to the invasive nature of implantation of the microdialysis probe, this technique only has a limited applicability in the human situation. (3) Due to the diluting effect of the dialysis, sensitive analytical methods are required to detect low concentrations. (4) The microdialysis technique is not always suitable for lipophilic compounds as they tend to adsorb to the microdialysis equipment (De Lange *et al.,* 1997; De Lange *et al.,* 2000; Sun and Stenken, 2003). However, the composition of the microdialysis perfusion fluid may be altered to improve the recovery, for example by addition of albumin or cyclodextrins to the perfusion fluid (Sun and Stenken, 2003).

Despite the very important advantage of being able to measure unbound brain concentrations as a function of time, the microdialysis technique is not often applied during early drug discovery because of the low throughput. However, it may provide information on the rate and extent of BBB and BCSFB transport, and modulations thereof. Furthermore, the microdialysis technique can be used to further distinguish the possible contribution of many dynamically regulated passive and active transport mechanisms.

One particular case is the investigation of the relationship between CSF and $brain_{ECF}$ concentrations, for the interpretation of human CSF data (De Lange and Danhof, 2002; Lin, 2008; Shen *et al.,* 2004). Several studies have been performed in which two microdialysis probes were implanted in a single animal; one in a selected brain region for measuring drug concentrations in the $brain_{ECF}$, and one in the lateral ventricle or cisterna magna for measuring drug concentrations in the CSF (Malhotra *et al.,* 1994; Matos *et al.,* 1992; Wong *et al.,* 1992).

Wong *et al.* (1992) found ventricular CSF concentrations being twice as high compared to rabbit $brain_{ECF}$ concentrations for zidovudine. Matos *et al.* (1992) measured morphine in CSF from the rat lateral ventricle, third ventricle, cisterna magna and spinal cord in the rat, and found morphine evenly distributed in all selected brain regions and CSF, except for cisternal CSF. Interestingly, cisternal CSF concentrations were about 5-fold higher than ventricular and lumbar CSF concentrations. This is counterintuitive, considering the CSF flow path. However, the concentration recovery was not addressed adequately. Finally, Malhotra *et al,* (1994) found that rat ventricular CSF concentrations were ~3-fold higher compared to $brain_{ECF}$ concentrations at steady state for EAB 515.

PET and SPECT

Positron emission tomography (PET) and single-photon emission computed tomography (SPECT) are very powerful techniques to study brain kinetics at multiple sites (Dresel *et al.,* 1998; Erlandsson *et al.,* 2005; Mamo *et al.,* 2004; Remington *et al.,* 2006; van Waarde, 2000). In short, small amounts of radiolabeled compounds are injected into the bloodstream, after which the total brain uptake can be estimated by calculating the ratio of the total brain radioactivity divided by the injected radioactivity.

The main difference between PET and SPECT is the type of radiation that is used. PET, as the name suggests, uses a positron emitter (usually ^{11}C or ^{18}F) for imaging, whereas SPECT uses a gamma emitter (often ^{123}I) (Erlandsson *et al.,* 2005; Haubner, 2010; Kouris, 1984). PET provides higher resolution images than SPECT. The major advantages of PET and SPECT are that these techniques are noninvasive and applicable to both animals and humans (van Waarde, 2000). As disadvantages, however, (1) PET and SPECT require radioactively labeled compounds, which is expensive and time-consuming in producing (Liu and Jia, 2007). Moreover, especially for PET radionuclides, the duration of a scan is limited by the decay of the radioactive label. For ^{11}C, which has a half-life of only 20 min, this means that synthesis of the radiolabeled compound should be performed on-site, right before the experiment. (2) While ^{18}F (half-life of 110 min) and ^{123}I (half-life of 13.2 h) can provide more flexibility in time, the labeling with these nuclei may change the compounds' properties. (3) Also, for animals, anesthesia is required, which may affect the physiological status of the animal, and may further limit the comparison to humans (Claassen, 1994). (4) Another disadvantage is that PET and SPECT signals do not distinguish between compounds and their metabolites, (5) nor between bound and unbound concentrations, as they can only localize the level of radioactivity (Neuwelt *et al.,* 2008).

CONSIDERATIONS IN ANIMAL-TO-HUMAN EXTRAPOLATION / PREDICTION

All vertebrates share the same mechanisms of blood-brain transport (Cserr and Bundgaard, 1984). However, the rate and extent of these mechanisms depend on conditions such as species, gender, tissue, genetic background, diet, disease, drug use, etc. As a result, observations in a particular setting are not necessarily predictive of what would be observed in another setting. In the following section, we will discuss the possible use of the different techniques in the clinical setting or for the prediction of human brain target site concentrations, as well as how different conditions may affect brain processes and therewith drug distribution into the brain.

Application of the different techniques in the extrapolation to the clinical setting

The brain perfusion technique, the brain homogenate free fraction method and the brain slice technique can all be applied to determine the rate and extent of brain target site exposure. This is often done during early CNS drug discovery, as these techniques have relatively high throughput and allow for good drug candidate selection (Read and Braggio 2010). However, these techniques have very limited applicability in the extrapolation to the clinical setting. The techniques that can be applied both in animals as well as in humans are the CSF sampling technique, the intracerebral microdialysis technique, PET, and SPECT. Of these techniques, PET and SPECT are the most promising, as they are very powerful techniques to study brain kinetics at multiple sites (Dresel *et al.,* 1998; Erlandsson *et al.,* 2005; Mamo *et al.,* 2004; Remington *et al.,* 2006; van Waarde, 2000). However, the time needed for the development of appropriate tracers and high costs of PET and SPECT scanning currently limit the use of these techniques during drug development.

So far, the CSF sampling technique is the technique that is most often used during drug development, as CSF sampling is relatively simple, straightforward, and cheap, compared to intracerebral microdialysis, PET, and SPECT (Lin, 2008). Moreover, this can be applied both to humans and animals. However, the use of CSF concentrations as a surrogate marker for brain target site concentrations is not that simple and straightforward, as a generally applicable relationship between CSF concentrations and brain target site concentrations does not exist (De Lange and Danhof, 2002; Lin, 2008; Shen *et al.,* 2004). Therefore, it is questionable whether brain target site concentrations can be predicted on the basis of CSF concentrations.

A number of studies have indicated that for most compounds there is not much difference between apparent steady-state concentrations in CSF and $brain_{ECF}$ in the rat (concentration ratios are < 3) (Fridén *et al.,* 2009b; Kalvass and Maurer, 2002; Liu *et al.,* 2006; Maurer *et al.,* 2005). However, the following questions still remain:

- Are such ratios predictive for the human situation?
- How does disease state influence such ratios?

- And, most importantly: if human CSF concentrations would have been predictive than why hasn't it proven itself as such?

The only technique that allows the measurement of unbound drug concentrations at the brain target site as well as in CSF *in vivo* is the intracerebral microdialysis technique. In the preclinical setting, the intracerebral microdialysis technique could very well be used to investigate the relationship between CSF concentrations and brain target site concentrations (Malhotra *et al.,* 1994; Matos *et al.,* 1992; Wong *et al.,* 1992). All in all, each of the different techniques has its advantages and disadvantages for extrapolating to the clinical setting.

Condition-dependent factors

In the drug development setting we would like to use animal data as best as possible for prediction of the human situation. This means that we have to consider sources of variation from controlled preclinical situations to clinical practice. One of the major issues in extrapolating from animal data to the human situation is that the vast majority of studies are being done in healthy animals, whereas there is increasing evidence that dysfunctional BBB mechanisms are at the core of CNS diseases (Jeffrey and Summerfield, 2010). However, for certain CNS disorders, there are simply no appropriate animal models available. In that case, animal experiments can improve our understanding of the biological system, which is essential to be able to understand the processes that underlie the disease. Then, for accurate prediction of CNS drug concentrations and effect in humans on the basis of animal data, one should take into account the possible influences of CNS diseases and genetic differences between species on the processes that govern CNS exposure (Syvänen *et al.,* 2009).

Inflammatory and oxidative stress, which are cofactors in nearly every CNS disease, can acutely disrupt the BBB and BCSFB at the level of the tight junctions (Miller, 2010). It has also been shown that a bacterial or viral infection of the CNS can cause a disruption in the integrity of the BBB and BCSFB (Paul *et al.,* 1998). So far, only limited information is available on the impact of CNS diseases on the expression levels of the different active transport systems that are located on the BBB and BCSFB. Of the different transport systems, most information is available on the regulation of expression levels of

P-gp. However, there is some evidence that also BCRP, MRP1, MRP2, and MRP4 expression is altered after exposure to certain xenobiotics, which include therapeutic agents and environmental toxicants (Miller, 2010). Some of these xenobiotics have also been found to increase expression of drug metabolizing enzymes in brain capillary endothelial cells. Increased expression levels of the different transport systems and drug metabolizing enzymes can make it very difficult to get sufficient amounts of drugs to their brain target site. Despite the success of specific transport inhibitors in improving drug delivery to the brain in animal studies, the results have not been translated to the clinic (Miller, 2010). It has been suggested that blocking of P-gp could improve drug delivery across the BBB. However, effective doses of P-gp inhibitors, such as cyclosporine and verapamil, are often toxic (Neuwelt, 2004).

The effect of inflammation on the activity and expression levels of transport systems is rather complex, as the direction and degree of change in expression levels is found to be dependent on the inflammatory signal and time after exposure. For instance, it has been found that P-gp activity is decreased after short-term exposure to proinflammatory signals, whereas there is no change in P-gp expression (Roberts and Goralski, 2008). Following a more prolonged exposure, the activity and expression of P-gp are both increased (Roberts and Goralski, 2008). However, rather than being an effect of CNS diseases, the change in transporter expression can also be the cause of CNS diseases. There have been some reports that a decrease in P-gp expression causes an increase in amyloid β protein levels in the brain, which is involved in the pathogenesis of Alzheimer's disease (Cirrito *et al.,* 2005; Vogelgesang *et al.,* 2002; Vogelgesang *et al.,* 2004). Reduced expression or activity of P-gp has also been associated with Creutzfeld-Jakob disease (Vogelgesang *et al.,* 2005), Parkinson's disease (Vautier *et al.,* 2009), HIV infection (Langford *et al.,* 2004), and normal aging (Bauer *et al.,* 2009). Furthermore, increased expression or activity of P-gp, but also BCRP, MRP1, and MRP2 is associated with epileptic seizures (Löscher and Potschka, 2005a).

Of all the different transporter systems, P-gp is considered to be the most clinically relevant, as it has a broad substrate specificity and plays an important role in drug disposition and response. Besides being expressed at the BBB and BCSFB, P-gp can also be found in the liver, kidneys, and intestine (Thiebaut *et al.,* 1987). As a result, a variable expression or activity of P-gp will alter the

extent of absorption, tissue distribution, and excretion of compounds that are substrates for P-gp (Marzolini *et al.,* 2004). The variable expression or activity could be caused by single-nucleotide polymorphisms (SNPs) that have been reported for the gene encoding P-gp (Marzolini *et al.,* 2004). While the effect of most SNPs on the expression or activity of P-gp still remains unclear, it has been reported that the absorption by the gut is altered by a specific polymorphism in exon 26 (C3435T), which results in a lower expression level of P-gp (Hoffmayer *et al.,* 2000). The same SNP has also been reported to be involved in drug-resistant epilepsy, where epileptic patients that have the specific SNP are more likely to respond to antiepileptic drugs (Siddiqui *et al.,* 2003). This is probably the result of a decreased expression and activity of P-gp at the BBB.

Even though most of the different transport systems at the BBB and BCSFB are expressed both in humans as well as in rats, their expression levels and activities might differ greatly between species (table 1) (Begley, 2004; Choudhuri *et al.,* 2003; Graff and Pollack, 2004; Hagenbuch and Meier, 2004; Hoshi *et al.,* 2013; Kusuhara and Sugiyama, 2004; Kusuhara and Sugiyama, 2005; Löscher and Potschka, 2005b; Perrière *et al.,* 2007; Syvänen *et al.,* 2009; Uchida *et al.,* 2011; Vannucci, 1994). This is probably the result of the genetic differences between humans and rats. The most profound differences can be seen for P-gp and the OATP family.

In humans, P-gp is encoded by the MDR1 gene, whereas in rodents it is encoded by two genes; mdr1a and mdr1b. Both mdr1a and mdr1b are present in rodent brain, but only mdr1a is located at the BBB, while mdr1b is present in brain parenchyma (Demeule *et al.,* 2002). The substrate specificity of mdr1a and mdra1b P-gp is largely overlapping, although there are some differences (Schinkel, 1999). As the tissue distribution of mdr1a and mdr1b P-gp is different, but partly overlapping, this suggests that the mdr1a and mdr1b P-gp in rodents functions the same as the MDR1 P-gp in humans (Schinkel, 1999). For the OATP family, the differences between species are more profound (Hagenbuch and Meier, 2004). However, because the OATP family has a broad and partially overlapping substrate specificity, it is likely that the functions of the different subtypes are comparable between rodents and humans (Hagenbuch and Meier, 2004).

Table 1. Overview of the different active transport systems that are located at the human and rat BBB and BCSFB

Transporter protein	Human BBB	Rat BBB	Human BCSFB	Rat BCSFB
P-gp	+ [1]	+ [5,a]	+ [2]	+ [2,a]
BCRP	+ [1]	+ [5]	-	-
MRP1	+ [2]	+ [6]	+ [2]	+ [11]
MRP2	+ [2]	+ [7]	-	+ [11]
MRP3	+ [2]	+ [6]	-	+ [11]
MRP4	+ [1]	+ [5]	+ [8]	+ [11]
MRP5	+ [2]	+ [6]	+ [8]	+ [11]
MRP6	+ [2]	-	-	+ [11]
OCT1	+ [2]	-	+ [2]	+ [11]
OCT2	+ [2]	+ [8]	+ [2]	+ [11]
OCT3	+ [2]	+ [8]	+ [2]	+ [8]
OCTN1	+ [2]	+ [8]	+ [8]	+ [11]
OCTN2	+ [2]	+ [8]	+ [8]	+ [11]
OATP A	+ [3]	-	-	-
OATP B	+ [3]	+ [8,b]	+ [8]	+ [11,b]
OATP E	+ [3]	+ [8,c]	+ [8]	+ [11,c]
OATP F	+ [3]	+ [8,d]	-	+ [11,d]
Oatp1	-	+ [3]	-	+ [2]
Oatp2	-	+ [3]	-	+ [2]
Oatp3	-	+ [3]	-	+ [2]
OAT1	+ [2]	+ [2]	+ [10]	+ [8]
OAT2	-	-	-	+ [8]
OAT3	+ [4]	+ [5]	+ [10]	+ [8]
GLUT-1	+ [1]	+ [5]	+ [2]	+ [9]

Notes to table 1: [1] Uchida et al., 2011; [2] Graff and Pollack, 2004; [3] Hagenbuch and Meier, 2004; [4] Löscher and Potschka, 2005b; [5] Hoshi et al., 2013; [6] Perrière et al., 2007; [7] Begley, 2004; [8] Kusuhara and Sugiyama, 2004; [9] Vannucci, 1994; [10] Kusuhara and Sugiyama, 2005; [11] Choudhuri et al., 2003.

[a] Human P-gp encoded by MDR1, rat P-gp encoded by mdr1a/mdr1b; [b] The rat ortholog of OATP B is Oatp9; [c] The rat ortholog of OATP E is Oatp12; [d] The rat ortholog of OATP F is Oatp14.

Another important difference between species is the relative rate of CSF production, which is estimated to be about 0.88 %/min in rats, compared to 0.29 %/min in humans (table 2). Thus, there is a higher CSF turnover in rats compared to humans. This could be important for hydrophilic compounds, as they can be taken along with the CSF and the relatively high flow of CSF could thereby prevent the diffusion to the brain target site. As for lipophilic compounds, even though the protein concentration in human CSF is reported to be about 400 times less than in human blood, the CSF protein concentration in the rat is 5-10 times higher compared to humans (Maurer, 2010). It has also been reported that CSF protein concentrations increase along the flow path. Therefore, a concentration gradient could exist along the CSF flow path for both hydrophilic as well as lipophilic compounds. This indicates that the location of CSF sampling is very important (Summerfield and Jeffrey, 2006).

These are all examples illustrative of the fact that we need a more thorough understanding of the processes that occur in the brain. To do so, we must gather and combine mechanistic information on the contribution of processes on the causal chain from drug administration, to drug brain target site PK, to ultimate CNS drug effects, including the variability in these contributions that will exist between conditions. Such will pave the way for adequate prediction of human drug effects. Consequently, a lot of data needs to be integrated, which is beyond individual intellectual capabilities. Therefore, we need to make use of mathematical modeling.

Table 2. Differences between rat and human physiological parameters

Parameter	Human value	Rat value
$Brain_{ECF}$ volume	240 ml [1]	290 µl [6]
$Brain_{ECF}$ production rate	0.15-0.2 ml/min (0.0625-0.083 %/min) [1,2]	0.2-0.5 µl/min (0.069-0.17 %/min) [6,7]
CSF volume	140 ml [3]	250 µl [8]
CSF production rate	0.4 ml/min (0.29 %/min) [4]	2.2 µl/min (0.88 %/min) [9]
Cerebral blood flow	700 ml/min (14% of cardiac output) [5]	1.1 ml/min (2.5% of cardiac output) [10]

[1] Begley, 2000; [2] Kimelberg, 2004; [3] Kohn et al., 1991; [4] Nilsson et al., 1992; [5] Ito et al., 2006; [6] Cserr et al., 1981; [7] Abbott, 2004; [8] Bass and Lundborg, 1973; [9] Cserr, 1965; [10] Harashima et al., 1985.

Mathematical modeling

We can learn more on the inter-relationship between plasma PK, BBB transport and intra-brain distribution, by performing integrative cross-compare designed studies in animals in which variables are systematically varied (e.g. inhibition of an efflux transporter, or induction of pathological state). This allows us to dissect contributions of individual mechanisms of blood-brain transport in animals, which provides links to the human situation. Humans have the same mechanisms as animals, but these may have a different rate and extent and therefore have different contributions to the dose-effect relationships (Cserr and Bundgaard, 1984). As many variables are in play, we need to organize and integrate all these, and further condense and store such knowledge in mathematical models.

Compartmental modeling - In order to be able to predict human brain target site concentrations and ultimate drug effect on the basis of preclinical data, different mathematical modeling techniques can be applied (Danhof *et al.,* 2008). The most commonly applied mathematical modeling technique is the relatively simple compartmental model analysis, viewing the body as a series of virtual and interconnected compartments (Fleishaker and Smith, 1987). Using mass balance differential equations, concentration-time profiles in different compartments can be described. These equations can also be used to calculate PK parameters like volume of distribution, systemic clearance, and elimination half-life.

Allometric scaling - Extrapolation of animal PK parameters to the human situation is necessary for designing first in human trials, which can sometimes be done reasonably well by allometric scaling (Bonati *et al.,* 1984; Lavé *et al.,* 1999; Mahmood and Balian, 1999; Obach *et al.,* 1997; Yassen *et al.,* 2007; Zuideveld *et al.,* 2007). Allometric scaling uses bodyweight or body surface area as the main determinant of PK parameters, assuming that there are anatomical, physiological and biochemical similarities among different species (Boxenbaum, 1982; Dedrick, 1973; Mordenti, 1986). However, for predicting human PK parameters that are involved in more complex systems on the basis of animal data, a physiologically-based (PB) PK model is more appropriate.

PBPK modeling - PBPK models integrate drug-dependent, physiological, and biological parameters as they vary in between species, subjects, or with age and disease state (Colburn, 1988a; Espié *et al.,* 2009; Ings, 1990). In a PBPK model the tissues of interest are viewed as body compartments and are arranged in anatomical order, based on blood circulation, to form an integrated physiological model (Colburn, 1988a; Espié *et al.,* 2009; Ings, 1990; Rowland *et al.,* 2004). Once a suitable model has been developed, the concentration-time profiles of the drug in each of the body compartments can be calculated based on a mass balance. The distribution of the drug can then be linked to the physicochemical properties of the drug and the type of tissue involved. Distribution of the drug into tissues can further be classified as either perfusion rate limited or permeability rate limited (Colburn, 1988a; Ings, 1990; Jones *et al.,* 2009).

A typical PBPK model consists of non-eliminating (adipose, bone, brain, gut, heart, lung, muscle, skin, spleen) and eliminating tissues (kidney and liver) (figure 3A) (Jones *et al.,* 2006; Jones *et al.,* 2009; Rowland *et al.,* 2004). However, to be able to properly predict brain target site concentrations, the brain compartment in the PBPK model should describe the complexity of the CNS (De Lange and Danhof, 2002; Ooie *et al.,* 1997; Shen *et al.,* 2004). Figure 3B shows the complexity of the CNS in the brain compartment of a PBPK model.

Even though the PBPK approach may be more suitable for complex systems, it also results in complex mathematical models that are expensive and time consuming. Therefore, PBPK models are often only used in the later stages of drug development (Espié *et al.,* 2009; Ings, 1990; Jones *et al.,* 2006; Jones *et al.,* 2009; Rowland *et al.,* 2004).

Modeling of drug effect - Ultimately, the goal of mathematical modeling is to be able to predict drug efficacy and safety in humans on the basis of animal data (Danhof *et al.,* 2008). To link drug concentration-time data to the physiologic response, PK-PD modeling is often applied. The primary objective of PK-PD modeling is prediction of the time course of the drug effect *in vivo* in health and disease (Breimer and Danhof, 1997). Depending on the concentration-effect relationship, as well as the type of response (inhibition or stimulation), different PK-PD models can be used (Csajka and Verotta, 2006; Swinghammer and

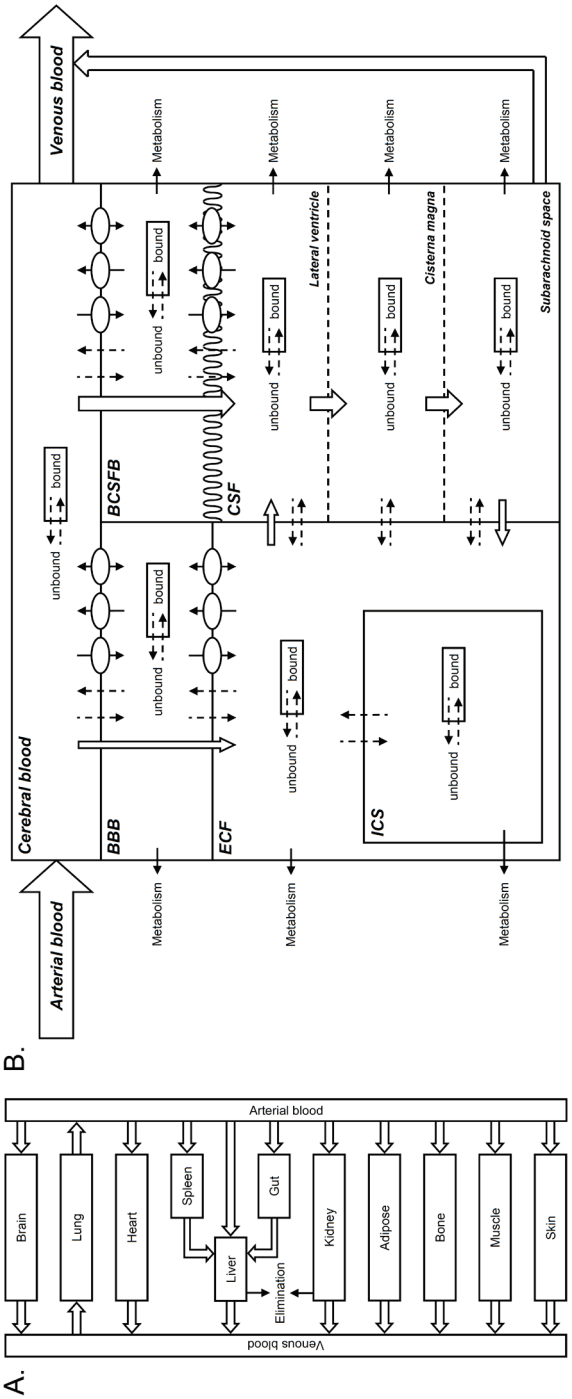

Figure 3. (A) Schematic representation of a typical PBPK model. (B) Schematic representation of the brain compartments on the basis of the information that is presented in this review. Block arrows indicate fluid flow; solid arrows indicate active transport processes; dashed arrows indicate permeability rate-limited transport; solid lines indicate restricted diffusion; dashed lines indicate free diffusion

Kroboth, 1988). When the effect is directly related to plasma concentrations, a PK compartmental model with the addition of an effect compartment could be sufficient (Sheiner *et al.,* 1979). However, as CNS drug effects often have their origin in the brain, an alternate model that relates the effect to drug concentrations in a peripheral compartment is more appropriate (Colburn, 1981; Colburn, 1988b).

Prediction of human drug effect - Extrapolation of animal PK-PD data to predict the time course of the drug effect in humans can sometimes be done by simple allometric scaling of the PK parameters and the PK-PD relationship (Mager *et al.,* 2009). However, for accurate prediction of human drug effect on the basis of animal data, one should also understand the biological processes that underlie the effect. These processes include target site distribution, target binding, target activation, transduction, homeostatic feedback, and disease processes (Danhof *et al.,* 2005; Danhof *et al.,* 2007). Information on these processes is included in mechanism-based (MB) PK-PD modeling. A major advantage of MBPK-PD modeling is the distinction between drug-specific parameters and biological system-specific parameters. Drug-specific parameters are dependent on the physicochemical properties of the drug and include target affinity and target activation, whereas biological system-specific parameters describe the functioning of the biological system (Danhof *et al.,* 2008). This indicates that MBPK-PD modeling can be applied for the extrapolation of animal data to the human situation, but also from one drug to another.

DISCUSSION AND CONCLUSIONS

The development of drugs for central nervous system (CNS) disorders has encountered high failure rates. In part this has been due to the sole focus on BBB permeability of drugs, without taking into account all other processes that determine drug concentrations at the target site. Moreover, conditional dependence of these processes has typically been neglected.

The impact of these processes can be studied in the preclinical setting with several *in vitro*, *ex vivo*, and *in vivo* techniques. However, considering the

animal-to-human extrapolation, the CSF sampling technique and intracerebral microdialysis technique are currently the best available techniques.

In practical terms, of special interest is CSF sampling as it can be performed in animals as well as in humans and provides information on unbound drug concentrations. A number of studies have shown that steady state CSF concentrations can be used very well for the prediction of steady state brain concentrations within a 3-fold error range for compounds that freely diffuse across the BBB and BCSFB, whereas the difference between CSF exposure and brain exposure may be beyond 3-fold for compounds that are substrates for the different active transport systems at the BBB and BCSFB (Fridén *et al.,* 2009b; Kalvass and Maurer, 2002; Liu *et al.,* 2006; Maurer *et al.,* 2005). On that basis it may be questioned:

- How useful are steady state concentration ratios? What is the degree of fluctuation in plasma concentrations and how does this correspond to the degree of variation in concentrations at the brain target site? And, in what extent are the CNS effects sensitive for such fluctuations?
- How useful are single time point CSF or total brain samples? One should consider that the use of a single time point sample as a marker for CSF or total brain exposure tells us nothing about the rate of blood-brain transport, which is relevant for drugs with a desired rapid onset of action.
- What is the impact of the 3-fold error that is allowed for the estimation of CSF-brain$_{ECF}$ concentration ratios? The 3-fold error is considered to be of little pharmacologic or pharmacokinetic consequence for the prediction of unbound brain concentrations on the basis of CSF concentrations (Maurer *et al.,* 2005). However, the 3-fold error is also allowed for the prediction of human CSF exposure on the basis of rat CSF exposure (Fridén *et al.,* 2009b). This results in a 9-fold error that is allowed for the prediction of human unbound brain exposure on the basis of human CSF exposure. This may have significant consequences if a drug has a steep concentration-effect relationship or a narrow therapeutic window.

This implicates that in order to be able to accurately predict CNS drug effect in humans, it is essential that we increase our understanding of the complexity of the CNS and CNS disorders. Given that CSF concentrations are often

considered to be the best available surrogate for brain target site concentrations in humans (Fridén *et al.,* 2009b; Kalvass and Maurer, 2002; Liu *et al.,* 2006; Liu *et al.,* 2009; Maurer *et al.,* 2005), future research should focus on studying the relationship between CSF concentrations and brain target site concentrations.

The only technique that allows the measurement of unbound drug concentrations at the brain target site, provided that the CNS drug target faces the $brain_{ECF}$, as well as in CSF *in vivo* is the intracerebral microdialysis technique. In the preclinical setting, the intracerebral microdialysis technique could very well be used to investigate the relationship between CSF concentrations and extracellular brain target site concentrations (Malhotra *et al.,* 1994; Matos *et al.,* 1992; Wong *et al.,* 1992). When the CNS drug target is located intracellularly, there is not a single technique that allows to study the relationship between CSF concentrations and intracellular concentrations. This indicates that a combination of different techniques should be applied. However, to be able to predict CNS drug effect in humans, it is also essential to study the underlying processes that govern the concentration-effect relationship.

In combination with CSF sampling, brain tissue sampling and serial blood sampling, the intracerebral microdialysis technique provides very useful data to determine the kinetics of transport equilibration across the BBB and BCSFB under a variety of conditions, in the species of choice, such as mice, rats, rabbits, piglets and monkeys, as well as in humans (intensive care patients). Therefore it is of importance to investigate the inter-relationship between plasma PK, BBB transport and intra-brain distribution in integrative cross-compare designed studies. By systematically influencing one (or a subset) of variables, one can decipher the impact of changes at the level of this variable on the blood-brain transport.

Such information on the rate and extent of BBB and BCSFB transport, and modulations thereof, will be useful to further distinguish the possible contribution of many dynamically regulated passive and active transport mechanisms. The knowledge thus provided on BBB and BCSFB transport mechanisms and regulation is critical for the understanding of brain homeostasis, and how disturbances thereof may lead to CNS diseases. Also, it will be critical in ultimately being able to predict the PK-PD relationship of CNS active compounds.

Apart from striving towards reduction of the use of animals and the fact that animal models of CNS diseases will never exactly reflect the disease conditions in human, we will move forward considerably by systematic research on CNS drugs in the preclinical setting, including animal models of CNS diseases that reflect important parts of disease mechanisms. As many variables are in play, we need to organize and integrate all these, and further condense and store such knowledge in mathematical frameworks.

REFERENCES

Abbott NJ. Evidence of bulk flow of brain interstitial fluid: significance for physiology and pathology. Neurochem Int 2004; 45: 545-552.

Abbott NJ, Rönnbäck L, Hansson E. Astrocyte-endothelial interactions at the blood-brain barrier. Nat Rev Neurosci 2006; 7: 41-53.

Bass NH, Lundborg P. Postnatal development of bulk flow in the cerebrospinal fluid system of the albino rat: clearance of carboxyl-[^{14}C]inulin after intrathecal infusion. Brain Res 1973; 52: 323-332.

Bauer M, Karch R, Neumann F, Abrahim A, Wagner CC, Kletter K, Müller M, Zeitlinger M, Langer O. Age dependency of cerebral P-gp function measured with (R)-[^{11}C]verapamil and PET. Eur J Clin Pharmacol 2009; 65: 941-946.

Begley DJ. Transport to the brain. In: D.J. Begley, M.W. Bradbury and J. Kreuter, editors. The blood-brain barrier and drug delivery to the CNS. 2000; New York: Dekker; p. 93–108.

Begley DJ. ABC transporters and the blood-brain barrier. Curr Pharm Des 2004; 10: 1295-1312.

Bernacki J, Dobrowolska A, Nierwińska K, Małecki, A. Physiology and pharmacological role of the blood-brain barrier. Pharmacol Rep 2008; 60: 600-622.

Bonati M, Latini R, Tognini G, Young JF, Garattini S. Interspecies comparison of in vivo caffeine pharmacokinetics in man, monkey, rabbit, rat and mouse. Drug Metab Rev 1984; 15: 1355-1383.

Bouman HJ, van Wimersma Greidanus TB. A rapid and simple cannulation technique for repeated sampling of cerebrospinal fluid in freely moving rats. Brain Res Bull 1979; 4: 575-577.

Boxenbaum H. Interspecies scaling, allometry, physiological time, and the ground plan of pharmacokinetics. J Pharmacokin Biopharm 1982; 10: 201-227.

Breimer DD, Danhof M. Relevance of the application of pharmacokinetic-pharmacodynamic modelling concepts in drug development. The 'wooden shoe' paradigm. Clin Pharmacokin 1997; 32: 259-267.

Bruce JN, Oldfield EH. Method for sequential sampling of cerebrospinal fluid in humans. Neurosurgery 1988; 23: 788-790.

Business Insights. In: *The CNS Market Outlook to 2014*, 2010.

Choudhuri S, Cherrington NJ, Li N, Klaassen CD. Constitutive expression of various xenobiotic and endobiotic transporter mRNAs in the choroid plexus of rats. Drug Metab Dispos 2003; 31: 1337-1345.

Cirrito JR, Deane R, Fagan AM, Spinner ML, Parsadanian M, Finn MB, Jiang H, Prior JL, Sagare A, Bales KR, Paul SM, Zlokovic B, Piwnica-Worms D, Holtzman DM. P-glycoprotein deficiency at the blood-brain barrier increases amyloid-β deposition in an Alzheimer disease mouse model. J Clin Invest 2005; 115: 3285-3290.

Claassen. In: *Techniques in the Behavioral and Neural Sciences, Neglected Factors in Pharmacology and Neuroscience Research, Vol. 12*, 1994.

Colburn WA. Simultaneous pharmacokinetic and pharmacodynamic modeling. J Pharmacokin Biopharm 1981; 9: 367-388.

Colburn WA. Physiologic pharmacokinetic modeling. J Clin Pharmacol 1988a; 28: 673-677.

Colburn WA. Combined pharmacokinetic/pharmacodynamic (PK/PD) modeling. J Clin Pharmacol 1988b; 28: 769-771.

Crone C. The permeability of brain capillaries to non-electrolytes. Acta Physiol Scand 1965; 64: 407-417.

Csajka C, Verotta D. Pharmacokinetic-pharmacodynamic modeling: history and perspectives. J Pharmacokin Pharmacodyn 2006; 33: 227-279.

Cserr HF. Potassium exchange between cerebrospinal fluid, plasma, and brain. Am J Physiol 1965; 209: 1219-1226.

Cserr HF. Physiology of the choroid plexus. Physiol Rev 1971; 51: 273-311.

Cserr HF, Cooper DN, Suri PK, Patlak CS. Efflux of radiolabeled polyethylene glycols and albumin from rat brain. Am J Physiol 1981; 240: F319-F328.

Cserr HF, Bundgaard M. Blood-brain interfaces in vertebrates: a comparative approach. Am J Physiol 1984; 246: R277-R288.

Dagenais C, Rousselle C, Pollack GM, Scherrmann J-M. Development of an in situ mouse brain perfusion model and its application to mdr1a P-glycoprotein-deficient mice. J Cereb Blood Flow Metab 2000; 20: 381-386.

Danhof M, Levy G. Kinetics of drug action in disease states. I. Effect of infusion rate on phenobarbital concentrations in serum, brain and cerebrospinal fluid of normal rats at onset of loss of righting reflex. J Pharmacol Exp Ther 1984; 229: 44-50.

Danhof M, Alvan G, Dahl SG, Kuhlmann J, Paintaud G. Mechanism-based pharmacokinetic-pharmacodynamic modelling – a new classification of biomarkers. Pharm Res 2005; 22: 1432-1437.

Danhof M, de Jongh J, de Lange ECM, Della Pasqua OE, Ploeger BA, Voskuyl RA. Mechanism-based pharmacokinetic-pharmacodynamic modeling: biophase distribution, receptor theory, and dynamical systems analysis. Annu Rev Pharmacol Toxicol 2007; 47: 357-400.

Danhof M, de Lange ECM, Della Pasqua OE, Ploeger BA, Voskuyl RA. Mechanism-based pharmacokinetic-pharmacodynamic (PK-PD) modeling in translational drug research. Trends Pharmacol Sci 2008; 29: 186-191.

Davson H, Oldendorf WH. Transport in the central nervous system. Proc R Soc Med 1967; 60: 326-329.

Deane R, Zheng W, Zlokovic BV. Brain capillary endothelium and choroid plexus epithelium regulate transport of transferring-bound and free iron into the rat brain. J Neurochem 2004; 88: 813-820.

Dedrick RL. Animal scale-up. J Pharmacokin Biopharm 1973; 1: 435-461.

De La Calle JL, Paíno CL. A procedure for direct lumbar puncture in rats. Brain Res Bull 2002; 59: 245-250.

De Lange ECM, Danhof M. Considerations in the use of cerebrospinal fluid pharmacokinetics to predict brain target concentrations in the clinical setting. Implications of the barriers between blood and brain. Clin Pharmacokin 2002; 41: 691-703.

De Lange ECM, Danhof M, de Boer AG, Breimer DD. Critical factors of intracerebral microdialysis as a technique to determine the pharmacokinetics of drugs in rat brain. Brain Res 1994; 666: 1-8.

De Lange ECM, de Boer AG, Breimer DD. Methodological issues in microdialysis sampling for pharmacokinetic studies. Adv Drug Del Rev 2000; 45: 125-148.

De Lange ECM, Danhof M, de Boer AG, Breimer DD. Methodological considerations of intracerebral microdialysis in pharmacokinetic studies on drug transport across the blood-brain barrier. Brain Res Rev 1997; 25: 27-49.

Demeule M, Régina A, Jodoin J, Laplante A, Dagenais C, Berthelet F, Moghrabi A, Béliveau R. Drug transport to the brain: key roles for the efflux pump P-glycoprotein in the blood-brain barrier. Vasc Pharmacol 2002; 38: 339-348.

Dohrmann GJ. The choroid plexus: a historical review. Brain Res 1970; 18: 197-218.

Dresel S, Tatsch K, Dähne I, Mager T, Scherer J, Hahn K. Iodine-123-iodobenzamide SPECT assessment of dopamine D_2 receptor occupancy in risperidone-treated schizophrenic patients. J Nucl Med 1998; 39: 1138-1142.

Erlandsson K, Sivananthan T, Lui D, Spezzi A, Townsend CE, Mu S, Lucas R, Warrington S, Ell PJ. Measuring SSRI occupancy of SERT using the novel tracer [^{123}I]ADAM: a SPECT validation study. Eur J Nucl Med Mol Im 2005; 32: 1329-1336.

Espié P, Tytgat D, Sargentini-Maier M-L, Poggesi I, Watelet J-P. Physiologically based pharmacokinetics (PBPK). Drug Metab Rev 2009; 41: 391-407.

Fleishaker JC, Smith RB. Compartmental model analysis in pharmacokinetics. J Clin Pharmacol 1987; 27: 922-926.

Fridén M, Gupta A, Antonsson M, Bredberg U, Hammarlund-Udenaes M. In vitro methods for estimating unbound drug concentrations in the brain interstitial and intracellular fluids. Drug Metab Disp 2007; 35: 1711-1719.

Fridén M, Ducrozet F, Middleton B, Antonsson M, Bredberg U, Hammarlund-Udenaes M. Development of a high-throughput brain slice method for studying drug distribution in the central nervous system. Drug Metab Dispos 2009a; 37: 1226-1233.

Fridén M, Winiwarter S, Jerndal G, Bengtsson O, Wan H, Bredberg U, Hammarlund-Udenaes M, Antonsson M. Structure – brain exposure relationships in rat and human using a novel data set of unbound drug concentrations in brain interstitial and cerebrospinal fluids. J Med Chem 2009b; 52: 6233-6243.

Gazzin S, Strazielle N, Schmitt C, Fevre-Montagne M, Ostrow JD, Tribelli C, Ghersi-Egea JF. Differential expression of the multidrug resistance-related proteins ABCb1 and ABCc1 between blood-brain interfaces. J Comp Neurol 2008; 510: 497-507.

Ghersi-Egea J-F, Perrin R, Leininger-Muller B, Grassiot M-C, Jeandel C, Floquet J, Cuny G, Siest G, Minn A. Subcellular localization of cytochrome P450, and activities of several enzymes responsible for drug metabolism in the human brain. Biochem Pharmacol 1993; 45: 647-658.

Ghersi-Egea J-F, Leininger-Muller B, Suleman G, Siest G, Minn A. Localization of drug-metabolizing enzyme activities to blood-brain interfaces and circumventricular organs. J Neurochem 1994; 62: 1089-1096.

Gjedde A. High- and low-affinity transport of D-glucose from blood to brain. J Neurochem 1981; 36: 1463-1471.

Graff CL, Pollack G. Drug transport at the blood-brain barrier and the choroid plexus. Curr Drug Metab 2004; 5: 95-108.

Gupta A, Chatelain P, Massingham R, Jonsson EN, Hammarlund-Udenaes M. Brain distribution of cetirizine enantiomers: comparison of three different tissue-to-plasma partition coefficients: K(p), K(p,u), and K(p,uu). Drug Metab Dispos 2006; 34: 318-323.

Hagenbuch B, Meier PJ. Organic anion transporting polypeptides of the OATP/*SLC21* family: polygenetic classification as OATP/*SLCO* superfamily, new nomenclature and molecular/functional properties. Eur J Physiol 2004; 447: 653-665.

Hammarlund-Udenaes M. Active-site concentrations of chemicals – are they a better predictor of effect than plasma/organ/tissue concentrations? Basic Clin Pharmacol Toxicol 2009; 106: 215-220.

Hammarlund-Udenaes M, Fridén M, Syvänen S, Gupta A. On the rate and extent of drug delivery to the brain. Pharm Res 2008; 25: 1737-1750.

Hammarlund-Udenaes M, Bredberg U, Fridén M. Methodologies to assess brain drug delivery in lead optimization. Curr Topics Med Chem 2009; 9: 148-161.

Harashima H, Sawada Y, Sugiyama Y, Iga T, Hanano M. Analysis of nonlinear tissue distribution of quinidine in rats by physiologically based pharmacokinetics. J Pharmacokin Biopharm 1985; 13: 425-440.

Haubner R. PET radiopharmaceuticals in radiation treatment planning – synthesis and biological characteristics. Radiother Oncol 2010; 96: 280-287.

Hill KK, West SA, Ekhator NN, Bruce AB, Wortman MD, Baker DG, Geracioti Jr TD. The effect of lumbar puncture stress on dopamine and serotonin metabolites in human cerebrospinal fluid. Neurosci Lett 1999; 276: 25-28.

Hoffmayer S, Burk O, von Richter O, Arnold HP, Brockmöller J, Johne A, Cascorbi I, Gerloff T, Roots I, Eichelbaum M, Brinkmann U. Functional polymorphisms of the human multidrug-resistance gene: multiple sequence variations and correlation of one allele with P-glycoprotein expression and activity *in vivo*. Proc Natl Acad Sci USA 2000; 97: 3473-3478.

Hoshi Y, Uchida Y, Tachikawa M, Inoue T, Ohtsuki S, Terasaki T. Quantitative atlas of blood-brain barrier transporters, receptors, and tight junction proteins in rats and common marmoset. J Pharm Sci 2013; 102: 3343-3355.

Ings RMJ. Interspecies scaling and comparisons in drug development and toxicogenetics. Xenobiotica 1990; 20: 1201-1231.

Ito H, Inoue K, Goto R, Kinomura S, Taki Y, Okada K, Sato K, Sato T, Kanno I, Fukuda H. Database of normal human cerebral blood flow measured by SPECT: I. Comparison between I-123-IMP, Tc-99m-HMPAO, and Tc-99m-ECD as referred with O-15 labeled water PET and voxel-based morphometry. Ann Nucl Med 2006; 20: 131-138.

Jeffrey P, Summerfield S. Assessment of the blood-brain barrier in CNS drug discovery. Neurobiol Dis 2010; 37: 33-37.

Jones HM, Parrott N, Jorga K, Lavé T. A novel strategy for physiologically based predictions of human pharmacokinetics. Clin Pharmacokin 2006; 45: 511-542.

Jones HM, Gardner IB, Watson KJ. Modelling and PBPK simulation in drug discovery. AAPS J 2009; 11: 155-166.

Kakee A, Terasaki T, Sugiyama Y. Brain efflux index as a novel method of analyzing efflux transport at the blood-brain barrier. J Pharmacol Exp Ther 1996; 277: 1550-1559.

Kalvass JC, Maurer TS. Influence of nonspecific brain and plasma binding of CNS exposure: implications for rational drug discovery. Biopharm Drug Dispos 2002; 23: 327-338.

Kassem NA, Deane R, Segal MB, Chen RL, Preston JE. Thyroxine (T_4) transfer from CSF to choroid plexus and ventricular brain regions in rabbit: contributory role of P-glycoprotein and organic anion transporting polypeptides. Brain Res 2007; 1181: 44-50.

Keep RF, Jones HC. A morphometric study on the development of the lateral ventricle choroid plexus, choroid plexus capillaries and ventricular ependyma in the rat. Dev Brain Res 1990a; 56: 47-53.

Keep RF, Jones HC. Cortical microvessels during brain development: a morphometric study in the rat. Microvasc Res 1990b; 40: 412-426.

Kimelberg HK. Water homeostasis in the brain: basic concepts. Neurosci 2004; 129: 851-860.

Kohn MI, Tanna NK, Herman GT, Resnick SM, Mozley PD, Gur RE, Alavi A, Zimmerman RA, Gur RC. Analysis of brain and cerebrospinal fluid volumes with MR imaging. Part I. Methods, reliability, and validation. Radiology 1991; 178: 115-122.

Kouris K. Emission tomography: a concise theoretical overview. Nucl Med Comm 1984; 5: 733-739.

Kusuhara H, Sugiyama Y. Efflux transport systems for organic anions and cations at the blood-CSF barrier. Adv Drug Del Rev 2004; 56: 1741-1763.

Kusuhara H, Sugiyama Y. Active efflux across the blood-brain barrier: role of the solute carrier family. NeuroRx 2005; 2: 73-85.

Langford D, Grigorian A, Hurford R, Adame A, Ellis RJ, Hansen L, Masliah E. Altered P-gp expression in AIDS patients with HIV encephalitis. J Neuropathol Exp Neurol 2004; 63: 1038-1047.

Lavé T, Portmann R, Schenker G, Gianni A, Guenzi A, Girometta MA, Schmitt M. Interspecies pharmacokinetic comparisons and allometric scaling of napsagatran, a low molecular weight thrombin inhibitor. J Pharm Pharmacol 1999; 49: 178-183.

Lee G, Bendayan R. Functional expression and localization of P-glycoprotein in the central nervous system: relevance to the pathogenesis and treatment of neurological disorders. Pharm Res 2004; 21: 1313-1330.

Lee G, Dallas S, Hong M, Bendayan R. Drug transporters in the central nervous system: brain barriers and brain parenchyma considerations. Pharmacol Rev 2001; 53: 569-596.

Levin VA. Relationship of octanol/water partition coefficient and molecular weight to rat brain capillary permeability. J Med Chem 1980; 23: 682-684.

Lin JH. CSF as a surrogate for assessing CNS exposure: an industrial perspective. Curr Drug Metab 2008; 9: 46-59.

Lin JH, Sugiyama Y, Awazu S, Hanano M. *In vitro* and *in vivo* evaluation of the tissue-to-blood partition coefficient for physiological pharmacokinetic models. J Pharmacokin Biopharm 1982; 10: 637-647.

Liu X, Jia L. The conduct of drug metabolism studies considered good practice (I): analytical systems and *in vivo* studies. Curr Drug Metab 2007; 8: 815-821.

Liu X, Smith BJ, Chen C, Callegari E, Becker SL, Chen X, Cianfrogna J, Doran AC, Doran SD, Gibbs JP, Hosea N, Liu J, Nelson FR, Szewc MA, Van Deusen J. Evaluation of cerebrospinal fluid concentration and plasma free concentration as a surrogate measurement for brain free concentration. Drug Metab Dispos 2006; 34: 1443-1447.

Liu X, Van Natta K, Yeo H, Vilenski O, Weller PE, Worboys PD, Monshouwer M. Unbound drug concentration in brain homogenate and cerebral spinal fluid at steady state as a surrogate for unbound concentration in brain interstitial fluid. Drug Metab Dispos 2009; 37: 787-793.

Lorenzo AV, Spector S. Transport of salicylic acid by the choroid plexus *in vitro*. J Pharmacol Exp Ther 1973; 184: 465-471.

Löscher W, Potschka H. Blood-brain barrier active efflux transporters: ATP-binding cassette gene family. Nat Rev Neurosci 2005a; 6: 591-602.

Löscher W, Potschka H. Role of drug efflux transporters in the brain for drug disposition and treatment of brain diseases. Prog Neurobiol 2005b; 76: 22-76.

Mager DE, Woo S, Jusko WJ. Scaling pharmacodynamics from *in vitro* and preclinical animal studies to humans. Drug Metab Pharmacokin 2009; 24: 16-24.

Mahmood I, Balian JD. The pharmacokinetic principles behind scaling from preclinical results to phase I protocols. Clin Pharmacokin 1999; 36: 1-11.

Malhotra BK, Lemaire M, Sawchuk, RJ. Investigation of the distribution of EAB 515 to cortical ECF and CSF in freely moving rats utilizing microdialysis. Pharm Res 1994; 11: 1223-1232.

Mamo D, Kapur S, Shammi CM, Papatheodorou G, Mann S, Therrien F, Remington G. A PET study of dopamine D_2 and serotonin 5-HT_2 receptor occupancy in patients with schizophrenia treated with therapeutic doses of ziprasidone. Am J Psych 2004; 161: 818-825.

Mandula H, Parepally JMR, Feng R, Smith QR. Role of site-specific binding to plasma albumin in drug availability to brain. J Pharmacol Exp Ther 2006; 317: 667-675.

Marzolini C, Paus E, Buclin T, Kim RB. Polymorphisms in human *MDR1* (P-glycoprotein): recent advances and clinical relevance. Clin Pharmacol Ther 2004; 75: 13-33.

Matos FF, Rollema H, Basbaum AI. Simultaneous measurement of extracellular morphine and serotonin in brain tissue and CSF by microdialysis in awake rats. J Neurochem 1992; 58: 1773-1781.

Maurer TS, DeBartolo DB, Tess DA, Scott D. Relationship between exposure and nonspecific binding of thirty-three central nervous system drugs in mice. Drug Metab Dispos 2005; 33: 175-181.

Maurer MH. Proteomics of brain extracellular fluid (ECF) and cerebrospinal fluid (CSF). Mass Spectrom Rev 2010; 29: 17-28.

Mayer S, Maickel RP, Brodie BB. Kinetics of penetration of drugs and other foreign compounds into cerebrospinal fluid and brain. J Pharmacol Exp Ther 1959; 127: 205-211.

Miller DS. Regulation of P-glycoprotein and other ABC drug transporters at the blood-brain barrier. Trends Pharmacol Sci 2010; 31: 246-254.

Miyan JA, Nabiyouni M, Zendah M. Development of the brain: a vital role for cerebrospinal fluid. Can J Physiol Pharmacol 2003; 81: 317-328.

Mordenti J. Man versus beast: pharmacokinetic scaling in mammals. J Pharm Sci 1986; 75: 1028-1040.

Morgan DJ, Huang JL. Effect of plasma protein binding on kinetics of capillary uptake and efflux. Pharm Res 1993; 10: 300-304.

Morrison PF, Bungay PM, Hsiao JK, Ball BA, Mefford IN, Dedrick RL. Quantitative microdialysis: analysis of transients and application to pharmacokinetics in brain. J Neurochem 1991; 57: 103-119.

Neuwelt EA. Mechanisms of disease: the blood-brain barrier. Neurosurg 2004; 54: 131-142.

Neuwelt EA, Abbott NJ, Abrey L, Banks WA, Blakley B, Davis T, Engelhardt B, Grammas P, Nedergaard M, Nutt J, Pardridge W, Rosenburg GA, Smith Q, Drewes LR. Strategies to advance translational research into brain barriers. Lancet Neurol 2008; 7: 84-96.

Newman GC, Hospod FE, Schissel SL. Ischemic brain slice glucose utilization: effects of slice thickness, acidosis, and K^+. J Cereb Blood Flow Metab 1991; 11: 398-406.

Nicolaysen LC, Pan H-T, Justice Jr JB. Extracellular cocaine and dopamine concentrations are linearly related in rat striatum. Brain Res 1988; 456: 317-323.

Nielsen JA, Fossom LH, Sparber SB. Metabolism of ^{3}H-dopamine continuously perfused through push-pull cannulas in rats' brains: modification by amphetamine or prostaglandin $F_{2\alpha}$. Pharmacol Biochem Behav 1980; 13: 235-242.

Nilsson C, Stahlberg F, Thomsen C, Henriksen O, Herning M, Owman C. Circadian variation in human cerebrospinal fluid production measured by magnetic resonance imaging. Am J Physiol 1992; 262: R20-R24.

Obach RS, Baxter JG, Liston TE, Silber BM, Jones BC, MacIntyre F, Rance DJ, Wastall P. The prediction of human pharmacokinetic parameters from preclinical and *in vitro* metabolism data. J Pharmacol Exp Ther 1997; 283: 46-58.

Ohno K, Pettigrew KD, Rapoport SI. Lower limits of cerebrovascular permeability to nonelectrolytes in the conscious rat. Am J Physiol 1978; 235: H299-H307.

Oldendorf WH. Measurement of brain uptake of radiolabeled substances using a tritiated water internal standard. Brain Res 1970; 24: 372-376.

Ooie T, Terasaki T, Suzuki H, Sugiyama Y. Kinetic evidence for active transport across the blood-brain barrier of quinolone antibiotics. J Pharmacol Exp Ther 1997; 283: 293-304.

Pardridge WM. Transport of small molecules through the blood-brain barrier: biology and methodology. Adv Drug Del Rev 1995; 15: 5-36.

Pardridge WM. Drug and gene targeting to the brain with molecular Trojan horses. Nat Rev Drug Discov 2002; 1:131-139.

Paul R, Lorenzl S, Koedel U, Sporer B, Vogel U, Frosch M, Pfister H-W. Matrix metalloproteinases contribute to the blood-brain barrier disruption during bacterial meningitis. Ann Neurol 1998; 44: 592-600.

Peletier LA, Benson N, van der Graaf PH. Impact of plasma-protein binding on receptor occupancy: an analytical description. J Theor Biol 2009; 265: 253-262.

Perrière N, Yousif S, Cazaubon S, Chaverot N, Bourasset F, Cisternino S, Declèves X, Hori S, Terasaki T, Deli M, Scherrmann J-M, Temsamani J, Roux F, Couraud P-O. A functional in vitro model of rat blood-brain barrier for molecular analysis of efflux transporters. Brain Res 2007; 1150: 1-13.

Preston JE, Al-Sarraf H, Segal MB. Permeability of the developing blood-brain barrier to ^{14}C-mannitol using the rat in situ brain perfusion technique. Dev Brain Res 1995; 87: 69-76.

Proescholdt MG, Hutto B, Brady LS, Herkenham M. Studies of cerebrospinal fluid flow and penetration into brain following lateral ventricle and cisterna magna injections of the tracer [^{14}C]inulin in rat. Neurosci 2000; 95: 577-592.

Rao VV, Dahlheimer JL, Bardgett ME, Snyder AZ, Finch RA, Sartorelli AC, Piwnica-Worms D. Choroid plexus epithelial expression of *MDR1* P-glycoprotein and multidrug resistance-associated protein contribute to the blood-cerebrospinal-fluid drug-permeability barrier. Proc Natl Acad Sci USA 1999; 96: 3900-3905.

Read KD, Braggio S. Assessing brain free fraction in early drug discovery. Expert Opin Drug Metab Toxicol 2010; 6: 337-344.

Remington G, Mamo D, Labelle A, Reiss J, Shammi C, Mannaert E, Mann S, Kapur S. A PET study evaluating dopamine D_2 receptor occupancy for long-acting injectable risperidone. Am J Psych 2006; 163: 396-401.

Roberts DJ, Goralski KB. A critical overview of the influence of inflammation and infection on P-glycoprotein expression and activity in the brain. Expert Opin Drug Metab Toxicol 2008; 4: 1245-1264.

Roberts LM, Black DS, Raman C, Woodford K, Zhou M, Haggerty JE, Yan AT, Cwirla SE, Grindstaff KK. Subcellular localization of transporters along the rat blood-brain barrier and blood-cerebral-spinal fluid barrier by *in vivo* biotinylation. Neurosci 2008; 155: 423-438.

Rowland M, Balant L, Peck C. Physiologically based pharmacokinetics in drug development and regulatory science: a workshop report (Georgetown university, Washington, DC, May 29-30, 2002). AAPS PharmSci. 2004; 6: E6.

Sabol KE, Freed CR. Brain acetaminophen measurement by in vivo dialysis, in vivo electrochemistry and tissue assay: a study of the dialysis technique in the rat. J Neurosci Meth 1988; 24: 163-168.

Schinkel AH. P-glycoprotein, a gatekeeper in the blood-brain barrier. Adv Drug Del Rev 1999; 36: 179-194.

Scism JL, Powers KM, Artru AA, Lewis L, Shen DD. Probenecid-inhibitable efflux transport of valproic acid in the brain parenchymal cells of rabbits: a microdialysis study. Brain Res 2000; 884: 77-86.

Segal MB. Extracellular and cerebrospinal fluids. J Inher Metab Dis 1993; 16: 617-638.

Sheiner LB, Stanski DR, Vozeh S, Miller RD, Ham J. Simultaneous modeling of pharmacokinetics and pharmacodynamics: application to d-tubocurarine. Clin Pharmacol Ther 1979; 25: 358-371.

Shen DD, Artru AA, Adkison KK. Principles and applicability of CSF sampling for the assessment of CNS drug delivery and pharmacodynamics. Adv Drug Del Rev 2004; 56: 1825-1857.

Siddiqui A, Kerb R, Weale ME, Brinkmann U, Smith A, Goldstein DB, Wood NW, Sisodiya SM. Association of multidrug resistance in epilepsy with a polymorphism in the drug-transporter gene ABCB1. N Engl J Med 2003; 348: 1442-1448.

Ståhle L, Segersvärd S, Ungerstedt U. Drug distribution studies with microdialysis II. Caffeine and theophylline in blood, brain and other tissues in rats. Life Sci 1991; 49: 1843-1852.

Summerfield SG, Jeffrey P. *In vitro* prediction of brain penetration – a case for free thinking? Expert Opin Drug Discov 2006; 1: 595-607.

Sun L, Stenken JA. Improving microdialysis extraction efficiency of lipophilic eicosanoids. J Pharm Biomed Anal 2003; 33: 1059-1071.

Swinghammer TL, Kroboth PD. Basic concepts in pharmacodynamic modeling. J Clin Pharmacokin 1988; 28: 388-394.

Syvänen S, Lindhe Ö, Palner M, Kornum BR, Rahman O, Långström B, Knudsen GM, Hammarlund-Udenaes M. Species differences in blood-brain barrier transport of three positron emission tomography radioligands with emphasis on P-glycoprotein transport. Drug Metab Dispos 2009; 37: 635-643.

Takasato Y, Rapoport S, Smith QR. An in situ brain perfusion technique to study cerebrovascular transport in the rat. Am J Physiol 1984; 247: H484-H493.

Tanaka H, Mizojiri K. Drug-protein binding and blood-brain barrier permeability. J Pharmacol Exp Ther 1999; 288: 912-918.

Terasaki T, Deguchi Y, Sato H, Hirai K, Tsuji A. *In vivo* transport of a dynorphin-like analgesic peptide, E-2078, through the blood-brain barrier: an application of brain microdialysis. Pharm Res 1991; 8: 815-820.

Thiebaut F, Tsuruo T, Hamada H, Gottesman MM, Pastan I, Willingham MC. Cellular localization of the multidrug-resistance gene product P-glycoprotein in normal human tissues. Proc Natl Acad Sci USA 1987; 84: 7735-7738.

Uchida Y, Ohtsuki S, Katsukara Y, Ikeda C, Suzuki T, Kamiie J, Terasaki T. Quantitative targeted absolute proteomics of human blood-brain barrier transporters and receptors. J Neurochem 2011; 117: 333-345.

van Bree JBMM, Baljet AV, van Geyt A, de Boer AG, Danhof M, Breimer DD. The unit impulse response procedure for the pharmacokinetic evaluation of drug entry into the central nervous system. J Pharmacokin Biopharm 1989; 17: 441-462.

van Waarde A. Measuring receptor occupancy with PET. Curr Pharm Des 2000; 6: 1593-1610.

Vannucci SJ. Developmental expression of GLUT1 and GLUT3 glucose transporters in rat brain. J Neurochem 1994; 62: 240-246.

Vautier S, Fernandez C. ABCB1: the role in Parkinson's disease and pharmacokinetics of antiparkinsonian drugs. Expert Opin Drug Metab Toxicol 2009; 5: 1349-1358.

Vogelgesang S, Cascorbi I, Schroeder E, Pahnke J, Kroemer HK, Siegmund W, Kunert-Keil C, Walker LC, Warzok RW. Deposition of Alzheimer's β-amyloid is inversely correlated with P-glycoprotein expression in the brain of elderly non-demented humans. Pharmacogenetics 2002; 12: 535-541.

Vogelgesang S, Warzok RW, Cascorbi I, Kunert-Keil C, Schroeder E, Kroemer HK, Siegmund W, Walker LC, Pahnke J. The role of P-glycoprotein in cerebral amyloid angiopathy; implications for the early pathogenesis of Alzheimer's disease. Curr Alzheimer Res 2004; 1: 121-125.

Vogelgesang S, Glatzel M, Walker LC, Kroemer HK, Aguzzi A, Warzok RW. Cerebrovascular P-glycoprotein expression is decreased in Creutzfeld-Jakob disease. Acta Neuropathol 2006; 111: 436-443.

Wang Q, Yang H, Miller DW, Elmquist WF. Effect of the P-glycoprotein inhibitor, cyclosporin A, on the distribution of rhodamine-123 to the brain: an in vivo microdialysis study in freely moving rats. Biochem Biophys Res Comm 1995; 211: 719-726.

Wang X, Kimura S, Yazawa T, Endo N. Cerebrospinal fluid sampling by lumbar puncture in rats – repeated measurements of nitric oxide metabolites. J Neurosci Meth 2005; 145: 89-95.

Watson J, Wright S, Lucas A, Clarke KL, Viggers J, Cheetham S, Jeffrey P, Porter R, Read KD. Receptor occupancy and brain free fraction. Drug Metab Dispos 2009; 37: 753-760.

Wolburg H, Paulus W. Choroid plexus: biology and pathology. Acta Neuropathol 2010; 119: 75-88.

Wong SL, Wang Y, Sawchuk RJ. Analysis of zidovudine distribution to specific regions in rabbit brain using microdialysis. Pharm Res 1992; 9: 332-338.

World Health Organization. In: "*Neurological Disorders: Public Health Challenges*", 2007.

Yassen A, Olofsen E, Kan J, Dahan A, Danhof M. Animal-to-human extrapolation of the pharmacokinetic and pharmacodynamic properties of buprenorphine. Clin Pharmacokin 2007; 46: 433-447.

Zuideveld KP, van der Graaf PH, Peletier LA, Danhof M. Allometric scaling of pharmacodynamic response: application to 5-HT_{1A} receptor mediated responses from rat to man. Pharm Res 2007; 24: 2031-2039.

Chapter 2

Scope and intent of the investigations

Drug distribution into the brain is governed by many processes, including plasma pharmacokinetics (PK), plasma protein binding, passive and active transport across the blood-brain (BBB) or blood-cerebrospinal fluid barrier (BCSFB). In addition, once within the brain, it includes bulk flow, diffusion, and extra-intracellular exchange. This multifactorial nature of brain distribution complicates the prediction of central nervous system (CNS) drug effects in man.

To predict (desired or undesired) CNS drug effects in humans, a mechanistic understanding is needed of the individual contributions of the abovementioned processes involved in brain target site distribution. With the unbound drug concentrations at the brain target site being responsible for the CNS effect it is important to determine or predict in particular the unbound drug concentration-time profiles at their site of action. For many CNS active compounds, brain target site concentrations are closely linked to, or even indistinguishable from, the unbound drug concentrations in the brain extracellular fluid ($brain_{ECF}$) (De Lange *et al.,* 2000; Hammarlund-Udenaes, 2009; Jeffrey and Summerfield, 2010; Watson *et al.,* 2009). This indicates that direct measurement of $brain_{ECF}$ concentrations in human would be very valuable. The only technique currently available to measure $brain_{ECF}$ concentration-time profiles is the intracerebral microdialysis technique. Unfortunately, this technique is invasive, though minimally, and therefore highly limited for general application in humans. The search is therefore for approaches to predict human $brain_{ECF}$ PK via other approaches.

In **Chapter 1** several techniques that can be applied during the preclinical phase of drug development to determine or predict human brain target site concentrations are reviewed. In practical terms, CSF sampling is of special interest as it can be performed in animals as well as in humans and provides information on unbound drug concentrations (Danhof and Levy, 1984). Furthermore, CSF concentrations are often considered to be the best available surrogate for brain target site concentrations in humans as it is assumed that CSF concentrations readily equilibrate with $brain_{ECF}$ concentrations due to the lack of a physical barrier between these sites (Lee *et al.,* 2001). However, qualitative and quantitative differences in processes that govern the PK of drugs in the brain exist between different conditions (species, gender, diet, disease etc.). This makes that a generally applicable relationship between CSF

concentrations and $brain_{ECF}$ concentrations does not exist (De Lange and Danhof, 2002; Lin, 2008; Shen *et al.,* 2004). This underscores the need for more quantitative understanding of the processes involved in brain target site distribution, and their individual and condition-dependent contributions to the brain PK and therewith to the ultimate CNS drug effect.

With the use of several different preclinical techniques mechanistic information on the rate and extent of unbound drug distribution into and within the brain can be gathered. However, most of the preclinical techniques appear to have very limited applicability in the extrapolation to the human situation due to fact that (total) brain tissue concentrations are measured that, for obvious reasons, can never be directly compared to human measurements. In both humans and animals, non-invasive techniques like positron emission tomography (PET) and single-photon emission computed tomography (SPECT) can be applied for measurement of total brain activity of the ligand, which may provide information on the total drug concentration to calculate PK or brain target occupancy. Also CSF can be sampled from both humans and animals. Thus far, CSF sampling in animal and human is most often used during drug development. As the compound is typically present in its unbound form in the CSF and CSF may be obtained at multiple time points, this fluid is of special value. Therefore, its usefulness as a surrogate marker for brain target site concentrations is of interest.

In a preclinical setting CSF sampling has been combined with other techniques to study the relationship between CSF concentrations and unbound brain target site concentrations. These studies have typically used single time-point CSF and brain tissue samples, in healthy animals and under the presumption of steady state conditions (Fridén *et al.,* 2009; Kalvass and Maurer, 2002; Liu *et al.,* 2006; Liu *et al*., 2009; Maurer *et al.,* 2005).

The only technique that allows the measurement of unbound drug concentrations at the brain target site as well as in CSF as a function of time is the intracerebral microdialysis technique. As this technique is (minimally) invasive it cannot readily be used in the clinical setting. However, it is anticipated that studies in experimental animals will provide data that can be used to build a mathematical brain distribution model that can be translated to the human situation if based on physiological systems parameters (Kielbasa and Stratford Jr, 2012).

Chapter 3 describes the application of multiple intracerebral microdialysis probes to single animals for direct comparison between unbound concentrations of acetaminophen, a paradigm compound for passive transport, in $brain_{ECF}$, CSF from lateral ventricle (CSF_{LV}) and CSF from cisterna magna (CSF_{CM}). In combination with advanced mathematical modeling, taking into account the physiology of the rat brain, a systems-based pharmacokinetic (SBPK) model was developed to describe our experimental data. Furthermore, by scaling the physiological parameters to the human values, the SBPK model was then used to predict human $brain_{ECF}$ concentrations by comparison with human CSF concentrations available from literature. As acetaminophen is a small, moderately lipophilic molecule, and distribution is governed by passive transport only, it was expected to be readily and evenly distributed over the brain, in both rats and humans.

For compounds subjected to active transport at the BBB and/or BCSFB, such as by the efflux transporter P-glycoprotein (P-gp), differences between $brain_{ECF}$ and CSF are anticipated to be more profound. With P-gp functioning as an efflux transporter at both the luminal and abluminal membranes of capillary endothelial cells of the BBB, as well as at the adjacent pericytes and astrocytes, it is suggested that P-gp may regulate drug transport processes within the brain at both the cellular and subcellular level. Although the localization and functionality of P-gp at the BCSFB is still subject of debate, this could result in significant differences between concentrations at the brain target site and in CSF for compounds that are substrates for P-gp mediated transport.

Chapter 4 describes the application of the multiple microdialysis probes approach for continuous measurement and direct comparison of $brain_{ECF}$ and CSF kinetics of quinidine, a well-known P-gp substrate. The impact of P-gp functionality on non-steady state relationships between CSF and $brain_{ECF}$ quinidine concentrations was investigated by co-administration of the P-gp blocker tariquidar. The previously developed SBPK model for acetaminophen was expanded to allow the characterization of the specific impact of P-gp functionality on the within brain distribution using quinidine as paradigm compound. This resulted in a number of key findings.

Besides P-gp, there is a wide range of other active transport systems located at the BBB and BCSFB, including organic cation transporters (OCT), organic

anion transporters (OAT), organic anion-transporting polypeptide (OATP), breast cancer resistance protein (BCRP), and the multidrug resistance-associated protein (MRP) family (Graff and Pollack, 2004).

Methotrexate is currently given in the clinic for CNS prophylaxis in case of malignant diseases with a high risk of prevalence of tumor metastases in the CNS. With the CNS being the target site for CNS prophylaxis, it is the aim to have the appropriate unbound methotrexate concentration at the brain target site. To characterize brain distribution of methotrexate, CSF concentrations are used, since $brain_{ECF}$ concentrations are not readily measurable in humans. However, methotrexate is known to be a substrate for a wide variety of transporters, including the reduced folate carrier 1 (RFC1), BCRP, MRP2, 3 and 4, OAT1 and 3, and OATP A and B. This could have major implications for the predictability of $brain_{ECF}$ methotrexate concentrations on the basis of CSF concentrations. Consequently, to be able to determine whether methotrexate $brain_{ECF}$ concentrations can be adequately predicted by CSF concentrations, one should first understand the mechanisms that determine the relationship between CSF concentrations and $brain_{ECF}$ concentrations.

Chapter 5 describes the application of the multiple microdialysis probes approach for continuous measurement and direct comparison of $brain_{ECF}$ and CSF kinetics of methotrexate. To investigate the specific contribution of the various transporters, probenecid is co-administered as inhibitor of MRPs, OATs and OATPs. The previously developed SBPK model for acetaminophen and quinidine was adapted to allow the identification of the specific impact of MRP/OAT/OATP functionality on the basis of our methotrexate rat data. Furthermore, the developed SBPK model was also applied to extrapolate our data to other conditions, and other species, including human.

In **Chapter 6** the results presented in this thesis for the prediction of brain target site concentrations on the basis of CSF PK are discussed and future perspectives are given for predicting CNS drug effect in humans on the basis of preclinical data.

REFERENCES

Danhof M, Levy G. Kinetics of drug action in disease states. I. Effect of infusion rate on phenobarbital concentrations in serum, brain and cerebrospinal fluid of normal rats at onset of loss of righting reflex. J Pharmacol Exp Ther 1984; 229: 44-50.

De Lange ECM, Danhof M. Considerations in the use of cerebrospinal fluid pharmacokinetic to predict brain target concentrations in the clinical setting. Implications of the barriers between blood and brain. Clin Pharmacokinet 2002; 41: 691-703.

De Lange ECM, de Boer AG, Breimer DD. Methodological issues in microdialysis sampling for pharmacokinetic studies. Adv Drug Del Rev 2000; 45: 125-148.

Fridén M, Winiwarter S, Jerndal G, Bengtsson O, Wan H, Bredberg U, Hammarlund-Udenaes M, Antonsson M. Structure – brain exposure relationships in rat and human using a novel data set of unbound drug concentrations in brain interstitial and cerebrospinal fluids. J Med Chem 2009; 52: 6233-6243.

Graff CL, Pollack G. Drug transport at the blood-brain barrier and the choroid plexus. Curr Drug Metab 2004; 5: 95-108.

Hammarlund-Udenaes M. Active-site concentrations of chemicals – are they a better predictor of effect than plasma/organ/tissue concentrations? Basic Clin Pharmacol Toxicol 2009; 106: 215-220.

Jeffrey P, Summerfield S. Assessment of the blood-brain barrier in CNS drug discovery. Neurobiol Dis 2010; 37: 33-37.

Kalvass JC, Maurer TS. Influence of nonspecific brain and plasma binding of CNS exposure: implications for rational drug discovery. Biopharm Drug Dispos 2002; 23: 327-338.

Kielbasa W, Stratford Jr RE. Exploratory translational modeling approach in drug development to predict human brain pharmacokinetics and pharmacologically relevant clinical doses. Drug Metab Dispos. 2012; 40: 877-883.

Lee G, Dallas S, Hong M, Bendayan R. Drug transporters in the central nervous system: brain barriers and brain parenchyma considerations. Pharmacol Rev 2001; 53: 6233-6243.

Lin JH. CSF as a surrogate for assessing CNS exposure: An industrial perspective. Curr Drug Metab 2008; 9: 46-59.

Liu X, Smith BJ, Chen C, Callegari E, Becker SL, Chen X, Cianfrogna J, Doran AC, Doran SD, Gibbs JP, Hosea N, Liu J, Nelson FR, Szewc MA, Van Deusen J. Evaluation of cerebrospinal

fluid concentration and plasma free concentration as a surrogate measurement for brain free concentration. Drug Metab Dispos 2006; 34: 1443-1447.

Liu X, Van Natta K, Yeo H, Vilenski O, Weller PE, Worboys PD, Monshouwer M. Unbound drug concentration in brain homogenate and cerebral spinal fluid at steady state as a surrogate for unbound concentration in brain interstitial fluid. Drug Metab Dispos 2009; 37: 787-793.

Maurer TS, DeBartolo DB, Tess DA, Scott D. Relationship between exposure and nonspecific binding of thirty-three central nervous system drugs in mice. Drug Metab Dispos 2005; 33: 175-181.

Shen DD, Artru AA, Adkison KK. Principles and applicability of CSF sampling for the assessment of CNS drug delivery and pharmacodynamics. Adv Drug Del Rev 2004; 56: 1825-1857.

Watson J, Wright S, Lucas A, Clarke KL, Viggers J, Cheetham S, Jeffrey P, Porter R, Read KD. Receptor occupancy and brain free fraction. Drug Metab Dispos 2009; 37: 753-760.

Section II

Studies on factors in blood-to-brain transport and within brain distribution

Chapter 3

Physiologically based pharmacokinetic modeling to investigate regional brain distribution kinetics in rats

J. Westerhout, B. Ploeger, J. Smeets, M. Danhof, E.C.M. de Lange

AAPS J. 2012; 14(3): 543-553

ABSTRACT

One of the major challenges in the development of central nervous system (CNS) targeted drugs is predicting CNS exposure in human from preclinical data. In this study we present a methodology to investigate brain disposition in rats using a physiologically-based modeling approach aiming at improving the prediction of human brain exposure. We specifically focused on quantifying regional diffusion and fluid flow processes within the brain.

Acetaminophen was used as a test compound as it is not subjected to active transport processes. Microdialysis probes were implanted in striatum, for sampling brain extracellular fluid ($brain_{ECF}$) concentrations, and in lateral ventricle (LV) and cisterna magna (CM), for sampling cerebrospinal fluid (CSF) concentrations. Serial blood samples were taken in parallel. These data, in addition to physiological parameters from literature, were used to develop a systems-based model to describe the regional brain pharmacokinetics of acetaminophen.

The concentration-time profiles of $brain_{ECF}$, CSF_{LV} and CSF_{CM} indicate a rapid equilibrium with plasma. However, $brain_{ECF}$ concentrations are on average 4-fold higher than CSF concentrations, with average brain-to-plasma $AUC_{0\text{-}240}$ ratios of 121%, 28% and 35% for $brain_{ECF}$, CSF_{LV} and CSF_{CM}, respectively.

It is concluded that for acetaminophen, a model compound for passive transport into, within and out of the brain, differences exist between the $brain_{ECF}$ and the CSF pharmacokinetics. The systems-based pharmacokinetic (SBPK) modeling approach is important, as it allowed the prediction of human $brain_{ECF}$ exposure on the basis of human CSF concentrations.

INTRODUCTION

Central nervous system (CNS) disorders are currently estimated to affect hundreds of millions of people worldwide (World Health Organization, 2007). While established treatments are currently available for most of these disorders, significant unmet medical needs still remain, as currently available drugs are treating symptoms rather than curing the disease (Pangalos *et al.,* 2007). Therefore, novel treatments or drugs with a different mechanism of action are needed. However, the failure rate of development of new CNS drugs is very high. The actual problem lies in the inability to predict human (wanted and unwanted) CNS drug effects.

It is known that unbound plasma concentrations may not necessarily represent the unbound brain concentrations available for target interaction, due to distributional mechanisms (**Chapter 1**). In recent years much attention has been given to blood-brain barrier (BBB) permeability, as this is assumed to be the main determinant of CNS exposure (Abbott *et al.,* 2008; Bickel, 2005; Feng, 2002; Hammarlund-Udenaes *et al.,* 2008; Jeffrey and Summerfield, 2010; Liu *et al.,* 2008). However, even though BBB permeability is a very important determinant, it is not the only relevant process. The brain is a dynamic multi-compartmental system, in which all processes of drug entry, within brain diffusion, metabolism, binding and elimination determine actual CNS target site concentrations (**Chapter 1**). To ultimately be able to predict CNS drug effects in humans, a more mechanistic understanding is needed of the individual contributions of the processes involved in brain target site distribution and ultimately drug effects.

The use of cerebrospinal fluid (CSF) as a surrogate for unbound brain target site concentrations has been discussed previously in **Chapter** 1 and by De Lange and Danhof (2002), Shen *et al.* (2004) and Lin (2008). In short, it has been concluded that a generally applicable relationship between CSF concentrations and brain extracellular fluid ($brain_{ECF}$) concentrations does not exist due to qualitative and quantitative differences in processes that govern the pharmacokinetics (PK) at these sites. However, CSF concentrations are often considered the best available surrogate for brain target site concentrations in humans (Fridén *et al.,* 2009; Kalvass and Maurer, 2002; Liu *et al.,* 2006; Liu *et al.,* 2009; Maurer *et al.,* 2005).

In rats, the most common method for collecting a CSF sample is by a single puncture or the implantation of a cannula in either the lateral ventricle or the cisterna magna (Bouman and van Wimersma Greidanus, 1979; Cserr, 1965; Cserr, 1971; De Lange and Danhof, 2002; Nielsen *et al.,* 1980). However, taking a CSF sample significantly affects the CSF volume, of which the impact is not yet known (De Lange *et al.,* 1997). The intracerebral microdialysis technique can be used for monitoring CSF concentrations, with minimal disturbance of the normal CSF physiology, and the application of multiple microdialysis probes to single animals allows for direct comparison between unbound concentrations in $brain_{ECF}$, CSF_{LV} and CSF_{CM}.

In this study we investigated the passive blood-brain transport processes that govern the relationship between the PK at different sites in the brain for acetaminophen, as a paradigm compound for passive transport (De Lange and Danhof, 2002; De Lange *et al.,* 1994). Concentration-time profiles of acetaminophen were obtained by microdialysis at different sites in the brain (striatum, lateral ventricle, and cisterna magna) and by serial blood sampling parallel plasma kinetics were obtained.

MATERIALS AND METHODS

Chemicals and solutions

Acetaminophen and saline were obtained from the Leiden University Medical Center Pharmacy (Leiden, the Netherlands). Sodium chloride, potassium chloride, calcium chloride, magnesium chloride, ethylenediaminetetraacetic acid (EDTA), perchloric acid, sodium acetate and L-(+)-Ascorbic acid were obtained from J.T. Baker (Deventer, the Netherlands). Disodium hydrogen phosphate dihydrate and sodium dihydrogen phosphate monohydrate were obtained from Merck (Amsterdam, the Netherlands). 3,4-Dihydroxy-benzylamine hydrobromide (DHBA), L-cysteine and 1-octane-sulfonic acid (OSA) were obtained from Sigma (Zwijndrecht, the Netherlands). Methanol and acetic acid were obtained from Biosolve B.V. (Valkenswaard, the Netherlands). Microdialysis perfusion fluid was prepared as previously described (Stevens *et*

al., 2009), containing 140.3 mM sodium, 2.7 mM potassium, 1.2 mM calcium, 1.0 mM magnesium and 147.7 mM chloride.

Animals

The study protocol was approved by the Animal Ethics Committee of Leiden University (UDEC nr. 07068) and all animal procedures were performed in accordance with Dutch laws on animal experimentation. A total of 36 Male Wistar WU rats (225-275 g, Charles River, Maastricht, the Netherlands) were randomly divided into two groups; the first group (n = 12) was used for the determination of the *in vivo* microdialysis probe recovery; the second group (n = 24) was used for brain disposition experiments.

After arrival, all animals were housed in groups for 5-7 days (Animal Facilities, Gorlaeus Laboratories, Leiden, the Netherlands), under standard environmental conditions (ambient temperature 21°C; humidity 60%; 12/12 h light/dark cycle, background noise, daily handling), with *ad libitum* access to food (Laboratory chow, Hope Farms, Woerden, the Netherlands) and acidified water. Between surgery and experiments, the animals were kept individually in Makrolon type three cages for 7 days to recover from the surgical procedures.

Surgery

All surgical procedures were performed under isoflurane (2%) anesthesia, while maintaining the body temperature at 37°C by an electric heating pad (CMA/150, CMA/Microdialysis AB, Stockholm, Sweden). First, cannulas were implanted in the left femoral artery and vein for blood sampling and drug administration, respectively. The cannulas were disinfected with 0.1% benzalkoniumchloride for at least 24h prior to the implantation. The arterial cannula consisted of 4 cm of non-sterile polyethylene tubing (ID 0.28 mm and OD 0.61 mm, Portex Fine Bore polythene tubing, Smiths Medical International Ltd, Kent, England) connected to 16 cm of non-sterile polyethylene tubing (ID 0.58 mm and OD 0.96 mm, Portex Fine Bore polythene tubing, Smiths Medical International Ltd, Kent, England). The thinner part of the cannula was inserted 4 cm into the artery. The venous cannula consisted of 19 cm non-sterile polyethylene tubing (ID 0.58 mm and OD 0.96 mm) with a small silicon ring

round the tubing at 3 cm from the tip. The cannula was inserted 3 cm into the vein. Both cannulas were subcutaneously led to the back of the head and fixated in the neck with a rubber ring.

Subsequently, after placing the rat in a stereotaxic frame (David Kopf Instruments, Tujunga, USA), the animals were chronically instrumented with two CMA/12 microdialysis guides (CMA/Microdialysis AB, Stockholm, Sweden) in different combinations of striatum (ST), for sampling in $brain_{ECF}$, and lateral ventricle (LV) and/or cisterna magna (CM) for sampling in CSF (ST+LV, ST+CM or LV+CM; each group with n = 8). For ST, the position of the microdialysis guide is: 1.0 mm anterior, 3.0 mm lateral, 3.4 mm ventral, relative to bregma. For LV, the position of the microdialysis guide is: 0.9 mm posterior, 1.6 mm lateral, 2.9 mm ventral, relative to the bregma. For CM, the position of the microdialysis guide is: 1.93 mm posterior, 3.15 mm lateral, 8.1 mm ventral, at an angle of 25° from the dorsoventral axis (towards anterior) and 18° lateral from the anteroposterior axis relative to lambda (figure 1). The microdialysis guides were secured to the skull with 3 anchor screws and dental cement.

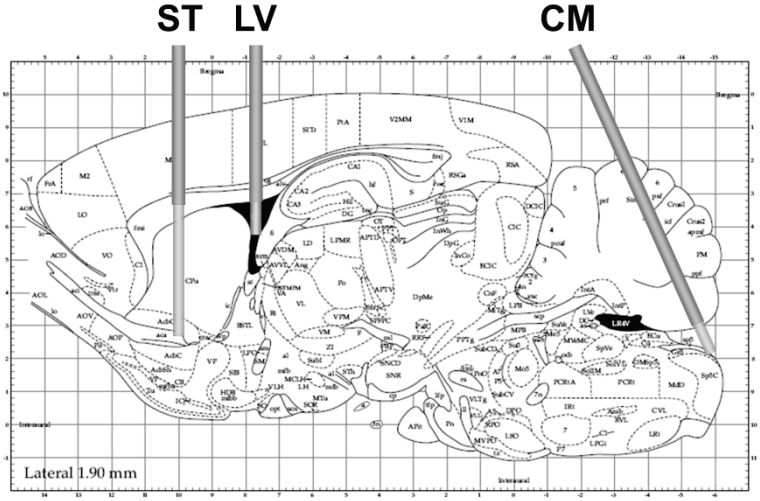

Figure 1. Graphical representation of the position of the microdialysis probes for ST, LV and CM

After the surgery the animals received 0.03 ml Temgesic ® intramuscular (Schering-Plough, Amstelveen, the Netherlands) and 0.3 ml Ampicillan® (Alfasan B.V., Woerden, the Netherlands) subcutaneously. One day prior to the experiment, the microdialysis dummies were replaced by the microdialysis

probes (CMA/12, Polycarbonate membrane, molecular weight cut-off 20 kDa, CMA/Microdialysis AB, Stockholm, Sweden, with a semi-permeable membrane length of 4 mm for ST, and 1 mm for LV and CM).

Experimental set-up

All experiments started between 9.00 and 10.00 AM to minimize the influences of circadian rhythms. First, microdialysis vials were weighed prior to the experiment to be able to validate the probe perfusion rate (a maximal deviation of 5% was allowed for the sample to be included in the data). All microdialysis vials were then placed in a cooled fraction collector (Univentor 820 Microsampler, AgnTho's AB, Lidingö, Sweden) to collect the microdialysate samples. Microdialysis perfusion fluid was prepared as described above. The microdialysis probes were connected to FEP-tubing (CMA/Microdialysis AB, Stockholm, Sweden) with tubing adapters (CMA/Microdialysis AB, Stockholm, Sweden). Microdialysis probes were then continuously flushed with microdialysis perfusion fluid (2 µl/min, Bee-Hive, Bioanalytical Systems Inc., W-Lafayette, USA), being equilibrated for 60 min before acetaminophen administration.

The *in vivo* microdialysis probe recovery of acetaminophen was determined on the basis of reverse dialysis (Ståhle *et al.,* 1991). The concept of the reverse dialysis method assumes directional independence of the solute through the dialysis membrane and that recovery is independent of the perfused concentration (Le Quellec *et al.,* 1995), as was true for acetaminophen under *in vitro* conditions. In short, the microdialysis probes in striatum, lateral ventricle and cisterna magna were perfused with different concentrations of acetaminophen (50, 200 and 1000 ng/ml) in perfusion fluid. The *in vivo* recovery for each microdialysis probe location is defined as the ratio of the concentration difference between the dialysate (C_{dial}) from striatum, lateral ventricle or cisterna magna and perfusion fluid (C_{in}) over the concentration in the perfusion fluid (equation 1) (Scheller and Kolb, 1991).

$$in\ vivo\ recovery = \frac{C_{in} - C_{dial}}{C_{in}} \quad (1)$$

For the brain disposition experiments, the rats received an intravenous infusion of 15 mg/kg acetaminophen dissolved in saline (200 µl/min/kg for a period of 10 minutes) with an automated pump (Pump 22 Multiple Syringe Pump, Harvard Apparatus, Holliston, USA). Start and duration of infusion was corrected for internal volume of the tubing so that infusion started at t=0 min. 10 min interval samples were collected between t=−1 h and t=2 h, followed by 20 min interval samples until t=4 h. After weighing the microdialysis vials they were stored at −80°C before analysis.

For the determination of acetaminophen plasma concentrations, blood samples of 100 µl were taken, in parallel to the microdialysate samples, from the arterial cannula at t=−5 (blank), 2, 7, 10, 15, 30, 60, 120, 180, and 240 min. For the determination of plasma protein binding of acetaminophen, blood samples of 300 µl were taken at t=−30 (blank) and 30 min (with a concentration assumed to be approximately 50% of C_{max}). After the blood sample at t=240 min, an additional dose of 15 mg/kg in 10 minutes was given to be able to determine plasma protein binding at C_{max} (at t=250 min). All blood samples were temporarily stored in heparin (10 IE) coated Eppendorf cups. The blank blood samples for the determination of plasma protein binding were spiked with acetaminophen to obtain a blood concentration of 150 ng/ml. The spiked blood samples were then incubated in a shaking water bath at 37°C for 30 minutes. All blood samples were centrifuged for 15 min at 5000 rpm and the plasma was pipetted into clean Eppendorf cups and stored at −20°C before analysis.

At the end of the experiments the animals were sacrificed with an overdose of Nembutal (Ceva Sante Animale, Libourne, France).

Plasma and microdialysate sample analysis

Plasma protein binding was determined with Centrifree® ultrafiltration devices (Millipore BV, Etten-Leur, the Netherlands). All procedures were performed according to the user's manual. The ultrafiltrate was diluted 10 times with saline before the analysis.

Acetaminophen concentrations in plasma, micdrodialysate and ultrafiltrate were determined as described by Stevens *et al.* (2009). In short, acetaminophen concentrations in plasma, microdialysate and ultrafiltrate were determined using

High Pressure Liquid Chromatography with Electro-Chemical Detection (HPLC-ECD).

To 50 µl of the plasma samples 50 µl purified Millipore water (resistivity 18.2 MΩ·cm, Millipore B.V., Amsterdam, the Netherlands) and 25 µl internal standard (IS), containing 150 ng/ml DHBA, was added. Proteins were then precipitated by adding 100 µl 6% perchloric acid, followed by vortexing and centrifugation (10 min at 4000 rpm). The supernatant was then transferred into a clean glass tube, after which 150 µl sodium acetate (1M) was added. After vortexing, the samples were injected into the HPLC-ECD. To 20 µl of the microdialysate or diluted ultrafiltrate samples 20 µl IS was added, followed by vortexing before being directly injected into the HPLC-ECD system.
Data acquisition and processing was performed using Empower® data acquisition software (Waters, Etten-Leur, the Netherlands). For constructing the calibration curve, linear regression analysis was applied using weight factor $1/(y)^2$. Data analysis, statistical analysis, and plotting were performed using Microsoft® Office Excel 2003 (Microsoft Corporation, USA).

Pharmacokinetic data analysis

All plasma concentrations were converted to unbound plasma concentrations, by correction for plasma protein binding. All microdialysate concentrations from striatum, lateral ventricle and cisterna magna were converted into brain$_{ECF}$ concentrations (C_{ECF}) or CSF concentrations (C_{CSF}) by division of the dialysate concentrations by the average *in vivo* recovery as determined for each microdialysis probe location (equation 2).

$$C_{ECF}\ or\ C_{CSF} = \frac{C_{dial}}{in\ vivo\ recovery} \qquad (2)$$

Areas under the curve from t=0 to t=240 min ($AUC_{0\text{-}240}$) were calculated by the trapezoidal rule and tested for differences by single factor ANOVA. The population PK models were developed and fitted to the data by means of non-linear mixed-effects modeling using the NONMEM software package (version 6.2, Icon Development Solutions, Ellicott City, Maryland, USA) and analyzed using the statistical software package S-Plus® for Windows (version 6.2 Professional, Insightful Corp., Seattle, USA).

Rather than applying a whole-body physiologically-based PK (PBPK) model, we focused on the brain physiology by implementing a systems-based approach. Here, the plasma kinetics were described by means of a compartmental approach, whereas the brain concentrations and the exchange between $brain_{ECF}$ and CSF were described by means of a physiologically-based approach. In order to do so, the volumes of the different brain compartments were fixed to their physiological volumes, which were based on the following considerations:

1. The $brain_{ECF}$ volume in a 250g rat is about 290 µl (Cserr *et al.,* 1981).
2. The brain intracellular space ($brain_{ICS}$) is approximately 80% of the brain volume (Thorne *et al.,* 2004). With an average brain weight of 1.8 g in a 250 g rat (own observations), this results in a $brain_{ICS}$ volume of 1.44 ml.
3. The total CSF volume in a 250g rat is about 300 µl (Bass and Lundborg 1973). The volume of the lateral ventricles is about 17% of the total CSF volume (Condon *et al.,* 1986; Kohn *et al.,* 1991). This results in a volume of the rat lateral ventricles of about 50 µl (0.17 × 300).
4. The volume of the cisterna magna is about 5.7% of the total CSF volume (Adam and Greenberg, 1978; Robertson, 1949). This results in a volume of the rat cisterna magna of about 17 µl (0.057 × 300).
5. The cranial subarachnoid space in rats is estimated to be about 60% of the total CSF volume (Bass and Lundborg, 1973; Levinger, 1971). This results in a volume of the cranial subarachnoid space of about 180 µl (0.60 × 300).
6. The unaccounted for CSF volume (17%; 50 µl) is considered to be mainly located in the third and fourth ventricles (Levinger, 1971).
7. The blood-brain transport is restricted by the presence of the BBB and the blood-CSF barrier (BCSFB), which is located at the choroid plexuses of the lateral, third and fourth ventricles (**Chapter 1**), as well as at the cisterna magna.
8. The intra-brain distribution was restricted by the physiological flow paths of $brain_{ECF}$, in which $brain_{ECF}$ flows towards the CSF compartments at a rate of 0.2 µl/min (Abbott, 2004; Cserr *et al.,* 1981), and CSF flows from lateral ventricle, through the third and fourth ventricle, to the cisterna magna and subsequently to the subarachnoid space (cranial and spinal) and back into blood at a rate of 2.2 µl/min (Cserr, 1965).

Structural model selections for the systems-based PK (SBPK) model were based on the likelihood ratio test ($p < 0.01$), diagnostic plots (observed concentrations vs. individual and population predicted concentrations, weighted residuals vs. predicted time and concentrations), parameter correlations and precision in parameter estimates. The inter-animal variability in pharmacokinetic parameters was assumed to be log normally distributed. The residual error, which accounts for unexplained variability (e.g. measurement and experimental error and model-misspecification), was best described with a proportional error model.

The validity of the SBPK model was investigated by means of a visual predictive check (Cox *et al.,* 1999; Duffull and Aarons, 2000; Yano *et al.,* 2001). Using the final PK parameter estimates, 1000 curves were simulated. Subsequently, the median and the 5^{th} and 95^{th} percentile of the predicted concentrations were calculated, which represent the 90% prediction interval. These were then compared with the observations.

In order to test the ruggedness of the model and estimate the precision of the parameters n=100 non-parametric (case resampling) bootstraps were performed. To create the bootstrapped datasets, specific rat data (plasma and microdialysate concentrations) were removed randomly from the datasets and replaced with randomly selected rat data from the complete original dataset. Each of these permutations of the original dataset were fitted with the final model determined based on the original dataset. This results in a series of model fits, each with its own set of parameters. These results were displayed graphically and the descriptive statistics of the parameters were compared to parameter estimates of the final model. Only bootstrap runs that successfully minimized were used in this analysis.

Systems-based scaling

The parameters of the rat SBPK model were extrapolated to humans to predict the human acetaminophen plasma, CSF and $brain_{ECF}$ concentration-time profiles. These concentration-time profiles were then compared to observed acetaminophen concentrations in plasma and CSF from the subarachnoid space (CSF_{SAS}), as presented by Bannwarth *et al.* (1992). To do so, the elimination clearance was scaled based on equation 3.

$$CL_{E,human} = CL_{E,rat} \times \left(\frac{BW_{human}}{BW_{rat}}\right)^{0.75} \quad (3)$$

Here, $CL_{E,human}$ and $CL_{E,rat}$ are the elimination clearances in humans and rats, respectively. BW_{human} and BW_{rat} are the human and rat bodyweights, respectively. The scaling factor of 0.75 is based on allometry (Boxenbaum, 1982). Next, the transfer clearances between plasma and the different peripheral and brain compartments were scaled based on equations 4 and 5.

$$CL_{PL-PER} = A_{PER} \times (V_{PER})^{0.67} \quad (4)$$

$$CL_{PL-BR} = A_{BR} \times (V_{BR})^{0.67} \quad (5)$$

Here, A_{PER} and A_{BR} are scaling coefficients for periphery and brain, respectively, and both are estimated on the basis of the rat data (Hosseini-Yeganeh and McLachlan, 2002). V_{PER} represents the physiological volume of the (lumped) peripheral tissues. V_{BR} represents the physiological volume of the different brain compartments. The scaling factor of 0.67 is based on the permeability surface area of the different brain compartments, which is related to the tissue weight (Kawai *et al.,* 1994). The physiological parameters of the rat SBPK model were changed accordingly.

RESULTS

All results are presented as average values ± standard deviation, unless stated otherwise.

Acetaminophen pharmacokinetics

The experimental set-up allowed for direct comparison of plasma concentrations with brain concentrations on two distinct sites, including the direct comparison of $brain_{ECF}$ concentrations with CSF concentrations within a single rat. Plasma protein binding was linear with concentration, at an extent of

19.5 ± 4.2 %. The average *in vivo* recoveries for the striatum, lateral ventricle and cisterna magna probes were 12.0 ± 3.3%, 8.1 ± 3.8% and 8.6 ± 4.7%, respectively. The average unbound acetaminophen concentrations for plasma, $brain_{ECF}$, CSF from lateral ventricle (CSF_{LV}) and cisterna magna (CSF_{CM}) is shown in figure 2.

The unbound plasma concentration-time profile shows a short distribution phase of about 15 min. During the elimination phase (t > 15 min) the unbound plasma concentrations reach an apparent plateau from t = 120 min onward. The concentration-time profiles of $brain_{ECF}$, CSF_{LV} and CSF_{CM} show a pattern similar to the unbound plasma concentration-time profile, indicating a relatively rapid distribution. However, $brain_{ECF}$ concentrations are on average 4-fold higher than CSF concentrations in both lateral ventricle and cisterna magna. The CSF concentration in both locations is similar.

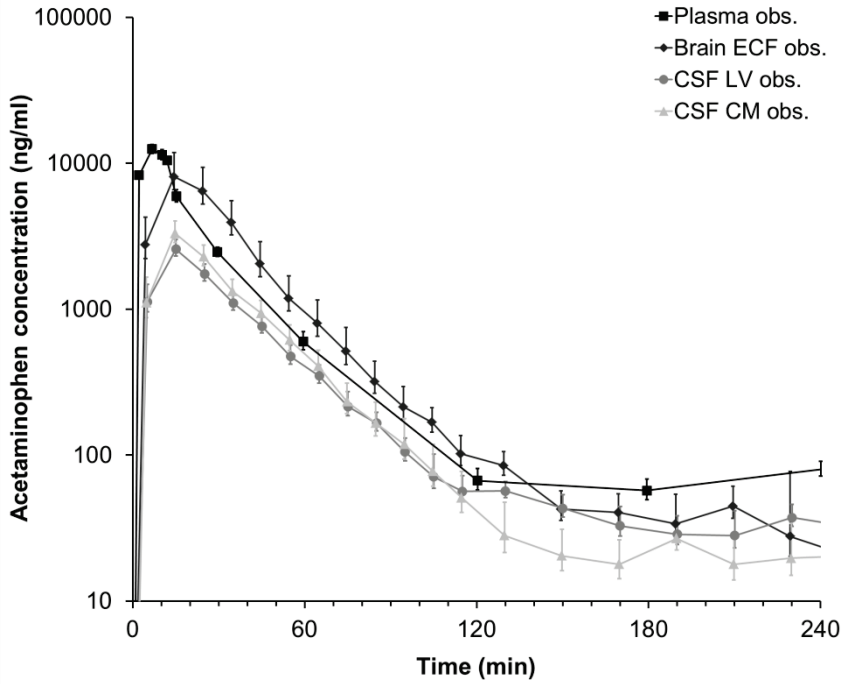

Figure 2. Observed data from the rat. Average (geometric mean ± S.E.M.) unbound acetaminophen concentration-time profile for plasma (n = 10), $brain_{ECF}$ (n = 10), CSF_{LV} (n = 14) and CSF_{CM} (n = 8)

The concentration-time profile for the $brain_{ECF}$ shows more similarities to the unbound plasma concentration-time profile than the concentration-time profiles of CSF_{LV} or CSF_{CM}. The acetaminophen concentration in $brain_{ECF}$ is significantly higher ($p < 0.05$) than that in CSF from t = 0 to t = 80 min. As a result, the $brain_{ECF}$-to-unbound plasma $AUC_{0\text{-}240}$ ratio is also higher than the CSF-to-unbound plasma $AUC_{0\text{-}240}$ ratio with an average ratio of 121 ± 72%, 28 ± 10% and 35 ± 17% for $brain_{ECF}$, CSF_{LV} and CSF_{CM}, respectively. This indicates that $brain_{ECF}$-to-CSF exposure ratio is approximately 4.

Compartmental modeling approach

All data were subjected first to compartmental pharmacokinetic analysis. The compartmental pharmacokinetic analysis showed that the plasma concentrations were best described by a 2 compartment model that included inter-compartmental clearance (Q), elimination clearance from the central compartment (CL_E) and an additional zero-order drug input into the plasma compartment. This additional, infusion-like, drug input represents the fraction of the administered acetaminophen that is reabsorbed (F_{abs}) within the study duration (240 min), presumably because of enterohepatic circulation (Hjelle and Klaassen, 1984; Siegers *et al.,* 1983; Watari *et al.,* 1983).

As the next step in the data analysis, to describe the concentrations in each of the brain compartments, a single brain compartment was added. Drug flow between the brain compartment and the plasma compartment was by a clearance in (CL_{in}) and clearance out (CL_{out}), rather than an intercompartmental clearance.

Subsequently, the addition of a second and third brain compartment was explored for the description of the plasma data, as well as the $brain_{ECF}$, CSF_{LV} and CSF_{CM} data (results not shown). As it was our goal to investigate the relationship between $brain_{ECF}$ and CSF pharmacokinetics, we have applied compartmental modeling to describe the relationships between $brain_{ECF}$ and CSF at the two sites.

However, this approach was without success, as the model had too much freedom to fit the plasma and brain data correctly. For this reason, and because of the improved value for extrapolation and prediction, we have applied a systems-based PK model to investigate the exchange between $brain_{ECF}$ and CSF.

Systems-based modeling approach

As CSF flows from lateral ventricle through the third and fourth ventricle, to the cisterna magna and subsequently to the subarachnoid space and back into blood, we added two CSF compartments that represent the combined third and fourth ventricle (CSF_{TFV}) and the subarachnoid space (CSF_{SAS}) to more adequately describe CSF physiology. Since we have no measurements of the concentrations in the third and fourth ventricle, the transfer clearance between plasma and third and fourth ventricle was assumed to be equal to the transfer clearance between plasma and lateral ventricle. For the correct representation of the brain physiology, we have also included the $brain_{ICS}$ to the model. However, since we have no measurements of total brain concentrations, it was assumed that $brain_{ICS}$ concentrations are equal to $brain_{ECF}$ concentrations. Therefore, the $brain_{ICS}$ volume is added to the $brain_{ECF}$ volume to account for the total brain volume.

Final SBPK model - The final SBPK model is shown in figure 3. The differential equations of this model can be found in the appendix. The final estimation of the PK parameters is summarized in table 1.

Here, CL_E is the elimination clearance from plasma, $Q_{PL\text{-}PER}$ is the inter-compartmental clearance between plasma and the peripheral compartment. Further, for transfer clearances between compartments ($CL_{from\ comp\text{-}to\ comp}$), denotations of the compartments are: PL = plasma; ECF = $brain_{ECF}$; ICS = $brain_{ICS}$; LV = lateral ventricle; TFV = third and fourth ventricle; CM = cisterna magna and SAS = subarachnoid space. Q_{ECF} is the flow rate of $brain_{ECF}$, Q_{CSF} is the flow rate of CSF. For the plasma and brain compartments V is the physiological volume; for the peripheral compartment V is the volume of distribution. F_{abs} is the fraction of the dose that is reabsorbed over time as a result of enterohepatic circulation, fu_p is the fraction unbound in plasma, η_i is the inter-individual variability of parameter i and ε_j is the residual error on the concentrations in compartment j.

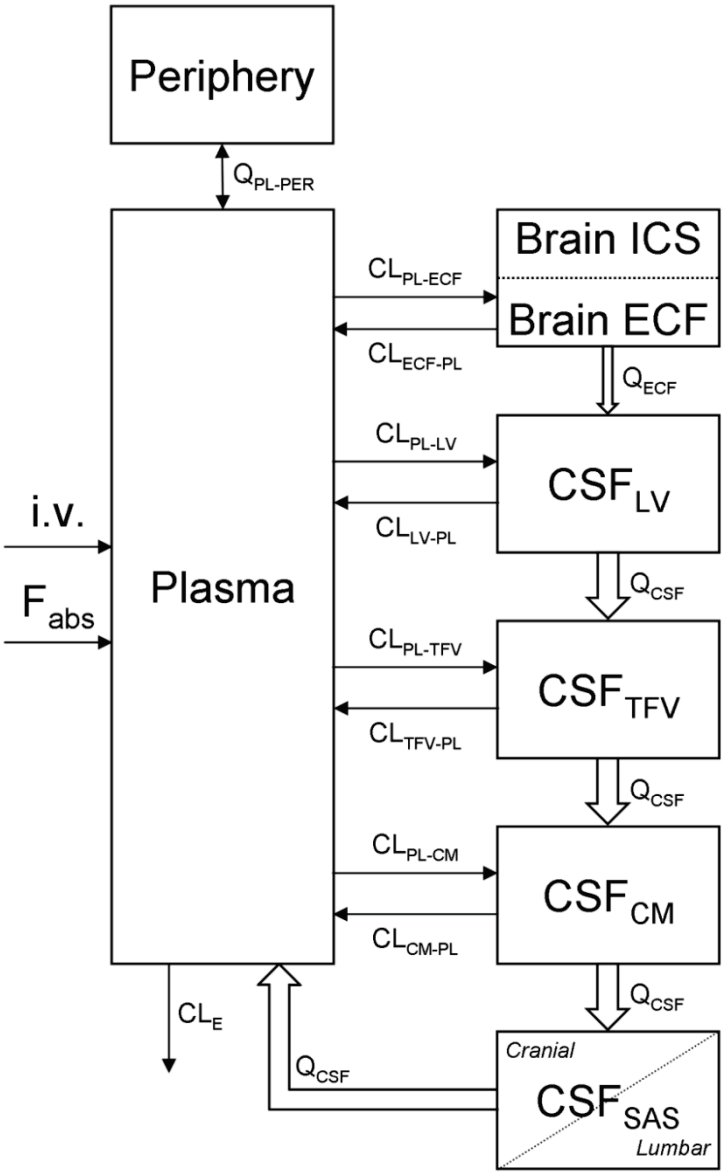

Figure 3. Graphical representation of the SBPK model that was used to describe the intra-brain distribution in the rat. CL_E is the elimination clearance from plasma, Q_{PL-PER} is the inter-compartmental clearance between plasma and the peripheral compartment. Further, for transfer clearances between compartments ($CL_{from\ comp-to\ comp}$), denotations of the compartments are: PL = plasma; ECF = $brain_{ECF}$; LV = lateral ventricle; TFV = third and fourth ventricle; and CM = cisterna magna. F_{abs} is the fraction of the dose that is reabsorbed over time as a result of enterohepatic circulation

The visual predictive check of the final model is given in figure 4. It can be seen that the final model describes the data very well within the 90% prediction interval, and also can cope with the large inter-individual variation in brain concentrations. This SBPK model was used to predict acetaminophen concentrations in rat $CSF_{SAS,}$ shown in figure 5. As a result of the CSF flow from lateral ventricle, through the third and fourth ventricle, to the cisterna magna and subsequently to the subarachnoid space, clear differences in the predicted concentration-time profiles of these CSF compartments can be observed.

Extrapolation to humans

The final SBPK model was used for the prediction of human $brain_{ECF}$ concentrations by scaling of the rat parameters to humans. However, scaling of the elimination clearance based on allometry resulted in an underestimation of plasma and CSF_{SAS} concentrations (results not shown). Therefore, it was decided to fit the plasma data to our model for estimating the elimination clearance in humans. This resulted in a reasonable prediction of plasma and CSF_{SAS} concentrations (figure 6). The final human PK parameters are given in table 1. Predictions indicate that $brain_{ECF}$ concentrations in humans are ~2-fold higher than plasma concentrations.

By comparing the acetaminophen concentrations in plasma and CSF_{SAS} between rats and humans (as presented by Bannwarth *et al.* (1992)), it can be seen that the kinetics in humans are slower compared to rats (figure 7). However, the peak concentrations in plasma appear to be similar, whereas the peak concentrations in CSF_{SAS} in humans are ~8-fold higher compared to rats.

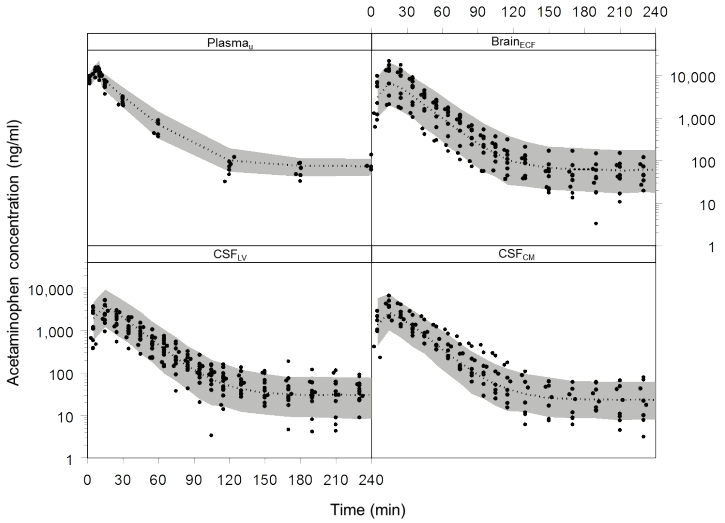

Figure 4. The visual predictive check of the final SBPK model. The dots represent the individual data points and the grey area represents the 90% prediction confidence interval. The x-axis represents the time in minutes, the y-axis represents the acetaminophen concentration in ng/ml. The different boxes represent the unbound plasma, brain$_{ECF}$, CSF$_{LV}$ and CSF$_{CM}$ data

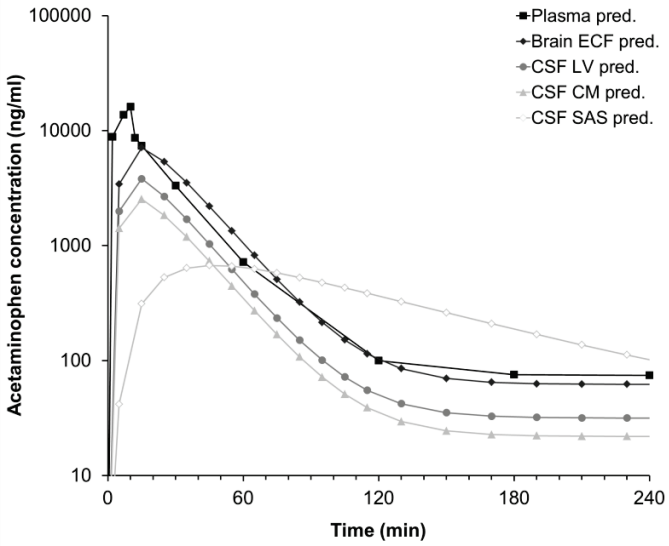

Figure 5. SBPK model predicted acetaminophen concentrations in rat plasma and the different brain compartments: brain$_{ECF}$, CSF$_{LV}$, CSF$_{CM}$ and CSF$_{SAS}$. Predictions are based on a 10 min i.v. infusion of 15 mg/kg acetaminophen in a 250 gr rat

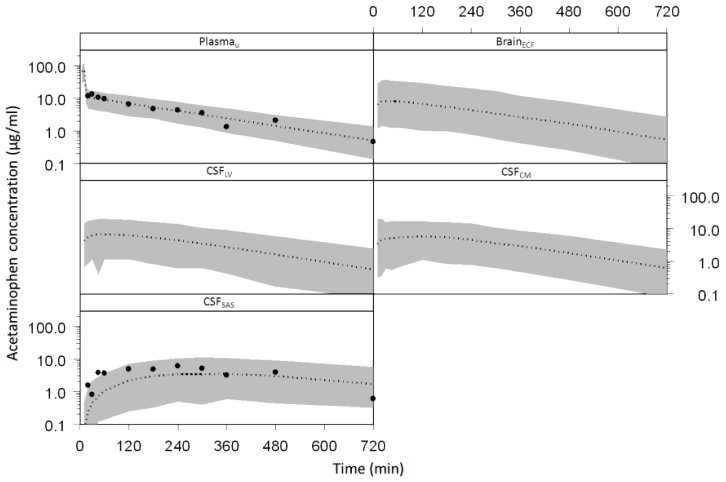

Figure 6. Observed and SBPK model predicted human acetaminophen concentrations in humans. The dots represent the data as presented by Bannwarth et al. (1992) and the grey area represents the 90% prediction confidence interval. The x-axis represents the time in minutes, the y-axis represents the acetaminophen concentration in µg/ml. The different boxes represent the unbound plasma, brain$_{ECF}$, CSF$_{LV}$, CSF$_{CM}$ and CSF$_{SAS}$. Predictions are based on a 10 min i.v. infusion of 15 mg/kg acetaminophen in a 70 kg human

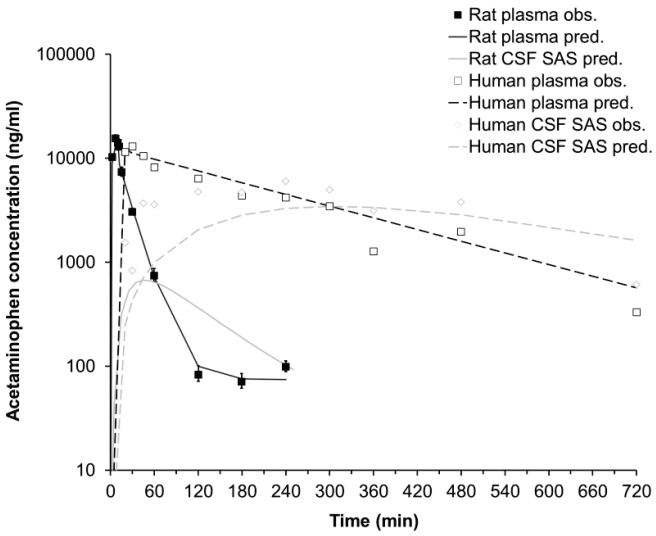

Figure 7. Observed and SBPK model predicted acetaminophen concentrations in rat and human plasma and CSF$_{SAS}$. Predictions are based on a 10 min i.v. infusion of 15 mg/kg acetaminophen in a 250 gr rat and a 70 kg human

Table 1. Final estimation of the rat and human PK parameters (± standard error)

Parameter	Rat value	Human value
CL_E	13.8 ± 1.0 ml/min	299 ml/min
$Q_{PL\text{-}PER}$	45.1 ± 5.8 ml/min	1100 ml/min
$CL_{PL\text{-}ECF}$	165 ± 39 µl/min	14.9 ml/min
$CL_{ECF\text{-}PL}$	198 ± 24 µl/min	17.8 ml/min
$CL_{PL\text{-}LV}$	2.9 ± 1.3 µl/min	0.17 ml/min
$CL_{LV\text{-}PL}$	5.0 ± 2.1 µl/min	0.05 ml/min
$CL_{PL\text{-}TFV}$	2.9 ± 1.3 µl/min	0.17 ml/min
$CL_{TFV\text{-}PL}$	5.0 ± 2.1 µl/min	0.05 ml/min
$CL_{PL\text{-}CM}$	0.8 ± 0.4 µl/min	0.05 ml/min
$CL_{CM\text{-}PL}$	4.5 ± 0.9 µl/min	0.27 ml/min
Q_{ECF}	*0.2 µl/min* [1,2]	*0.175 ml/min* [12,13]
Q_{CSF}	*2.2 µl/min* [3]	*0.4 ml/min* [14]
V_{PL}	*10.6 ml* [4]	*2.9 l* [15]
V_{PER}	188 ± 11 ml	51.6 l
V_{ICS}	*1440 µl* [5]	*960 ml* [5]
V_{ECF}	*290 µl* [1]	*240 ml* [12]
V_{LV}	*50 µl* [6,7]	*22.5 ml* [6,7,16]
V_{TFV}	*50 µl* [8]	*22.5 ml* [8]
V_{CM}	*17 µl* [9,10]	*7.5 ml* [9,10]
V_{SAS}	*180 µl* [8,11]	*90 ml* [17]
F_{abs}	0.025 %/min	N.A.
fu_p	80.5 ± 4.2%	95% [18]
$\eta_{CL\ E}$	0.03 ± 0.01	N.A.
$\eta_{CL\ PL\text{-}ECF}$	0.45 ± 0.25	N.A.
$\eta_{CL\ PL\text{-}LV}$	0.28 ± 0.13	N.A.
$\eta_{CL\ PL\text{-}CM}$	1.11 ± 0.54	N.A.
ε_{PL}	0.08 ± 0.02	0.06
ε_{ECF}	0.14 ± 0.03	N.A.
$\varepsilon_{CSF\ LV}$	0.19 ± 0.05	N.A.
$\varepsilon_{CSF\ CM}$	0.18 ± 0.04	N.A.
$\varepsilon_{CSF\ SAS}$	N.A.	N.A.

Parameter values in italic are derived from literature. CL_E is the elimination clearance from plasma, $Q_{PL\text{-}PER}$ is the inter-compartmental clearance between plasma and the peripheral compartment. Further, for transfer clearances between compartments ($CL_{from\ comp\text{-}to\ comp}$), denotations of the compartments are: PL = plasma; ECF = brain$_{ECF}$; LV = lateral ventricle; TFV = third and fourth ventricle; and CM = cisterna magna. For plasma and brain compartments V is the physiological volume; for peripheral compartment V is the volume of distribution. η_i = inter-individual variability of parameter i; ε_j = residual error on concentrations in compartment j.

Notes to table 1 continued: [1] Cserr et al., 1981; [2] Abbott, 2004; [3] Cserr, 1965; [4] Lee and Blaufox, 1985; [5] Thorne et al., 2004; [6] Condon et al., 1986; [7] Kohn et al., 1991; [8] Levinger, 1971; [9] Robertson, 1949; [10] Adam and Greenberg, 1978; [11] Bass and Lundborg, 1973; [12] Begley, 2000; [13] Kimelberg, 2004; [14] Nilsson et al., 1992; [15] Frank and Gray, 1953; [16] Dickey et al., 2000; [17] Pardridge, 2011; [18] Bailey and Briggs, 2004.

DISCUSSION

In the development of CNS targeted drugs, the prediction of human CNS target exposure is a big challenge. Often it is assumed that CSF concentrations are more or less equal to unbound brain concentrations, and the most common method for collecting a CSF sample from humans is by a lumbar puncture (Hill *et al.,* 1999). However, the brain is a dynamic multi-compartmental system, in which all processes of entry, diffusion, metabolism, binding and elimination determine local CNS concentrations. Not much is currently known about the impact of these processes on brain disposition of different drugs. Here we present a methodology to investigate brain disposition in rats using a systems-based modeling approach aiming at improving the prediction of human brain exposure.

In this study we compared the unbound concentration-time profiles of acetaminophen, as a paradigm compound for passive transport, obtained from the brain striatum and different sites of CSF. To that end we have used the multiple microdialysis probes approach, with probes placed into different sites of the brain. Thus, the PK information is obtained by the same technique, without the need of taking CSF samples that influences brain physiology. Our hypothesis was that acetaminophen would distribute homogeneously over the brain.

Since the inter-individual variation in brain concentrations is reasonably large, the statistical significance of the results could be questioned. However, the variability in brain concentrations is most likely the result of the large variation in *in vivo* recovery, which is the sum of the intra-individual variation, the analytical error and the true inter-individual variability.

With an assumed log-normal distribution of the inter-individual variability and the residual error, it can be assumed that the observed differences between

$brain_{ECF}$ and CSF concentrations are the result of actual differences, rather than a result of the variability in the *in vivo* recoveries.

Preferably, the *in vivo* recovery should have been determined in the same animals in which the brain disposition experiments were performed to eliminate the inter-individual variability. However, we decided to perform these experiments in a separate group of animals to keep the duration of experiments within realistic limits.

With *in vivo* recoveries of approximately 10%, we are working at the limit of the methodology. Therefore, in retrospect, the level of *in vivo* recovery could have been increased by decreasing the microdialysis perfusion flow rate. However, as our analytical method required a certain sample volume we decided to use a flow rate of 2 µl/min. Furthermore, we have used 10 minute sample intervals to reveal the initial rate of brain distribution, which is crucial information for estimating clearance values into and out of the different brain compartments.

Even though the final resulting variability of the brain disposition data was high, the modeling does take into consideration this variability by means of the inter-individual variability in plasma to $brain_{ECF}$, plasma to CSF_{LV} and plasma to CSF_{CM} clearance, as well as a residual error on the $brain_{ECF}$, CSF_{LV} and CSF_{CM} data.

Acetaminophen PK in plasma, together with $brain_{ECF}$ PK or CSF PK, has been studied before (De Lange *et al.,* 1994; De Lange *et al.,* 1995; Hjelle and Klaassen, 1984; Morrison *et al.,* 1991; Siegers *et al.,* 1983; Stevens *et al.,* 2009; van Bree *et al.,* 1989; Watari *et al.,* 1983), but $brain_{ECF}$ PK and CSF PK have never been directly related to each other. The plasma concentration-time profile obtained in this study shows great similarities with those reported previously. For example, Morrison *et al.* (1991), showed a distribution phase of approximately 20 minutes, after an i.v. bolus dose of 15 mg/kg, followed by an elimination phase until the end of the experiment at t = 120 min. Watari *et al.* (1983), reported a distribution phase of 15 min and that the disposition of acetaminophen was best described by a 2-compartment model. As in previous studies from our group (De Lange *et al.,* 1994; Stevens *et al.,* 2009; van Bree *et al.,* 1989), we observed in this study a plateau in plasma concentrations at time points later than 120 min. The plateau of the plasma concentrations is presumably caused by enterohepatic circulation of acetaminophen. This has

been described by Watari *et al.* (1983), Siegers *et al.* (1983), and Hjelle and Klaassen (1984). Acetaminophen is metabolized / biotransformed in the liver into acetaminophen-sulfate and acetaminophen-glucuronide. Acetaminophen-sulfate is subsequently transported both into the bile and into the bloodstream, after which it is mainly excreted via urine. Acetaminophen-glucuronide is mainly transported into bile, which is then released in the intestines. After the release in the small intestine, the acetaminophen-sulfate and acetaminophen-glucuronide can be hydrolyzed into acetaminophen, which is then re-absorbed. The time course of the re-uptake of acetaminophen spans several hours (Hjelle and Klaassen, 1984; Siegers *et al.,* 1983; Watari *et al.,* 1983), which therefore could explain the plateau in plasma concentrations from t = 120 min onward.

It is often assumed that CSF concentrations equilibrate readily with $brain_{ECF}$ concentrations due to the lack of a physical barrier between the two (Lee *et al.,* 2001). The rate of equilibration between CSF concentrations and $brain_{ECF}$ concentrations by passive diffusion through brain tissue is dependent on the lipophilicity of the compound (De Lange *et al.,* 1995). For acetaminophen, which is a moderately lipophilic compound with known fast equilibrium between blood and brain, and no indication of active transport at the BBB or BCSFB, we expected the $brain_{ECF}$ and CSF concentrations to be similar. However, we have observed that $brain_{ECF}$ concentrations are approximately 4-fold higher than CSF concentrations. This can probably be explained by the relatively high turnover rate of CSF. With a total CSF volume of 300 µl, and a flow rate of 2.2 µl/min, the total CSF volume is replaced every 2.5 h. However, the volumes of the lateral ventricle and cisterna magna are calculated to be 50 and 17 µl, respectively. This indicates that the CSF in the lateral ventricle and cisterna magna is replaced every 23 and 8 minutes, respectively. Due to the slow distribution from the brain tissue to the CSF, the CSF acts as a sink, causing the observed concentration gradient within the brain. This has been observed for other passively transported compounds as well (Kielbasa and Stratford Jr, 2012).

Several studies have reported acetaminophen concentration-time profiles in $brain_{ECF}$ (De Lange *et al.,* 1994; Morrison *et al.,* 1991; Stevens *et al.,* 2009), and CSF (De Lange *et al.,* 1995). We have found more or less similar unbound plasma and $brain_{ECF}$ concentration-time profiles, while in literature $brain_{ECF}$ concentrations have been reported that were several-fold lower than plasma

concentrations. Importantly, in the previous studies, $brain_{ECF}$ concentrations were estimated on the basis of *in vitro* recovery, while in this study it was based on *in vivo* recovery correction. We found an *in vitro* recovery value of acetaminophen of 31.9 ± 5.2%, for a 4 mm microdialsyis membrane, which is ~3 fold higher than the *in vivo* recovery of 12.0 ± 3.3% estimated in this study. This might be an explanation for the discrepancy between earlier reports and the current one. Assuming the same ratio between *in vitro* and *in vivo* recoveries (~factor 3), it would indicate a concentration-time profile in $brain_{ECF}$ that is more similar to unbound plasma concentrations than to CSF.

On the other hand, using serial CSF sampling – from the cisterna magna, van Bree *et al.* (1989) have found that acetaminophen slowly distributed into and out of CSF, resulting in a delayed maximum concentration in CSF, and a slower elimination. We think that the sampling of CSF jeopardizes brain fluid homeostasis, as it causes a decrease in CSF pressure that normally serves as a trigger for elimination of CSF into blood via the basal cisterns and subarachnoid spaces (Kazama *et al.,* 1994).

Calculations of brain distribution are often performed by modeling the brain compartment as an effect compartment (Hammarlund-Udenaes *et al.,* 1997; Sheiner *et al.,* 1979). Here, the plasma concentration is the driving force for brain concentrations, without the uptake into or elimination from the brain influencing the concentration-time profile in blood. However, for a more realistic approach in describing the data we have included the brain compartment in the mass balance of acetaminophen disposition. Rather than applying a whole-body PBPK model, we implemented a systems-based approach where the plasma kinetics were described by means of a compartmental approach, while the brain concentrations, and the exchange between $brain_{ECF}$ and CSF, were described by means of a physiologically-based approach. In order to do so, the volumes of the different brain compartments were fixed to their physiological volumes. Since the physiological volumes of the different brain compartments are over 35-fold lower than that of plasma, only a small fraction of the amount of acetaminophen in plasma is transported into brain tissue.

Interestingly, the clearance values between plasma and $brain_{ECF}$ are over 40-fold higher than the clearance values between plasma and CSF. This indicates

that the transport across the BBB is more substantial compared to transport across the BCSFB.

Given that CSF concentrations are considered to be the best available surrogate for $brain_{ECF}$ concentrations in humans (Fridén *et al.,* 2009; Kalvass and Maurer, 2002; Liu *et al.,* 2006; Liu *et al.,* 2009; Maurer *et al.,* 2005), we have focused on the prediction of human $brain_{ECF}$ concentrations based on human CSF concentrations. Bannwarth and colleagues have measured acetaminophen concentrations in plasma and CSF following a 3 min i.v. infusion of 2 g propacetamol, a prodrug which is hydrolysed to acetaminophen within 7 minutes (Bannwarth *et al.,* 1992). The dosage used corresponded to ~15 mg/kg acetaminophen in 10 minutes, which is equal to the dose used in this study. The observed plasma and spinal CSF_{SAS} concentration-time profile in humans are similarly shaped as the observed acetaminophen plasma concentration-time profile and the predicted CSF_{SAS} concentration-time profile in rat. However, the kinetics in humans are different from that in rats.

For the prediction of human $brain_{ECF}$ exposure on the basis of human CSF concentrations the SBPK modeling approach is important, as it allowed the extrapolation of our rat data. This was done by changing the different physiological parameters of the rat to the human values and systems-based scaling of the brain clearances. A similar approach has been applied by Kielbasa and Stratford (2012), where brain compartmental volumes were fixed to their physiological volumes and human brain PK parameters were predicted on the basis of allometric scaling of rat brain PK parameters. These predictions were then compared to clinical PK parameters based on human plasma or CSF concentrations.

As the possibility to validate human predictions of $brain_{ECF}$ exposure on the basis of direct measurement of $brain_{ECF}$ concentrations in human is highly restricted, there is the need for more mechanistic understanding of the processes involved in the causal path from drug dosing to CNS drug effects. This will possibly allow the validation of predictions on the basis of appropriate biomarkers in human CSF or plasma samples. To that end, the physiological brain disposition model presented here will be extended on the basis of brain disposition measurements of a series of other drugs with different physicochemical properties in order to fully characterize the processes involved in brain disposition. For drugs that are known to be actively transported into or

out of the brain, a cross-compare designed study with or without the inhibition of the specific transporter will be informative on the contribution of the specific transporter in blood-brain transport. By adding this information to the current SBPK model, together with quantitative information on the transporter expression levels in animals and humans, the SBPK model will serve as a basis for extrapolation of preclinical findings and ultimately only *in vitro* determinations of physicochemical properties of drugs, to the human situation.

CONCLUSION

Even for acetaminophen, a drug without active transport processes into, within and out of the brain, significant differences exist between the striatal $brain_{ECF}$ and the CSF concentrations after acute dosing.

With the ultimate goal of being able to predict CNS drug effects in humans, a more mechanistic understanding of the relative importance of the processes involved in brain target site distribution can be obtained *in vivo* by applying the intracerebral microdialysis technique in combination with physiologically based pharmacokinetic modeling.

APPENDIX

Differential equations

The mass balance equations describing the final SBPK model were expressed as follows:

Plasma:

$$\frac{dA_{PL,u}}{dt} = dose - k_{PL-PER} \times A_{PL,u} + k_{PER-PL} \times A_{PER} - k_{PL-ECF} \times A_{PL,u}$$
$$+k_{ECF-PL} \times A_{ECF} - k_{PL-LV} \times A_{PL,u} + k_{LV-PL} \times A_{LV} - k_{PL-TFV} \times A_{PL,u}$$
$$+k_{TFV-PL} \times A_{TFV} - k_{PL-CM} \times A_{PL,u} + k_{CM-PL} \times A_{CM} + \left(\frac{Q_{CSF}}{V_{SAS}}\right) \times A_{SAS}$$

$$-k_E \times A_{PL,u} + F_{abs} \times dose$$

$$C_{PL,u} = \frac{A_{PL,u}}{V_{PL}}$$

Periphery:

$$\frac{dA_{PER}}{dt} = k_{PL-PER} \times A_{PL,u} - k_{PER-PL} \times A_{PER}$$

$$C_{PER} = \frac{A_{PER}}{V_{PER}}$$

$Brain_{ECF}$:

$$\frac{dA_{ECF}}{dt} = k_{PL-ECF} \times A_{PL,u} - k_{ECF-PL} \times A_{ECF} - \left(\frac{Q_{ECF}}{V_{ECF}}\right) \times A_{ECF}$$

$$C_{ECF} = \frac{A_{ECF}}{V_{ECF}}$$

CSF_{LV}:

$$\frac{dA_{LV}}{dt} = k_{PL-LV} \times A_{PL,u} - k_{LV-PL} \times A_{LV} + \left(\frac{Q_{ECF}}{V_{ECF}}\right) \times A_{ECF} - \left(\frac{Q_{CSF}}{V_{LV}}\right) \times A_{LV}$$

$$C_{LV} = \frac{A_{LV}}{V_{LV}}$$

CSF_{TFV}:

$$\frac{dA_{TFV}}{dt} = k_{PL-TFV} \times A_{PL,u} - k_{TFV-PL} \times A_{TFV} + \left(\frac{Q_{CSF}}{V_{LV}}\right) \times A_{LV} - \left(\frac{Q_{CSF}}{V_{TFV}}\right) \times A_{TFV}$$

$$C_{TFV} = \frac{A_{TFV}}{V_{TFV}}$$

CSF_{CM}:

$$\frac{dA_{CM}}{dt} = k_{PL-CM} \times A_{PL,u} - k_{CM-PL} \times A_{CM} + \left(\frac{Q_{CSF}}{V_{TFV}}\right) \times A_{TFV} - \left(\frac{Q_{CSF}}{V_{CM}}\right) \times A_{CM}$$

$$C_{CM} = \frac{A_{CM}}{V_{CM}}$$

CSF_{SAS}:

$$\frac{dA_{SAS}}{dt} = \left(\frac{Q_{CSF}}{V_{CM}}\right) \times A_{CM} - \left(\frac{Q_{CSF}}{V_{SAS}}\right) \times A_{SAS}$$

$$C_{SAS} = \frac{A_{SAS}}{V_{SAS}}$$

Where:

$$k_E = \frac{CL_E}{V_{PL}}$$

$$k_{PL-PER} = \frac{Q_{PL-PER}}{V_{PL}}$$

$$k_{PER-PL} = \frac{Q_{PL-PER}}{V_{PER}}$$

$$k_{PL-ECF} = \frac{CL_{PL-ECF}}{V_{PL}}$$

$$k_{ECF-PL} = \frac{CL_{ECF-PL}}{V_{ECF}}$$

$$k_{PL-LV} = \frac{CL_{PL-LV}}{V_{PL}}$$

$$k_{LV-PL} = \frac{CL_{LV-PL}}{V_{LV}}$$

$$k_{PL-TFV} = \frac{CL_{PL-TFV}}{V_{PL}}$$

$$k_{TFV-PL} = \frac{CL_{TFV-PL}}{V_{TFV}}$$

$$k_{PL-CM} = \frac{CL_{PL-CM}}{V_{PL}}$$

$$k_{CM-PL} = \frac{CL_{CM-PL}}{V_{CM}}$$

NOMENCLATURE

A_i	Amount of acetaminophen in compartment i (ng)
C_i	Concentration of acetaminophen in compartment i (ng/ml)
k	rate constant (min^{-1})
Q	flow rate (ml/min)
CL	clearance (ml/min)
V	volume (ml)

Subscripts

PL	plasma
PL,u	unbound acetaminophen in plasma
PER	peripheral compartment
ECF	$brain_{ECF}$
CSF	CSF
LV	lateral ventricle
TFV	third and fourth ventricle
CM	cisterna magna
SAS	subarachnoid space

REFERENCES

Abbott NJ. Evidence for bulk flow of brain interstitial fluid: significance for physiology and pathology. Neurochem Int 2004; 45: 545-552.

Abbott NJ, Dolman DEM, Patabendige AK. Assays to predict drug permeation across the blood-brain barrier, and distribution to brain. Curr Drug Metab 2008; 9: 901-910.

Adam R, Greenberg JO. The mega cisterna magna. J Neurosurg 1978; 48: 190-192.

Bailey DN, Briggs JR. The binding of selected therapeutic drugs to human serum α_1 acid glycoprotein and to human serum albumin in vitro. Ther Drug Monit 2004; 26: 40-43.

Bannwarth B, Netter P, Lapicque F, Gillet P, Péré P, Boccard E, Royer RJ, Gaucher A. Plasma and cerebrospinal fluid concentrations of paracetamol after a single intravenous dose of propacetamol. Br J Clin Pharmacol 1992; 34: 79-81.

Bass NH, Lundborg P. Postnatal development of bulk flow in the cerebrospinal fluid system of the albino rat: clearance of carboxyl-[^{14}C]inulin after intrathecal infusion. Brain Res 1973; 52: 323-332.

Begley DJ. Transport to the brain. In: D.J. Begley, M.W. Bradbury and J. Kreuter, editors. The blood-brain barrier and drug delivery to the CNS. 2000; New York: Dekker; p. 93-108.

Bickel U. How to measure drug transport across the blood-brain barrier. NeuroRx 2005; 2: 15-26.

Bouman HJ, van Wimersma Greidanus TB. A rapid and simple cannulation technique for repeated sampling of cerebrospinal fluid in freely moving rats. Brain Res Bull 1979; 4: 575-577.

Boxenbaum H. Interspecies scaling, allometry, physiological time, and the ground plan of pharmacokinetics. J Pharmacokin Biopharm 1982; 10: 201-227.

Condon P, Patterson J, Wyper D, Hadley D, Grant R, Teasdale G, Rowan J. Use of magnetic resonance imaging to measure intracranial cerebrospinal fluid volume. Lancet 1986; 327: 1355-1357.

Cox EH, Veyrat-Follet C, Beal SL, Fuseau E, Kenkare S, Sheiner LB. A population pharmacokinetic-pharmacodynamic analysis of repeated measures time-to-event pharmacodynamic responses: the antiemetic effect of ondansetron. J Pharmacokinet Biopharm 1999; 27: 625-644.

Cserr HF. Potassium exchange between cerebrospinal fluid, plasma, and brain. Am J Physiol 1965; 209: 1219-1226.

Cserr HF. Physiology of the choroid plexus. Physiol Rev 1971; 51: 273-311.

Cserr HF, Cooper DN, Suri PK, Patlak CS. 1981. Efflux of radiolabeled polyethylene glycols and albumin from rat brain. Am J Physiol 240: F319-F328.

De Lange ECM, Danhof M. Considerations in the use of cerebrospinal fluid pharmacokinetics to predict brain target site concentrations in the clinical setting. Implications of the barriers between blood and brain. Clin Pharmacokinet 2002; 41: 691-703.

De Lange ECM, Danhof M, de Boer AG, Breimer DD. Critical factors of intracerebral microdialysis as a technique to determine the pharmacokinetics of drugs in rat brain. Brain Res 1994; 666: 1-8.

De Lange ECM, Bouw MR, Mandema JW, Danhof M, de Boer AG, Breimer DD. Application of intracerebral microdialysis to study regional distribution kinetics of drugs in rat brain. Br J Pharmacol 1995; 116: 2538-2544.

De Lange ECM, Danhof M, de Boer AG, Breimer DD. Methodological considerations of intracerebral microdialysis in pharmacokinetic studies on drug transport across the blood-brain barrier. Brain Res Behav 1997; 25: 27-49.

Dickey CC, Shenton ME, Hirayasu Y, Fischer I, Voglmaier MM, Niznikiewicz MA, Seidman LJ, Fraone S, McCarley RW. Large CSF volume not attributable to ventricular volume in schizotypical personality disorder. Am J Psychiatry 2000; 157: 48-54.

Duffull SB, Aarons L. Development of a sequential linked pharmacokinetic and pharmacodynamic simulation model for ivabradine in healthy volunteers. Eur J Pharm Sci 2000; 10: 275-284.

Feng MR. Assessment of blood-brain barrier penetration: in silico, in vitro and in vivo. Curr Drug Metab 2002; 3: 647-657.

Frank H, Gray SJ. The determination of plasma volume in man with radioactive chromic chloride. J Clin Invest 1953; 32: 991-999.

Fridén M, Winiwarter S, Jerndal G, Bengtsson O, Wan H, Bredberg U, Hammarlund-Udenaes M, Antonsson M. Structure—Brain exposure relationships in rat and human using a novel data set of unbound drug concentrations in brain interstitial and cerebrospinal fluids. J Med Chem 2009; 52: 6233-6243.

Hammarlund-Udenaes M, Paalzow LK, de Lange ECM. Drug equilibration across the blood-brain barrier – pharmacokinetic considerations based on the microdialysis method. Pharm Res 1997; 14: 128-134.

Hammarlund-Udenaes M, Fridén M, Syvänen S, Gupta A. On the rate and extent of drug delivery to the brain. Pharm Res 2008; 25: 1737-1750.

Hill KK, West SA, Ekhator NN, Bruce AB, Wortman MD, Baker DG, Geracioti Jr TD. The effect of lumbar puncture stress on dopamine and serotonin metabolites in human cerebrospinal fluid. Neurosci Lett 1999; 276: 25-28.

Hjelle JJ, Klaassen CD. Glucuronidation and biliary excretion of acetaminophen in rats. J Pharmacol Exp Ther 1984; 228: 407-413.

Hosseini-Yeganeh M, McLachlan AJ. Physiologically based pharmacokinetic model for terbinafine in rats and humans. Antimicrob Agents Chemother 2002; 46: 2219-2228.

Jeffrey P, Summerfield S. Assessment of the blood-brain barrier in CNS drug discovery. Neurobiol Dis 2010; 37: 33-37.

Kalvass JC, Maurer TS. Influence of nonspecific brain and plasma binding of CNS exposure: Implications for rational drug discovery. Biopharm Drug Dispos 2002; 23: 327-338.

Kawai R, Lemaire M, Steimer J-L, Bruelisauer A, Niederberger W, Rowland M. Physiologically based pharmacokinetic study on a cyclosporine derivative, SDZ IMM 125. J Pharmacokinet Biopharm 1994; 22: 327-365.

Kazama S, Masaki Y, Maruyama S, Ishihara A. Effect of altering cerebrospinal fluid pressure on spinal cord blood flow. Ann Thorac Surg 1994; 58: 112-115.

Kielbasa W, Stratford Jr RE. Exploratory translational modeling approach in drug development to predict human brain pharmacokinetics and pharmacologically relevant clinical doses. Drug Metab Dispos. 2012; 40: 877-883.

Kimelberg HK. Water homeostasis in the brain: Basic concepts. Neurosci 2004; 129: 851-860.

Kohn MI, Tanna NK, Herman GT, Resnick SM, Mozley PD, Gur RE, Alavi A, Zimmerman RA, Gur GC. Analysis of brain and cerebrospinal fluid volumes with MR imaging. Part I. Methods, reliability, and validation. Radiology 1991; 178: 115-122.

Le Quellec A, Dupin S, Genissel P, Saivin S, Marchand B, Houin G. Microdialysis probes calibration: gradient and tissue dependent changes in no net flux and reverse dialysis methods. J Pharmacol Toxicol Meth 1995; 33: 11-16.

Lee HB, Blaufox MD. Blood volume in the rat. J Nucl Med 1985; 26: 72-76.

Lee G, Dallas S, Hong M, Bendayan R. Drug transporters in the central nervous system: Brain barriers and brain parenchyma considerations. Pharmacol Rev 2001; 53: 569-596.

Levinger IM. The cerebral ventricles of the rat. J Anat 1971; 108: 447-451.

Lin JH. CSF as a surrogate for assessing CNS exposure: an industrial perspective. Curr Drug Metab 2008; 9: 46-59.

Liu X, Smith BJ, Chen C, Callegari E, Becker SL, Chen X, Cianfrogna J, Doran AC, Doran SD, Gibbs JP, Hosea N, Liu J, Nelson FR, Szewc MA, Van Deusen J. Evaluation of cerebrospinal fluid concentration and plasma free concentration as a surrogate measurement for brain free concentration. Drug Metab Dispos 2006; 34: 1443-1447.

Liu X, Chen C, Smith BJ. Progress in brain penetration evaluation in drug discovery and development. J Pharmacol Exp Ther 2008; 325: 349-356.

Liu X, Van Natta K, Yeo H, Vilenski O, Weller PE, Worboys PD, Monshouwer M. Unbound drug concentration in brain homogenate and cerebral spinal fluid at steady state as a surrogate for unbound concentration in brain interstitial fluid. Drug Metab Dispos 2009; 37: 787-793.

Maurer TS, DeBartolo DB, Tess DA, Scott D. Relationship between exposure and nonspecific binding of thirty-three central nervous system drugs in mice. Drug Metab Dispos 2005; 33: 175-181.

Morrison PF, Bungay PM, Hsiao JK, Ball BA, Mefford IN, Dedrick RL. Quantitative microdialysis: analysis of transients and application to pharmacokinetics in brain. J Neurochem 1991; 57: 103-119.

Nielsen JA, Fossom LH, Sparber SB. Metabolism of ^{3}H-dopamine continuously perfused through push-pull cannulas in rats' brains: modification by amphetamine or prostaglanding $F_{2\alpha}$. Pharmacol Biochem Behav 1980; 13: 235-242.

Nilsson C, Stahlberg F, Thomsen C, Henriksen O, Herning M, Owman C. Circadian variation in human cerebrospinal fluid production measured by magnetic resonance imaging. Am J Physiol 1992; 262: R20-R24.

Pangalos MN, Schechter LE, Hurko O. Drug development for CNS disorders: strategies for balancing risk and reducing attrition. Nat Rev Drug Disc 2007; 6: 521-532.

Pardridge WM. Drug transport in brain via the cerebrospinal fluid. Fluids Barriers CNS 2011; 8: 7.

Robertson EG. Developmental defects of the cisterna magna and dura mater. J Neurol Neurosurg Psychiatry 1949; 12: 39-51.

Scheller D, Kolb J. The internal reference technique in microdialysis: a practical approach to monitoring dialysis efficiency and to calculating tissue concentration from dialysate samples. J Neurosci Meth 1991; 40: 31-38.

Sheiner LB, Stanski DR, Vozeh S, Miller RD, Ham J. Simultaneous modeling of pharmacokinetics and pharmacodynamics: application to d-tubocurarine. Clin Pharmacol Ther 1979; 25: 358-371.

Shen DD, Artru AA, Adkison KK. Principles and applicability of CSF sampling for the assessment of CNS drug delivery and pharmacodynamics. Adv Drug Del Rev 2004; 56: 1825-1857.

Siegers C-P, Rozman K, Klaassen CD. Biliary excretion and enterohepatic circulation of paracetamol in the rat. Xenobiotica 1983; 13: 591-596.

Ståhle L, Segersvärd S, Ungerstedt U. A comparison between three methods for estimation of extracellular concentrations of exogenous and endogenous compounds by microdialysis. J Pharmacol Meth 1991; 25: 41-52.

Stevens J, Suidgeest E, van der Graaf PH, Danhof M, de Lange ECM. A new minimal-stress freely-moving rat model for preclinical studies on intranasal administration of CNS drugs. Pharm Res 2009; 26: 1911-1917.

Thorne RG, Hrabětová S, Nicholson C. Diffusion of epidermal growth factor in rat brain extracellular space measured by integrative optical imaging. J Neurophysiol 2004; 92: 3471-3481.

van Bree JBMM, Baljet AV, van Geyt A, de Boer AG, Danhof M, Breimer DD. The unit impulse response procedure for the pharmacokinetic evaluation of drug entry into the central nervous system. J Pharmacokinet Biopharm 1989; 17: 441-462.

Watari N, Iwai M, Kaneniwa N. Pharmacokinetic study of the fate of acetaminophen and its conjugates in rats. J Pharmacokinet Biopharm 1983; 11: 245-272.

World Health Organization. In: Neurological Disorders: Public Health Challenges. 2007. http://www.who.int/mental_health/neurology/neurodiso/en/. Accessed 19 Dec 2011.

Yano Y, Beal SL, Sheiner LB. Evaluating pharmacokinetic/pharmacodynamic models using the posterior predictive check. J Pharmacokinet Pharmacodyn 2001; 28: 171-192.

Chapter 4

The impact of P-glycoprotein functionality on non-steady state relationships between CSF and brain extracellular fluid

J. Westerhout, J. Smeets, M. Danhof, E.C.M. de Lange

J. PK. PD. 2013; 40(3): 327-342

ABSTRACT

In the development of central nervous system (CNS)-targeted drugs, the prediction of human CNS target exposure is a big challenge. Cerebrospinal fluid (CSF) concentrations have often been suggested as a 'good enough' surrogate for brain extracellular fluid ($brain_{ECF}$, brain target site) concentrations in humans. However, brain anatomy and physiology indicates prudence.

We have applied a multiple microdialysis probes approach in rats, for continuous measurement and direct comparison of quinidine kinetics in $brain_{ECF,}$ CSF, and plasma.

The data obtained indicated important differences between $brain_{ECF}$ and CSF kinetics, with $brain_{ECF}$ kinetics being most sensitive to P-gp inhibition. To describe the data we developed a systems-based pharmacokinetic (SBPK) model. Our findings indicated that: 1) $brain_{ECF}$- and CSF-to-unbound plasma $AUC_{0\text{-}360}$ ratios were all over 100%; 2) P-gp also restricts brain intracellular exposure; 3) a direct transport route of quinidine from plasma to brain cells exists; 4) P-gp-mediated efflux of quinidine at the blood-brain barrier (BBB) seems to result of combined efflux enhancement and influx hindrance; 5) P-gp at the blood-CSF barrier (BCSFB) either functions as an efflux transporter or is not functioning at all.

It is concluded that in parallel obtained data on unbound $brain_{ECF}$, CSF and plasma concentrations, under dynamic conditions, is a complex but most valid approach to reveal the mechanisms underlying the relationship between $brain_{ECF}$ and CSF concentrations. This relationship is significantly influenced by the activity of P-gp. Therefore, information on the activity of P-gp is required for the prediction of human brain target site concentrations of P-gp substrates on the basis of human CSF concentrations.

INTRODUCTION

To be able to predict desired or undesired central nervous system (CNS) drug effects in humans, a mechanistic understanding is needed of the individual contributions of the processes involved in brain target site distribution and ultimately drug effects. With the unbound drug concentrations at the brain target site being responsible for the (un)wanted effect it is important to be able to determine or predict unbound drug concentrations at their site of action.

During the preclinical phase of drug development several techniques can be applied to determine or predict brain target site concentrations, which are often closely linked, or equal, to brain extracellular fluid ($brain_{ECF}$) concentrations (De Lange *et al.,* 2000; Hammarlund-Udenaes, 2009). However, most of the preclinical techniques have very limited applicability in the extrapolation of preclinical findings to the human situation (**Chapter 1**; De Lange *et al.,* 1997; Hammarlund-Udenaes *et al.,* 2009).

Cerebrospinal fluid (CSF) concentrations are often considered to be the best available surrogate for brain target site concentrations in humans (Fridén *et al.,* 2009; Kalvass and Maurer, 2002; Liu *et al.,* 2006; Liu *et al.,* 2009; Maurer *et al.,* 2005). It is often assumed that CSF concentrations readily equilibrate with $brain_{ECF}$ concentrations due to the lack of a physical barrier between these sites (Lee *et al.,* 2001). However, due to qualitative and quantitative differences in processes that govern the pharmacokinetics (PK) of drugs in the brain, a generally applicable relationship between CSF concentrations and $brain_{ECF}$ concentrations does not exist (**Chapter 1**; De Lange and Danhof, 2002; Lin, 2008; Shen *et al.,* 2004).

Transport of drugs into and out of the brain is not solely governed by the blood-brain barriers (the blood-brain barrier (BBB) and the blood-CSF barrier (BCSFB)), but also by the anatomy of the brain and physiological processes. In combination with drug specific properties (Danhof *et al.,* 2007; Keep and Jones, 1990; Mayer *et al.,* 1959; Oldendorf, 1979), this determines the concentrations of a drug within a specific part of the CNS, including the target site concentrations, which we are ultimately interested in.

We have previously shown that even for acetaminophen, a model compound for passive transport into, within and out of the brain, differences exist between CSF and $brain_{ECF}$ kinetics (**Chapter 3**). For compounds subjected to active

transport at the level of the brain barriers, such as by P-gp, differences between $brain_{ECF}$ and CSF are anticipated to be larger. With P-gp localized at both the luminal and abluminal membranes of capillary endothelial cells, as well as to adjacent pericytes and astrocytes (Bendayan *et al.,* 2006), this suggests that P-gp may regulate drug transport processes in the entire brain at both the cellular and subcellular level. In contrast, P-gp presence and localization at the BCSFB is still subject of debate, with the only report of presence at the apical surface of the choroid plexus epithelial cells in the rat by Rao *et al.* (1999). Furthermore, it has been well established that P-gp functions as an efflux transporter at the BBB (Schinkel, 1999), whereas, there has been some evidence that P-gp could function as an influx transporter at the BCSFB (Kassem *et al.,* 2007; Rao *et al.,* 1999). This could result in significant differences between concentrations at the brain target site and in CSF for compounds that are substrates for P-gp mediated transport.

The presence of P-gp at multiple sites, with in part a yet uncertain transport direction, could have major implications for the predictability of human $brain_{ECF}$ concentrations on the basis of human CSF concentrations for compounds that are substrates for active (e.g. P-gp-mediated) transport. Consequently, to be able to predict human $brain_{ECF}$ concentrations on the basis of human CSF concentrations, one should first understand the mechanisms that determine the relationship between CSF concentrations and $brain_{ECF}$ concentrations.

Previous studies have indicated that, under steady-state conditions, CSF concentrations were comparable to steady-state $brain_{ECF}$ concentrations for compounds that freely diffuse across the BBB and BCSFB, but may differ for compounds that are substrate for the various active transport systems at the BBB and BCSFB (Fridén *et al.,* 2009; Kalvass and Maurer, 2002; Liu *et al.,* 2006; Liu *et al.,* 2009; Maurer *et al.,* 2005). CSF and $brain_{ECF}$ concentration ratios were considered comparable if smaller than 3-fold, and assumed to be of little pharmacological consequence.

However, we have previously questioned this arbitrary threefold range in ratio of CSF and $brain_{ECF}$ (target site) kinetics, especially with regard to the unknown impact of the steady-state situation *versus* the more realistic multiple dosing conditions (troughs and peaks), the unknown of the changes therein in disease conditions as well as the unknown impact of this range on pharmacodynamics (**Chapter 1**). These unknowns need to be investigated

before we can really predict human target site pharmacokinetics and finally CNS effects.

Using the multiple intracerebral microdialysis probes approach (striatum, lateral ventricle, and cisterna magna) with parallel blood sampling, continuous measurement and direct comparison of changes in concentrations in plasma, $brain_{ECF}$ and CSF kinetics of quinidine could be assessed. Quinidine, a well-known P-gp substrate (Doran *et al.,* 2005; Kusuhara *et al.,* 1997; Syvänen *et al.,* 2012; Sziráki *et al.,* 2011; Varma and Panchagnula, 2005), was administered by means of a short infusion of 10 mg/kg and 20 mg/kg, with and without co-administration of the P-gp blocker tariquidar (Fox and Bates, 2007; Kurnik *et al.,* 2008). Mathematical modeling was applied to the data to result in a number of key findings.

MATERIALS AND METHODS

Chemicals and solutions

Quinidine, quinidine sulfate dehydrate, quinidine hemi sulfate and quinine hemi sulfate were obtained from Sigma Aldrich (Zwijndrecht, the Netherlands). Tariquidar (XR9576) was obtained from Xenova Group PLC (Cambridge, England) or API Services Inc. (Westford, USA). Triethyl amine was obtained from J.T. Baker (Deventer, the Netherlands). Boric acid and orthophosphoric acid 85% were obtained from Merck (Darmstadt, Germany). Methyl tert-butyl ether was obtained from Biosolve B.V. (Valkenswaard, the Netherlands). Isoflurane was obtained from Pharmachemie B.V. (Haarlem, the Netherlands). Saline and 5% glucose were obtained from the Leiden University Medical Centre pharmacy (Leiden, the Netherlands). Microdialysis perfusion fluid was prepared as previously described (**Chapter 3**), containing 140.3 mM sodium, 2.7 mM potassium, 1.2 mM calcium, 1.0 mM magnesium and 147.7 mM chloride.

Animals

The study protocol was approved by the Animal Ethics Committee of Leiden University (UDEC nr. 07142) and all animal procedures were performed in accordance with Dutch laws on animal experimentation. A total of 60 male Wistar WU rats (225-275 g, Charles River, Maastricht, the Netherlands) were randomly divided into two groups; the first group (n = 12) was used for the determination of the *in vivo* microdialysis probe recovery; the second group (n = 48) was used for brain disposition experiments. This second group was further divided into four subgroups, designated for 10 or 20 mg/kg quinidine without or with co-administration of tariquidar (10^-, 10^+, 20^- and 20^+, respectively).

After arrival, all animals were housed in groups for 5-7 days (Animal Facilities, Gorlaeus Laboratories, Leiden, the Netherlands), under standard environmental conditions (ambient temperature 21°C; humidity 60%; 12/12 h light/dark cycle, background noise, daily handling), with *ad libitum* access to food (Laboratory chow, Hope Farms, Woerden, the Netherlands) and acidified water. Between surgery and experiments, the animals were kept individually in Makrolon type three cages for 7 days to recover from the surgical procedures.

Surgery

All surgical procedures were performed as described in **Chapter 3**. In short, cannulas were implanted in the left femoral artery and vein for blood sampling and drug administration, respectively. Both cannulas were subcutaneously led to the back of the head and fixated in the neck with a rubber ring. Subsequently, the animals were chronically instrumented with two CMA/12 microdialysis guides (CMA/Microdialysis AB, Stockholm, Sweden) in different combinations of striatum (ST), for sampling in $brain_{ECF}$, and lateral ventricle (LV) and/or cisterna magna (CM) for sampling in CSF (ST+LV, ST+CM or LV+CM). For ST, the position of the microdialysis guide is: 1.0 mm anterior, 3.0 mm lateral, 3.4 mm ventral, relative to bregma. For LV, the position of the microdialysis guide is: 0.9 mm posterior, 1.6 mm lateral, 2.9 mm ventral, relative to the bregma. For CM, the position of the microdialysis guide is: 1.93 mm posterior, 3.15 mm lateral, 8.1 mm ventral, at an angle of 25° from the dorsoventral axis (towards anterior) and 18° lateral from the anteroposterior axis relative to

lambda. The microdialysis guides were secured to the skull with 3 anchor screws and dental cement.

After the surgery the animals received 0.03 ml Temgesic ® intramuscularly (Schering-Plough, Amstelveen, the Netherlands) and 0.3 ml Ampicillan® (Alfasan B.V., Woerden, the Netherlands) subcutaneously. One day prior to the experiment, the microdialysis dummies were replaced by the microdialysis probes (CMA/12 Elite, Polyarylethersulfone membrane, molecular weight cut-off 20 kDa, CMA/Microdialysis AB, Stockholm, Sweden, with a semi-permeable membrane length of 4 mm for ST, and 1 mm for LV and CM).

Experimental set-up

All experiments were performed as described in **Chapter 3** with some modifications. In short, the *in vivo* microdialysis probe recovery of quinidine was determined on the basis of reverse dialysis (Ståhle *et al.,* 1991). The microdialysis probes in striatum, lateral ventricle and cisterna magna were perfused with different concentrations of quinidine (50, 200 and 1000 ng/ml) in perfusion fluid. To evaluate the potential effect of co-administration of tariquidar on the *in vivo* recovery of quinidine, several animals received an intravenous infusion of 15 mg/kg in 5% glucose solution (100 µl/min/kg for a period of 10 minutes) with an automated pump (Pump 22 Multiple Syringe Pump, Harvard Apparatus, Holliston, USA) 30 minutes prior to the start of the reverse dialysis experiment. Control animals received an intravenous infusion of vehicle (100 µl/min/kg for a period of 10 minutes).

The *in vivo* recovery is defined as the ratio of the concentration difference between the dialysate (C_{dial}) and perfusion fluid (C_{in}) over the concentration in the perfusion fluid (equation 1) (Scheller and Kolb, 1991).

$$in\ vivo\ recovery = \frac{C_{in} - C_{dial}}{C_{in}} \quad (1)$$

For the brain disposition experiments, the rats first received an intravenous infusion of 15 mg/kg tariquidar in 5% glucose solution or vehicle 30 minutes prior to the administration of 10 or 20 mg/kg quinidine in saline (100 µl/min/kg for a period of 10 minutes). The start and duration of the infusion was corrected for internal volume of the tubing so that infusion started at t=0 min. 10 min

interval samples were collected between t=−1 h and t=4 h, followed by 20 min interval samples until t=6 h. After weighing the microdialysis vials they were stored at −80°C before analysis.

For the determination of quinidine plasma concentrations, blood samples of 100 µl were taken, in parallel to the microdialysate samples, from the arterial cannula at t=−5 (blank), 2, 7, 10, 12, 17, 30, 60, 140, 240, and 360 min. All blood samples were temporarily stored in heparin (10 IU) coated Eppendorf cups before being centrifuged for 15 min at 5000 rpm. The plasma was then pipetted into clean Eppendorf cups and stored at −20°C before analysis.

At the end of the experiments the animals were sacrificed with an overdose of Nembutal (Ceva Sante Animale, Libourne, France). The animals were then perfused and decapitated to isolate the brain. After cleaning with saline, weighing, and freezing in liquid nitrogen, the brain was stored at -80˚C before analysis.

Plasma protein binding

For the determination of plasma protein binding of quinidine, blood samples of 300 µl were taken at t=−30 (blank) and 60 min (with a concentration assumed to be approximately 50% of C_{max} (Harashima *et al.,* 1985)). After the blood sample at t=360 min, an additional dose of 10 or 20 mg/kg in 10 minutes was given to be able to determine plasma protein binding at C_{max} (at t=370 min). All blood samples were temporarily stored in heparin (10 IU) coated Eppendorf cups. The blank blood samples were spiked with quinidine to obtain a blood concentration of 100 ng/ml for the 10 mg/kg dose group and 200 ng/ml for the 20 mg/kg dose group. The spiked blood samples were then incubated in a shaking water bath at 37°C for 30 minutes. All blood samples were centrifuged for 15 min at 5000 rpm and the plasma was pipetted into clean Eppendorf cups and stored at −20°C before analysis.

Plasma protein binding was determined with Centrifree® ultrafiltration devices (Millipore BV, Etten-Leur, the Netherlands). All procedures were performed according to the user's manual. The ultrafiltrate was diluted 10 times with saline before the analysis.

Concentration analysis

Quinidine concentrations in plasma, plasma ultrafiltrate, microdialysate, and total brain were determined as described by Syvänen *et al.* (2012), using High Pressure Liquid Chromatography (HPLC) with fluorescence detection. In short, to 20 µl of plasma, 50 µl internal standard (IS; 500 ng/ml quinine) was added. After homogenization with 200 µl borate buffer pH 10, 5 ml of methyl tert-butyl ether was added. After vortexing, centrifugation, and freezing of the aqueous layer, the organic phase was evaporated to dryness. The extracts were reconstituted in 100 µl of mobile phase and centrifuged at 4000 g during 5 min. The clean plasma extracts were injected using a mobile phase with an acetonitrile/buffer ratio of 1:6.

To 20 µl of the plasma ultrafiltrate or microdialysate samples 20 µl IS was added, followed by vortexing before being directly injected into the HPLC system.

Quinidine concentration in brain tissue was analyzed by the following steps: whole brain was homogenized in 50 mM phosphate buffer at pH 7.4. To 600 µl of the homogenate 100 µl IS and 100 µl 1M sodium hydroxide was added. 5 ml methyl tert-butyl ether was then added, followed by vortexing and centrifugation. 4 ml of the supernatant was then transferred to a clean glass tube and 100 µL of 30 mM phosphoric acid was added. After vortexing and centrifugation, the supernatants were aspirated and discarded. The remaining aqueous phase was centrifuged for 10 min at 11000 g. An aliquot of 50 µl was then transferred to clean glass vials and 20 µl was injected into the HPLC system.

Data acquisition and processing was performed using Empower® data acquisition software (Waters, Etten-Leur, the Netherlands). For constructing the calibration curve, linear regression analysis was applied using weight factor $1/(y)^2$. Data analysis, statistical analysis, and plotting were performed using Microsoft® Office Excel 2003 (Microsoft Corporation, USA).

Pharmacokinetic data analysis

All plasma concentrations were converted to unbound plasma concentrations, by correction for plasma protein binding. All microdialysate concentrations

from striatum, lateral ventricle and cisterna magna were converted into $brain_{ECF}$ concentrations (C_{ECF}) or CSF concentrations (C_{CSF}) by division of the dialysate concentrations by the average *in vivo* recovery as determined for each microdialysis probe location (equation 2).

$$C_{ECF}\ or\ C_{CSF} = \frac{C_{dial}}{in\ vivo\ recovery} \quad (2)$$

Areas under the curve from t=0 to t=360 min ($AUC_{0\text{-}360}$) were calculated by the trapezoidal rule and tested for differences by single factor ANOVA. The population PK models were developed and fitted to the data by means of non-linear mixed-effects modeling using the NONMEM software package (version 6.2, Icon Development Solutions, Ellicott City, Maryland, USA) and analyzed using the statistical software package S-Plus® for Windows (version 6.2 Professional, Insightful Corp., Seattle, USA).

The pharmacokinetic model for quinidine plasma and brain concentrations was based on the systems-based PK (SBPK) approach we have previously applied to investigate the exchange between $brain_{ECF}$ and CSF of acetaminophen (**Chapter 3**). For this approach, the volumes of the different brain compartments were fixed to their physiological volumes. The rat brain intracellular space and $brain_{ECF}$ volume were assumed to be 1.44 ml (Thorne *et al.,* 2004), and 290 µl (Cserr *et al.,* 1981), respectively. With a total CSF volume of 300 µl in the rat (Bass and Lundborg 1973), the volumes of the lateral ventricles, third and fourth ventricles, cisterna magna and subarachnoid space were assumed to be 50 µl (Condon *et al.,* 1986; Kohn *et al.,* 1991), 50 µl (Levinger, 1971), 17 µl (Adam and Greenberg, 1978; Robertson, 1949), and 180 µl (Bass and Lundborg, 1973; Levinger, 1971), respectively. The intra-brain distribution was restricted by the physiological flow paths of $brain_{ECF}$, in which $brain_{ECF}$ flows towards the CSF compartments at a rate of 0.2 µl/min (Abbott, 2004; Cserr *et al.,* 1981), and CSF flows from lateral ventricle, through the third and fourth ventricle, to the cisterna magna and subsequently to the subarachnoid space (cranial and spinal) and back into blood at a rate of 2.2 µl/min (Cserr, 1965).

Structural model selections for the SBPK model were based on the likelihood ratio test ($p < 0.01$), diagnostic plots (observed concentrations vs. individual and population predicted concentrations, weighted residuals vs.

predicted time and concentrations), parameter correlations and precision in parameter estimates. The inter-animal variability in pharmacokinetic parameters was assumed to be log normally distributed. The residual error, which accounts for unexplained variability (e.g. measurement and experimental error and model-misspecification), was best described with a proportional error model.

The validity of the SBPK model was investigated by means of a visual predictive check (Cox *et al.,* 1999; Duffull and Aarons, 2000; Yano *et al.,* 2001). Using the final PK parameter estimates, 1000 curves were simulated. Subsequently, the median and the 5^{th} and 95^{th} percentile of the predicted concentrations were calculated, which represent the 90% prediction interval. These were then compared with the observations.

In order to test the ruggedness of the model and estimate the precision of the parameters n=100 non-parametric (case resampling) bootstraps were performed. To create the bootstrapped datasets, specific rat data (plasma and microdialysate concentrations) were removed randomly from the datasets and replaced with randomly selected rat data from the complete original dataset. Each of these permutations of the original dataset were fitted with the final model determined based on the original dataset. This results in a series of model fits, each with its own set of parameters. These results were displayed graphically and the descriptive statistics of the parameters were compared to parameter estimates of the final model. Only bootstrap runs that successfully minimized were used in this analysis.

RESULTS

All results are presented as average values ± standard error of the mean, unless stated otherwise.

Quinidine pharmacokinetics

The average unbound plasma ($plasma_u$), $brain_{ECF}$, lateral ventricle (CSF_{LV}) and cisterna magna (CSF_{CM}) quinidine concentrations following the 10 and 20 mg/kg dose with or without co-administration of tariquidar are shown in figure 1. Plasma protein binding of quinidine was linear at an extent of 86.5 ± 5.5 %. It

was not affected by co-administration of tariquidar. The co-administration of tariquidar slightly reduced the plasma elimination rate of $plasma_u$ for both 10 and 20 mg/kg dose of quinidine. Data obtained by microdialysis from the $brain_{ECF}$, CSF_{LV} and CSF_{CM} were corrected for *in vivo* recovery. The average *in vivo* recoveries for the quinidine concentrations in striatum, lateral ventricle and cisterna magna probes were not influenced by co-administration of tariquidar and were determined to be 9.1 ± 0.5%, 2.9 ± 0.5% and 3.5 ± 0.5%, respectively.

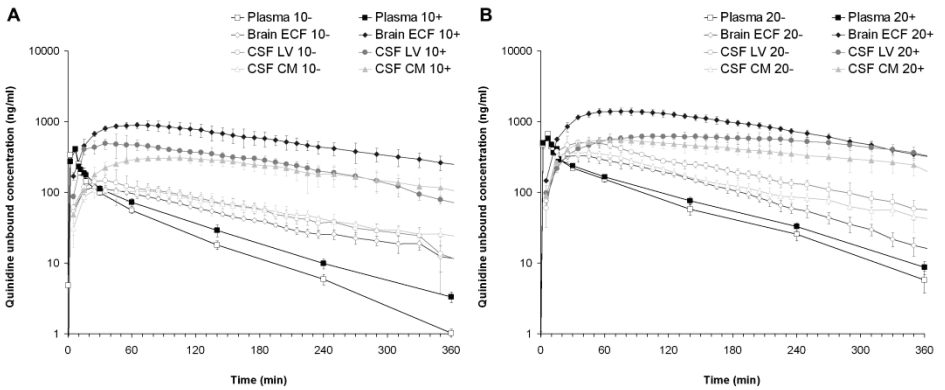

Figure 1. Average (geometric mean ± S.E.M.) unbound quinidine concentration-time profiles following intravenous administration of quinidine, with (+) or without (-) co-administration of tariquidar (15/mg/kg). (A) 10 mg/kg quinidine dose: for plasma (n = 11 (-) and 6 (+)), $brain_{ECF}$ (n = 6 (-) and 4 (+)), CSF_{LV} (n = 4 (-) and 3 (+)) and CSF_{CM} (n = 4 (-) and 4 (+). (B) 20 mg/kg quinidine dose. Plasma (n = 9 (-) and 11 (+)), $brain_{ECF}$ (n = 5 (-) and 6 (+)), CSF_{LV} (n = 4 (-) and 4 (+)) and CSF_{CM} (n = 6 (-) and 6 (+))

It can be seen that a higher dose of quinidine leads to higher quinidine concentrations in all brain compartments, but not to the same extent. Tariquidar increased quinidine concentrations significantly ($p < 0.01$) in all brain compartmens, but most pronouncedly for $brain_{ECF}$. The effect of tariquidar was dependent on the quinidine dose; at the higher dose of quinidine, the increase in quinidine concentrations in all brain compartments was less profound, as can be seen by the average $brain_u$-to-$plasma_u$ $AUC_{0\text{-}360}$ ratios (table 1). However, the difference between the unbound brain ($brain_u$)-to-$plasma_u$ $AUC_{0\text{-}360}$ ratios for the 10 and 20 mg/kg dose with co-administration of tariquidar was only significant ($p < 0.05$) for $brain_{ECF}$. The $brain_{ECF}$-to-CSF concentrations ratios were also very much dependent on tariquidar, and on average were increased from 0.77 ± 0.19 to 2.41 ± 0.56 and from 0.67 ± 0.21 to 2.02 ± 0.52, for the 10

and 20 mg/kg dose, respectively (table 2). Significant differences in AUC ratios and concentrations between $brain_{ECF}$ and CSF (either from lateral ventricle or cisterna magna) were only observed for the groups that received the co-administration of tariquidar.

Table 1. $Brain_u$-to-$plasma_u$ AUC_{0-360} ratios for $brain_{ECF}$, CSF_{LV} and CSF_{CM} for the 10 mg/kg and 20 mg/kg dose without (-) and with (+) co-administration of tariquidar

$Brain_u$-to-$plasma_u$ AUC_{0-360} ratios	10^-	10^+	20^-	20^+
$Brain_{ECF}$	135 ± 17%	1265 ± 213%**‡	150 ± 16%‡	864 ± 64%**‡†
CSF_{LV}	177 ± 39%	624 ± 41%**	257 ± 24%	498 ± 74%**
CSF_{CM}	167 ± 16%	479 ± 76%**	184 ± 15%	383 ± 33%**

** *Significantly ($p < 0.01$) different from the group without co-administration of tariquidar*
‡ *Significantly ($p < 0.05$) different from the CSF-to-$plasma_u$ AUC_{0-360} ratios*
† *Significantly ($p < 0.05$) different from the 10 mg/kg dose group with co-administration of tariquidar*

Table 2. $Brain_{ECF}$-to-CSF concentration ratios for the 10 mg/kg and 20 mg/kg dose without (-) and with (+) co-administration of tariquidar

$Brain_{ECF}$-to-CSF concentration ratios	10^-	10^+	20^-	20^+
$Brain_{ECF}$-to-CSF_{LV}	0.75 ± 0.09*	2.13 ± 0.47*	0.56 ± 0.18*	1.81 ± 0.57
$Brain_{ECF}$-to-CSF_{CM}	0.79 ± 0.25	2.70 ± 0.51*	0.78 ± 0.17	2.23 ± 0.37*
$Brain_{ECF}$-to-$CSF_{average}$	0.77 ± 0.19	2.41 ± 0.56*	0.67 ± 0.21	2.02 ± 0.52*

* *Significantly ($p < 0.05$) different from 1*

Also, end-of-experiment total brain concentrations ($brain_{total}$) were obtained. These data were corrected for corresponding $brain_{ECF}$ concentrations to represent deep brain ($brain_{deep}$) concentrations. The $brain_{deep}$ concentrations were determined to be on average 3.6 ± 1.6-fold higher than final $brain_{ECF}$ concentrations for the control group and 6.3 ± 1.5-fold higher for the animals that received a co-administration of tariquidar (not significantly different). This indicates that P-gp also influences brain intracellular exposure.

Compartmental modeling approach

All data were subjected first to compartmental pharmacokinetic analysis. It was shown that the plasma concentrations were best described by a three compartment model with inter-compartmental clearance (Q), and elimination clearance from the central compartment (CL_E). The effect of the co-administration of tariquidar on the elimination clearance was found to be significant ($p < 0.01$, objective function value reduction of 6.63 units).

To describe the concentrations in each of the brain compartments, four brain compartments were added ($brain_{ECF}$, $CSF_{LV,}$ CSF_{CM} and $brain_{deep}$). Drug transport between the plasma and the different brain compartments was determined by a transfer clearance between plasma and each of the brain compartments ($CL_{PL\text{-}BR}$) and vice versa ($CL_{BR\text{-}PL}$). In this model (figure 2) it was not possible to include drug transport between the different brain compartments because each brain compartment then has multiple routes of entry. The model was not able to identify the specific contribution of each route, resulting in transfer clearance value estimations near 0, which is not realistic. Therefore, we decided to remove the transport between the different brain compartments.

Distinction between passive and active transport clearances - The effect of P-gp on the different transfer clearances between plasma and the brain compartments was determined by comparing the parameter estimations for the rats that did to those rats that did not receive the co-administration of tariquidar. Thus, a distinction could be made between the passive and the active component of the transfer clearances.

The data were best described by a model in which P-gp reduced the transfer clearance from plasma to the brain compartments (i.e. influx hindrance; equation 3) and increased the transfer clearance from the brain compartments to plasma (i.e. efflux enhancement; equation 4). The transfer clearances between plasma and the different brain compartments that could be assigned to P-gp were incorporated into the model as previously described by Syvänen *et al.* (2006):

$$CL_{PL-BR} = CL_{PL-BR,p} - CL_{PL-BR,P-gp} \quad (3)$$

$$CL_{BR-PL} = CL_{BR-PL,p} + CL_{BR-PL,P-gp} \quad (4)$$

Where the subscript 'p' denotes passive transport and 'P-gp' denotes P-gp-mediated transport.

Modeling quinidine concentration-dependent P-gp-mediated transport - Since P-gp-mediated transport is an active (saturable) process we have also tried to identify the maximal transport rate (T_m) and the blood- or brain concentration for half-maximal transport (K_m) as follows:

$$CL_{PL-BR,P-gp} = \frac{T_{m,PL-BR}}{K_{m,PL-BR}+C_{PL,u}} \quad (5)$$

$$CL_{BR-PL,P-gp} = \frac{T_{m,BR-PL}}{K_{m,BR-PL}+C_{BR}} \quad (6)$$

Where $C_{PL,u}$ is the unbound plasma concentration and C_{BR} is the concentration in one of the brain compartments. The parameter estimations of T_m and K_m resulted in high values for both T_m and K_m (results not shown), indicating that the plasma and brain concentrations in this study are not sufficiently high for saturating P-gp-mediated transport. The parameter estimations of T_m and K_m also resulted in too large coefficients of variation. Thus, our data were insufficient to determine the values of these parameters, and for the next modeling steps, P-gp-mediated transport had to be incorporated by means of a single clearance value, rather than by T_m and K_m.

Modeling deep brain concentrations - $Brain_{deep}$ concentrations were determined for samples obtained at the end-of-experiment time point. Based on previous studies in our lab with male Wistar WU rats (unpublished results), it was found that the $brain_{deep}$-to-$brain_{ECF}$ concentration ratio of quinidine was constant throughout the entire experimental period. We used this information to estimate $brain_{deep}$ concentrations during the experiment.

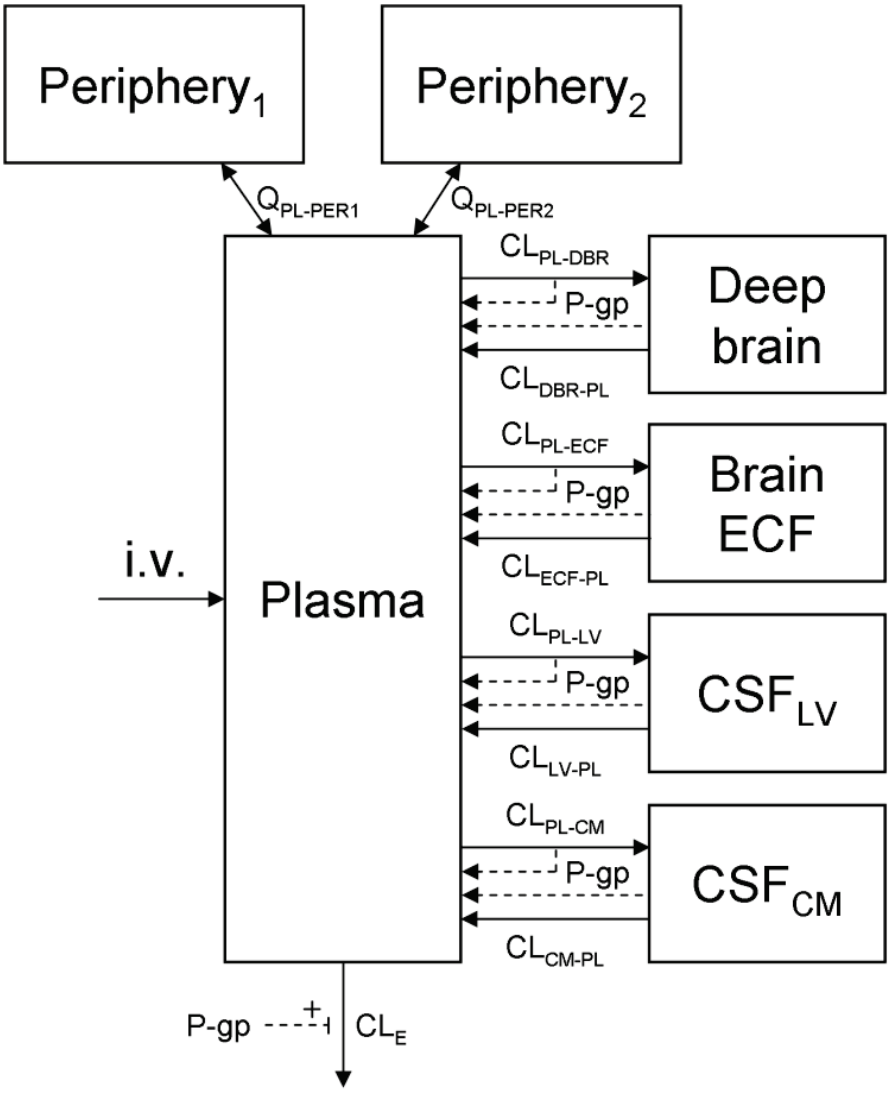

Figure 2. Diagram of the compartmental model that was used to describe the brain distribution of quinidine in the rat. CL_E is the elimination clearance from plasma, $Q_{PL\text{-}PERx}$ is the inter-compartmental clearance between plasma and the first (x=1) or second (x=2) peripheral compartment. Further, for transfer clearances between compartments ($CL_{from\ comp\text{-}to\ comp}$), denotations of the compartments are: PL = plasma; DBR = $brain_{deep}$; ECF = $brain_{ECF}$; LV = lateral ventricle; and CM = cisterna magna

Final compartmental model - The final estimation of the PK parameters of the compartmental model is summarized in table 3. The visual predictive check of the final compartmental model is given in figure 3. It can be seen that the compartmental model describes the data very well within the 90% prediction interval, and also can cope with the large inter-individual variation as observed in the different brain concentrations.

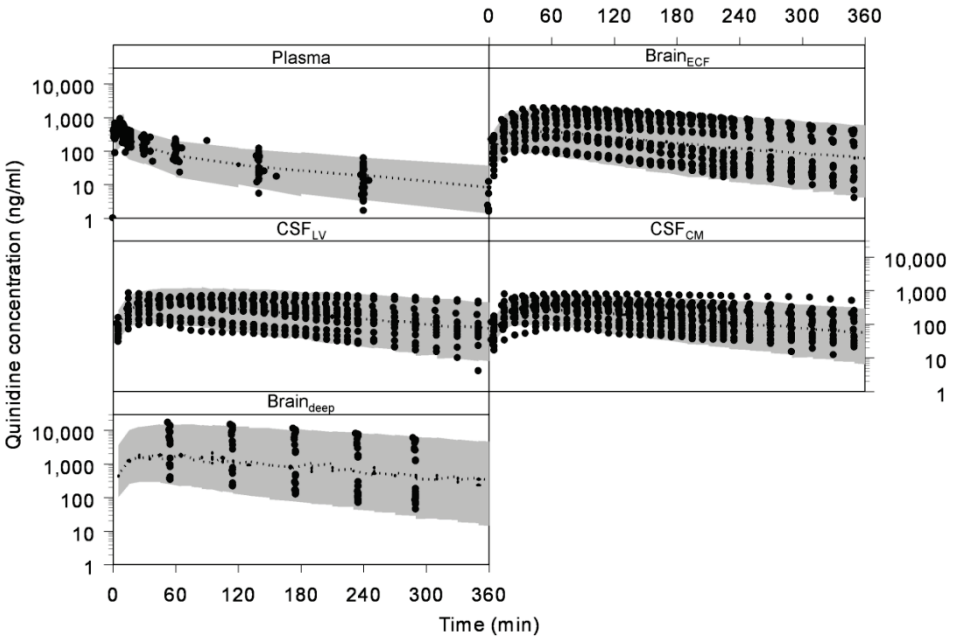

Figure 3. The visual predictive check of the compartmental model. The dots represent the individual data points and the gray area represents the 90% prediction confidence interval. The different boxes represent the plasma, brain$_{ECF}$, CSF$_{LV}$, CSF$_{CM}$ and brain$_{deep}$ data

Table 3. Final estimation of the rat PK parameters for the compartmental model (± standard error)

Parameter	Value
CL_E	158 ± 11 ml/min
P-gp effect on CL_E	1.2 ± 0.1-fold increase
$Q_{PL\text{-}PER1}$	822 ± 95 ml/min
$Q_{PL\text{-}PER2}$	171 ± 28 ml/min
$CL_{PL\text{-}DBR,p}$	1430 ± 188 µl/min
$CL_{PL\text{-}DBR,P\text{-}gp}$	1270 ± 165 µl/min
$CL_{DBR\text{-}PL,p}$	16.1 ± 1.3 µl/min
$CL_{DBR\text{-}PL,P\text{-}gp}$	17.3 ± 2.4 µl/min
$CL_{PL\text{-}ECF,p}$	36.6 ± 3.9 µl/min
$CL_{PL\text{-}ECF,P\text{-}gp}$	25.8 ± 3.7 µl/min
$CL_{ECF\text{-}PL,p}$	3.2 ± 0.2 µl/min
$CL_{ECF\text{-}PL,P\text{-}gp}$	4.4 ± 0.7 µl/min
$CL_{PL\text{-}LV,p}$	3.4 ± 0.7 µl/min
$CL_{PL\text{-}LV,P\text{-}gp}$	1.1 ± 0.3 µl/min
$CL_{LV\text{-}PL,p}$	0.4 ± 0.09 µl/min
$CL_{LV\text{-}PL,P\text{-}gp}$	0.5 ± 0.2 µl/min
$CL_{PL\text{-}CM,p}$	0.7 ± 0.08 µl/min
$CL_{PL\text{-}CM,P\text{-}gp}$	0.07 ± 0.02 µl/min
$CL_{CM\text{-}PL,p}$	0.1 ± 0.02 µl/min
$CL_{CM\text{-}PL,P\text{-}gp}$	0.2 ± 0.06 µl/min
V_{PL}	*10.6 ml* [1]
V_{PER1}	5.9 ± 0.5 l
V_{PER2}	11.7 ± 1.6 l
V_{DBR}	*1.44 ml* [2]
V_{ECF}	*290 µl* [3]
V_{LV}	*50 µl* [4,5]
V_{CM}	*17 µl* [6,7]
η_{CLE}	0.08 ± 0.02
ε_{PL}	0.13 ± 0.02
ε_{DBR}	0.06 ± 0.01
ε_{ECF}	0.05 ± 0.01
ε_{LV}	0.09 ± 0.02
ε_{CM}	0.07 ± 0.01

Parameter values in italic are derived from literature. CL_E is the elimination clearance from plasma, $Q_{PL\text{-}PERx}$ is the inter-compartmental clearance between plasma and the first (x=1) or second (x-=2) peripheral compartment. Further, for transfer clearances between compartments ($CL_{from\ comp\text{-}to\ comp}$), denotations of the compartments are: PL = plasma; ECF = $brain_{ECF}$; DBR = $brain_{deep}$; LV = lateral ventricle; and CM = cisterna magna. For plasma and brain compartments V is the physiological volume; for peripheral compartments V is the volume of distribution. η_i = inter-individual variability of parameter i; ε_j = residual error on concentrations in compartment j.

Notes to table 3 continued: The additional subscripts 'p' and 'P-gp' denote passive transport and P-gp-mediated transport, respectively.
[1] Lee and Blaufox, 1985; [2] Thorne et al., 2004; [3] Cserr et al., 1981; [4] Condon et al., 1986; [5] Kohn et al., 1991; [6] Adam and Greenberg, 1978; [7] Robertson, 1949.

Systems-based modeling approach

As it was our goal to investigate the relationship between $brain_{ECF}$ and CSF pharmacokinetics, we have applied a SBPK modeling approach. To more adequately describe CSF physiology, we have added two CSF compartments that represent the combined third and fourth ventricle (CSF_{TFV}) and the subarachnoid space (CSF_{SAS}), like we did previously for analysis of acetaminophen regional brain distribution (**Chapter 3**). Since we have no measurements of the concentrations in the third and fourth ventricle, the transfer clearance between plasma and third and fourth ventricle was assumed to be equal to the transfer clearance between plasma and lateral ventricle.

Modeling CSF flow - In our first attempt of the SBPK approach the values of the $brain_{ECF}$ flow (Q_{ECF}) and CSF flow (Q_{CSF}) were fixed to their physiological values. However, it appeared that this value for Q_{CSF} was too high for proper description of quinidine concentration in the CSF compartments. Therefore the CSF production rate was estimated. To do so, the clearance from CSF_{LV} to plasma was fixed to 0, as otherwise Q_{CSF} was estimated to be 0. Thereby, the model was 'forced' to estimate the Q_{CSF}, being 0.52 ± 0.25 µl/min. This value of Q_{CSF} was much lower than the physiological one (2.2 µl/min). An explanation for the reduced Q_{CSF} was searched for. It was found that quinidine is capable of inhibiting Na^+-K^+-ATPase activity (Ball *et al.,* 1981), which is an enzyme at the apical membrane of the choroid plexus that leads to the formation of CSF (Brown *et al.,* 2004; Ernst *et al.,* 1986). A potential influence of quinidine reducing CSF flow was investigated by a CSF quinidine concentration (C_{CSF})-dependent inhibition of Q_{CSF} by means of an E_{max} model (equation 7), in which $Q_{CSF,EF}$ was the effective CSF flow.

$$Q_{CSF,EF} = Q_{CSF} \times \left(1 - \frac{C_{CSF}}{C_{CSF} + IC_{50}}\right) \quad (7)$$

The resulting estimated IC_{50} of quinidine was 209 ± 66 ng/ml. This value was 143-fold lower than reported (~30 µg/ml (Ball *et al.,* 1981)) and therefore not considered realistic. As an alternative, we needed to fix the Q_{CSF} to its physiological value and to define the rate of transfer of quinidine from blood to CSF_{LV} and vice versa being equal.

Modeling P-gp-mediated transport - P-gp has been well described as an efflux transporter at the BBB. However, the mechanism by which P-gp can exert its effect could be by so-called efflux enhancement or influx hindrance or both. The data were best described by the model with P-gp function solely as influx hindrance or combined influx hindrance and efflux enhancement. The observation that *in vivo* probe recovery of quinidine was not affected by tariquidar would be an indication that quinidine is transported by P-gp only via the influx hindrance mechanism (Kusuhara *et al.,* 1997; Stein *et al.,* 1994; Sun *et al.,* 2001). However, as the largest reduction in the objective function value in the model was observed for a combined influx hindrance and efflux enhancement, this indicates that this model is most probably the best.

Based on the suggestion that P-gp functions as an influx transporter at the BCSFB (Kassem *et al.,* 2007; Rao *et al.,* 1999), the effect of P-gp on the clearance values between plasma and CSF was described as such. However, with our data we could not identify P-gp influx at the BCSFB. Therefore, we have tested models in which P-gp was considered to be an efflux transporter at the BCSFB or not present at the BCSFB at all. The data were best described by a model with P-gp as an efflux transporter at the BCSFB for lateral ventricle, whereas it was absent for cisterna magna.

Again, we have tried to identify T_m and K_m values for P-gp-mediated transport of the SBPK model, but without success (results not shown). Therefore, P-gp-mediated transport had to be incorporated by means of a single clearance value, rather than by T_m and K_m.

Modeling deep brain concentrations - Our assumption was that compounds, after passing the BBB and BCSFB would first enter $brain_{ECF}$, before reaching the $brain_{deep}$ compartment. However, since the $brain_{deep}$ concentrations are much higher than the $brain_{ECF}$ concentrations, and the physiological volume of the $brain_{deep}$ compartment is much larger than the $brain_{ECF}$ compartment, the mass

transfer of quinidine from plasma, via the $brain_{ECF}$ compartment, to the deep brain needs to be quite substantial. This route did not result in a model that could adequately describe the data. In contrast, a direct mass transfer from plasma into the $brain_{deep}$ compartment did. Actually, the direct route through lipid membranes seems a rather plausible explanation for a lipohilic drug like quinidine, which has a logP of 2.36 in its neutral form (Machatha and Yalkowsky, 2005).

Final SBPK model - The final SBPK model is shown in figure 4. The differential equations of this model can be found in the appendix. The final estimation of the PK parameters is summarized in table 4. Here, the parameters are the same as for table 3, with the addition of the following: $CL_{PL\text{-}TFV}$ is the clearance from plasma to CSF_{TFV}, $CL_{TFV\text{-}PL}$ is the clearance from CSF_{TFV} to plasma, Q_{ECF} is the flow rate of $brain_{ECF}$, Q_{CSF} is the flow rate of CSF, V_{TFV} is the volume of the third and fourth ventricle combined and V_{SAS} is the volume of the subarachnoid space.

The visual predictive check of the final model is given in figure 5. It can be seen that the final model describes the data very well within the 90% prediction interval, and also can cope with the large inter-individual variation in brain concentrations.

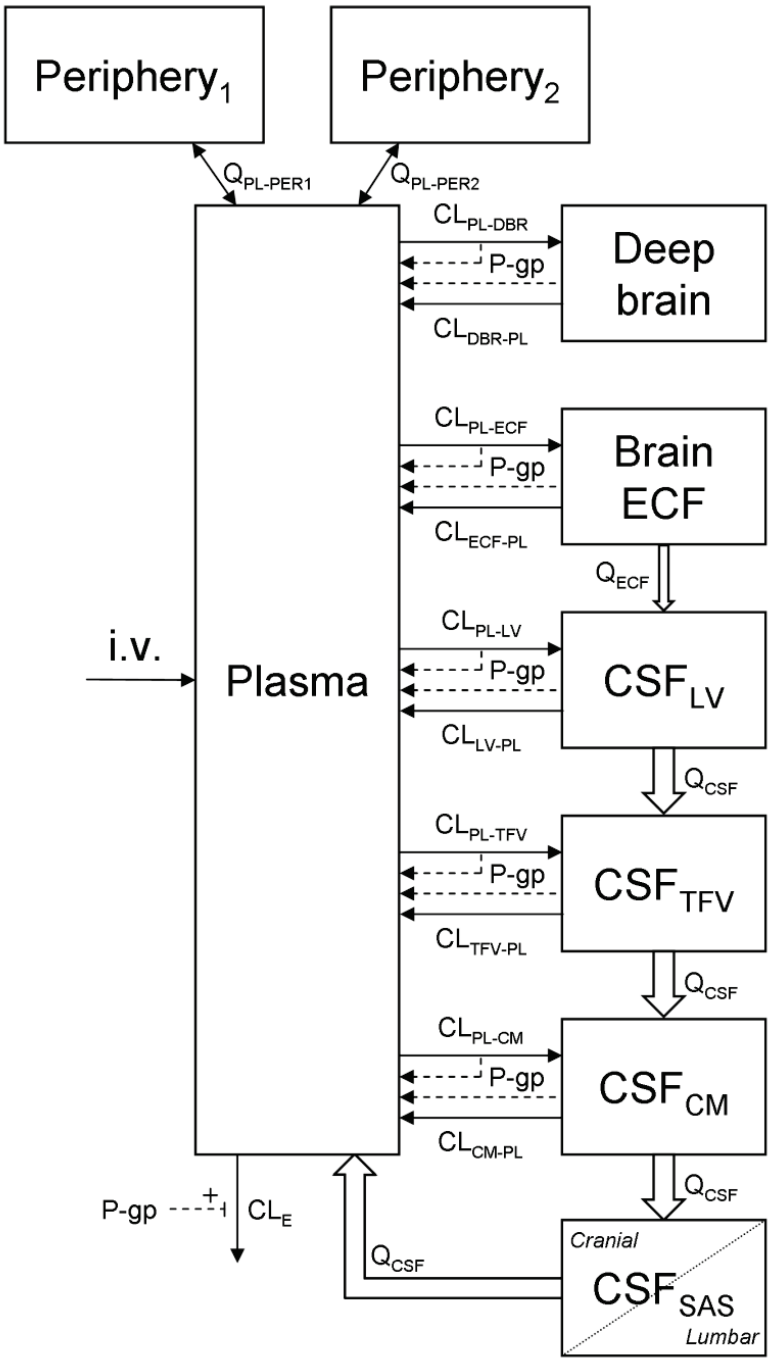
Periphery1
Periphery2
QPL-PER1
QPL-PER2
CLPL-DBR
P-gp
CLDBR-PL
Deep brain
CLPL-ECF
P-gp
CLECF-PL
Brain ECF
QECF
i.v.
Plasma
CLPL-LV
P-gp
CLLV-PL
CSFLV
QCSF
CLPL-TFV
P-gp
CLTFV-PL
CSFTFV
QCSF
CLPL-CM
P-gp
CLCM-PL
CSFCM
QCSF
P-gp
CLE
QCSF
Cranial
CSFSAS
Lumbar

Figure 4 (left). Diagram of the SBPK model that was used to describe the intra-brain distribution in the rat. CL_E is the elimination clearance from plasma, $Q_{PL\text{-}PERx}$ is the inter-compartmental clearance between plasma and the first (x=1) or second (x=2) peripheral compartment. Further, for transfer clearances between compartments ($CL_{from\ comp\text{-}to\ comp}$), denotations of the compartments are: PL = plasma; DBR = $brain_{deep}$; ECF = $brain_{ECF}$; LV = lateral ventricle; TFV = third and fourth ventricle; CM = cisterna magna and SAS = subarachnoid space. Q_{ECF} is the flow rate of $brain_{ECF}$, Q_{CSF} is the flow rate of CSF

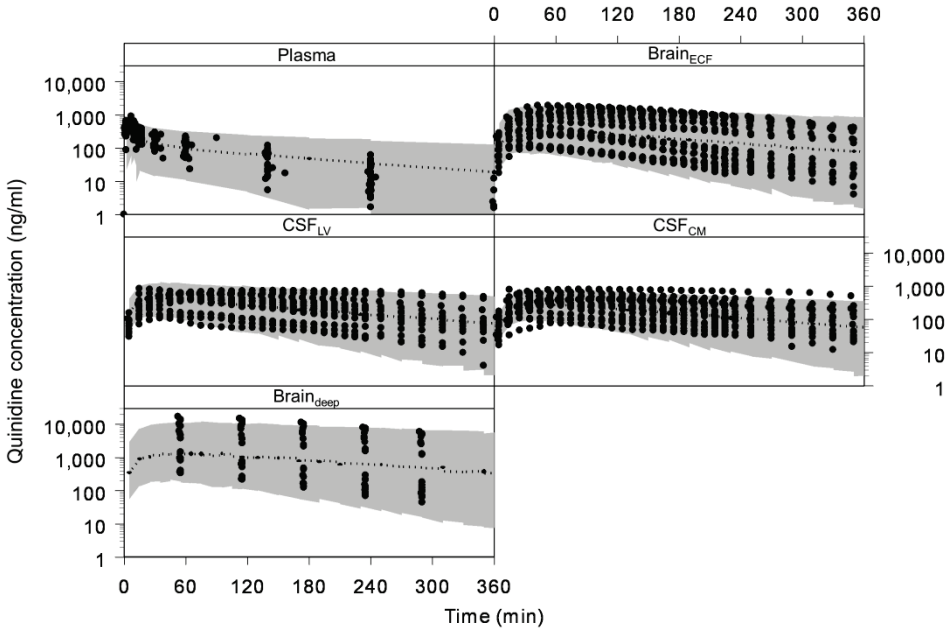

Figure 5. The visual predictive check of the final SBPK model. The dots represent the individual data points and the gray area represents the 90% prediction confidence interval. The x-axis represents the time (min) and the y-axis represents the quinidine concentrations (ng/ml). The different boxes represent the plasma, $brain_{ECF}$, CSF_{LV}, CSF_{CM} and $brain_{deep}$ data, respectively

Table 4. Final estimation of the rat PK parameters for the different SBPK models (± standard error)

Parameter	efflux enhancement	influx hindrance	efflux enhancement and influx hindrance
Objective function value	18105	18030	17969
CL_E	81.6 ± 11.4 ml/min	87.4 ± 10.5 ml/min	95.9 ± 11.0 ml/min
P-gp effect on CL_E	1.9 ± 0.2-fold increase	2.1 ± 0.3-fold increase	1.9 ± 0.2-fold increase
$Q_{PL\text{-}PER1}$	1520 ± 177 ml/min	1150 ± 138 ml/min	1190 ± 135 ml/min
$Q_{PL\text{-}PER2}$	84.2 ± 57.6 ml/min	360 ± 105 ml/min	333 ± 94 ml/min
$CL_{PL\text{-}DBR,p}$	1540 ± 182 µl/min	2670 ± 501 µl/min	2180 ± 384 µl/min
$CL_{PL\text{-}DBR,P\text{-}gp}$	N.A.	2430 ± 466 µl/min	1900 ± 373 µl/min
$CL_{DBR\text{-}PL,p}$	17.8 ± 1.5 µl/min	48.5 ± 9.6 µl/min	37.2 ± 7.2 µl/min
$CL_{DBR\text{-}PL,P\text{-}gp}$	253 ± 40.4 µl/min	N.A.	19.6 ± 10.9 µl/min
$CL_{PL\text{-}ECF,p}$	48.6 ± 6.3 µl/min	68.4 ± 9.1 µl/min	50.2 ± 5.0 µl/min
$CL_{PL\text{-}ECF,P\text{-}gp}$	N.A.	54.8 ± 8.1 µl/min	33.8 ± 5.1 µl/min
$CL_{ECF\text{-}PL,p}$	7.1 ± 1.2 µl/min	9.3 ± 1.4 µl/min	6.3 ± 0.8 µl/min
$CL_{ECF\text{-}PL,P\text{-}gp}$	33.1 ± 8.1 µl/min	N.A.	5.3 ± 1.7 µl/min
$CL_{PL\text{-}LV,p}$	7.2 ± 0.8 µl/min	8.4 ± 0.8 µl/min	9.0 ± 0.9 µl/min
$CL_{PL\text{-}LV,P\text{-}gp}$	N.A.	3.0 ± 0.7 µl/min	3.8 ± 0.8 µl/min
$CL_{LV\text{-}PL,p}$	0.03 ± 0.01 µl/min	0.04 ± 0.01 µl/min	0.04 ± 0.01 µl/min
$CL_{LV\text{-}PL,P\text{-}gp}$	1.2 ± 0.4 µl/min	N.A.	0 µl/min
$CL_{PL\text{-}CM,p}$	1.3 ± 0.3 µl/min	1.1 ± 0.3 µl/min	1.1 ± 0.3 µl/min
$CL_{PL\text{-}CM,P\text{-}gp}$	N.A.	0 µl/min	0 µl/min
$CL_{CM\text{-}PL,p}$	3.7 ± 0.5 µl/min	4.0 ± 0.5 µl/min	4.1 ± 0.5 µl/min
$CL_{CM\text{-}PL,P\text{-}gp}$	0 µl/min	N.A.	0 µl/min
Q_{ECF}	*0.2 µl/min* [1,2]	*0.2 µl/min* [1,2]	*0.2 µl/min* [1,2]
Q_{CSF}	*2.2 µl/min* [3]	*2.2 µl/min* [3]	*2.2 µl/min* [3]
V_{PL}	*10.6 ml* [4]	*10.6 ml* [4]	*10.6 ml* [4]
V_{PER1}	13.2 ± 1.8 l	6.4 ± 1.6 l	6.8 ± 1.7 l
V_{PER2}	5.8 ± 2.6 l	13.9 ± 2.0 l	13.3 ± 2.2 l
V_{DBR}	*1.44 ml* [5]	*1.44 ml* [5]	*1.44 ml* [5]
V_{ECF}	*290 µl* [6]	*290 µl* [6]	*290 µl* [6]
V_{LV}	*50 µl* [7,8]	*50 µl* [7,8]	*50 µl* [7,8]
V_{TFV}	50 µl [9]	50 µl [9]	50 µl [9]
V_{CM}	*17 µl* [10,11]	*17 µl* [10,11]	*17 µl* [10,11]
V_{SAS}	*180 µl* [9,12]	*180 µl* [9,12]	*180 µl* [9,12]
η_{CLE}	0.20 ± 0.09	0.16 ± 0.08	0.14 ± 0.06
ε_{PL}	0.29 ± 0.04	0.22 ± 0.02	0.22 ± 0.03
ε_{DBR}	0.06 ± 0.01	0.07 ± 0.02	0.07 ± 0.02
ε_{ECF}	0.07 ± 0.01	0.07 ± 0.01	0.06 ± 0.01
ε_{LV}	0.10 ± 0.01	0.10 ± 0.01	0.11 ± 0.02
ε_{CM}	0.06 ± 0.01	0.07 ± 0.01	0.08 ± 0.02

Notes to table 4: Parameter values in italic are derived from literature; N.A. implicates that the parameter is not available in the specific model. CL_E is the elimination clearance from plasma, $Q_{PL\text{-}PERx}$ is the inter-compartmental clearance between plasma and the first (x=1) or second (x-=2) peripheral compartment. Further, for transfer clearances between compartments ($CL_{from\ comp\text{-}to\ comp}$), denotations of the compartments are: PL = plasma; ECF = $brain_{ECF}$; DBR = $brain_{deep}$; LV = lateral ventricle; and CM = cisterna magna. For plasma and brain compartments, V = physiological volume; for peripheral compartments, V = volume of distribution. η_i = inter-individual variability of parameter i; ε_j = residual error on concentrations in compartment j. The additional subscripts 'p' and 'P-gp' denote passive transport and P-gp-mediated transport, respectively.
[1] Abbott, 2004; [2] Cserr et al., 1981; [3] Cserr, 1965; [4] Lee and Blaufox, 1985; [5] Thorne et al., 2004; [6] Cserr et al., 1981; [7] Condon et al., 1986; [8] Kohn et al., 1991; [9] Levinger, 1971; [10] Adam and Greenberg, 1978; [11] Robertson, 1949; [12] Bass and Lundborg, 1973.

DISCUSSION

In the development of CNS-targeted drugs, the prediction of human CNS target exposure is a big challenge. While CSF concentrations are often considered to be the best available surrogate for brain target site concentrations in humans, a generally applicable relationship between CSF concentrations and $brain_{ECF}$ concentrations does not exist (**Chapter 1**; De Lange and Danhof, 2002; Lin, 2008; Shen *et al.,* 2004). Previous studies have indicated that, at steady-state conditions, CSF to $brain_{ECF}$ concentration ratios were between 3-fold (either higher or lower) for compounds that freely diffuse across the BBB and BCSFB, while for compounds being brain barrier transporter substrates the difference may be higher (Fridén *et al.,* 2009; Kalvass and Maurer, 2002; Liu *et al.,* 2006; Liu *et al.,* 2009; Maurer *et al.,* 2005). Combining their data showed that 24% (21/89) of the P-gp substrates had a CSF/$brain_{ECF}$ concentration ratio larger than 3. Then, prediction of $brain_{ECF}$ concentrations on the basis of CSF concentrations gets inadequate. This indicates that we need to improve our understanding of the impact of P-gp functionality at the brain barriers in order to be able to predict human CNS $brain_{ECF}$ concentrations.

By using the multiple microdialysis probes approach (**Chapter 3**), we investigated the direct relationships between brain striatum concentrations and those in different CSF locations, and unbound plasma concentrations in the rat. We have focused on P-gp-mediated efflux transport functionality at the BBB,

whereas it has been reported to function as an influx transporter at the BCSFB (Kassem *et al.,* 2007; Rao *et al.,* 1999). This could have major implications for the relationship between CSF concentrations and $brain_{ECF}$ concentrations for compounds that are substrates for P-gp-mediated transport. To investigate the specific contribution of P-gp-mediated transport, quinidine was used as a paradigm P-gp substrate, with inhibition of P-gp by co-administration of tariquidar. Tariquidar is known to inhibit P-gp with a half-maximum inhibition constant (IC_{50}) of approximately 25 ng/ml (Mistry *et al.,* 2001). Previous work by Bankstahl *et al.* (2008), and Syvänen *et al*. (2011) have indicated that a 15 mg/kg dose of tariquidar results in plasma and brain concentrations over 50-fold higher than the IC_{50} value up to 3 hours after administration. Therefore, it is plausible to assume that the dose of tariquidar is sufficient to fully inhibit P-gp throughout the entire experimental period. Advanced mathematical modeling was used to finally determine the interaction between systems physiology and quinidine. Our key findings indicated that: 1) $brain_{ECF}$- and CSF-to-unbound plasma $AUC_{0\text{-}360}$ ratios were all over 100%, indicating influx transport by using unbound concentrations; 2) P-gp also restricts brain intracellular exposure; 3) a direct transport route of quinidine from plasma to brain cells exists; 4) P-gp-mediated efflux of quinidine at the BBB seems to result of combined efflux enhancement and influx hindrance; 5) P-gp at the BCSFB at the level of the lateral ventricle functions as an efflux transporter or, at the cisterna magna, is not functioning at all.

In previous studies $brain_{ECF}$ concentrations were estimated on the basis of total brain concentrations and the brain unbound fraction, determined by equilibrium dialysis of drug-spiked brain homogenates (Kalvass and Maurer, 2002; Liu *et al.,* 2006; Maurer *et al.,* 2005). However, brain tissue homogenization destroys cell structures unmasking binding sites that are normally not accessible to a drug (Liu *et al.,* 2009), potentially leading to underestimation of the *in vivo* brain unbound fraction. The use of the brain slice technique is an improvement (Kakee *et al.,* 1996). Liu *et al.* (2006), and Fridén *et al.* (2009), have applied this technique to calculate the brain unbound fraction, being further used to estimate $brain_{ECF}$ concentrations. Comparison of the brain homogenate method with brain slice technique indicated that the brain unbound fraction was over 50% different for 5 out of 7 compounds (Liu *et al.,* 2006). Liu *et al.* (2009) have later applied the microdialysis technique for direct

measurement of unbound $brain_{ECF}$ concentrations and compared those to CSF concentrations sampled at steady-state. They found that the ratio of CSF over $brain_{ECF}$ concentrations was larger for 1 out of the 7 P-gp substrates.

To our surprise, we found that unbound quinidine concentrations in brain were significantly higher than unbound concentrations in plasma. This appears to be in contrast to previous studies by Liu *et al.* (2009), and Kodaira *et al.* (2011), in which unbound brain-to-unbound plasma ($brain_u/plasma_u$) concentration ratios at assumed steady state were well below unity. While our results were quite comparable to the results of Liu *et al.* (2009), and Kodaira *et al.* (2011), a substantial difference was found for the (calculated) unbound brain (ECF) concentrations between these studies, and ours. Liu *et al.* (2009) determined the brain free fraction with the brain homogenate method and found an unbound brain fraction comparable to the unbound brain fraction that was found by Kodaira *et al.* (2011) by the brain slice technique (3.6% and 2.4%, respectively). In contrast, the unbound brain fraction in our study was calculated to be 28% ($brain_{ECF}$ concentration divided by the total brain concentration). However, Liu *et al.* (2009) reported a 3-fold difference in the $brain_u$ concentrations when calculated on the basis of the brain homogenate free fraction, compared to using microdialysis data when corrected for *in vitro* recovery. We measured both *in vitro* (33%) and *in vivo* recovery (9%), and found that the *in vivo* recovery was 3.5-fold lower. If we would calculate the $brain_{ECF}/plasma_u$ concentration ratio at maximal concentrations, like Liu *et al.* did, and assume that for Liu also a 3.5-fold lower *in vivo* recovery would apply, then the $brain_{ECF}/plasma_u$ concentration ratio would be comparable to ours.

For the $brain_{ECF}/plasma_u$ $AUC_{0\text{-}360}$ ratios, we found values significantly larger than unity as in the elimination phase the rate of decline in plasma concentrations was larger than those observed in CSF and $brain_{ECF}$. We cannot compare these findings with Kodaira and Liu because their studies did not include an elimination phase.

Therefore, based on our data, it appears that quinidine is also transported by other transporters at the BBB and BCSFB, in the direction of the brain. However, there is no direct information in literature to support this. We could only find the following potential contributions: Van Montfoort *et al.* (2001) reported that quinidine is transported by organic cation transporters (OCTs). This observation was made in an *in vitro* study, and was found to occur for a pH

of 6, but not significantly at pH 7.4. The question remains how this relates to the *in vivo* situation, like ours. Giacomini *et al.* (2010) stated that quinidine is a potential inhibitor of OCTs. OCTs have been localized both at the BBB (Lin *et al.,* 2010), as well as at the BCSFB (Choudhuri *et al.,* 2003). Thus, the possibility of active influx transport for quinidine at the BBB and BCSFB remains to be further investigated. Alternatively, it could reflect a passive "ion-trapping" process, governed by lower pH values in $brain_{ECF}$ (pH=~7.3) than in plasma (pH=~7.4). However, as quinidine is a diprotic base with pKas 4.2 and 7.9 (Varma and Panchagnula, 2005), the low difference between the % ionized at pH=7.3 (80%) and pH=7.4 (76%) does not seem to explain our findings.

According to the "smaller than 3-fold concentration ratio paradigm" (Maurer *et al.,* 2005), differences between $brain_{ECF}$ and CSF concentrations of quinidine as found in this study (on average 0.72 ± 0.20) would be considered pharmacokinetically irrelevant. However, upon co-administration of tariquidar this ratio increased 3.1-fold (to the value of 2.22 ± 0.57). This means that P-gp functionality and variations thereof may have an important effect on the $brain_{ECF}$-CSF ratio and the extrapolation from rats to humans, as is discussed by De Lange (2013a; 2013b). However, quinidine is a strong P-gp substrate and it remains to be investigated what the impact of P-gp functionality on the $brain_{ECF}$-CSF concentration relationships would be for weaker substrates.

Several different models for P-gp-mediated transport have been suggested (Higgins and Gottesman, 1992; Kusuhara *et al.,* 1997; Sahrom, 1997; Sharom, 2006; Stein *et al.,* 1994; Sun *et al.,* 2001; Syvänen *et al.,* 2006). The first model is described as the "classical pump model" in which a P-gp substrate is transported from the cytosol to the extracellular space against a concentration gradient (so-called "efflux enhancement") (Higgins and Gottesman, 1992; Sharom, 1997; Sharom, 2006; Stein *et al.,* 1994; Syvänen *et al.,* 2006). The second model can be described as a "vacuum cleaner model" in which a lipophilic compound that is diffusing across the cellular membrane, is interacting with P-gp within the lipid bilayer of the cellular membrane and is then transported back into the extracellular space (Higgins and Gottesman, 1992; Kusuhara *et al.,* 1997; Sharom, 1997; Sharom, 2006). The third model is described as the "flippase model" in which a lipophilic compound within the lipid bilayer at the cytosolic side is flipped to the extracellular side where it diffuses back into the extracellular space (Higgins and Gottesman, 1992;

Sharom, 1997; Sharom, 2006; Stein *et al.,* 1994; Sun *et al.,* 2001; Syvänen *et al.,* 2006). In the second and third model P-gp prevents the entry of compounds to the brain by a process which is called "influx hindrance". Based on the SBPK modeling results, it appears that for quinidine P-gp acts via combined influx hindrance and efflux enhancement. This is in line with the localization of P-gp at both the luminal and abluminal membrane of the BBB (Bendayan *et al.,* 2006).

For the potential role of P-gp at the BCSFB, there have been some indications that P-gp could function as an influx transporter at the BCSFB (Kassem *et al.,* 2007; Rao *et al.,* 1999). We anticipated this to be among our findings, however, with our data we could not identify P-gp influx at the level of the BCSFB. Instead, the results of the SBPK modeling suggest that P-gp at the BCSFB functions as an efflux transporter (lateral ventricle) or is not functioning at all (cisterna magna).

Then, interestingly, the co-administration of tariquidar results in an increase of the total brain-to-brain$_{ECF}$ concentration ratio, which has also been observed in an earlier study on quinidine at our lab by Syvänen *et al.* (2012). This indicates that P-gp is also located beyond the BBB at the parenchymal and perivascular astrocytes, which is in line with several reports (Declèves *et al.,* 2000; Golden and Pardridge, 2000; Pardridge *et al.,* 1997; Seegers *et al.,* 2002a; Seegers *et al.,* 2002b; Volk *et al.,* 2005).

In our current study we obtained in parallel brain striatum, CSF and plasma$_u$ concentration-time profiles, under dynamic conditions, included corrections for *in vivo* probe recoveries, and plasma protein binding to finally obtain unbound concentrations in these body compartments. It is anticipated that this approach, combined with advanced mathematical modeling, will further improve revealing the mechanisms underlying the relationship between brain$_{ECF}$ and CSF concentrations than will steady-state and/or single end-of-experiment CSF concentrations (Kielbasa *et al.,* 2009). Having information on concentration-time profiles following a single administration is relevant as we need time-dependent data to decipher the rate and extent of processes of drug transport into, within, and out of the brain (Hammarlund-Udenaes *et al.,* 2008). It provides the best basis to further explore the multiple dose regimens as used in the clinic, for which it is know that a true steady state condition is actually not reached.

Finally, in striving towards reduction on the use of animals on one hand, and the fact that systematic studies on the inter-relationship of plasma PK, BBB transport and intra-brain distribution, cannot be performed in human, the use of the multiple microdialysis probes approach, obtaining a total of 84 samples per animal, results in a great reduction in the number of animals required for these type of studies compared to the single time point measurements.

CONCLUSION

It is concluded that in parallel obtained data on unbound $brain_{ECF}$, CSF and $plasma_u$ concentrations, under dynamic conditions, combined with advanced mathematical modeling is a most valid approach to reveal the mechanisms underlying the relationship between $brain_{ECF}$ and CSF concentrations, which is significantly influenced by activity of P-gp. This indicates that information on functionality of P-gp is important for the prediction of human brain target site concentrations of P-gp substrates on the basis of human CSF concentrations, and provides further guide to unravelling mechanisms and drug properties that govern the transport into, within, and out of the brain, for translational purposes.

APPENDIX

DIFFERENTIAL EQUATIONS

The mass balance equations describing the final SBPK model were expressed as follows:

Plasma:

$$\frac{dA_{PL,u}}{dt} = dose - k_{PL-PER1} \times A_{PL,u} + k_{PER1-PL} \times A_{PER1} - k_{PL-PER2} \times A_{PL,u}$$
$$+k_{PER2-PL} \times A_{PER2} - k_{PL-DBR} \times A_{PL,u} + k_{DBR-PL} \times A_{DBR} - k_{PL-ECF} \times A_{PL,u}$$
$$+k_{ECF-PL} \times A_{ECF} - k_{PL-LV} \times A_{PL,u} + k_{LV-PL} \times A_{LV} - k_{PL-TFV} \times A_{PL,u}$$

$$+k_{TFV-PL} \times A_{TFV} - k_{PL-CM} \times A_{PL,u} + k_{CM-PL} \times A_{CM} + \left(\frac{Q_{CSF}}{V_{SAS}}\right) \times A_{SAS} - k_E \times A_{PL,u}$$

$$C_{PL,u} = \frac{A_{PL,u}}{V_{PL}}$$

Periphery:

$$\frac{dA_{PER1}}{dt} = k_{PL-PER1} \times A_{PL,u} - k_{PER1-PL} \times A_{PER1}$$

$$C_{PER1} = \frac{A_{PER1}}{V_{PER1}}$$

$$\frac{dA_{PER2}}{dt} = k_{PL-PER2} \times A_{PL,u} - k_{PER2-PL} \times A_{PER2}$$

$$C_{PER2} = \frac{A_{PER2}}{V_{PER2}}$$

$Brain_{deep}$:

$$\frac{dA_{DBR}}{dt} = k_{PL-DBR} \times A_{PL,u} - k_{DBR-PL} \times A_{DBR}$$

$$C_{DBR} = \frac{A_{DBR}}{V_{DBR}}$$

$Brain_{ECF}$:

$$\frac{dA_{ECF}}{dt} = k_{PL-ECF} \times A_{PL,u} - k_{ECF-PL} \times A_{ECF} - \left(\frac{Q_{ECF}}{V_{ECF}}\right) \times A_{ECF}$$

$$C_{ECF} = \frac{A_{ECF}}{V_{ECF}}$$

CSF_{LV}:

$$\frac{dA_{LV}}{dt} = k_{PL-LV} \times A_{PL,u} - k_{LV-PL} \times A_{LV} + \left(\frac{Q_{ECF}}{V_{ECF}}\right) \times A_{ECF} - \left(\frac{Q_{CSF}}{V_{LV}}\right) \times A_{LV}$$

$$C_{LV} = \frac{A_{LV}}{V_{LV}}$$

CSF_{TFV}:

$$\frac{dA_{TFV}}{dt} = k_{PL-TFV} \times A_{PL,u} - k_{TFV-PL} \times A_{TFV} + \left(\frac{Q_{CSF}}{V_{LV}}\right) \times A_{LV} - \left(\frac{Q_{CSF}}{V_{TFV}}\right) \times A_{TFV}$$

$$C_{TFV} = \frac{A_{TFV}}{V_{TFV}}$$

CSF_{CM}:

$$\frac{dA_{CM}}{dt} = k_{PL-CM} \times A_{PL,u} - k_{CM-PL} \times A_{CM} + \left(\frac{Q_{CSF}}{V_{TFV}}\right) \times A_{TFV} - \left(\frac{Q_{CSF}}{V_{CM}}\right) \times A_{CM}$$

$$C_{CM} = \frac{A_{CM}}{V_{CM}}$$

CSF_{SAS}:

$$\frac{dA_{SAS}}{dt} = \left(\frac{Q_{CSF}}{V_{CM}}\right) \times A_{CM} - \left(\frac{Q_{CSF}}{V_{SAS}}\right) \times A_{SAS}$$

$$C_{SAS} = \frac{A_{SAS}}{V_{SAS}}$$

Where:

$$k_E = \frac{CL_{E,p} + CL_{E,P-gp}}{V_{PL}}$$

$$k_{PL-PER1} = \frac{Q_{PL-PER1}}{V_{PL}}$$

$$k_{PER1-PL} = \frac{Q_{PL-PER1}}{V_{PER1}}$$

$$k_{PL-PER2} = \frac{Q_{PL-PER2}}{V_{PL}}$$

$$k_{PER2-PL} = \frac{Q_{PL-PER2}}{V_{PER2}}$$

$$k_{PL-DBR} = \frac{CL_{PL-DBR,p} - CL_{PL-DBR,P-gp}}{V_{PL}}$$

$$k_{DBR-PL} = \frac{CL_{DBR-PL,p} + CL_{DBR-PL,P-gp}}{V_{DBR}}$$

$$k_{PL-ECF} = \frac{CL_{PL-ECF,p} - CL_{PL-ECF,P-gp}}{V_{PL}}$$

$$k_{ECF-PL} = \frac{CL_{ECF-PL,p} + CL_{ECF-PL,P-gp}}{V_{ECF}}$$

$$k_{PL-LV} = \frac{CL_{PL-LV,p} - CL_{PL-LV,P-gp}}{V_{PL}}$$

$$k_{LV-PL} = \frac{CL_{LV-PL,p} + CL_{LV-PL,P-gp}}{V_{LV}}$$

$$k_{PL-TFV} = \frac{CL_{PL-TFV,p} - CL_{PL-TFV,P-gp}}{V_{PL}}$$

$$k_{TFV-PL} = \frac{CL_{TFV-PL,p} + CL_{TFV-PL,P-gp}}{V_{TFV}}$$

$$k_{PL-CM} = \frac{CL_{PL-CM,p} - CL_{PL-CM,P-gp}}{V_{PL}}$$

$$k_{CM-PL} = \frac{CL_{CM-PL,p} + CL_{CM-PL,P-gp}}{V_{CM}}$$

NOMENCLATURE

A_i	Amount of quinidine in compartment i (ng)
C_i	Concentration of quinidine in compartment i (ng/ml)
k	rate constant (min^{-1})
Q	flow rate (ml/min)
CL	clearance (ml/min)
V	volume (ml)

Subscripts

PL	plasma
PL,u	unbound quinidine in plasma
PERi	peripheral compartment i
DBR	$brain_{deep}$
ECF	$brain_{ECF}$
CSF	CSF
LV	lateral ventricle

TFV third and fourth ventricle
CM cisterna magna
SAS subarachnoid space

REFERENCES

Abbott NJ. Evidence for bulk flow of brain interstitial fluid: significance for physiology and pathology. Neurochem Int 2004; 45: 545-552.

Adam R, Greenberg JO. The mega cisterna magna. J Neurosurg 1978; 48: 190-192.

Ball WJ Jr, Tse-Eng D, Wallick ET, Bilezikian JP, Schwartz A, Butler VP. Effect of quinidine on the digoxin receptor in vitro. J Clin Invest 1981; 68: 1065-1074.

Bankstahl JP, Kuntner C, Abrahim A, Karch R, Stanek J, Wanek T, Wadsak W, Kletter K, Müller M, Löscher W, Langer O. Tariquidar-induced P-glycoprotein inhibition at the rat blood-brain barrier studied with (R)-^{11}C-Verapamil and PET. J Nucl Med 2008; 49: 1328-1335.

Bass NH, Lundborg P. Postnatal development of bulk flow in the cerebrospinal fluid system of the albino rat: clearance of carboxyl-[14C]inulin after intrathecal infusion. Brain Res 1973; 52: 323-332.

Bendayan R, Ronaldson PT, Gingras D, Bendayan M. In situ localization of P-glycoprotein (ABCB1) in human and rat brain. J Histochem Cytochem 2006; 54: 1159-1167.

Betz AL, Goldstein GW. Specialized properties and solute transport in brain capillaries. Annu Rev Physiol 1986; 48: 241-250.

Brown PD, Davies SL, Speake T, Millar ID. Molecular mechanisms of cerebrospinal fluid production. Neurosci 2004; 129: 957-970.

Choudhuri S, Cherrington NJ, Li N, Klaassen CD. Constitutive expression of various xenobiotic and endobiotic transporter mRNAs in the choroid plexus of rats. Drug Metab Dispos 2003; 31: 1337-1345.

Condon P, Patterson J, Wyper D, Hadley D, Grant R, Teasdale G, Rowan J. Use of magnetic resonance imaging to measure intracranial cerebrospinal fluid volume. Lancet 1986; 327: 1355-1357.

Cox EH, Veyrat-Follet C, Beal SL, Fuseau E, Kenkare S, Sheiner LB. A population pharmacokinetic-pharmacodynamic analysis of repeated measures time-to-event

pharmacodynamic responses: the antiemetic effect of ondansetron. J Pharmacokinet Biopharm 1999; 27: 625-644.

Cserr HF. Potassium exchange between cerebrospinal fluid, plasma, and brain. Am J Physiol 1965; 209: 1219-1226.

Cserr HF, Cooper DN, Suri PK, Patlak CS. Efflux of radiolabeled polyethylene glycols and albumin from rat brain. Am J Physiol 1981; 240: F319-F28.

Danhof M, de Jongh J, de Lange ECM, Della Pasqua OE, Ploeger BA, Voskuyl RA. Mechanism-based pharmacokinetic-pharmacodynamic modeling: biophase distribution, receptor theory, and dynamical systems analysis. Annu Rev Pharmacol Toxicol 2007; 47: 357-400.

De Lange ECM. Utility of CSF in translational neuroscience. J Pharmacokinet Pharmacodyn. 2013a; 40: 315-26.

De Lange ECM. The mastermind approach to CNS drug therapy: translational prediction of human brain distribution, target site kinetics, and therapeutic effects. Fluids Barriers CNS 2013b; 10: 12.

De Lange ECM, Danhof M. Considerations in the use of cerebrospinal fluid pharmacokinetic to predict brain target concentrations in the clinical setting. Implications of the barriers between blood and brain. Clin Pharmacokinet 2002; 41: 691-703.

De Lange ECM, Danhof M, de Boer AG, Breimer DD. Methodological Considerations of Intracerebral Microdialysis in Pharmacokinetic Studies on Drug Transport Across the Blood-Brain Barrier. Brain Res Rev 1997; 25: 27-49.

De Lange ECM, de Boer AG, Breimer DD. Methodological issues in microdialysis sampling for pharmacokinetic studies. Adv Drug Del Rev 2000; 45: 125-148.

Declèves X, Regina A, Laplanche JL, Roux F, Boval B, Launay JM, Scherrmann JM. Functional expression of P-glycoprotein and multidrug resistance-associated protein (Mrp1) in primary cultures of rat astrocytes. J Neurosci Res 2000; 60: 594-602.

Doran A, Obach RS, Smith BJ, Hosea NA, Becker S, Callegari E, Chen C, Chen X, Choo E, Cianfrogna J, Cox LM, Gibbs JP, Gibbs MA, Hatch H, Hop CECA, Kasman IN, LaPerle J, Liu JH, Liu X, Logman M, Maclin D, Nedza FM, Nelson F, Olson E, Rahematpura S, Raunig D, Rogers S, Schmidt K, Spracklin DK, Szewc M, Troutman M, Tseng E, Tu M, Van Deusen JW, Venkatakrishnan K, Walens G, Wang, EQ, Wong D, Yasgar AS, Zhang C. The impact of P-glycoprotein on the disposition of drugs targeted for indications of the central nervous system: evaluation using the mdr1a/1b knockout mouse model. Drug Metab Dispos 2005; 33: 165-174.

Duffull SB, Aarons L. Development of a sequential linked pharmacokinetic and pharmacodynamic simulation model for ivabradine in healthy volunteers. Eur J Pharm Sci 2000; 10: 275-284.

Ernst SA, Palacios JR 2nd, Siegel GJ. Immunocytochemical localization of Na+,K+-ATPase catalytic polypeptide in mouse choroid plexus. J Histochem Cytochem 1986; 34: 189-195.

Fox E, Bates SE. Tariquidar (XR9576): a P-glycoprotein drug efflux pump inhibitor. Expert Rev Anticancer Ther 2007; 7: 447-459.

Fridén M, Winiwarter S, Jerndal G, Bengtsson O, Wan H, Bredberg U, Hammarlund-Udenaes M, Antonsson M. Structure—Brain exposure relationships in rat and human using a novel data set of unbound drug concentrations in brain interstitial and cerebrospinal fluids. J Med Chem 2009; 52: 6233-6243.

Giacomini KM, Huang S-M, Tweedie DJ, Benet LZ, Brouwer KLR, Chu X, Dahlin A, Evers R, Fischer V, Hillgren KM, Hoffmaster KA, Ishikawa T, Keppler D, Kim RB, Lee CA, Niemi M, Polli JW, Sugiyama Y, Swaan PW, Ware JA, Wright SH, Wah Yee S, Zamek-Gliszczyncski MJ, Zhang L. Membrane transporters in drug development. Nat Rev Drug Discov 2010; 9: 215-236.

Golden PL, Pardridge WM. Brain microvascular P-glycoprotein and a revised model of multidrug resistance in brain. Cell Mol Neurobiol 2000; 20: 165-181.

Hammarlund-Udenaes M. Active-site concentrations of chemicals – are they a better predictor of effect than plasma/organ/tissue concentrations? Basic Clin Pharmacol Toxicol 2009; 106: 215-220.

Hammarlund-Udenaes M, Fridén M, Syvänen S, Gupta A. On The Rate and Extent of Drug Delivery to the Brain. Pharm Res 2008; 25: 1737-1750.

Hammarlund-Udenaes M, Bredberg U, Fridén M. Methodologies to assess brain drug delivery in lead optimization. Curr Top Med Chem 2009; 9: 148-162.

Harashima H, Sawada Y, Sugiyama Y, Iga T, Hanano M. Analysis of nonlinear tissue distribution of quinidine in rats by physiologically based pharmacokinetics. J Pharmacokinet Biopharm 1985; 13: 425-440.

Higgins CF, Gottesman MM. Is the multidrug transporter a flippase? Trends Biochem Sci 1992; 17: 18-21.

Kakee A, Terasaki T, Sugiyama Y. Brain efflux index as a novel method of analyzing efflux transport at the blood-brain barrier. J Pharmacol Exp Ther 1996; 277: 1550-1559.

Kalvass JC, Maurer TS. Influence of nonspecific brain and plasma binding of CNS exposure: Implications for rational drug discovery. Biopharm Drug Dispos 2002; 23: 327-338.

Kassem NA, Deane R, Segal MB, Chen RL, Preston JE. Thyroxine (T_4) transfer from CSF to choroid plexus and ventricular brain regions in rabbit: Contributory role of P-glycoprotein and organic anion transporting polypeptides. Brain Res 2007; 1181: 44-50.

Keep RF, Jones HC. A morphometric study on the development of the lateral ventricle choroid plexus, choroid plexus capillaries and ventricular ependyma in the rat. Dev Brain Res 1990; 56: 47-53.

Kielbasa W, Kalvass JC, Stratford R. Microdialysis evaluation of atomoxetine brain penetration and central nervous system pharmacokinetics in rats. Drug Metab Dispos 2009; 37: 137-142.

Kodaira H, Kusuhara H, Fujita T, Ushiki J, Fuse E, Sugiyama Y. Quantitative evaluation of the impact of active efflux by P-glycoprotein and breast cancer resistance protein at the blood-brain barrier on the predictability of the unbound concentrations of drugs in the brain using cerebrospinal fluid concentrations as a surrogate. J Pharmacol Exp Ther 2011; 339: 935-944.

Kohn MI, Tanna NK, Herman GT, Resnick SM, Mozley PD, Gur RE, Alavi A, Zimmerman RA, Gur RC. Analysis of brain and cerebrospinal fluid volumes with MR imaging. Part I. Methods, reliability, and validation. Radiology 1991; 178: 115-122.

Kurnik D, Sofowora GG, Donahue JP, Nair UB, Wilkinson GR, Wood AJJ, Muszkat M. Tariquidar, a selective P-glycoprotein inhibitor, does not potentiate loperamide's opioid brain effects in humans despite full inhibition of lymphocyte P-glycoprotein. Anesthesiology 2008; 109: 1092-1099.

Kusuhara H, Suzuki H, Terasaki T, Kakee A, Lemaire M, Sugiyama Y. P-glycoprotein mediates the efflux of quinidine across the blood-brain barrier. J Pharmacol Exp Ther 1997; 283: 574-580.

Lee HB, Blaufox MD. Blood volume in the rat. J Nucl Med 1985; 26: 72-76.

Lee G, Dallas S, Hong M, Bendayan R. Drug transporters in the central nervous system: Brain barriers and brain parenchyma considerations. Pharmacol Rev 2001; 53: 569-596.

Levinger IM. The cerebral ventricles of the rat. J Anat 1971; 108: 447-451.

Lin JH. CSF as a surrogate for assessing CNS exposure: An industrial perspective. Curr Drug Metab 2008; 9: 46-59.

Lin C-J, Tai Y, Huang M-T, Tsai Y-F, Hsu H-J, Tzen K-Y, Liou H-H. Cellular localization of the organic cation transporters, OCT1 and OCT2, in brain microvessel endothelial cells and its

implication for MPTP transport across the blood-brain barrier and MPTP-induced dopaminergic toxicity in rodents. J Neurochem 2010; 114: 717-727.

Liu X, Smith BJ, Chen C, Callegari E, Becker SL, Chen X, Cianfrogna J, Doran AC, Doran SD, Gibbs JP, Hosea N, Liu J, Nelson FR, Szewc MA, Van Deusen J. Evaluation of cerebrospinal fluid concentration and plasma free concentration as a surrogate measurement for brain free concentration. Drug Metab Dispos 2006; 34: 1443-1447.

Liu X, Van Natta K, Yeo H, Vilenski O, Weller PE, Worboys PD, Monshouwer M. Unbound drug concentration in brain homogenate and cerebral spinal fluid at steady state as a surrogate for unbound concentration in brain interstitial fluid. Drug Metab Dispos 2009; 37: 787-793.

Machatha SG, Yalkowsky SH. Comparison of the octanol/water partition coefficients calculated by ClogP®, ACDlogP and KowWin® to experimentally determined values. Int J Pharmaceut 2005; 294: 185-192.

Maurer TS, DeBartolo DB, Tess DA, Scott D. Relationship between exposure and nonspecific binding of thirty-three central nervous system drugs in mice. Drug Metab Dispos 2005; 33: 175-181.

Mayer S, Maickel RP, Brodie BB. Kinetics of penetration of drugs and other foreign compounds into cerebrospinal fluid and brain. J Pharmacol Exp Ther 1959; 127: 205-211.

Mistry P, Stewart AJ, Dangerfield W, Okiji S, Liddle C, Bootle D, Plumb JA, Templeton D, Charlton P. In vitro and in vivo reversal of P-glycoprotein-mediated multidrug resistance by a novel potent modulator, XR9576. Cancer Res 2001; 61: 749-758.

Oldendorf WH. Lipid solubility and drug penetration of the blood-brain barrier. Proc Soc Exp Biol Med 1974; 147: 813-815.

Pardridge WM, Golden PL, Kang YS, Bickel U. Brain microvascular and astrocyte localization of P-glycoprotein. J Neurochem 1997; 68: 1278-1285.

Rao VV, Dahlheimer JL, Bardgett ME, Snyder AZ, Finch RA, Sartorelli AC, Piwnica-Worms D. Choroid plexus epithelial expression of MDR1 P-glycoprotein and multidrug resistance-associated protein contribute to the blood-cerebrospinal-fluid drug-permeability barrier. Proc Natl Acad Sci USA 1999; 96: 3900-3905.

Robertson EG. Developmental defects of the cisterna magna and dura mater. J Neurol Neurosurg Psychiatry 1949; 12: 39-51.

Scheller D, Kolb J. The internal reference technique in microdialysis: a practical approach to monitoring dialysis efficiency and to calculating tissue concentration from dialysate samples. J Neurosci Methods 1991; 40: 31-38.

Schinkel AH. P-glycoprotein, a gatekeeper in the blood-brain barrier. Adv Drug Del Rev 1999; 36: 179-194.

Seegers U, Potschka H, Löscher W. Transient increase of P-glycoprotein expression in endothelium and parenchyma of limbic brain regions in the kainate model of temporal lobe epilepsy. Epilepsy Res 2002a; 51: 257-268.

Seegers U, Potschka H, Löscher W. Expression of the multidrug transporter P-glycoprotein in brain capillary endothelial cells and brain parenchyma of amygdala-kindled rats. Epilepsia 2002b; 43: 675-684.

Sharom FJ. The P-glycoprotein efflux pump: how does it transport drugs? J Membrane Biol 1997; 160: 161-175.

Sharom FJ. Shedding light on drug transport: structure and function of the P-glycoprotein multidrug transporter (ABCB1). Biochem Cell Biol 2006; 84: 979-992.

Shen DD, Artru AA, Adkison KK. Principles and applicability of CSF sampling for the assessment of CNS drug delivery and pharmacodynamics. Adv Drug Del Rev 2004; 56: 1825-1857.

Ståhle L, Segersvärd S, Ungerstedt U. A comparison between three methods for estimation of extracellular concentrations of exogenous and endogenous compounds by microdialysis. J Pharmacol Methods 1991; 25: 41-52.

Stein WD, Cardarelli C, Pastan I, Gottesman MM. Kinetic evidence suggesting that the multidrug transporter differentially handles influx and efflux of its substrates. Mol Pharmacol 1994; 45: 763-772.

Sun H, Bungay PM, Elmquist WF. Effect of capillary efflux transport inhibition on the determination of probe recovery during in vivo microdialysis in the brain. J Pharmacol Exp Ther 2001; 297: 991-1000.

Syvänen S, Xie R, Sahin S, Hammarlund-Udenaes M. Pharmacokinetic consequences of active drug efflux at the blood-brain barrier. Pharm Res 2006; 23: 705-717.

Syvänen S, Luurtsema G, Molthoff CFM, Windhorst AD, Huisman MC, Lammertsma AA, Voskuyl RA, de Lange ECM. (R)-[^{11}C]Verapamil PET studies to assess changes in P-

glycoprotein expression and functionality in rat blood-brain barrier after exposure to kainate-induced status epilepticus. BMC Med Imaging 2011; doi:10.1186/1471-2342-11-1.

Syvänen S, Schenke M, van den Berg D-J, Voskuyl RA, de Lange ECM. Alteration in P-glycoprotein functionality affects intrabrain distribution of quinidine more than brain entry – a study in rats subjected to status epilepticus by kainate. AAPS J 2012; 14: 87-96.

Sziráki I, Erdo F, Beéry E, Molnar PM, Fazakas C, Wilhelm I, Makai I, Kis E, Herédi-Szabó K, Abonyi T, Krizbai I, Tóth GK, Krajcsi P. Quinidine as an ABCB1 probe for testing drug interactions at the blood-brain barrier: An in vitro in vivo correlation study. J Biomol Screen 2011; 16: 886-894.

Thorne RG, Hrabětová S, Nicholson C. Diffusion of epidermal growth factor in rat brain extracellular space measured by integrative optical imaging. J Neurophysiol 2004; 92: 3471-3481.

Van Montfoort JE, Müller M, Groothuis GMM, Meijer DKF, Koepsell H, Meier PJ. Comparison of “type I” and “type II” organic cation transport by organic cation transporters and organic anion-transporting polypeptides. J Pharmacol Exp Ther 2001; 298: 110-115.

Varma MVS, Panchagnula R. pH-dependent functional activity of P-glycoprotein in limiting intestinal absorption of protic drugs: kinetic analysis of quinidine efflux in situ. J Pharm Sci 2005; 94: 2632-2643.

Volk HA, Potschka H, Löscher W. Immunohistochemical localization of P-glycoprotein in rat brain and detection of its increased expression by seizures are sensitive to fixation and staining variables. J Histochem Cytochem 2005; 53: 517-531.

Yano Y, Beal SL, Sheiner LB. Evaluating pharmacokinetic/pharmacodynamic models using the posterior predictive check. J Pharmacokinet Pharmacodyn 2001; 28: 171-192.

Chapter 5

Prediction of methotrexate CNS distribution in different species – influence of disease conditions

J. Westerhout, D-J. van den Berg, R. Hartman, M. Danhof, E.C.M. de Lange

Accepted for publication in Eur. J. Pharm. Sci.

ABSTRACT

Children and adults with malignant diseases have a high risk of prevalence of the tumor in the central nervous system (CNS). As prophylaxis treatment methotrexate is often given. In order to monitor methotrexate exposure in the CNS, cerebrospinal fluid (CSF) concentrations are often measured. However, the question is in how far we can rely on CSF concentrations of methotrexate as appropriate surrogate for brain target site concentrations, especially under disease conditions.

In this study, we have investigated the spatial distribution of unbound methotrexate in healthy rat brain by parallel microdialysis, with or without inhibition of Mrp/Oat/Oatp-mediated active transport processes by a co-administration of probenecid. Specifically, we have focused on the relationship between brain extracellular fluid ($brain_{ECF}$) and CSF concentrations. The data were used to develop a systems-based pharmacokinetic (SBPK) brain distribution model for methotrexate. This model was subsequently applied on literature data on methotrexate brain distribution in other healthy and diseased rats ($brain_{ECF}$), healthy dogs (CSF) and diseased children (CSF) and adults ($brain_{ECF}$ and CSF).

Important differences between $brain_{ECF}$ and CSF kinetics were found, but we have found that inhibition of Mrp/Oat/Oatp-mediated active transport processes does not significantly influence the relationship between $brain_{ECF}$ and CSF methotrexate concentrations.

The prediction of methotrexate data obtained in other healthy rats and dogs works reasonably well, provided that information on the different elimination routes, or the lack thereof, is included in the systems-based scaling approach. The prediction of data from diseased rats and humans, together with SBPK model-based simulations, indicates that disease conditions significantly affect brain distribution.

It is concluded that in parallel obtained data on unbound $brain_{ECF}$, CSF and plasma concentrations, under dynamic conditions, combined with advanced mathematical modeling is a most valid approach to develop SBPK models that allow revealing the mechanisms underlying the relationship between $brain_{ECF}$ and CSF concentrations in health and disease.

INTRODUCTION

Methotrexate was introduced into the treatment of malignant diseases more than 50 years ago (Hertz *et al.,* 1956). Today, many treatment protocols for malignant diseases, like acute lymphoblastic leukemia, have established the combination of high-dose methotrexate (to decrease the fraction of plasma protein binding), combined with leucovorin rescue (Djerassi *et al.,* 1967; Moe and Holen, 2000). Before the use of central nervous system (CNS) prophylaxis, the CNS was the most frequently reported site of initial recurrence in children with acute lymphoblastic leukemia, accounting for up to 75% of cases (Bleyer and Poplack, 1985; Evans *et al.,* 1970). However, in the treatment of acute lymphoblastic leukemia, prophylactic CNS therapy effectively reduced the rate of CNS relapses (Balis and Poplack, 1989; Blaney and Poplack, 1996, Clarke *et al.,* 2003; Smith *et al.,* 1996). Still, CNS recurrence remains a major limitation to achieving complete cure, accounting for 30–40% of recurrences in some pediatric clinical trials (Hutchinson *et al.,* 2003; Lange *et al.,* 2002).

The use of cranial irradiation for CNS prophylaxis is effective but associated with severe late effects (Clarke *et al.,* 2003; Ochs and Mulhern, 1994). Today, the combination of high-dose methotrexate and intrathecal methotrexate, employed to reduce such treatment-related late effects, has successfully replaced cranial irradiation as CNS prophylaxis in most patients (about 80 to 90%) of acute lymphoblastic leukemia (Káp *et al.,* 1998; Pui *et al.,* 2009). However, the intrathecal methotrexate procedure is susceptible to complications and stressful for the patient, especially for children (Keidan *et al.,* 2005). Therefore, it has been suggested that the use of high-dose intravenous methotrexate alone could be sufficient for CNS prophylaxis (Niemann *et al.,* 2010).

On the basis of *in vitro* testing, a methotrexate concentration of 0.45 μg/ml at the target site is commonly acknowledged as effective in killing tumor cells (Hryniuk and Bertino, 1969). With the CNS being the target site for CNS prophylaxis, it is the aim to have the appropriate methotrexate concentration in the brain extracellular fluid ($brain_{ECF}$). However, as blood-brain barrier (BBB) transport is highly restricted for methotrexate, plasma concentrations need to be far higher than the 0.45 μg/ml to be able to reach appropriate concentrations in the CNS. As a result, the exposure of the rest of the body to cytotoxic

concentrations is quite substantial (Chabner and Young, 1973; Ferreri *et al.,* 2004).

The information on the relationship between plasma and CNS methotrexate concentrations appears to be inconsistent, with linear relationships reported by Borsi and Moe (1987), Jönsson *et al.* (2007), Millot *et al.* (1994), whereas Milano *et al.* (1990), Thyss *et al.* (1987) and Vassal *et al.* (1990) reported non-linear relationships. Therefore, CNS concentrations are often monitored for appropriate dose selection (Niemann *et al.,* 2010). To that end, CSF concentrations are used, since $brain_{ECF}$ concentrations are not readily measurable in humans. CSF concentrations are considered to be the best available surrogate (Fridén *et al.,* 2009; Kalvass and Maurer, 2002; Liu *et al.,* 2006; Liu *et al.,* 2009; Maurer *et al.,* 2005), with the assumption that CSF concentrations readily equilibrate with $brain_{ECF}$ concentrations due to the lack of a physical barrier between these sites (Lee *et al.,* 2001). However, due to qualitative and quantitative differences between processes that govern the pharmacokinetics (PK) of drugs in the $brain_{ECF}$ versus CSF, a generally applicable relationship between the PK at these two sites does not exist and needs evaluation (**Chapter 1**; De Lange and Danhof, 2002; Lin, 2008; Shen *et al.,* 2004).

We have previously shown that even for acetaminophen, investigated as model compound for passive transport into, within and out of the brain, differences exist between CSF and $brain_{ECF}$ kinetics (**Chapter 3**). Furthermore, we have also shown that for quinidine, a model compound for P-gp mediated transport, differences exist between CSF and $brain_{ECF}$ kinetics, which are very much dependent on P-gp functionality (**Chapter 4**). With methotrexate being a substrate for a wide variety of transporters that are all located at the BBB and BCSFB (including the reduced folate carrier 1 (RFC1) (Hinken *et al.,* 2011), breast cancer resistance protein (BCRP) (Breedveld *et al.,* 2007), multidrug resistance-associated proteins (MRP) 2, 3 and 4 (Vlaming *et al.,* 2011), organic anion transporter (OAT) 1 and 3 (Takeda *et al.,* 2002), and organic anion-transporting polypeptides (OATP) A (Badagnani *et al.,* 2006) and OATP B (van de Steeg *et al.,* 2009)), this could have major implications for the predictability of $brain_{ECF}$ methotrexate concentrations on the basis of CSF concentrations. Consequently, to be able to know whether methotrexate $brain_{ECF}$ concentrations can be adequately predicted by CSF concentrations, one should first understand

the mechanisms that determine the relationship between CSF concentrations and $brain_{ECF}$ concentrations.

In this study we have used the parallel intracerebral microdialysis probes approach (striatum, lateral ventricle, and cisterna magna (**Chapter 3**)) in conjunction with parallel blood sampling, for continuous measurement and direct comparison of changes in concentrations in plasma, $brain_{ECF}$ and CSF kinetics of methotrexate. To investigate the specific contribution of the various transporters, probenecid is co-administered as inhibitor of MRPs (Bakos *et al.,* 2000), OATs (Sugiyama *et al.,* 2001) and OATPs (Kis *et al.,* 2013). Advanced mathematical modeling is applied to extrapolate the data to other conditions, and other species, including human.

MATERIALS AND METHODS

Chemicals and solutions

Methotrexate solution for injection (Emthexate PF) and isoflurane were obtained from Pharmachemie B.V. (Haarlem, the Netherlands). Methotrexate (powder), aminopterin and ammonium formate were from Sigma-Aldrich (Zwijndrecht, the Netherlands). Probenecid, 5% glucose and saline were obtained from the Leiden University Medical Centre pharmacy (Leiden, the Netherlands). Acetonitrile (HPLC-S grade), methanol (ULC-grade) and formic acid (ULC grade) were from Biosolve (Valkenswaard, the Netherlands). Ammonium hydroxide (25%), magnesium chloride, sodium acetate, sodium chloride, calcium chloride and perchloric acid, were obtained from Baker (Deventer, the Netherlands). Potassium chloride was from Merck (Darmstadt, Germany). All other chemicals were of analytical grade. Microdialysis perfusion fluid was prepared as previously described (**Chapter 3**), containing 140.3 mM sodium, 2.7 mM potassium, 1.2 mM calcium, 1.0 mM magnesium and 147.7 mM chloride.

Animals

The study protocol was approved by the Animal Ethics Committee of Leiden University (UDEC nr. 10094). All animal procedures were performed in accordance with Dutch laws on animal experimentation. A total of 40 male Wistar WU rats (225-275 g, Charles River, Maastricht, the Netherlands) were randomly divided into two groups; the first group (n = 8) was used for the determination of the *in vivo* microdialysis probe recovery; the second group (n = 32) was used for brain disposition experiments. This second group was further divided into four subgroups, designated for 40 or 80 mg/kg methotrexate without or with co-administration of probenecid (denoted as 40^-, 40^+, 80^- and 80^+, respectively).

After arrival, all animals were housed in groups for 5-7 days (Animal Facilities, Gorlaeus Laboratories, Leiden, the Netherlands), under standard environmental conditions (ambient temperature 21°C; humidity 60%; 12/12 h light/dark cycle, background noise, daily handling), with *ad libitum* access to food (Laboratory chow, Hope Farms, Woerden, the Netherlands) and acidified water. Between surgery and experiments, the animals were kept individually in Makrolon type three cages for 7 days to recover from the surgical procedures.

Surgery

All surgical procedures were performed as described in **Chapter 3**. In short, cannulas were implanted in the left femoral artery and vein for blood sampling and drug administration, respectively. Both cannulas were subcutaneously led to the back of the head and fixated in the neck with a rubber ring. Subsequently, the animals were chronically instrumented with two CMA/12 microdialysis guides (CMA/Microdialysis AB, Stockholm, Sweden) in different combinations of striatum (ST), for sampling in $brain_{ECF}$, and lateral ventricle (LV) and/or cisterna magna (CM) for sampling in CSF (ST+LV, ST+CM or LV+CM). For ST, the position of the microdialysis guide is: 1.0 mm anterior, 3.0 mm lateral, 3.4 mm ventral, relative to bregma. For LV, the position of the microdialysis guide is: 0.9 mm posterior, 1.6 mm lateral, 2.9 mm ventral, relative to the bregma. For CM, the position of the microdialysis guide is: 1.93 mm posterior, 3.15 mm lateral, 8.1 mm ventral, at an angle of 25° from the dorsoventral axis

(towards anterior) and 18° lateral from the anteroposterior axis relative to lambda. The microdialysis guides were secured to the skull with 3 anchor screws and dental cement.

After the surgery the animals received 0.03 ml Temgesic ® intramuscularly (Schering-Plough, Amstelveen, the Netherlands) and 0.3 ml Ampicillan® (Alfasan B.V., Woerden, the Netherlands) subcutaneously. One day prior to the experiment, the microdialysis dummies were replaced by the microdialysis probes (CMA/12 Elite, Polyarylethersulfone membrane, molecular weight cut-off 20 kDa, CMA/Microdialysis AB, Stockholm, Sweden, with a semi-permeable membrane length of 4 mm for ST, and 1 mm for LV and CM).

Experimental set-up

All experiments were performed as described in **Chapter 4**, with some modifications. In short, the *in vivo* microdialysis probe recovery of methotrexate was determined on the basis of reverse dialysis (Ståhle *et al.,* 1991). The microdialysis probes in striatum, lateral ventricle and cisterna magna were perfused with different concentrations of methotrexate (50, 200 and 1000 ng/ml) in perfusion fluid. To evaluate the potential effect of co-administration of probenecid on the *in vivo* recovery of methotrexate, several animals received an intravenous infusion of 150 mg/kg probenecid in 5% $NaHCO_3$ in saline (150 µl/min/kg for a period of 10 minutes) with an automated pump (Pump 22 Multiple Syringe Pump, Harvard Apparatus, Holliston, USA) 30 minutes prior to the start of the reverse dialysis experiment. Control animals received an intravenous infusion of vehicle (150 µl/min/kg, for a period of 10 minutes).

The *in vivo* recovery is defined as the ratio of the concentration difference between the dialysate (C_{dial}) and perfusion fluid (C_{in}) over the concentration in the perfusion fluid (equation 1) (Scheller and Kolb, 1991).

$$in\ vivo\ recovery = \frac{C_{in} - C_{dial}}{C_{in}} \quad (1)$$

For the brain disposition experiments, the rats first received an intravenous infusion of 150 mg/kg probenecid in 5% $NaHCO_3$ in saline or vehicle (150 µl/min/kg, for a period of 10 minutes) 30 minutes prior to the administration of 40 or 80 mg/kg methotrexate in saline (200 µl/min/kg for a period of 10

minutes). The start and duration of the infusion was corrected for internal volume of the tubing so that infusion started at t=0 min. 10 min interval samples were collected between t=−1 h and t=5 h. After weighing the microdialysis vials they were stored at −80°C before analysis.

For the determination of methotrexate plasma concentrations, blood samples of 100 µl were taken, in parallel to the microdialysate samples, from the arterial cannula at t=−5 (blank), 2, 7, 9, 10, 12, 17, 30, 90, 180, and 300 min. All blood samples were temporarily stored in heparin (10 IU) coated Eppendorf cups before being centrifuged for 15 min at 5000 rpm. The plasma was then pipetted into clean Eppendorf cups and stored at −20°C before analysis.

At the end of the experiments the animals were sacrificed with an overdose of Nembutal (Ceva Sante Animale, Libourne, France).

Plasma protein binding

For the determination of plasma protein binding of methotrexate, plasma samples of different time points were pooled (combining t = 2 and 7; t = 9 and 10; t = 12 and 17; t = 30 and 90; t = 180 and 300) to span the entire concentration range. Plasma protein binding was determined with Centrifree® ultrafiltration devices (Millipore BV, Etten-Leur, the Netherlands). All procedures were performed according to the user's manual. The ultrafiltrate was diluted 10 times with saline before the analysis.

Concentration analysis

Methotrexate concentrations in plasma, plasma ultrafiltrate and microdialysate were quantified using an on-line solid phase extraction (SPE) with liquid chromatography-tandem mass spectrometry (LC/MS/MS) system, based on previous work by Rule *et al.* (2001) and Guo *et al*. (2007).

To 20 µl of plasma and plasma ultrafiltrate, 20 µl internal standard (10 µg/ml aminopterin) was added. After mixing with 40 µl of 6% perchloric acid and centrifugation for 10 minutes at 10000 g, 60 µl of the supernatant was thoroughly mixed with 40 µl of 1 M sodium acetate. 20 µl was then injected on the SPE column.

To 15 µl of the microdialysate samples, 15 µl of the internal standard (250 ng/ml aminopterin) was added. After mixing, 10 µl was injected on the SPE column.

HySphere™ SPE cartridges and a cartridge holder from Spark (Emmen, the Netherlands) were used in combination with the divert/inject valve of the mass spectrometer to prevent salt entering the mass spectrometer. After flushing under acidic conditions, the SPE was switched onto the LC system and methotrexate and its internal standard were eluted from the SPE to the LC column. For plasma precipitates, C-8 HD SE cartridges were used, while for microdialysate samples C-18 cartridges were used. After injection of the sample on the SPE column, salts from either precipitated plasma or microdialysate samples were flushed to waste before analysis on the HPLC column. A quaternary gradient HPLC pump (P580) from Dionex (Breda, the Netherlands) was used for the on-line SPE method, while a Surveyor pump (Thermo Scientific, Breda, the Netherlands) served as delivery unit for the HPLC column.

The VisionHT® C-18B column (Grace Alltech, Breda, the Netherlands) was thermostatted at 37°C. The mobile phase consisted of 21% methanol and 79% lab water, derived from a PURELAB Ultra system (Veolia Water Solutions, Ede, the Netherlands), containing 0.2% formic acid and 1 mM ammonium formate. After isocratic elution of the peaks of methotrexate and internal standard, the column was flushed with 90% methanol and 10% lab water containing 0.2% formic acid and 1mM ammonium formate 7–9.5 minutes after injection.

Sample analysis was performed on a Finnigan TSQ Quantum Ultra Mass Spectrometer System (Thermo Scientific, Breda, the Netherlands). Electrospray ionization was used in the positive mode at 3500V. Methotrexate was quantified using selected reaction monitoring (SRM) with the transition 455–308 (*m/z*). The internal standard, aminopterin, had a SRM transition of 441–294 (*m/z*). The collision energy used was 18 V, scan width was set at 0.7 *m/z* and both Q1 and Q3 were set to 0.70 full width at half maximum (FWHM). The scan time was 0.11 seconds. Argon served as the collision gas.

Pharmacokinetic data analysis

All plasma concentrations were converted to unbound plasma concentrations, by correction for plasma protein binding. All microdialysate concentrations from striatum, lateral ventricle and cisterna magna were converted into $brain_{ECF}$ concentrations (C_{ECF}) or CSF concentrations (C_{CSF}) by division of the dialysate concentrations by the average *in vivo* recovery as determined for each microdialysis probe location (equation 2).

$$C_{ECF}\ or\ C_{CSF} = \frac{C_{dial}}{in\ vivo\ recovery} \qquad (2)$$

Areas under the curve from t=0 to t=300 min ($AUC_{0\text{-}300}$) were calculated by the trapezoidal rule and tested for differences by single factor ANOVA. The population PK models were developed and fitted to the data by means of non-linear mixed-effects modeling using the NONMEM software package (version 6.2, Icon Development Solutions, Ellicott City, Maryland, USA) and analyzed using the statistical software package S-Plus® for Windows (version 6.2 Professional, Insightful Corp., Seattle, USA).

The pharmacokinetic model for methotrexate plasma and brain concentrations was based on the systems-based PK (SBPK) approach we have previously applied to investigate the exchange between $brain_{ECF}$ and CSF of acetaminophen (**Chapter 3**) and quinidine (**Chapter 4**). For this approach, the volumes of the different brain compartments were fixed to their physiological volumes. The rat brain intracellular space and $brain_{ECF}$ volume were assumed to be 1.44 ml (Thorne *et al.,* 2004) and 290 µl (Cserr *et al.,* 1981), respectively. With a total CSF volume of 300 µl in the rat (Bass and Lundborg, 1973), the volumes of the lateral ventricles, third and fourth ventricles, cisterna magna and subarachnoid space were assumed to be 50 µl (Condon *et al.,* 1986; Kohn *et al.,* 1991), 50 µl (Levinger, 1971), 17 µl (Adam and Greenberg, 1978; Robertson, 1949) and 180 µl (Bass and Lundborg, 1973; Levinger, 1971), respectively. The intra-brain distribution was restricted by the physiological flow paths of $brain_{ECF}$, in which $brain_{ECF}$ flows towards the CSF compartments at a rate of 0.2 µl/min (Abbott, 2004; Cserr *et al.,* 1981), and CSF flows from lateral ventricle, through the third and fourth ventricle, to the cisterna magna and subsequently to

the subarachnoid space (cranial and spinal) and back into blood at a rate of 2.2 µl/min (Cserr, 1965).

Structural model selections for both the blood and brain PK model were based on the likelihood ratio test ($p < 0.01$), diagnostic plots (observed concentrations vs. individual and population predicted concentrations, weighted residuals vs. predicted time and concentrations), parameter correlations and precision in parameter estimates. The inter-animal variability in pharmacokinetic parameters was assumed to be log normally distributed. The residual error, which accounts for unexplained variability (e.g. measurement and experimental error and model-misspecification), was best described with a proportional error model.

The validity of the pharmacokinetic models was investigated by means of a visual predictive check. (Cox *et al.,* 1999; Duffull and Aarons, 2000; Yano *et al.,* 2001) Using the final PK parameter estimates, 1000 curves were simulated. Subsequently, the median and the 5^{th} and 95^{th} percentile of the predicted concentrations were calculated, which represent the 90% prediction interval. These were then compared with the observations.

In order to test the ruggedness of the model and estimate the precision of the parameters n=100 non-parametric (case resampling) bootstraps were performed. To create the bootstrapped datasets, specific rat data (plasma and microdialysate concentrations) were removed randomly from the datasets and replaced with randomly selected rat data from the complete original dataset. Each of these permutations of the original dataset was fitted with the final model determined based on the original dataset. This results in a series of model fits, each with its own set of parameters. These results were displayed graphically and the descriptive statistics of the parameters were compared to parameter estimates of the final model. Only bootstrap runs that successfully minimized were used in this analysis.

Systems-based scaling

The SBPK model was first used to predict the methotrexate plasma and $brain_{ECF}$ concentration-time profiles of brain tumor-bearing rats (De Lange *et al.,* 1995), to investigate the impact of disease-status on the kinetics of methotrexate. Next, the parameters of the rat SBPK were extrapolated to healthy dogs (Neuwelt *et*

al., 1985), to investigate the validity of using this approach for interspecies scaling. To do so, the elimination clearance was first divided into renal clearance and hepatic clearance, with renal clearance assumed to be identical to the glomerular filtration rate (Brcakova *et al.,* 2009) and the remaining clearance assigned to hepatic clearance. The hepatic clearance was then scaled to the number of hepatocytes in rat or dog liver. Next, the transfer clearances between plasma and the different peripheral and brain compartments were scaled based on

$$CL_{PL-PER} = A_{PER} \times (V_{PER})^{0.67} \quad (3)$$

$$CL_{PL-BR} = A_{BR} \times (V_{BR})^{0.67} \quad (4)$$

In which A_{PER} and A_{BR} are scaling coefficients for periphery and brain, respectively, and both are estimated on the basis of the rat data (Hosseini-Yeganeh and McLachlan, 2002). V_{PER} represents the physiological volume of the (lumped) peripheral tissues for rapid (including muscle, kidney, intestine and liver) and slow equilibration (including adipose, skin, heart, bone and remaining tissue). V_{BR} represents the physiological volume of the different brain compartments. The scaling factor of 0.67 is based on the permeability surface area of the different brain compartments, which is related to the tissue weight (Kawai *et al.,* 1994). The physiological parameters of the rat SBPK model were changed accordingly.

Finally, the parameters of the rat SBPK were extrapolated to the human setting, which included adults and children with different disease-states, using the same approach as applied for extrapolation to dogs.

RESULTS

All results are presented as average values ± standard error of the mean, unless stated otherwise.

Methotrexate pharmacokinetics

The average unbound plasma ($plasma_u$), $brain_{ECF}$, lateral ventricle (CSF_{LV}) and cisterna magna (CSF_{CM}) methotrexate concentrations following the 40 and 80 mg/kg dose with or without co-administration of probenecid are shown in figure 1. Plasma protein binding of methotrexate was linear at an extent of 55.2 ± 7.7%. It was not affected by co-administration of probenecid. The co-administration of probenecid slightly altered the distribution phase for both the 40 and 80 mg/kg dose of methotrexate. Data obtained by microdialysis from the $brain_{ECF}$, CSF_{LV} and CSF_{CM} were corrected for *in vivo* recovery. The average *in vivo* recoveries for the methotrexate concentrations in striatum, lateral ventricle and cisterna magna probes were influenced by co-administration of probenecid and were determined to be 22.1 ± 2.0%, 28.1 ± 2.9% and 35.9 ± 2.5%, for the control group and 7.1 ± 0.9%, 16.9 ± 1.7% and 21.6 ± 5.6% for the probenecid group, respectively.

It can be seen that a higher dose of methotrexate leads to higher methotrexate concentrations in all brain compartments, but not to the same extent. Probenecid increased methotrexate concentrations significantly ($p < 0.01$) in all brain compartments. The effect of probenecid was dependent on the methotrexate dose; at the higher dose of methotrexate, the increase in methotrexate concentrations was more profound for $brain_{ECF}$ and CSF_{LV}, as can be seen by the average unbound brain ($brain_u$)-to-$plasma_u$ $AUC_{0\text{-}300}$ ratios (table 1). However, the dose-dependency was not significant. The relationship between $brain_{ECF}$-to-CSF concentration ratios was not significantly affected by probenecid co-administration, and was on average 7.7 ± 3.7 (table 2).

Table 1. $Brain_u$-to-$plasma_u$ $AUC_{0\text{-}360}$ ratios for $brain_{ECF}$, CSF_{LV} and CSF_{CM} for the 40 mg/kg and 80 mg/kg dose without (-) and with (+) co-administration of probenecid

$Brain_u$-to-$plasma_u$ $AUC_{0\text{-}300}$ ratios	40^-	40^+	80^-	80^+
$Brain_{ECF}$	2.5 ± 1.7%‡	5.9 ± 1.1%*‡	2.5 ± 0.3%‡	9.8 ± 3.3%*‡
CSF_{LV}	0.6 ± 0.1%	1.6 ± 1.0%	0.5 ± 0.3%	3.5 ± 0.4%*
CSF_{CM}	0.4 ± 0.1%	0.8 ± 0.1%	0.7 ± 0.4%	0.9 ± 0.5%

* *Significantly ($p < 0.05$) different from the group without co-administration of probenecid*

‡ *Significantly ($p < 0.05$) different from the CSF-to-$plasma_u$ $AUC_{0\text{-}300}$ ratios*

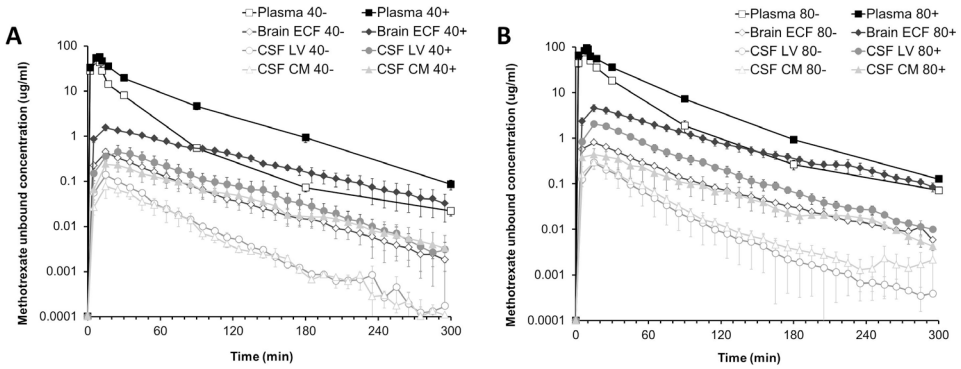

Figure 1. Average (geometric mean ± S.E.M.) unbound methotrexate concentration-time profiles following intravenous administration of methotrexate, with (+) or without (-) co-administration of probenecid (150 mg/kg). (A) 40 mg/kg methotrexate dose: for plasma (n = 7 (-) and 6 (+)), $brain_{ECF}$ (n = 5 (-) and 4 (+)), CSF_{LV} (n = 4 (-) and 3 (+)) and CSF_{CM} (n = 3 (-) and 4 (+). (B) 80 mg/kg methotrexate dose. Plasma (n = 7 (-) and 7 (+)), $brain_{ECF}$ (n = 4 (-) and 5 (+)), CSF_{LV} (n = 5 (-) and 4 (+)) and CSF_{CM} (n = 6 (-) and 3 (+))

Table 2. $Brain_{ECF}$-to-CSF concentration ratios for the 40 mg/kg and 80 mg/kg dose without (-) and with (+) co-administration of probenecid. (No significant differences were found).

$Brain_{ECF}$-to-CSF concentration ratios	40^-	40^+	80^-	80^+
$Brain_{ECF}$-to-CSF_{LV}	9.6 ± 5.0	6.0 ± 2.9	11.6 ± 7.0	5.2 ± 2.4
$Brain_{ECF}$-to-CSF_{CM}	11.5 ± 5.5	8.3 ± 1.6	6.0 ± 2.3	12.7 ± 3.0
$Brain_{ECF}$-to-$CSF_{average}$	10.2 ± 4.8	6.8 ± 2.1	7.6 ± 3.3	7.2 ± 2.7

Systems-based modeling approach

As it was our goal to investigate the relationship between $brain_{ECF}$ and CSF pharmacokinetics, we have applied a SBPK modeling approach like we did previously for analysis of regional brain distribution of acetaminophen (**Chapter 3**) and quinidine (**Chapter 4**). To adequately describe CSF physiology, we have used four CSF compartments that represent the CSF_{LV}, the combined third and fourth ventricle (CSF_{TFV}), the CSF_{CM} and the subarachnoid space (CSF_{SAS}). Since we have no measurements of the concentrations in the third and fourth ventricle, the transfer clearance between plasma and third and fourth ventricle was assumed to be equal to the transfer clearance between plasma and lateral ventricle.

Distinction between passive and active transport clearances - The active component of the different transfer clearances between plasma and the brain compartments was determined by comparing the parameter estimations for the rats that did to those rats that did not receive the co-administration of probenecid. Even though methotrexate is transported by a wide variety of transporters, the co-administration of the Mrp-, Oat- and Oatp-inhibitor probenecid allowed us to investigate the impact of combined Mrp-, Oat- and Oatp-mediated transport. The active component of the transfer clearances between plasma and the different brain compartments was incorporated into the model as previously described by Syvänen *et al.* (2006):

$$CL_{PL-BR} = CL_{PL-BR,p} - CL_{PL-BR,a} \quad (5)$$

$$CL_{BR-PL} = CL_{BR-PL,p} + CL_{BR-PL,a} \quad (6)$$

Where the subscript 'p' denotes passive transport and 'a' denotes active transport. For the animals that received a co-administration of probenecid, both $CL_{PL\text{-}BR,a}$ and $CL_{BR\text{-}PL,a}$ were considered to be 0.

Modeling Mrp-, Oat- and Oatp-mediated transport - Both Mrps, Oats, as well as Oatps have been well described as efflux transporters at the BBB and BCSFB (Graff and Pollack, 2004). However, the mechanism by which Mrps, Oats and Oatps can exert their effect could be by reducing the transfer clearance from plasma to the brain compartments (i.e. influx hindrance; equation 5) or by increasing the transfer clearance from the brain compartments to plasma (i.e. efflux enhancement; equation 6) or both. The data were best described by the model with Mrp, Oat and Oatp functioning solely by influx hindrance. Interestingly, the observation that *in vivo* probe recovery of methotrexate was affected by probenecid indicates that methotrexate is transported by Mrps, Oats and Oatps via the efflux enhancement mechanism (Syvänen *et al.,* 2006). However, estimation of the active components when Mrp, Oat and Oatp were considered to function by efflux enhancement resulted in too large coefficients of variation. Also, the estimation of the active component in the transfer between plasma and cisterna magna resulted in too large coefficients of variation and was therefore assumed to be absent.

Modeling methotrexate concentration-dependent Mrp-, Oat- or Oatp-mediated transport - Since Mrp-, Oat- or Oatp-mediated transport is an active (saturable) process we have also tried to identify the maximal transport rate (T_m) and the blood- or brain concentration for half-maximal transport (K_m) as follows:

$$CL_{PL-BR,a} = \frac{T_{m,PL-BR}}{K_{m,PL-BR}+C_{PL,u}} \quad (7)$$

$$CL_{BR-PL,a} = \frac{T_{m,BR-PL}}{K_{m,BR-PL}+C_{BR}} \quad (8)$$

Where $C_{PL,u}$ is the unbound plasma concentration and C_{BR} is the concentration in one of the brain compartments. The parameter estimations of T_m and K_m resulted in high values for both T_m and K_m (results not shown), indicating that the plasma and brain concentrations in this study are not sufficiently high for saturating Mrp-, Oat- or Oatp-mediated transport. The parameter estimations of T_m and K_m also resulted in too large coefficients of variation. Thus, our data were insufficient to determine the values of these parameters. Therefore, Mrp-, Oat- or Oatp-mediated transport had to be incorporated by means of a single active transport clearance value, rather than by T_m and K_m.

Final SBPK model - The final SBPK model is shown in figure 2. The differential equations of this model can be found in the appendix. The final estimation of the PK parameters is summarized in table 3. Interestingly, no active component on the elimination clearance could be identified, whereas this was the case for the compartmental pharmacokinetic analysis of the plasma concentrations only (results not shown).

According to Brcakova *et al.* (2009), the rate of renal clearance of unbound methotrexate in rats equals the rate of renal creatinine clearance, which is a measure of the glomerular filtration rate (GFR; 1.4 ml/min in the rat (Atherton, 1983)). Consequently, the remaining methotrexate clearance is hepatically. Based on our results, the rate of hepatic clearance is therefore 7.35 ml/min in the rat. With a total hepatic blood flow of approximately 11.8 ml/min (Davies and Morris, 1993), this results in a hepatic extraction ratio of 62%, which is comparable to the 53% reported previously by Kates and Tozer (1976).

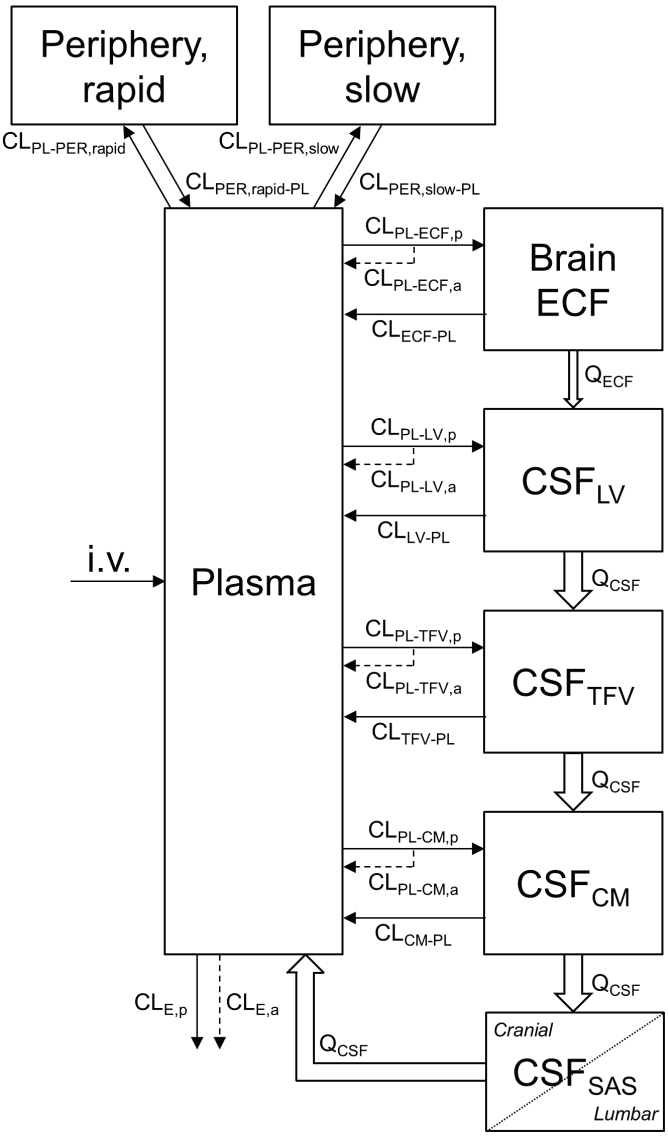

Figure 2. Diagram of the SBPK model that was used to describe the intra-brain distribution of methotrexate in the rat. CL_E is the elimination clearance from plasma. Further, for transfer clearances between compartments ($CL_{from\ comp\text{-}to\ comp}$), denotations of the compartments are: PL = plasma; PER,rapid = rapidly equilibrating periphery; PER,slow = slowly equilibrating periphery; ECF = brain$_{ECF}$; LV = lateral ventricle; TFV = third and fourth ventricle; CM = cisterna magna and SAS = subarachnoid space. Q_{ECF} is the flow rate of brain$_{ECF}$, Q_{CSF} is the flow rate of CSF. The subscript 'p' denotes passive transport and 'a' denotes active transport.

The visual predictive check of the final model is given in figure 3. It can be seen that the final model describes the data very well within the 90% prediction interval, and also can cope with the large inter-individual variation in brain concentrations.

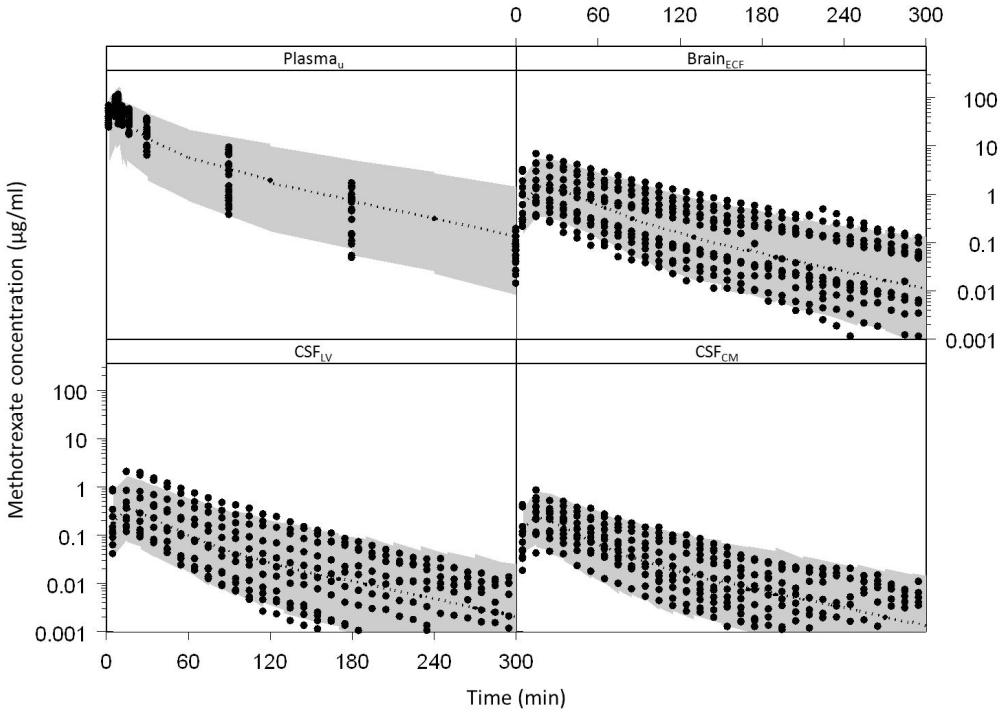

Figure 3. The visual predictive check of the final SBPK model. The dots represent the individual data points and the gray area represents the 90% prediction confidence interval. The different boxes represent the plasma$_u$, brain$_{ECF}$, CSF$_{LV}$ and CSF$_{CM}$ data

Systems-based scaling

The physiological and PK parameters of the rat, dog and human children and adults that were used for the extrapolation are given in table 3.

Table 3. Final estimation of the rat PK parameters of methotrexate for the SBPK model (± standard error) and predicted dog and human parameters.

Parameter	Rat value	Dog value (20-25 kg)	Human child value (9 year old, 30 kg bodyweight)	Human adult value
$f_{u,p}$	44.8 ± 7.7 %	*60%* [13]	*67.7%* [19]	*67.7%* [19]
$CL_{E,p}$	8.75 ± 0.85 ml/min	88.2 ml/min (based on 1.1*GFR) [13]	163.2 ml/min (based on 2*GFR) [20]	250 ml/min (based on 2*GFR) [20]
GFR	*1.4 ml/min* [1]	*80.2 ml/min* [14]	*81.6 ml/min* [21]	*125 ml/min* [6]
$CL_{E,a}$	N.A.	N.A.	N.A.	N.A.
$CL_{PL\text{-}PER,rapid}$	31.5 ± 4.9 ml/min	748.2 ml/min	606.0 ml/min	1047.2 ml/min
$CL_{PER,rapid\text{-}PL}$	2.45 ± 0.34 ml/min	582.0 ml/min	471.3 ml/min	814.5 ml/min
$CL_{PL\text{-}PER,slow}$	2.94 ± 0.91 ml/min	38.1 ml/min	72.6 ml/min	146.5 ml/min
$CL_{PER,slow\text{-}PL}$	0.25 ± 0.04 ml/min	32.4 ml/min	61.8 ml/min	124.5 ml/min
$CL_{PL\text{-}ECF,p}$	1.81 ± 0.48 µl/min	29.8 µl/min	176.6 µl/min	180.9 µl/min
$CL_{PL\text{-}ECF,a}$	1.29 ± 0.41 µl/min	21.3 µl/min	125.8 µl/min	128.9 µl/min
$CL_{ECF\text{-}PL}$	17.0 ± 4.4 µl/min	280.2 µl/min	1658.3 µl/min	1699.2 µl/min
$CL_{PL\text{-}LV,p}$	0.12 ± 0.04 µl/min	2.18 µl/min	5.55 µl/min	7.19 µl/min
$CL_{PL\text{-}LV,a}$	0.09 ± 0.03 µl/min	1.64 µl/min	4.17 µl/min	5.39 µl/min
$CL_{LV\text{-}PL}$	3.69 ± 1.57 µl/min	67.2 µl/min	170.8 µl/min	221.1 µl/min
$CL_{PL\text{-}TFV,p}$	0.12 ± 0.04 µl/min	2.18 µl/min	5.55 µl/min	7.19 µl/min
$CL_{PL\text{-}TFV,a}$	0.09 ± 0.03 µl/min	1.64 µl/min	4.17 µl/min	5.39 µl/min
$CL_{TFV\text{-}PL}$	3.69 ± 1.57 µl/min	67.2 µl/min	170.8 µl/min	221.1 µl/min
$CL_{PL\text{-}CM,p}$	0.017 ± 0.007 µl/min	0.24 µl/min	0.81 µl/min	1.01 µl/min
$CL_{PL\text{-}CM,a}$	N.A.	N.A.	N.A.	N.A.
$CL_{CM\text{-}PL}$	4.37 ± 1.81 µl/min	62.4 µl/min	207.4 µl/min	258.4 µl/min
Q_{ECF}	*0.2 µl/min* [2,3]	*10.5 µl/min (based on 0.11 µl/min/g brain)* [3]	*0.1 ml/min (based on 50% of Q_{CSF})* [22]	*0.175 ml/min* [22]
Q_{CSF}	*2.2 µl/min* [4]	*63 µl/min* [15]	*0.2 ml/min* [23]	*0.4 ml/min* [29]
V_{PL}	*10.6 ml* [5]	*1112 ml* [16]	*1600 ml* [24]	*2900 ml* [30]
$V_{PER,rapid}$	*49.7% of bodyweight* [6]	*64.1% of bodyweight* [6]	*36.1% of bodyweight* [25]	*35.0% of bodyweight* [25]

Table 3 Continued.

$V_{PER,slow}$	*45.5% of bodyweight* [6]	*26.2% of bodyweight* [6]	*48.0% of bodyweight* [25]	*58.6% of bodyweight* [25]
V_{ECF}	*290 µl* [3]	*19 ml (based on 95.5 gr brain)* [15]	*270 ml* [26] *(based on 1350 gr brain)* [27]	*280 ml* [26] *(based on 1400 gr brain)* [27]
$V_{CSF,total}$	*300 µl* [7]	*15.6 ml* [17]	*90 ml* [28]	*140 ml* [22]
V_{LV}	*50 µl* [8,9]	*3.8 ml (24% of total CSF volume)* [18]	*15.3 ml (17% of total CSF volume)* [8,9]	*22.5 ml* [8,9,31]
V_{TFV}	*50 µl* [10]	*1.3 ml (8% of total CSF volume)* [18]	*15.3 ml (17% of total CSF volume)* [8,9]	*22.5 ml* [8,9]
V_{CM}	*17 µl* [11,12]	*0.9 ml (6% of total CSF volume (human value))* [11,12]	*5.1 ml (5.7% of total CSF volume)* [11,12]	*7.5 ml* [11,12]
V_{SAS}	*180 µl* [7,10]	*9.0 ml (60% of total CSF volume (human value))* [7,10]	*54 ml (60% of total CSF volume)* [7,10]	*90 ml* [32]
η_{CLE}	0.11 ± 0.02	0.11	0.11	0.11
ε_{PL}	0.18 ± 0.03	0.18	0.18	0.18
ε_{ST}	0.07 ± 0.02	0.07	0.07	0.07
ε_{LV}	0.31 ± 0.09	0.31	0.31	0.31
ε_{CM}	0.25 ± 0.06	0.25	0.25	0.25

Parameter values in italic are derived from literature. $F_{u,p}$ is the fraction unbound in plasma, CL_E is the elimination clearance from plasma. For transfer clearances between compartments ($CL_{from\ comp\text{-}to\ comp}$), denotations of the compartments are: PL = plasma; PER,rapid = rapidly equilibrating peripheral tissues; PER,slow = slowly equilibrating peripheral tissues; ECF = brain$_{ECF}$; LV = lateral ventricle; TFV = third and fourth ventricle; CM = cisterna magna; and SAS = subarachnoid space. V is the physiological volume. η_i = inter-individual variability of parameter i; ε_j = residual error on concentrations in compartment j. The additional subscripts 'p' and 'a' denote passive and active transport, respectively. N.A. implicates that the parameter is not available in the specific model.

[1] Atherton, 1983; [2] Abbott, 2004; [3] Cserr et al., 1981; [4] Cserr, 1965; [5] Lee and Blaufox, 1985; [6] Davies and Morris, 1993; [7] Bass and Lundborg, 1973; [8] Condon et al, 1986; [9] Kohn et al., 1991; [10] Levinger, 1971; [11] Adam and Greenberg, 1978; [12] Robertson, 1949; [13] Henderson et al., 1965; [14] Von Hendy-Willson and Pressler, 2011; [15] Bering, 1959; [16] Visser et al., 1982; [17] Löfgren et al., 1973; [18] Vladic et al 2009; [19] Skibińska et al., 1990; [20] Hendel and Brodthagen, 1984; [21] Schwartz et al., 1976; [22] Kimelberg, 2004; [23] Yasuda et al., 2002; [24] Linderkamp et al., 1977; [25] ICRP, 2002; [26] Thorne et al., 2004; [27] Dekaban and Sadowsky, 1978; [28] Troncin and Dadure, 2009; [29] Nilsson et al., 1992; [30] Frank and Gray, 1953; [31] Dickey et al., 2000; [32] Pardridge, 2011.

Extrapolation to other healthy and to diseased rats

We have applied the final SBPK model to investigate the impact of disease-status on the PK of methotrexate in $plasma_u$ and $brain_{ECF}$ of brain tumor-bearing rats, compared to healthy control rats (De Lange *et al.,* 1995). By using the same PK parameter values that were estimated based on our data (table 3), there appears to be a small underestimation of the elimination from plasma as well as a small underestimation of the initial $brain_{ECF}$ concentrations for the control rats (figure 4A) (but both $plasma_u$ and $brain_{ECF}$ data are in general still within the range of 5-95% of the model prediction of the data). However, for the group of rats with measurement of plasma and ipsilateral $brain_{ECF}$ concentrations at 11 days post-tumor implantation, the concentration-time profiles in $brain_{ECF}$ in brain tumor were substantially higher than was the case for the healthy situation (figure 4B). Presence and size of tumor were determined histologically after the end of the experiment. Simulations indicated that these higher $brain_{ECF}$ concentrations are most likely caused by an increased plasma-to-$brain_{ECF}$ clearance rate in brain tumor conditions (results not shown).

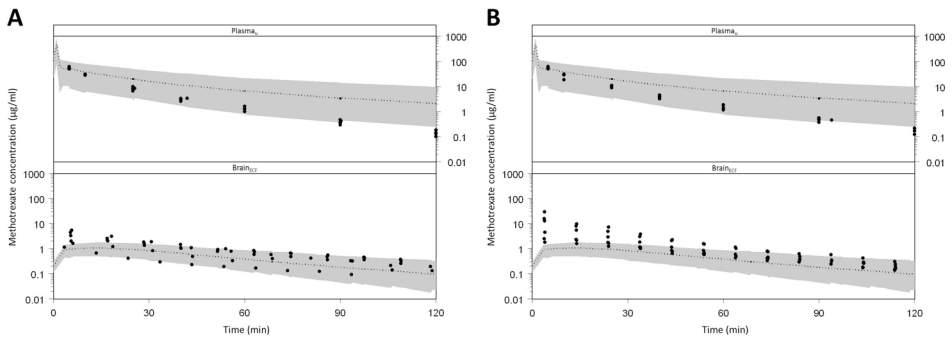

Figure 4. Observed and SBPK model predicted methotrexate $plasma_u$ and $brain_{ECF}$ concentrations in (A) control rats ($plasma_u$, n=5; $brain_{ECF}$, n=6); (B) tumor implanted rats with ipsilateral $brain_{ECF}$ measurement after 11 days ($plasma_u$, n=6; $brain_{ECF}$, n=6) (De Lange et al., 1995). Note that the two lowest concentration-time profiles in (B) represent animals in which no tumor was present on subsequent histological examinations. The dots represent the individual data points and the gray area represents the 90% prediction confidence interval. The different boxes represent the $plasma_u$ and $brain_{ECF}$ data

Extrapolation to healthy dogs

We have also tried to predict the $plasma_u$ and CSF kinetics of methotrexate in healthy dogs by systems-based scaling of our rat data. Predictions were then compared to literature data presented by Neuwelt *et al.* (1985). Plasma concentrations were first corrected for the level of protein binding, which was assumed to be 40% (Henderson *et al.,* 1965). The rate of renal clearance was assumed to equal the glomerular filtration rate (80.2 ml/min (Von Hendy-Willson and Pressler, 2011)). Systems-based scaling of our data initially resulted in a 10-to-100-fold underestimation of dog $plasma_u$ and CSF_{CM} concentrations, whereas the CSF_{CM}-to-$plasma_u$ concentration ratio was predicted correctly. The underestimation of the $plasma_u$ and CSF_{CM} concentrations was primarily caused by an overestimation of the plasma elimination clearance. As the number of hepatocytes per gram liver in dogs is twice as much compared to rats (Bayliss *et al.,* 1999), the rate of hepatic clearance was scaled to the liver weight and then multiplied by 2. With an assumed liver weight of 720 g in the dog (Davies and Morris, 1993), the rate of hepatic clearance was estimated to be 1094 ml/min. However, in the rat, methotrexate is eliminated both via the kidneys as well as the liver, whereas in dogs methotrexate is eliminated primarily via the kidneys (Henderson *et al.,* 1965). This indicates that the estimation of the hepatic clearance rate in dogs was much too high. For healthy dogs, with a hepatic clearance being approximately 10% of the renal clearance (Henderson *et al.,* 1965), using the physiological and adapted PK parameters presented in table 3, the prediction was much improved and resulted in a slight underestimation of $plasma_u$ and CSF_{CM} concentrations (figure 5). Yet the CSF_{CM}-to-$plasma_u$ concentration ratio was still predicted correctly.

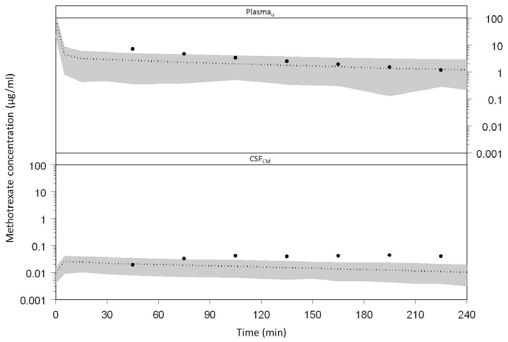

Figure 5. Observed and SBPK model predicted methotrexate plasma$_u$ and CSF$_{CM}$ concentrations in (healthy) dogs (plasma$_u$, n=12; CSF$_{CM}$, n=4). The dots represent the average data points as could be obtained from Neuwelt et al. (1985) and the gray area represents the 90% prediction confidence interval. The different boxes represent the plasma$_u$ and CSF$_{CM}$ data. The hepatic clearance was assumed to be 10% of the renal clearance for the final SBPK predictions

Extrapolation to diseased human adults and children

The only available human brain$_{ECF}$ concentration-time profiles were derived from Blakeley *et al*. (2009), from 2 adult patients with supratentorial glioma. Other data included human plasma and CSF$_{LV}$ concentration-time profiles in adults with meningeal leukemia or meningeal carcinomatosis (n = 21, Shapiro *et al.,* 1975), primary tumor (n = 16, Glantz *et al.,* 1998), or only plasma concentration-time profiles in adults with small-cell lung carcinoma (n = 9, Creaven *et al.,* 1976), various neoplastic diseases (n = 8, Bore et al., 1987) or rheumatoid arthritis (n = 56, Herman et al., 1989; Stewart *et al.,* 1990). Also included were plasma and CSF$_{CM}$ concentration-time profiles from children with medulloblastoma or ependymoblastoma (n = 4, Chatelut *et al.,* 1991), plasma and CSF$_{SAS}$ concentration-time profiles from children with non-Hodgkin's lymphoma (n = 29, Vassal *et al.,* 1990), or only plasma concentration-time profiles from children with acute lymphoblastic leukemia (n = 49, Aumente *et al.,* 2006) or osteosarcoma (n = 14, Colom *et al.,* 2009). For constructing the adult and child plasma, CSF$_{LV}$, CSF$_{CM}$ and CSF$_{SAS}$ dataset, either the individual or average data points from the different references were used, when available. Otherwise, simulations were performed based on the PK parameters presented in the different references.

All plasma concentrations were first corrected for the level of protein binding, which was assumed to be 32% for high dose methotrexate (Skibińska *et al.,* 1990). Systems-based scaling of our data initially resulted in a 100-fold underestimation of human $plasma_u$, $brain_{ECF}$ and CSF concentrations for both adults and children (results not shown). Again, the underestimation of the $plasma_u$, $brain_{ECF}$ and CSF concentrations was primarily caused by an overestimation of the elimination clearance. For the systems-based scaling of the elimination clearance of methotrexate it was assumed that the rate of human renal clearance equals the glomerular filtration rate (125 ml/min in adults (Davies and Morris, 1993) and approximately 80 ml/min in 9 year-old children (the average age of the available datasets)). As the number of hepatocytes per gram liver is equal between rats and humans (Bayliss *et al.,* 1999), the rate of hepatic clearance is scaled to the liver weight. With an assumed liver weight of 10 g in the rat (Davies and Morris, 1993), 780 g in 9 year old children and 1820 g in adults (ICRP, 2002), the rate of hepatic clearance is estimated to be 593 ml/min and 1380 ml/min in 9 years old children and adults, respectively. However, due to the extensive enterohepatic circulation of methotrexate in humans, the hepatic elimination rate is effectively reduced to the same level as the renal elimination rate (Hendel and Brodthagen, 1984). So, when taking into account that the hepatic clearance rate of methotrexate in humans is much lower than the extrapolated value, i.e. equal to the renal clearance rate, the predicted human $plasma_u$ concentrations are comparable to the observed concentrations (figure 6). However, even though the human $plasma_u$ concentrations can be predicted reasonably well with systems-based scaling of our rat data and adaption of the hepatic clearance rate to those reported for human (table 3), this approach still results in an up to 10-fold underestimation of $brain_{ECF}$, CSF_{CM} and CSF_{LV} concentrations in both children and adults, respectively. Scaling of the blood-to-brain clearance values on the basis of the total surface area of the BBB (150 cm^2 in rats (Gjedde, 1981; Keep and Jones, 1990a); 200,000 cm^2 in human adults (Pardridge, 2002)) and BCSFB (75 cm^2 in rats (Keep and Jones, 1990b), 2000-100,000 cm^2 in human adults (Dohrmann, 1970)), rather than to the tissue weight to the power 0.67, did not improve the predictions (results not shown).

$Brain_{ECF}$ and CSF_{LV} concentrations in adults, as shown in figure 6a, were not obtained in parallel, but from different subjects, also having other diseases. However, these are the only data available to make a comparison between these

two unbound brain concentrations. Both $brain_{ECF}$ and CSF_{LV} concentrations are higher than predicted by the SBPK model, while the observed $brain_{ECF}$-to-CSF_{LV} concentration ratio is in accordance with the predicted $brain_{ECF}$-to-CSF_{LV} concentration ratio. It therefore seems that the plasma-to-brain concentration ratio is increased by disease conditions. Specifically, simulations indicated that the $brain_{ECF}$-to-CSF concentration ratio in diseased adults and children is equal to 2.6, which is approximately 3-fold lower than the $brain_{ECF}$-to-CSF concentration ratio observed in healthy rats, being most likely caused by an overestimation of the $brain_{ECF}$-to-plasma clearance rate. It indicates that under disease conditions there is a decreased active efflux from the $brain_{ECF}$ to plasma (results not shown). On the other hand, simulations indicated that the underestimation of CSF concentrations in disease conditions is most likely caused by an overestimation of the CSF flow. This is in line with the observation that several adult patients had an obstruction to normal CSF flow (Glantz *et al.,* 1998) (results not shown).

Overall, the observed and SBPK model predicted $plasma_u$, $brain_{ECF}$, CSF_{LV}, CSF_{CM} and CSF_{SAS} concentration-time profiles in healthy and diseased rats, dogs, children and adults are summarized in figure 7.

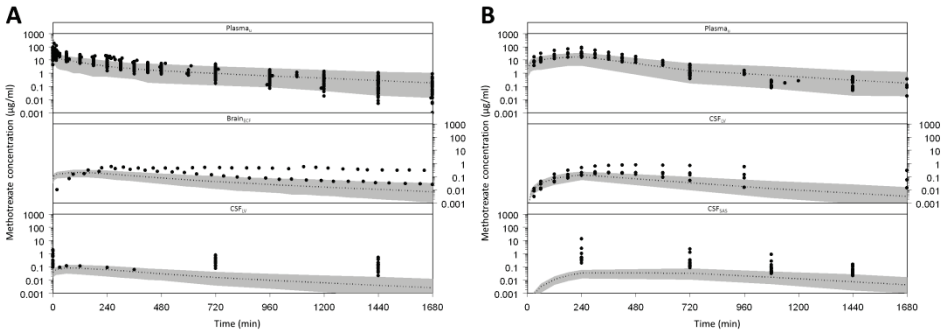

Figure 6. (A) Observed and predicted methotrexate plasma, CSF_{LV} and CSF_{SAS} concentrations in (diseased) children; (B) observed and SBPK model predicted methotrexate plasma, $brain_{ECF}$ and CSF_{LV} concentrations in (diseased) adults. Plasma data from adults and children were collected from different studies (see text and table 4). Adult $brain_{ECF}$ data were obtained from 2 patients with supratentorial glioma (Blakeley et al., 2009). Adult CSF_{LV} data were obtained from 21 patients with meningeal leukemia or meningeal carcinomatosis (Shapiro et al., 1975) or 16 patients with primary tumor (Glantz et al., 1998). Child CSF_{LV} data were obtained from 4 patients (serial sampling) with medulloblastoma or ependymoblastoma (Chatelut et al., 1991). Child CSF_{SAS} data were obtained from 29 patients (single sample) with non-Hodgkin's lymphoma (Vassal et al., 1990). The dots represent the individual data points and the gray area represents the 90% prediction confidence interval. The different boxes represent the $plasma_u$, $brain_{ECF}$, CSF_{LV} and CSF_{SAS} data. The hepatic clearance was assumed to be equal to the renal clearance for the final SBPK predictions

DISCUSSION

By using the parallel microdialysis probes approach, we have previously shown that, even for acetaminophen, a model compound for passive transport into, within and out of the brain, differences exist between CSF and $brain_{ECF}$ kinetics (**Chapter 3**). Furthermore, we have also shown that for quinidine, a model compound for P-gp mediated transport, differences exist between CSF and $brain_{ECF}$ kinetics, which are very much dependent of P-gp functionality (**Chapter 4**). With methotrexate being a substrate for a wide variety of transporters that are all located at the BBB and BCSFB, including RFC1 (Hinken *et al.,* 2011), BCRP (Breedveld *et al.,* 2007), MRP 2, 3 and 4 (Vlaming *et al.,* 2011), OAT 1 and 3 (Takeda *et al.,* 2002), and OATP A (Badagnani *et*

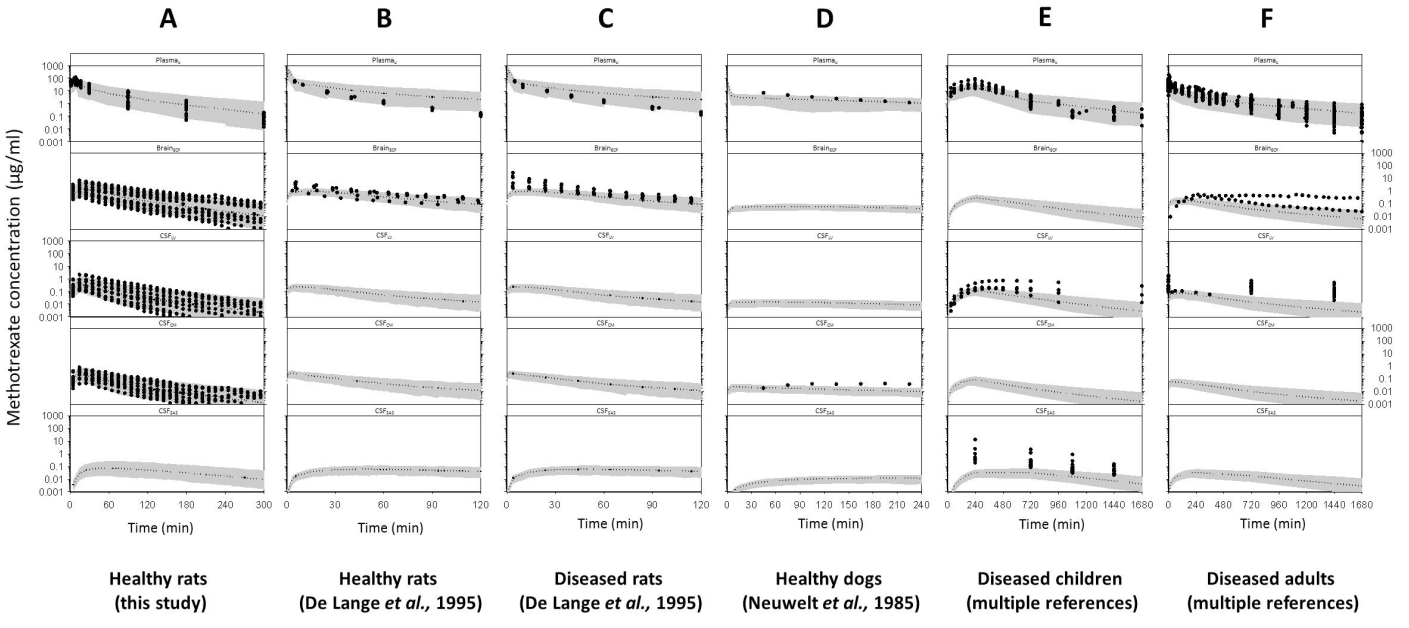

Figure 7. Observed and SBPK model predicted methotrexate plasma$_u$, brain$_{ECF}$, CSF$_{LV}$, CSF$_{CM}$ and CSF$_{SAS}$ concentration-time profiles in (A) healthy rats (this study); (B) healthy rats (De Lange et al., 1995); (C) diseased rats (De Lange et al., 1995); (D) healthy dogs (Neuwelt et al., 1985); (E) diseased children (multiple references); (F) diseased adults (multiple references). The dots represent the individual data points and the gray area represents the 90% prediction confidence interval. The different boxes represent the plasma$_u$, brain$_{ECF}$, CSF$_{LV}$, CSF$_{CM}$ and CSF$_{SAS}$ data. For healthy dogs and diseased humans the hepatic clearance was adapted as described in the text. Note: please mind the differences in the time-scales presented here

al., 2006) and OATP B (van de Steeg *et al.,* 2009), this could have major implications for the predictability of $brain_{ECF}$ methotrexate concentrations on the basis of CSF methotrexate concentrations.

In this study, the parallel microdialysis probes approach was used to investigate methotrexate distribution to and within the brain, and the specific contribution of the various transporters on the brain distribution of methotrexate. Probenecid was co-administered as inhibitor of Mrps (Bakos *et al.,* 2000), Oats (Sugiyama *et al.,* 2001) and Oatps (Kis *et al.,* 2013). Probenecid is known to inhibit Mrps, Oats and Oatps with a half-maximum inhibition constant (IC50) of approximately 50-300 µg/ml (Bakos *et al.,* 2000), 5-20 µg/ml (Sugiyama *et al.,* 2001) and 1.1 µg/ml (Kis *et al.,* 2013), respectively. Previous work by Emanuelsson and Paalzow (1988) has indicated that a 150 mg/kg dose of probenecid results in plasma concentrations over 10-fold higher than the IC_{50} value up to 3 h after administration. Therefore, it is plausible to assume that the dose of probenecid is sufficient to fully inhibit Mrps, Oats and Oatps throughout the entire experimental period.

We investigated the direct relationships between brain ST methotrexate concentrations and those in different CSF locations, and unbound plasma methotrexate concentrations in the rat. Previous work from our group has indicated that the methotrexate $brain_{ECF}$-to-$plasma_{total}$ AUC ratio is approximately 5% in healthy rats (De Lange *et al.,* 1995). Similar findings have been reported for the CSF-to-$plasma_{total}$ AUC ratio (Wang *et al.,* 2003). When taking into consideration the level of plasma protein binding and the differences in sampling methods, our current results are in line with these findings. Combined results of De Lange *et al.* (1995), and Wang *et al.* (2003), would indicate that $brain_{ECF}$ exposure and CSF exposure are more-or-less similar. However, in the current study, measuring parallelly at both sites within individual rats, we have found that $brain_{ECF}$ exposure of methotrexate is significantly higher than CSF exposure. Inhibition of Mrps, Oats and Oatps by probenecid resulted in a significant increase in $brain_{ECF}$ concentrations only. CSF concentrations seemed to be affected, but not to a significant extent, due to variability (as expected for a drug like methotrexate (Spector and Johanson, 2010)). Interestingly, the $brain_{ECF}$-to-CSF concentration ratio was not significantly influenced by co-administration of probenecid. This is in contrast

with the P-gp substrate quinidine, for which the relation between $brain_{ECF}$ and CSF concentrations was dependent on P-gp functionality (**Chapter 4**)

Advanced mathematical modeling was applied, using the same structural SBPK model that was previously used for acetaminophen (**Chapter 3**) and quinidine (**Chapter 4**). For methotrexate the model parameters were estimated using the experimental data obtained in this study. The resulting SBPK model was further used to predict data obtained in other conditions and species, taking into account changes in physiological parameters.

First, the SBPK model was used to investigate the impact of disease-status on the PK of methotrexate in $plasma_u$ and $brain_{ECF}$ of brain tumor-bearing rats, compared to healthy control rats as presented by De Lange et al. (1995). Figure 4A shows that the model prediction of plasma and $brain_{ECF}$ concentrations is reasonably good. Then, figure 4B shows the SBPK prediction for healthy rat conditions, for rats in which a tumor (rhabdomyosarcoma) had been implanted in the brain (De Lange *et al.,* 1995). It shows that tumor-bearing rats have specifically increased early methotrexate $brain_{ECF}$ concentrations.

Then, systems-based scaling of our healthy rat data to healthy dogs initially resulted in a 10-to-100-fold underestimation of $plasma_u$ and CSF concentrations. However, by taking into account that hepatic elimination of methotrexate in dogs is only a fraction of the renal clearance (Henderson *et al.,* 1965), the prediction of $plasma_u$ and CSF concentrations is much improved. The CSF_{CM}-to-$plasma_u$ concentration ratio was predicted correctly. This implicates that the SBPK model of brain distribution developed for the healthy rat seemed to apply correctly for healthy dogs, provided that the hepatic clearance is corrected. Our ultimate aim is to predict human brain distribution, in health and disease. The human methotrexate data available in literature, however, were all obtained under disease conditions, hampering a direct evaluation of the SBPK model in predicting human brain distribution of methotrexate. But, with the assumption that the SBPK model could appropriately predict methotrexate brain distribution in humans, the SBPK model can be used to identify changes brought about by disease conditions. To that end, it should be realized that not only brain diseases can influence brain distribution, as was demonstrated by changes in BBB transport of the permeability marker fluorescein for rats with peripheral inflammation upon chronic exposure to rotenone (Ravenstijn *et al.,* 2008).

Extrapolation of our healthy rat data to humans with different disease states initially resulted in a 100-fold underestimation of $plasma_u$, $brain_{ECF}$ and CSF concentrations. However, by taking into account that methotrexate undergoes extensive enterohepatic circulation in humans (Hendel and Brodthagen, 1984), the prediction of $plasma_u$ concentrations is much improved. Yet, under the given disease conditions, the $brain_{ECF}$ and CSF concentrations are up to 10-fold higher than predicted for healthy conditions. Using the SBPK model, simulations indicate a possible decreased active efflux from the $brain_{ECF}$ as well as a lower CSF flow under disease conditions. Actually, Glantz *et al.* (1998) reported that several patients had abnormal (low) CSF flow. It should be realized however, that the human data available from literature reflect methotrexate disposition in body and brain in a variety of diseases that probably do not affect body processes in the same manner. So, more specific data are needed to identify specific disease-related processes that influence brain distribution of methotrexate, and could lead to more personalized treatment.

Alternatively, or in addition, differences between SBPK predicted human healthy and the observed human disease methotrexate data might originate from influences of co-medication, sampling methods and analysis methods (table 4).

Possible species differences in the abundance levels and activities of the different active transport proteins at the BBB and BCSFB, under healthy and diseased conditions, probably also play an important role. It has been previously shown that the genetic variability in transporters in humans leads to an altered sensitivity to methotrexate and thus influences the toxicity and/or efficacy of methotrexate treatment (Kotnik *et al.,* 2011). This indicates that additional information on the species differences in abundance levels and activities of the different active transport proteins and drug-metabolizing enzymes at the BBB and BCSFB, as well as at the liver and kidney, under healthy or diseased conditions, is essential for extrapolation purposes.

Table 4. Different variables in disease states and experimental conditions of the available datasets in rats, dogs, children and adults

Reference	Subjects	Disease state	Dose (i.v.)	$Brain_{ECF}$ or CSF (sampling method)	Analysis
This manuscript	Rats (225-275 g; n=32)	Healthy	40 and 80 mg/kg (10 min)	$Brain_{ECF}$, CSF_{LV} and CSF_{CM} (microdialysis)	LC/MS/MS
De Lange *et al.,* 1995	Rats (160-200 g; n=12)	Brain tumor (implanted rhabdomyo-sarcoma)	75 mg/kg (bolus)	$Brain_{ECF}$ (microdialysis)	HPLC
Neuwelt *et al.,* 1985	Dogs (20-25 kg; n=4)	Healthy	4 mg/kg (bolus) + Evans blue	CSF_{CM} (Cisterna magna sampling)	Radioimmuno-assay
Aumente *et al.,* 2006	Children (0.5-17y; n=49)	Acute lympho-blastic leukemia	3 g/m^2 (4 h) + remission-induction therapy (>24h after methotrexate)	N.A.	Fluorescence polarization immunoassay
Blakeley *et al.,* 2009	Human adults (>18y; n=2)	Recurrent high grade gliomas	12 g/m^2 (4h) + sodium bicarbonate	$Brain_{ECF}$ (intratumoral microdialysis)	LC/MS
Bore *et al.,* 1987	Human adults (17-67y; n=8)	Sarcoma, carcinoma, lung metastasis	50 mg/m^2 (bolus) (no co-medication)	N.A.	Radioimmuno-assay
Chatelut *et al.,* 1991	Children (2-17y; n=4)	Medullo-blastoma or ependymo-blastoma	8 g/m^2 (4 h) + sodium bicarbonate (i.v. hydration)	CSF_{LV} (ventriculo-peritoneal derivation)	Enzymatic assay
Colom *et al.,* 2009	Children (n=14)	Osteo-sarcoma	12 g/m^2 (4 h) + leucovorin (24h after methotrexate)	N.A.	Fluorescence polarization immunoassay
Creaven *et al.,* 1976	Human adults (n=9)	Small-cell lung carcinoma	15 mg/m^2 (bolus) (no co-medication)	N.A.	[^{3}H]methotrex-ate

Table 4 continued

Glantz *et al.,* 1998	Human adults (>18y; n=16)	Histologically diagnosed primary tumor	8 g/m^2 (4 h) + leucovorin (24h after methotrexate)	CSF_{LV} (ventricular reservoirs)	Fluorescence polarization immunoassay
Herman *et al.,* 1989	Human adults (16-80y; n=41)	Rheumatoid arthritis	10 mg/m^2 (bolus) (no co-medication)	N.A.	Radiochemical-ligand binding assay
Shapiro *et al.,* 1975	Human adults (18-63y; n=21)	Leukemia and carcinoma	50 mg (bolus) (no co-medication)	CSF_{LV} (Ommaya reservoir)	microbiologic disk assay
Stewart *et al.,* 1990	Human adults (30-78y; n=15)	Rheutmatoid arthritis	15 mg (5 min) (received naproxen 3 days before)	N.A.	Radioenzymatic assay
Vassal *et al.,* 1990	Children (3-15y; n=29)	Non-Hodgkin's lymphoma	3 g/m^2 (3 h) + sodium bicarbonate (i.v. hydration)	CSF_{SAS} (lumbar puncture)	Fluorescence polarization immunoassay

CONCLUSION

It is concluded that in parallel obtained data on unbound $brain_{ECF}$, CSF and plasma concentrations, under dynamic conditions, combined with advanced mathematical modeling is a most valid approach to develop SBPK models that allow revealing the mechanisms underlying the relationship between $brain_{ECF}$ and CSF concentrations. In contrast to the P-gp substrate quinidine and P-gp mediated active transport, for methotrexate we have found that inhibition of Mrp/Oat/Oatp-mediated active transport processes does not significantly influence the relationship between $brain_{ECF}$ and CSF concentrations.

Our results suggest that the extrapolation of our healthy rat data to healthy dogs works reasonably well, provided that information on the different elimination routes, or the lack thereof, is included in the systems-based scaling approach. For the correct prediction of $plasma_u$, $brain_{ECF}$ or CSF concentrations in diseased humans, additional information is needed on specific disease states in order to identify which processes are influenced by the disease condition to improve personalized treatment, in which the SBPK model is anticipated to be a useful tool.

APPENDIX

DIFFERENTIAL EQUATIONS

The mass balance equations describing the final SBPK model were expressed as follows:

Plasma:

$$\frac{dA_{PL,u}}{dt} = dose - k_{PL-PER,rapid} \times A_{PL,u} + k_{PER,rapid-PL} \times A_{PER,rapid}$$
$$-k_{PL-PER,slow} \times A_{PL,u} + k_{PER,slow-PL} \times A_{PER,slow} - k_{PL-ECF} \times A_{PL,u}$$
$$+k_{ECF-PL} \times A_{ECF} - k_{PL-LV} \times A_{PL,u} + k_{LV-PL} \times A_{LV} - k_{PL-TFV} \times A_{PL,u}$$
$$+k_{TFV-PL} \times A_{TFV} - k_{PL-CM} \times A_{PL,u} + k_{CM-PL} \times A_{CM} + \left(\frac{Q_{CSF}}{V_{SAS}}\right) \times A_{SAS} - k_E \times A_{PL,u}$$

$$C_{PL,u} = \frac{A_{PL,u}}{V_{PL}}$$

Periphery:

$$\frac{dA_{PER,rapid}}{dt} = k_{PL-PER,rapid} \times A_{PL,u} - k_{PER,rapid-PL} \times A_{PER,rapid}$$

$$C_{PER,rapid} = \frac{A_{PER,rapid}}{V_{PER,rapid}}$$

$$\frac{dA_{PER,slow}}{dt} = k_{PL-PER,slow} \times A_{PL,u} - k_{PER,slow-PL} \times A_{PER,slow}$$

$$C_{PER,slow} = \frac{A_{PER,slow}}{V_{PER,slow}}$$

$Brain_{ECF}$:

$$\frac{dA_{ECF}}{dt} = k_{PL-ECF} \times A_{PL,u} - k_{ECF-PL} \times A_{ECF} - \left(\frac{Q_{ECF}}{V_{ECF}}\right) \times A_{ECF}$$

$$C_{ECF} = \frac{A_{ECF}}{V_{ECF}}$$

CSF_{LV}:

$$\frac{dA_{LV}}{dt} = k_{PL-LV} \times A_{PL,u} - k_{LV-PL} \times A_{LV} + \left(\frac{Q_{ECF}}{V_{ECF}}\right) \times A_{ECF} - \left(\frac{Q_{CSF}}{V_{LV}}\right) \times A_{LV}$$

$$C_{LV} = \frac{A_{LV}}{V_{LV}}$$

CSF_{TFV}:

$$\frac{dA_{TFV}}{dt} = k_{PL-TFV} \times A_{PL,u} - k_{TFV-PL} \times A_{TFV} + \left(\frac{Q_{CSF}}{V_{LV}}\right) \times A_{LV} - \left(\frac{Q_{CSF}}{V_{TFV}}\right) \times A_{TFV}$$

$$C_{TFV} = \frac{A_{TFV}}{V_{TFV}}$$

CSF_{CM}:

$$\frac{dA_{CM}}{dt} = k_{PL-CM} \times A_{PL,u} - k_{CM-PL} \times A_{CM} + \left(\frac{Q_{CSF}}{V_{TFV}}\right) \times A_{TFV} - \left(\frac{Q_{CSF}}{V_{CM}}\right) \times A_{CM}$$

$$C_{CM} = \frac{A_{CM}}{V_{CM}}$$

CSF_{SAS}:

$$\frac{dA_{SAS}}{dt} = \left(\frac{Q_{CSF}}{V_{CM}}\right) \times A_{CM} - \left(\frac{Q_{CSF}}{V_{SAS}}\right) \times A_{SAS}$$

$$C_{SAS} = \frac{A_{SAS}}{V_{SAS}}$$

Where:

$k_E = (CL_{E,p} + CL_{E,a})/V_{PL}$

$k_{PL-PER,rapid} = CL_{PL-PER,rapid}/V_{PL}$

$k_{PER,rapid-PL} = CL_{PL-PER,rapid}/V_{PER,rapid}$

$k_{PL-PER,slow} = CL_{PL-PER,slow}/V_{PL}$

$k_{PER,slow-PL} = CL_{PL-PER,slow}/V_{PER,slow}$

$k_{PL-ECF} = (CL_{PL-ECF,p} - CL_{PL-ECF,a})/V_{PL}$

$k_{ECF-PL} = (CL_{ECF-PL,p} + CL_{ECF-PL,a})/V_{ECF}$

$k_{PL-LV} = (CL_{PL-LV,p} - CL_{PL-LV,a})/V_{PL}$

$k_{LV-PL} = (CL_{LV-PL,p} + CL_{LV-PL,a})/V_{LV}$

$k_{PL-TFV} = (CL_{PL-TFV,p} - CL_{PL-TFV,a})/V_{PL}$

$k_{TFV-PL} = (CL_{TFV-PL,p} + CL_{TFV-PL,a})/V_{TFV}$

$k_{PL-CM} = (CL_{PL-CM,p} - CL_{PL-CM,a})/V_{PL}$

$k_{CM-PL} = (CL_{CM-PL,p} + CL_{CM-PL,a})/V_{CM}$

NOMENCLATURE

A_i	Amount of methotrexate in compartment i (ng)
C_i	Concentration of methotrexate in compartment i (ng/ml)
k	rate constant (min^{-1})
Q	flow rate (ml/min)
CL	clearance (ml/min)
V	volume (ml)

Subscripts

PL	plasma
PL,u	unbound methotrexate in plasma
PER,rapid	rapidly equilibrating peripheral compartment
PER,slow	slowly equilibrating peripheral compartment
ECF	$brain_{ECF}$

CSF	CSF
LV	lateral ventricle
TFV	third and fourth ventricle
CM	cisterna magna
SAS	subarachnoid space

REFERENCES

Abbott NJ. Evidence for bulk flow of brain interstitial fluid: significance for physiology and pathology. Neurochem Int 2004; 45: 545-552.

Adam R, Greenberg JO. The mega cisterna magna. J Neurosurg 1978; 48: 190-192.

Atherton JC. Glomerular filtration rate and salt and water reabsorption during pregnancy in the conscious rat. J Physiol 1983; 334: 493-504.

Aumente D, Santos Buelga D, Lukas JC, Gomez P, Torres A, García MJ. Population pharmacokinetics of high-dose methotrexate in children with acute lymphoblastic leukaemia. Clin Pharmacokinet 2006; 45: 1227-1238.

Badagnani I, Castro RA, Taylor TR, Brett CM, Huang CC, Stryke D, Kawamoto M, Johns SJ, Ferrin TE, Carlson EJ, Burchard EG, Giacomini KM. Interaction of methotrexate with organic-anion transporting polypeptide 1A2 and its genetic variants. J Pharmacol Exp Ther 2006; 318: 521-529.

Bakos É, Evers R, Sinkó E, Váradi A, Borst P, Sarkadi B. Interactions of the human multidrug resistance proteins MRP1 and MRP2 with organic anions. Mol Pharmacol 2000; 57: 760-768.

Balis FM, Poplack DG. Central nervous system pharmacology of antileukemic drugs. Am J Pediatr Hematol Oncol 1989; 11: 74-86.

Bass NH, Lundborg P. Postnatal development of bulk flow in the cerebrospinal fluid system of the albino rat: clearance of carboxyl-[14C]inulin after intrathecal infusion. Brain Res 1973; 52: 323-332.

Bayliss MK, Bell JA, Jenner WN, Park GR, Wilson K. Utility of hepatocytes to model species differences in the metabolism of loxtidine and to predict pharmacokinetic parameters in rat, dog and man. Xenobiotica 1999; 29: 253-268.

Bering EA Jr. Cerebrospinal fluid production and its relationship to cerebral metabolism and cerebral blood flow. Am J Physiol 1959; 197: 825-828.

Blakeley JO, Olson J, Grossman SA, He X, Weingart J, Supko JG. Effect of blood brain barrier permeability in recurrent high grade gliomas on the intratumoral pharmacokinetics of methotrexate: a microdialysis study. J Neurooncol 2009; 91: 51-58.

Blaney SM, Poplack DG. Pharmacologic strategies for the treatment of meningeal malignancy. Invest New Drugs 1996; 14: 69-85.

Bleyer WA, Poplack DG. Prophylaxis and treatment of leukemia in the central nervous system and other sanctuaries. Semin Oncol 1985; 12: 131-148.

Bore P, Bruno R, Lena N, Favre R, Cano JP. Methotrexate and 7-hydroxy-methotrexate pharmacokinetics following intravenous bolus administration and high-dose infusion of methotrexate. Eur J Cancer Clin Oncol 1987; 23: 1385-1390.

Borsi JD, Moe PJ. A comparative study on the pharmacokinetics of methotrexate in a dose range of 0.5 g to 33.6 g/m2 in children with acute lymphoblastic leukemia. Cancer 1987; 60: 5-13.

Brcakova E, Fuksa L, Cermanova J, Kolouchova G, Hroch M, Hirsova P, Martinkova J, Staud F, Micuda S. Alteration of methotrexate biliary and renal elimination during extrahepatic and intrahepatic cholestasis in rats. Biol Pharm Bull 2009; 32: 1978-1985.

Breedveld P, Pluim D, Cipriani G, Dahlhaus F, van Eijndhoven MAJ, de Wolf CJF, Kuil A, Beijnen JH, Scheffer GL, Jansen G, Borst P, Schellens JHM. The effect of low pH on breast cancer resistance protein (ABCG2)-mediated transport of methotrexate, 7-hydroxymethotrexate, methotrexate diglutamate, folic acid, mitoxantrone, topotecan, and resveratrol in in vitro drug transport models. Mol Pharmacol 2007; 71: 240-249.

Cáp J, Foltinová A, Kaiserová E, Mojzesová A, Sejnová D, Jamárik M. Is high dose methotrexate without irradiation of the brain sufficiently effective in prevention of CNS disease in children with acute lymphoblastic leukemia? Neoplasma 1998; 45: 176-179.

Chabner BA, Young RC. Threshold methotrexate concentration for in vivo inhibition of DNA synthesis in normal and tumorous target tissues. J Clin Invest 1973; 52: 1804-1811.

Chatelut E, Roche H, Plusquellec Y, Peyrille F, De Biasi J, Pujol A, Canal P, Houin G. Pharmacokinetic modeling of plasma and cerebrospinal fluid methotrexate after high-dose intravenous infusion in children. J Pharm Sci 1991; 80: 730-734.

Clarke M, Gaynon P, Hann I, Harrison G, Masera G, Peto R, Richards S. CNS-directed therapy for childhood acute lymphoblastic leukemia: childhood ALL collaborative group overview of 43 randomized trials. J Clin Oncol 2003; 21: 1798-1809.

Colom H, Farré R, Soy D, Peraire C, Cendros J-M, Pardo N, Torrent M, Domenech J, Mangues M-A. Population pharmacokinetics of high-dose methotrexate after intravenous administration in pediatric patients with osteosarcoma. Ther Drug Monit 2009; 31: 76-85.

Condon P, Patterson J, Wyper D, Hadley D, Grant R, Teasdale G, Rowan J. Use of magnetic resonance imaging to measure intracranial cerebrospinal fluid volume. Lancet 1986; 327: 1355-1357.

Cox EH, Veyrat-Follet C, Beal SL, Fuseau E, Kenkare S, Sheiner LB. A population pharmacokinetic-pharmacodynamic analysis of repeated measures time-to-event pharmacodynamic responses: the antiemetic effect of ondansetron. J Pharmacokinet Biopharm 1999; 27: 625-644.

Creaven PJ, Cohen MH, Allen LM. Methotrexate plasma decay kinetics: possible alteration in patients undergoing gut sterilization. Br J Cancer 1976; 34: 571-575.

Cserr HF. Potassium exchange between cerebrospinal fluid, plasma, and brain. Am J Physiol 1965; 209: 1219-1226.

Cserr HF, Cooper DN, Suri PK, Patlak CS. Efflux of radiolabeled polyethylene glycols and albumin from rat brain. Am J Physiol 1981; 240: F319-F328.

Davies B, Morris T. Physiological parameters in laboratory animals and humans. Pharm Res 1993; 10: 1093-1095.

Dekaban AS, Sadowsky D. Changes in brain weights during the span of human life: relation of brain weights to body heights and body weights. Ann Neurol 1978; 4: 345-356.

De Lange ECM, Danhof M. Considerations in the use of cerebrospinal fluid pharmacokinetics to predict brain target site concentrations in the clinical setting. Implications of the barriers between blood and brain. Clin Pharmacokin 2002; 41: 691-703.

de Lange ECM, de Vries JD, Zurcher C, Danhof M, de Boer AG, Breimer DD. The use of intracerebral microdialysis for the determination of pharmacokinetic profiles in anticancer drugs in tumor-bearing rat brain. Pharm Res 1995; 12: 1924-1931.

Dickey CC, Shenton ME, Hirayasu Y, Fischer I, Voglmaier MM, Niznikiewicz MA, Seidman LJ, Fraone S, McCarley RW. Large CSF volume not attributable to ventricular volume in schizotypical personality disorder. Am J Psychiatry 2000; 157: 48-54.

Djerassi I, Farber S, Abir E, Neikirk W. Continuous infusion of methotrexate in children with acute leukemia. Cancer 1967; 20: 233-242.

Dohrmann GJ. The choroid plexus: a historical review. Brain Res 1970; 18: 197-218.

Duffull SB, Aarons L. Development of a sequential linked pharmacokinetic and pharmacodynamics simulation model for ivabradine in healthy volunteers. Eur J Pharm Sci 2000; 10: 275-284.

Emanuelsson B-M, Paalzow LK. Dose-dependent pharmacokinetics of probenecid in the rat. Biopharm Drug Dispos 1988; 9: 59-70.

Evans AE, Gilbert ES, Zandstra R. The increasing incidence of central nervous system leukemia in children. Cancer 1970; 26: 404-409.

Ferreri AJM, Guerra E, Regazzi M, Pasini F, Ambrosetti A, Pivnik A, Gubkin A, Calderoni A, Spina M, Brandes A, Ferrarese F, Rognone A, Govi S, Dell'Oro S, Locatelli M, Villa E, Reni M. Area under the curve of methotrexate and creatinine clearance are outcome-determining factors in primary CNS lymphomas. Br J Cancer 2004; 90: 353-358.

Frank H, Gray SJ. The determination of plasma volume in man with radioactive chromic chloride. J Clin Invest 1953; 32: 991-999.

Fridén M, Winiwarter S, Jerndal G, Bengtsson O, Wan H, Bredberg U, Hammarlund-Udenaes M, Antonsson M. Structure-brain exposure relationships in rat and human using a novel data set of unbound drug concentrations in brain interstitial and cerebrospinal fluids. J Med Chem 2009; 52: 6233-6243.

Gjedde A. High- and low-affinity transport of D-glucose from blood to brain. J Neurochem 1981; 36: 1463-1471.

Glantz MJ, Cole BF, Recht L, Akerley W, Milles P, Saris S, Hochberg F, Calabresi P, Egorin MJ. High-dose intravenous methotrexate for patients with nonleukemic leptomeningeal cancer: is intrathecal chemotherapy necessary? J Clin Oncol 1998; 16: 1561-1567.

Graff CL, Pollack GM. Drug transport at the blood-brain barrier and the choroid plexus. Curr Drug Metab 2004; 5: 95-108.

Guo P, Wang X, Liu L, Belinsky MG, Kruh GD, Gallo JM. Determination of methotrexate and its major metabolite 7-hydroxymethotrexate in mouse plasma and brain tissue by liquid chromatography-tandem mass spectrometry. J Pharm Biomed Anal 2007; 43: 1789-1795.

Hendel J, Brodthagen H. Entero-hepatic cycling of methotrexate estimated by use of the D-isomer as a reference marker. Eur J Clin Pharmacol 1984; 26: 103-107.

Henderson ES, Adamson RH, Denham C, Oliverio VT. The metabolic fate of tritiated methotrexate I. absorption, excretion, and distribution in mice, rats, dogs and monkeys. Cancer Res 1965; 25: 1008-1017.

Herman RA, Veng-Pedersen P, Hoffman J, Koehnke R, Furst DE. Pharmacokinetics of low-dose methotrexate in rheumatoid arthritis patients. J Pharm Sci 1989; 78: 165-171.

Hertz R, Li MC, Spencer DB. Effect of methotrexate therapy upon choriocarcinoma and chorioadenoma. Proc Soc Exp Biol Med 1956; 93: 361-366.

Hinken W, Halwachs S, Kneuer C, Honscha W. Subcellular localization and distribution of the reduced folate carrier in normal rat tissues. Eur J Histochem 2011; 55: 11-18.

Hosseini-Yeganeh M, McLachlan AJ. Physiologically based pharmacokinetic model for terbinafine in rats and humans. Antimicrob Agents Chemother 2002; 46: 2219-2228.

Hryniuk WM, Bertino JR. Treatment of leukemia with large doses of methotrexate and folinic acid: clinical-biochemical correlates. J Clin Invest 1969; 48: 2140-2155.

Hutchinson RJ, Gaynon PS, Sather H, Bertolone SJ, Cooper HA, Tannous R, Wells LM, Heerema NA, Sailer S, Trigg ME. Intensification of therapy for children with lower-risk acute lymphoblastic leukemia: long-term follow-up of patients treated on Children's Cancer Group trial 1881. J Clin Oncol 2003; 21: 1790-1797.

ICRP. Basic anatomical and physiological data for use in radiological protection reference values. ICRP Publication 89. Ann ICRP 2002; 32: 3-4.

Jönsson P, Höglund P, Wiebe T, Schrøder H, Seidel H, Skärby T. Methotrexate concentrations in cerebrospinal fluid and serum, and the risk of central nervous system relapse in children with acute lymphoblastic leukaemia. Anticancer Drugs 2007; 18: 941-948.

Kalvass JC, Maurer TS. Influence of nonspecific brain and plasma binding of CNS exposure: implications for rational drug discovery. Biopharm Drug Dispos 2002; 23: 327-338.

Kates RE, Tozer TN. Biliary secretion of methotrexate in rats and its inhibition by probenecid. J Pharm Sci 1976; 65: 1348-1352.

Kawai R, Lemaire M, Steimer J-L, Bruelisauer A, Niederberger W, Rowland M. Physiologically based pharmacokinetic study on a cyclosporine derivative, SDZ IMM 125. J Pharmacokinet Biopharm 1994; 22: 327-365.

Keep RF, Jones HC. Cortical microvessels during brain development: a morphometric study in the rat. Microvasc Res 1990a; 40: 412-426

Keep RF, Jones HC. A morphometric study on the development of the lateral ventricle choroid plexus, choroid plexus capillaries and ventricular ependymal in the rat. Dev Brain Res 1990b; 56: 47-53.

Keidan I, Bielorei B, Berkenstadt H, Aizenkraft A, Harel B, Huna-Baron R, Kaplinsky C. Prospective evaluation of clinical and laboratory effects of intrathecal chemotherapy on children with acute leukemia. J Pediatr Hematol Oncol 2005; 27: 307-310.

Kimelberg HK. Water homeostasis in the brain: basic concepts. Neurosci 2004; 129: 851-860.

Kis O, Zastre JA, Hoque MT, Walmsley SL, Bendayan R. Role of drug efflux and uptake transporters in atazanavir intestinal permeability and drug-drug interactions. Pharm Res 2013; 30: 1050-1064.

Kohn MI, Tanna NK, Herman GT, Resnick SM, Mozley PD, Gur RE, Alavi A, Zimmerman RA, Gur GC. Analysis of brain and cerebrospinal fluid volumes with MR imaging. Part I. Methods, reliability, and validation. Radiology 1991; 178: 115-122.

Kotnik BF, Grabnar I, Grabar PB, Dolžan, Jazbec J. Association of genetic polymorphism in the folate metabolic pathway with methotrexate pharmacokinetics and toxicity in acute lymphoblastic leukaemia and malignant lymphoma. Eur J Clin Pharmacol 2011; 67: 993-1006.

Lange BJ, Bostrom BC, Cherlow JM, Sensel MG, La MKL, Rackoff W, et al. Double-delayed intensification improves event-free survival for children with intermediate-risk acute lymphoblastic leukemia: a report from the Children's Cancer Group. Blood 2002; 99: 825-833.

Lee HB, Blaufox MD. Blood volume in the rat. J Nucl Med 1985; 26: 72-76.

Lee G, Dallas S, Hong M, Bendayan R. Drug transporters in the central nervous system: brain barriers and brain parenchyma considerations. Pharmacol Rev 2001; 53: 6233-6243.

Levinger IM. The cerebral ventricles of the rat. J Anat 1971; 108: 447-451.

Lin JH. CSF as a surrogate for assessing CNS exposure: an industrial perspective. Curr Drug Metab 2008; 9: 46-59.

Linderkamp O, Versmold HT, Riegel KP, Betke K. Estimation and prediction of blood volume in infants and children. Eur J Pediat 1977; 125: 227-234.

Liu X, Smith BJ, Chen C, Callegari E, Becker SL, Chen X, Cianfrogna J, Doran AC, Doran SD, Gibbs JP, Hosea N, Liu J, Nelson FR, Szewc MA, Van Deusen J.. Evaluation of cerebrospinal fluid concentration and plasma free concentration as surrogate measurement for brain free concentration. Drug Metab Dispos 2006; 34: 1443-1447.

Liu X, Van Natta K, Yeo H, Vilenski O, Weller PE, Worboys PS, Monshouwer M. Unbound drug concentration in brain homogenate and cerebrospinal fluid at steady state as a surrogate for unbound concentration in brain interstitial fluid. Drug Metab Dispos 2009; 37: 787-793.

Löfgren J, von Essen C, Zwetnow N. The pressure-volume curve of the cerebrospinal fluid space in dogs. Acta Neurol Scandinav 1973; 49: 557-574.

Maurer TS, DeBartolo DB, Tess DA, Scott D. Relationship between exposure and nonspecific binding of thirty-three central nervous system drugs in mice. Drug Metab Dispos 2005; 33: 175-181.

Milano G, Thyss A, Serre Debeauvais F, Laureys G, Benoit Y, Deville A, Dutour C, Robert A, Otten J, Behar C, Frappaz D. CSF drug levels for children with acute lymphoblastic leukemia treated by 5 g/m2 methotrexate. A study from the EORTC Children's Leukemia Cooperative Group. Eur J Cancer 1990; 26: 492-495.

Millot F, Rubie H, Mazingue F, Mechinaud F, Thyss A. Cerebrospinal fluid drug levels of leukemic children receiving intravenous 5 g/m2 methotrexate. Leuk Lymphoma 1994; 14: 141-144.

Moe PJ, Holen A. High-dose methotrexate in childhood ALL. Pediatr Hematol Oncol 2000; 17: 615-622.

Neuwelt EA, Barnett PA, McCormick CI, Frenkel EP, Minna JD. Osmotic blood-brain barrier modification: monoclonal antibody, albumin, and methotrexate delivery to cerebrospinal fluid and brain. Neurosurg 1985; 17: 419-423.

Niemann A, Mühlisch J, Frühwald MC, Gerß J, Hempel G, Boos J. Therapeutic drug monitoring of methotrexate in cerebrospinal fluid after systemic high-dose infusion in children: can the burden of intrathecal methotrexate be reduced? Ther Drug Monit 2010; 32: 467-475.

Nilsson C, Stahlberg F, Thomsen C, Henriksen O, Herning M, Owman C. Circadian variation in human cerebrospinal fluid production measured by magnetic resonance imaging. Am J Physiol 1992; 262: R20-R24.

Ochs J, Mulhern R. Long-term sequalae of therapy for childhood acute lymphoblastic leukemia. Baillieres Clin Haematol 1994; 7: 365-376.

Pardridge WM. Drug and gene targeting to the brain with molecular Trojan horses. Nat Rev Drug Discov 2002; 1: 131-139.

Pardridge WM. Drug transport in brain via the cerebrospinal fluid. Fluids Barriers CNS 2011; 8: 7.

Pui CH, Campana D, Pei D, Bowman WP, Sandlund JT, Kaste SC, Ribeiro RC, Rubnitz JE, Raimondi SC, Onciu M, Coustan-Smith E, Kun LE, Jeha S, Cheng C, Howard SC, Simmons V, Bayles A, Metzger ML, Boyett JM, Leung W, Handgretinger R, Downing JR, Evans WE, Relling MV. Treating childhood acute lymphoblastic leukemia without cranial irradiation. N Engl J Med 2009; 360: 2730-2741.

Ravenstijn PG, Merlini M, Hameetman M, Murray TK, Ward MA, Lewis H, Ball G, Mottart C, de Ville de Goyet C, Lemarchand T, van Belle K, O'Neill MJ, Danhof M, De Lange ECM. The exploration of rotenone as a toxin for inducing Parkinson's disease in rats, for application in BBB transport and PK-PD experiments. J Pharmacol Toxicol Methods 2008; 57: 114-130.

Robertson EG. Developmental defects of the cisterna magna and dura mater. J Neurol Neurosurg Psychiatry 1949; 12: 39-51.

Rule G, Chapple M, Henion J. A 384-well solid-phase extraction for LC/MS/MS determination of methotrexate and its 7-hydroxy metabolite in human urine and plasma. Anal Chem 2001; 73: 439-443.

Scheller D, Kolb J. The internal reference technique in microdialysis: a practical approach to monitoring dialysis efficiency and to calculating tissue concentration from dialysate samples. J Neurosci Methods 1991; 40: 31-38.

Schwartz GJ, Haycock GB, Edelmann CM Jr, Spitzer A. A simple estimate of glomerular filtration rate in children derived from body length and plasma creatinine. Pediatrics 1976; 58: 259-263.

Shapiro WR, Young DF, Mehta BM. Methotrexate: distribution in cerebrospinal fluid after intravenous, ventricular and lumbar injections. N Engl J Med 1975; 293: 161-166.

Shen DD, Artru DD, Adkison KK. Principles and applicability of CSF sampling for the assessment of CNS drug delivery and pharmacodynamics. Adv Drug Del Rev 2004; 56: 1825-1857.

Skibińska L, Ramlau C, Załuski J, Olejniczak B. Methotrexate binding to human plasma proteins. Pol J Pharmacol Pharm 1990; 42: 151-157.

Smith M, Arthur D, Camitta B, Carroll AJ, Crist W, Gaynon P, Gelber R, Heerema N, Korn EL, Link M, Murphy S, Pui C-H, Pullen J, Reaman G, Sallan SE, Sather H, Shuster J, Simon R, Trigg M, Tubergen D, Uckun F, Ungerleider R. Uniform approach to risk classification and treatment assignment for children with acute lymphoblastic leukemia. J Clin Oncol 1996; 14: 18-24.

Spector R, Johanson CE. Vectorial ligand transport through mammalian choroid plexus. Pharm Res 2010; 27: 2054-2062.

Ståhle L, Segersvärd S, Ungerstedt U. A comparison between three methods for estimation of extracellular concentrations of exogenous and endogenous compounds by microdialysis. J Pharmacol Methods 1991; 25: 41-52.

Stewart CF, Fleming RA, Arkin CR, Evans WE. Coadministration of naproxen and low-dose methotrexate in patients with rheumatoid arthritis. Clin Pharmacol Ther 1990; 47: 540-546.

Sugiyama D, Kusuhara H, Shitara Y, Abe T, Meier PJ, Sekine T, Endou H, Suzuki H, Sugiyama Y. Characterization of the efflux transport of 17β-estradiol-D-17β-glucuronide from the brain across the blood-brain barrier. J Pharmacol Exp Ther 2001; 298: 316-322.

Syvänen S, Xie R, Sahin S, Hammarlund-Udenaes M. Pharmacokinetic consequences of active drug efflux at the blood-brain barrier. Pharm Res 2006; 23: 705-717.

Takeda M, Khamdang S, Narikawa S, Kimura H, Hosoyamada M, Cha SH, Sekine T, Endou H. Characterization of methotrexate transport and its drug interactions with human organic anion transporters. J Pharmacol Exp Ther. 2002; 302: 666-671.

Thorne RG, Hrabětová S, Nicholson C. Diffusion of epidermal growth factor in rat brain extracellular space measured by integrative optical imaging. J Neurophysiol 2004; 92:3471-3481.

Thyss A, Milano G, Deville A, Manassero J, Renee N, Schneider M. Effect of dose and repeat intravenous 24 hr infusions of methotrexate on cerebrospinal fluid availability in children with hematological malignancies. Eur J Cancer Clin Oncol 1987; 23: 843-847.

Troncin R, Dadure C. Pediatric spinal anaesthesia. Update Anaesthesia 2009; 25: 22-24.

van de Steeg E, van der Kruijssen CMM, Wagenaar E, Burggraaf JEC, Mesman E, Kenworthy KE, Schinkel AH. Methotrexate pharmacokinetics in transgenic mice with liver-specific expression of human organic anion-transporting polypeptide 1B1 (SLCO1B1). Drug Metab Dispos 2009; 37: 277-281.

Vassal G, Valteau D, Bonnay M, Patte C, Aubier F, Lemerle J. Cerebrospinal fluid and plasma methotrexate levels following high-dose regimen given as a 3-hour intravenous infusion in children with nonHodgkin's lymphoma. Pediatr Hematol Oncol 1990; 7: 71-77.

Visser MP, Krill MTA, Willems GM, Hermens WT. Plasma volume determination by use of enzyme dilution in the dog. Lab Animals 1982; 16: 248-255.

Vladić A, Klarica M, Bulat M. Dynamics of distribution of ^{3}H-inulin between the cerebrospinal fluid compartments. Brain Res 2009; 1248: 127-135.

Vlaming MLH, van Esch A, van de Steeg E, Pala Z, Wagenaar E, van Tellingen O, Schinkel AH. Impact of Abcc2 [multidrug resistance-associated protein (Mrp) 2], Abcc3 (Mrp3), and Abcg2 (breast cancer resistance protein) on the oral pharmacokinetics of methotrexate and its main metabolite 7-hydroxymethotrexate. Drug Metab Dispos 2011; 39: 1338-1344.

Von Hendy-Willson VE, Pressler BM. An overview of glomerular filtration rate testing in dogs and cats. Vet J 2011; 188: 156-165.

Wang F, Jiang X, Lu W. Profiles of methotrexate in blood and CSF following intranasal and intravenous administration to rats. Int J Pharm 2003; 263: 1-7.

Yano Y, Beal SL, Sheiner SL. Evaluating pharmacokinetic/pharmacodynamics models using the posterior predictive check. J Pharmacokinet Pharmacodyn 2001; 27: 171-192.

Yasuda T, Tomita T, McLone DG, Donovan M. Measurement of cerebrospinal fluid output through external ventricular drainage in one hundred infants and children: correlation with cerebrospinal fluid production. Pediatr Neurosurg 2002; 36: 22-28.

Section III

General discussion and future perspectives

Chapter 6

Prediction of brain target site concentrations on the basis of CSF PK: General discussion and perspectives

FACTORS THAT GOVERN THE PHARMACOKINETICS IN THE BRAIN

In the development of drugs for the treatment of central nervous system (CNS) disorders, the prediction of human CNS drug action is a big challenge. In part this has been due to the sole focus on the blood-brain barrier (BBB) permeability of drugs, which, as classical paradigm, is governed by the lipophilicity and molecular weight of drugs (Levin, 1980). However, not all processes that determine drug concentrations at the relevant target site within the CNS are taken into account. Besides plasma pharmacokinetics (PK), plasma protein binding, and passive and active transport across the blood-brain barriers (BBB and the blood-cerebrospinal fluid barrier (BCSFB)), processes within the brain can also influence brain target site PK, including bulk flow, diffusion, and extra-intracellular exchange (**Chapter 1**). Moreover, it is important to distinguish between the rate and the extent of all processes. For example, passing of the BBB occurs with a certain rate and to a certain extent (Hammarlund-Udenaes *et al.,* 2008). The rate of transport across the BBB is reflecting the time needed for a drug molecule to traverse this barrier, while the extent of BBB transport expresses the ratio of unbound drug concentrations in the brain compared to those in plasma at steady state ($K_{p,uu}$). It can also be calculated as the ratio of the area under the unbound concentration-time curve ($AUC_{0-\infty}$) in brain relative to that in plasma. The rate as well as the extent of BBB transport on one hand is dependent on both the (condition-dependent) characteristics of this barrier and on the physicochemical properties of the drugs (De Lange and Danhof, 2002; Levin, 1980). Likewise, for other processes the rate and extent can be defined. Each of the different processes that determine drug concentrations at the relevant CNS target has its particular influence on the overall rate and extent, and thereby plays a more or less important role in having the drug in the *right place*, at the *right time*, and at the *right concentration*.

For many CNS active compounds, brain target site concentrations are best reflected by, or may even be equal to unbound drug concentrations in the brain extracellular fluid ($brain_{ECF}$) (De Lange *et al.,* 2000; Hammarlund-Udenaes*,* 2009; Watson *et al*., 2009). However, the possibility of direct measurement of $brain_{ECF}$ concentrations is highly limited in the clinical phase of drug

development. Therefore, unbound drug concentrations in human CSF are used as a surrogate for human $brain_{ECF}$ concentrations. It is often assumed that CSF concentrations readily equilibrate with $brain_{ECF}$ concentrations due to the lack of a physical barrier between the two (Lee *et al.,* 2001). However, the brain is a dynamic, multi-compartmental system in which all processes of entry, diffusion, metabolism, binding and elimination determine local CNS concentrations. Due to qualitative and quantitative differences in processes that govern the PK of drugs in the brain, a generally applicable relationship between CSF concentrations and $brain_{ECF}$ concentrations does not exist (**Chapter 1**, De Lange, 2013a; De Lange and Danhof, 2002; Lin, 2008; Shen *et al.,* 2004). This all implies the need for mechanistic investigations on the contribution of the different processes that govern the brain target site exposure.

The rate and extent of drug penetration into the brain can be studied in the preclinical setting with several *in vitro*, *ex vivo* and *in vivo* techniques (**Chapter 1**), such as the brain perfusion technique or the brain slice technique. So far, most of these preclinical techniques determine total brain concentrations, or calculate unbound $brain_{ECF}$ concentrations using the fraction unbound in brain homogenate. When using brain homogenate, cell structures are destroyed and binding sites that are normally not accessible to a drug *in vivo* may be unmasked (Liu *et al.,* 2009). This could result in an erroneous estimation of the unbound fraction in brain tissue. Moreover, in the drug discovery phase these techniques are often used such that information on solely equilibrium distribution is obtained. However, this may limit the extrapolative power of the results to the human situation. Furthermore, most of these techniques cannot be applied to humans, which makes a direct comparison of preclinical and clinical findings impossible. In contrast, CSF sampling can be used in both animals and humans, and as it provides information on unbound concentrations (with some time-dependency) it is of special interest. Most useful would be to use the intracerebral microdialysis technique for monitoring unbound brain concentrations at one (or more) selected site(s) in the brain, but its use in humans is highly restricted. However, if applied in animals, intracerebral microdialysis may still reveal mechanistic information on the inter-relationships of different processes that govern the $brain_{ECF}$-CSF PK in different conditions *in vivo*, and may investigate such in conjunction with pharmacodynamic (PD) read-outs. Such information may provide useful links to the human situation.

PARALLEL INTRACEREBRAL MICRODIALYSIS

With intracerebral microdialysis it is possible to monitor local unbound concentrations of compounds at one or more specific sites in the brain. Thus, with the use of multiple intracerebral microdialysis probes in individual animals one can directly compare unbound concentrations in $brain_{ECF}$, CSF from lateral ventricle (CSF_{LV}) and CSF from cisterna magna (CSF_{CM}), thereby gaining insight into the relationship between $brain_{ECF}$ and CSF concentrations. However, special care should be taken in determining the concentration recovery. Because of the continuous flow of the perfusion solution through the microdialysis probe, the concentration in the dialysate will be lower than in the surrounding $brain_{ECF}$ or CSF. (De Lange *et al.,* 2000). This indicates the need for determination of the *in vivo* recovery for proper correction of the dialysate to $brain_{ECF}$ and CSF concentrations, preferably for each brain location and for each experimental condition.

The aim of the research presented in this thesis was to develop a preclinical brain distribution model, allowing the prediction of human brain target site concentrations on the basis of preclinical data. In order to be able to build a brain distribution model understanding of time-dependent (also non-steady state) kinetics of the unbound drug in $brain_{ECF}$ and CSF is essential. To that end, systematic studies on the inter-relationship of plasma PK, BBB transport, BCSFB transport and intra-brain distribution were performed in the rat by using probes at multiple brain sites in individual animals.

As a general approach, three compounds with different physicochemical properties were selected as paradigm compounds (table 1). Acetaminophen was chosen as paradigm compound for passive transport into, within and out of the brain, with a medium logP and no ionization at physiological pH (**Chapter 3**). Quinidine was selected as a paradigm compound with a high logP, indicative of high passive BBB transport, and a positive charge at physiological pH. Furthermore, quinidine is a known substrate for P-glycoprotein (P-gp)-mediated transport out of the brain. To investigate the specific contribution of P-gp-mediated transport P-gp was inhibited by co-administration of tariquidar, a selective P-gp inhibitor (**Chapter 4**). Methotrexate was selected as a paradigm compound with a low logP, indicative of low passive BBB transport, and a negative charge at physiological pH. Furthermore, methotrexate is known to be

transported by a wide variety of transporters, including the reduced folate carrier 1 (RFC1), breast cancer resistance protein (BCRP), the multidrug resistance-associated protein (MRP) family, organic anion transporters (OATs) and organic anion-transporting polypeptides (OATPs). To investigate the specific contribution of the various transporters, probenecid was co-administered as inhibitor of MRPs, OATs and OATPs (**Chapter 5**).

Table 1. Physicochemical properties of the selected paradigm compounds

Compound	MW	PSA	logP	Ionization	pKa1	pKa2	Ionized at physio-logical pH	Substrate for	Reference
Acetamino-phen	151.2	49.3	0.46	monoprotic acid	9.38	-	0% (neutral)	-	DrugBank DB00316
Quinidine	324.4	45.6	3.44	diprotic base	4.0	9.1	98% (positive)	P-gp	DrugBank DB00908
Methotrex-ate	454.4	210.5	-1.85	diprotic acid	3.4	4.1	99.9% (negative)	BCRP, MRPs, OATPs, OATs	DrugBank DB00563

Abbreviations: MW, molecular weight; PSA, polar surface area; logP, log octanol:water partition coefficient; pKa, acid dissociation constant

Since the rate of equilibration between CSF and $brain_{ECF}$ concentrations by passive diffusion is dependent on the lipophilicity and size of the compound (De Lange *et al.,* 2000; Levin, 1980), we expected the CSF and $brain_{ECF}$ concentrations to be similar for acetaminophen, because acetaminophen is a small and moderately lipophilic compound with anticipated fast transport between blood and brain. However, we have observed that $brain_{ECF}$ concentrations of acetaminophen are ~4-fold higher than its CSF concentrations. This can probably be explained by the relatively slow distribution from $brain_{ECF}$ to CSF compared to the turnover rate of CSF. This makes the CSF act as a sink, causing the observed lower concentrations in CSF compared to $brain_{ECF}$.

For the P-gp substrate quinidine we expected significant differences between $brain_{ECF}$ and CSF concentrations, since it has been well established that P-gp functions as an efflux transporter at the BBB (Schinkel, 1999), whereas there has been some evidence that P-gp could also function as an influx transporter at the BCSFB (Kassem *et al.,* 2007; Rao *et al.,* 1999). Interestingly, we found only small differences between $brain_{ECF}$ and CSF concentrations of quinidine (0.72 ±

0.20 without inhibition of P-gp and 2.22 ± 0.57 with inhibition of P-gp). On the basis of the "smaller than threefold $brain_{ECF}$-to-CSF concentration ratio paradigm" (Maurer *et al.,* 2005), this result would not be of much importance. However, in our perspective, even a small difference in PK could potentially lead to quite distinct PD, in case of a steep concentration-effect relationship, and therefore still needs to be considered. These results indicate that P-gp functionality and variations thereof may have an important effect on the $brain_{ECF}$-to-CSF concentration ratio and the extrapolation from rats to humans. For quinidine, furthermore, we also expected the unbound brain concentrations to be lower than the unbound plasma concentrations. However, to our surprise, the unbound brain concentrations in all brain compartments were significantly higher than those in plasma. Since quinidine is actively transported out of the brain, this suggests that quinidine is also transported by other transporters at the BBB and BCSFB, in the direction of the brain, possibly by organic cation transporters (Van Montfoort *et al.,* 2001). This illustrates the importance of interplay of the different transporters at the BBB and BCSFB. The influence of a particular transporter can only be dissected if specific blockers are available. Actually, only for P-gp specific blockers are available (e.g. tariquidar).

Another example of a drug that is transported by multiple active transport systems located at the BBB and BCSFB, including BCRP, MRPs, OATs and OATPs, is methotrexate. Based on differences in the direction of flux and subcellular localization of the different transporter systems at the BBB and BCSFB (**Chapter 1**), for methotrexate we were expecting significant differences between $brain_{ECF}$ and CSF concentrations. As methotrexate is a very hydrophilic compound, the extent of distribution to the brain is much lower than for acetaminophen and quinidine. Interestingly, for methotrexate we found that $brain_{ECF}$ concentrations were significantly higher than CSF concentrations (> 3-fold), and this difference seemed to be independent of probenecid co-administration. This indicates that the active transport by Mrps, Oats and Oatps does not influence the $brain_{ECF}$-CSF relationship. However, inhibition of Mrps, Oats and Oatps did result in a significant increase in both $brain_{ECF}$ and CSF concentrations. Also, for methotrexate, as transported by multiple active transport systems that cannot be inhibited in a specific manner, it becomes difficult to identify the specific contribution of each transporter. It is therefore more efficient to investigate the transport processes by systematically

influencing a subset of variables, either by varying the conditions of the system or by varying the drug properties. Using different drugs, with different drug properties, such as affinities for the different transporters, one can decipher the impact of changes at the level of these variables on the blood-brain transport and the distribution beyond.

SYSTEMS-BASED PHARMACOKINETIC MODELING

In order to predict human CNS effects, different mathematical modeling techniques can be applied (Danhof *et al.,* 2008). The most commonly applied has been the compartmental model analysis (Fleishaker and Smith, 1987), in which the brain compartment is modeled as an effect compartment (Hammarlund-Udenaes *et al.,* 1997; Sheiner *et al.*, 1979). Here the plasma concentration is the driving force for brain concentrations, without uptake into or elimination from the brain influencing the concentration-time profile in blood. Extrapolation of animal PK parameters to the human situation can sometimes be performed reasonably well by allometric scaling, using bodyweight or body surface area as the main determinant of PK parameters.

The physiologically-based pharmacokinetic (PBPK) modeling approach has provided the basis for interspecies extrapolation. It has focused on quantitative modeling of mass transport into and out of physiological compartments and made highly significant contributions to knowledge of the body (system) and the fates of drugs (Rowland *et al*., 2011). It has not, however, taken into account the distinction between the bound and unbound drug. Inclusion of unbound concentrations, however, will provide more accurate information on specifically membrane transport processes and can be named systems-based pharmacokinetic (SBPK) modeling.

Information on species- and/or condition-dependent differences in abundance levels and activities of the different active transport proteins and drug-metabolizing enzymes at the BBB and BCSFB, as well as at the liver and kidney, under healthy or diseased conditions, is essential for extrapolation purposes. With the use of advanced SBPK modeling the contributions of individual mechanisms in animals can be revealed to serve as links to the human situation. Thus, SBPK models integrate drug-specific and system-

specific physiological parameters that vary between species, subjects, or within subjects with different age and/or disease state (Colburn, 1988; Espié *et al.,* 2009; Ings, 1990). However, even though the whole body SBPK approach would provide the best information for prediction, it requires an extensive amount of information to be able to identify the impact on specific parameters, making the whole body SBPK modeling approach highly time-consuming and costly. We therefore chose to limit the SBPK approach to the brain only, with the plasma kinetics to be defined by a simple compartmental modeling approach to determine the input function; the PK exposure of the brain. In the SBPK brain model the data that were produced on (unbound) concentrations in plasma, $brain_{ECF}$, CSF_{LV} and CSF_{CM} from single animals were used to define the time-dependent parameters on exchange between plasma, $brain_{ECF}$ and CSF concentrations between several real brain compartments with their volumes and surfaces, by diffusion, fluid flows, and active transport processes. This was all performed using non-linear mixed-effects modeling using the NONMEM software package. Thereby, also the relationship between $brain_{ECF}$ and CSF concentrations could be determined.

Using the same structural model for all three paradigm compounds, the impact of drug characteristics on brain kinetics and the $brain_{ECF}$-CSF concentration relationship is investigated in a mechanistic manner. This will contribute to the predictability of human brain target site concentrations on the basis of preclinical data.

EXTRAPOLATION TO THE HUMAN SETTING

Given that CSF concentrations are considered to be the best available surrogate for $brain_{ECF}$ concentrations in humans (Fridén *et al.,* 2009; Kalvass and Maurer, 2002; Liu *et al.,* 2006; Liu *et al.,* 2009; Maurer *et al.,* 2005), we focused on predicting human $brain_{ECF}$ concentrations. Thereby human acetaminophen CSF concentrations as presented by Bannwarth *et al.* (1992) were used as a reference in **Chapter 3**. By changing the different values of the physiological parameters of the rat to their corresponding human values, and by fitting the human plasma data to our model while extrapolating the plasma-brain exchange in a systems-based manner, we were able to adequately predict human lumbar CSF

concentrations as observed by Bannwarth *et al.* (1992). For acetaminophen in humans, it was predicted that $brain_{ECF}$ concentrations are on average ~2-fold higher than unbound plasma concentrations, whereas the $brain_{ECF}$-to-CSF (from the subarachnoid space) concentration relationship is highly dependent on the time after dose. Though we do not have data on human acetaminophen $brain_{ECF}$ data, the data as predicted for human CSF lumbar concentrations that are in line with observed lumbar concentrations (Bannwarth *et al.,* 1992) gives confidence in the usefulness of our model.

Next, for quinidine (**Chapter 4**), the inclusion of the influence of P-gp-mediated transport at the blood-brain barriers was taken into account. It was clear that P-gp functionality is an important factor in the relationship between CSF and $brain_{ECF}$ exposure, given the fact that the relative distribution of quinidine over the brain compartments changes with blocking P-gp-mediated transport by co-administration of tariquidar. No data were available on quinidine CSF distribution in human, so at this moment in time this observation cannot be validated for the human situation.

For methotrexate there is quite some clinical data available, including $brain_{ECF}$ concentrations in humans (Blakeley *et al.,* 2009). However, all published human data (children and adults) has been obtained from patients with different disease states. It is therefore not logical to expect proper prediction of diseased human concentrations in different brain compartments on the basis of a preclinical model developed on data obtained in healthy rats. This is because diseases may influence the rate and extent of several processes that govern brain target site concentrations of (also non-) CNS active compounds. Actually, it is of high value to identify disease-specific induced changes in particular PK processes (and therewith PD impact). Assuming proper predictions of human brain concentrations under healthy conditions by the preclinical derived model, deviations of particular brain concentrations in disease conditions may as well be used to identify parameter "suspects" responsible for or contributing to changes in brain compartment concentrations.

In **Chapter 5** we therefore applied the SBPK model on literature data on methotrexate brain distribution, first, to predict data obtained in other healthy rats (plasma and $brain_{ECF}$ data), then, to investigate the impact of disease-status on the PK of methotrexate. By using the same PK parameter values that were estimated based on our data, we were able to predict the methotrexate plasma

and $brain_{ECF}$ concentrations in other healthy rats reasonably well. For earlier reported $brain_{ECF}$ concentrations of methotrexate in brain tumor-bearing rats (De Lange et al., 1995) the predictions by the preclinical brain distribution model were found to be significantly lower, indicating increased distribution of methotrexate at the brain tumor site. The next step was to use our SBPK model to predict plasma and CSF concentrations in healthy dogs. When taking into account that the hepatic elimination of methotrexate in dogs is only a fraction of the renal clearance (Henderson *et al.,* 1965), whereas in rats the hepatic elimination of methotrexate is estimated to be over 5-fold higher than the renal clearance, the predictions of plasma and CSF concentrations were reasonable.

In the case where a disease condition is the variable in a cross-compare designed study, the SBPK brain distribution model can be used in helping to identify which parameters (e.g. the elimination from plasma or the blood-brain transport) are possibly influenced. Furthermore, provided that the SBPK brain distribution model is able to describe the different processes well in healthy conditions, simulations will help in our understanding of the impact of parameter changes in disease conditions. With the assumption that our SBPK brain distribution model can appropriately predict methotrexate brain distribution in healthy humans, this model could be used to identify changes in methotrexate distribution brought about by disease conditions (like for the tumor-bearing rats).

In humans, methotrexate undergoes extensive enterohepatic circulation, effectively reducing the hepatic elimination rate to the same level as the renal elimination rate (Hendel and Brodthagen, 1984). With this information incorporated into the model, the prediction of human unbound methotrexate plasma concentrations is reasonable. However, under the given disease conditions, the $brain_{ECF}$ and CSF concentrations are significantly higher than predicted for healthy conditions. Simulations indicate a possible decreased active efflux from the $brain_{ECF}$ as well as a lower CSF flow could be the cause of these higher $brain_{ECF}$ and CSF concentrations under the given disease conditions. The reduced CSF flow as "suspect" contributor to changed methotrexate brain PK is in line with the observation that several adult patients had an obstruction to normal CSF flow (Glantz *et al.,* 1998).

So, interestingly, apart from blood-brain transport, the CSF flow seems to play an important role in the $brain_{ECF}$-CSF relationship. For acetaminophen and

methotrexate, the CSF acts as a sink, causing the observed lower concentrations in CSF compared to $brain_{ECF}$. As the relative rate of CSF turnover in rats is much higher than in humans, the sink effect in humans could be smaller as compared to that in rats. Then, certain drugs and certain diseases may influence CSF formation. This indicates that CSF turnover should also be considered in the $brain_{ECF}$-CSF relationship.

FUTURE PERSPECTIVES

To be able to predict CNS drug effects in humans on the basis of preclinical data, it is essential to study the underlying processes and mechanisms that govern the ultimate concentration-effect relationship. Therefore, it is of importance to investigate the inter-relationship between plasma PK, BBB and BCSFB transport, intra-brain distribution, target binding, target activation, transduction, homeostatic feedback, and disease processes (Danhof *et al.,* 2007; De Lange, 2013b; De Lange *et al.,* 2005). The current preclinical SBPK brain distribution model is a first step into that direction. It allows the investigation of the relationship between plasma PK, BBB and BCSFB transport and intra-brain distribution, in a systems-specific manner.

By systematically varying one (or a subset) of conditions (such as P-gp functionality), one can decipher the impact of changes on brain distribution in integrative cross-compare designed studies. To that end we also need advanced mathematical modeling procedures to dissect contributions of individual mechanisms, being key to translation from one condition to the other (De Lange, 2013b). The current preclinical SBPK brain distribution model follows that approach, and needs to be further developed/refined by using more data on other drugs with distinct physicochemical properties. By doing so we will be able to pin-point the influence of particular drug properties on the pharmacokinetic brain distribution behavior of drugs. Furthermore, the PK of a drug at different sites in the brain should be connected to (biomarkers of) the effect in order to unravel those concentrations that can be considered as target site concentrations.

Other aspects that need to be included for improving the SBPK brain distribution model are target-mediated drug disposition and target association

and dissociation kinetics. This may cause non-linearity in PK and/or PD, which may complicate the characterization of the PK-PD relationship. When drugs are bound with high affinity and to a significant extent (relative to the dose) to their target sites, the drug can be retained much longer in target rich tissue spaces than expected on the basis of the plasma elimination rate (Levy, 1996; Mager, 2006; Mager and Jusko, 2001). As an example, this may hold for the antipsychotic drugs risperidone and paliperidone with their targets being the dopamine D_2 and serotonin 5-HT_{2A} receptor. For these compounds, information on the regional brain distribution, together with information on the target density as well as the target association and dissociation kinetics provides a better understanding of processes that govern the PK-PD relationship (Johnson *et al.,* 2011; Kozielska *et al.,* 2012).

Thus, apart from blood-brain and intra-brain transport processes, target-mediated disposition adds on to the limited value of plasma PK to predict target site PK and stresses the importance of having additional information on target site PK that actually drives the PK-PD relationship. Since CNS target site concentrations cannot be obtained directly from humans, the aim should be to predict target site concentrations and effects in humans on the best indirect way, such as based on preclinical data.

The value of intracerebral microdialysis in this prediction is clearly exemplified by recent work by Stevens *et al.* (2012). They have shown that the effect of remoxipride, a dopamine D_2/D_3-receptor antagonist, on prolactin concentrations in plasma could be directly linked to remoxipride $brain_{ECF}$ concentrations as measured by microdialysis in the rat. To that end, human $brain_{ECF}$ remoxipride concentrations were predicted by allometric and physiological scaling of the rat data, which were then used to predict human plasma prolactin concentrations by applying the same structural PK-PD model as was developed on the basis of the rat data. The predicted human plasma prolactin concentrations show a great similarity to clinically observed plasma prolactin concentrations, indicating that advanced PK-PD modeling of preclinical data allows the prediction of drug effects in humans.

Further development of the preclinical SBPK brain distribution-effect model lies in improvement of the quality of the CNS effect data. Often, the focus has been on a single biomarker to reflect the CNS drug effect. However, given the complexity of brain diseases, it can be seen that the search for a single

biomarker to explain the disease relative to the healthy condition, and/or changes in the disease condition by (drug) treatment will never lead to a success. Actually we do not deal with "the" effect, but a composite of effects. The search should therefore be on "fingerprints" of multiple biomarkers, in a time-dependent manner, for investigations on the "effect spectrum". With metabolomics as an emerging scientific tool, many more compounds in brain fluids and in plasma can be measured in parallel, in a quantitative and time-dependent manner. Furthermore, the emphasis should lie on measures that can be obtained both preclinically and clinically, to enhance translational insights and therewith predictive power of preclinically obtained information (De Lange, 2014).

In conclusion, the future perspective is that by combining drug-specific and system-specific information on brain target site distribution with mechanistic information on the concentration-effect spectrum relationship (as they vary in between species, between subjects, or within subjects with age and/or disease state) will ultimately result in a systems-based PK-PD model that is anticipated to be able to predict human CNS drug effect on the basis of preclinical PK data (figure 1).

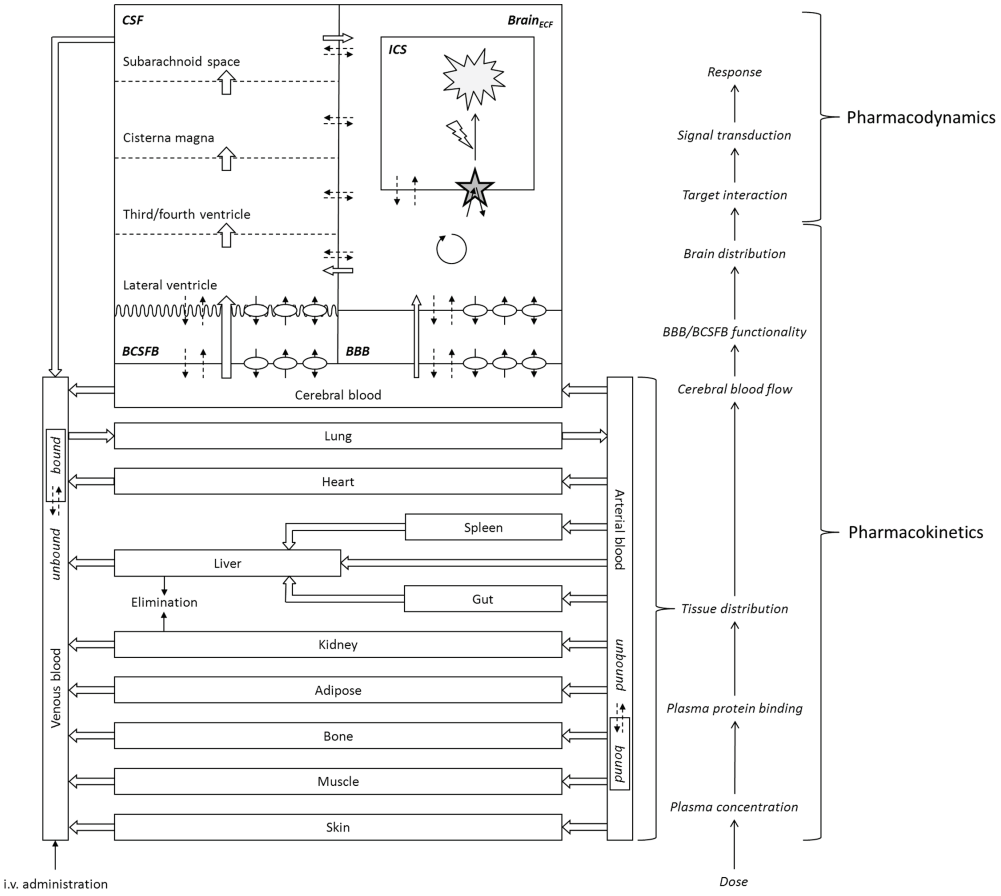

Figure 1. Schematic representation of a systems-based PK-PD model. On the right several underlying processes or mechanisms that are important for the pharmacokinetics and pharmacodynamics of a (unbound) drug are highlighted

REFERENCES

Bannwarth B, Netter P, Lapicque F, Gillet P, Péré P, Boccard E, Royer RJ, Gaucher A. Plasma and cerebrospinal fluid concentrations of paracetamol after a single intravenous dose of propacetamol. Br J Clin Pharmacol 1992; 34: 79-81.

Blakeley JO, Olson J, Grossman SA, He X, Weingart J, Supko JG. Effect of blood brain barrier permeability in recurrent high grade gliomas on the intratumoral pharmacokinetics of methotrexate: a microdialysis study. J Neurooncol 2009; 91: 51-58.

Colburn WA. Physiologic pharmacokinetic modeling. J Clin Pharmacol 1988; 28: 673-677.

Danhof M, de Jongh J, de Lange ECM, Della Pasqua OE, Ploeger BA, Voskuyl RA. Mechanism-based pharmacokinetic-pharmacodynamic modeling: biophase distribution, receptor theory, and dynamical systems analysis. Annu Rev Pharmacol Toxicol 2007; 47: 357-400.

Danhof M, de Lange ECM, Della Pasqua OE, Ploeger BA, Voskuyl RA. Mechanism-based pharmacokinetic-pharmacodynamic (PK-PD) modeling in translational drug research. Trends Pharmacol Sci 2008; 29: 186-191.

De Lange ECM, Danhof M. Considerations in the use of cerebrospinal fluid pharmacokinetics to predict brain target concentrations in the clinical setting. Implications of the barriers between blood and brain. Clin Pharmacokin 2002; 41: 691-703.

De Lange ECM. Utility of CSF in translational neuroscience. J Pharmacokinet Pharmacodyn. 2013a; 40: 315-26.

De Lange ECM. The mastermind approach to CNS drug therapy: translational prediction of human brain distribution, target site kinetics, and therapeutic effects. Fluids Barriers CNS 2013b; 10: 12.

De Lange ECM. Pharmacometrics in psychiatric diseases. In "Applied Pharmacometrics". Eds S. Schmidt and H. Derendorf. Springer. 2014.

De Lange ECM, de Vries JD, Zurcher C, Danhof M, De Boer AG, Breimer DD. The use of intracerebral microdialysis to study blood-brain barrier transport of anticancer drugs in tumor-bearing tat brain. Pharm Res 1995; 12: 1924-1931.

De Lange ECM, de Boer AG, Breimer DD. Methodological issues in microdialysis sampling for pharmacokinetic studies. Adv Drug Del Rev 2000; 45: 125-148.

De Lange ECM, Ravenstijn PGM, Groenendaal D, van Steeg TS. Toward the prediction of CNS drug effect profiles in physiological and pathological conditions using microdialysis and mechanism-based pharmacokinetic-pharmacodynamic modeling. AAPS J 2005; 7: article 54.

Espié P, Tytgat D, Sargentini-Maier M-L, Poggesi I, Watelet J-P. 2009. Physiologically based pharmacokinetics (PBPK). Drug Metab Rev 41: 391-407.

Fleishaker JC, Smith RB. Compartmental model analysis in pharmacokinetics. J Clin Pharmacol 1987; 27: 922-926.

Fridén M, Winiwarter S, Jerndal G, Bengtsson O, Wan H, Bredberg U, Hammarlund-Udenaes M, Antonsson M. Structure-brain exposure relationships in rat and human using a novel data set of

unbound drug concentrations in brain interstitial and cerebrospinal fluids. J Med Chem 2009; 52: 6233-6243.

Glantz MJ, Cole BF, Recht L, Akerley W, Milles P, Saris S, Hochberg F, Calabresi P, Egorin MJ. High-dose intravenous methotrexate for patients with nonleukemic leptomeningeal cancer: is intrathecal chemotherapy necessary? J Clin Oncol 1998; 16: 1561-1567.

Hammarlund-Udenaes M. Active-site concentrations of chemicals – are they a better predictor of effect than plasma/organ/tissue concentrations? Basic Clin Pharmacol Toxicol 2009; 106: 215-220.

Hammarlund-Udenaes M, Paalzow LK, de Lange ECM. Drug equilibration across the blood-brain barrier – pharmacokinetic considerations based on the microdialysis method. Pharm Res 1997; 14: 128-134.

Hammarlund-Udenaes M, Fridén M, Syvänen S, Gupta A. On the rate and extent of drug delivery to the brain. Pharm Res 2008; 25: 1737-1750.

Hendel J, Brodthagen H. Entero-hepatic cycling of methotrexate estimated by use of the D-isomer as a reference marker. Eur J Clin Pharmacol 1984; 26: 103-107.

Henderson ES, Adamson RH, Denham C, Oliverio VT. The metabolic fate of tritiated methotrexate I. absorption, excretion, and distribution in mice, rats, dogs and monkeys. Cancer Res 1965; 25: 1008-1017.

Ings RMJ. Interspecies scaling and comparisons in drug development and toxicogenetics. Xenobiotica 1990; 20: 1201-1231.

Johnson M, Kozielska M, Pilla Reddy V, Vermeulen A, Li C, Grimwood S, de Greef R, Groothuis GMM, Danhof M, Proost JH. Mechanism-based pharmacokinetic-pharmacodynamic modeling of the dopamine D_2 receptor occupancy of olanzapine in rats. Pharm Res 2011; 28: 2490-2504.

Kalvass JC, Maurer TS. Influence of nonspecific brain and plasma binding of CNS exposure: implications for rational drug discovery. Biopharm Drug Dispos 2002; 23: 327-338.

Kassem NA, Deane R, Segal MB, Chen RL, Preston JE. Thyroxine (T_4) transfer from CSF to choroid plexus and ventricular brain regions in rabbit: contributory role of P-glycoprotein and organic anion transporting polypeptides. Brain Res 2007; 1181: 44-50.

Kozielska M, Johnson M, Pilla Reddy V, Vermeulen A, Li C, Grimwood S, de Greef R, Groothuis GMM, Danhof M, Proost JH. Pharmacokinetic-pharmacodynamic modeling of the D_2

and 5-HT_{2A} receptor occupancy of risperidone and paliperidone in rats. Pharm Res 2012; 29: 1932-1948.

Lee G, Dallas S, Hong M, Bendayan R. Drug transporters in the central nervous system: brain barriers and brain parenchyma considerations. Pharmacol Rev 2001; 53: 569-596.

Levin VA. Relationship of octanol/water partition coefficient and molecular weight to rat brain capillary permeability. J Med Chem 1980; 23: 682-684.

Levy G. Pharmacological target-mediated drug disposition. Clin Pharmacol Ther 1994; 56: 248-52.

Lin JH. CSF as a surrogate for assessing CNS exposure: an industrial perspective. Curr Drug Metab 2008; 9: 46-59.

Liu X, Smith BJ, Chen C, Callegari E, Becker SL, Chen X, Cianfrogna J, Doran AC, Doran SD, Gibbs JP, Hosea N, Liu J, Nelson FR, Szewc MA, Van Deusen J.. Evaluation of cerebrospinal fluid concentration and plasma free concentration as surrogate measurement for brain free concentration. Drug Metab Dispos 2006; 34: 1443-1447.

Liu X, Van Natta K, Yeo H, Vilenski O, Weller PE, Worboys PD, Monshouwer M. Unbound drug concentration in brain homogenate and cerebral spinal fluid at steady state as a surrogate for unbound concentration in brain interstitial fluid. Drug Metab Dispos 2009; 37: 787-793.

Mager DE, Jusko WJ. General pharmacokinetic model for drugs exhibiting target-mediated drug disposition. J Pharmacokin Pharmacodyn 2001; 28: 507-532.

Mager DE. Target-mediated drug disposition and dynamics. Biochem Pharmacol 2006; 72: 1-10.

Maurer TS, DeBartolo DB, Tess DA, Scott D. Relationship between exposure and nonspecific binding of thirty-three central nervous system drugs in mice. Drug Metab Dispos 2005; 33: 175-181.

Rao VV, Dahlheimer JL, Bardgett ME, Snyder AZ, Finch RA, Sartorelli AC, Piwnica-Worms D. Choroid plexus epithelial expression of *MDR1* P-glycoprotein and multidrug resistance-associated protein contribute to the blood-cerebrospinal-fluid drug-permeability barrier. Proc Natl Acad Sci USA 1999; 96: 3900-3905.

Rowland M, Peck C, Tucker G. Physiologically-based pharmacokinetics in drug development and regulatory science. Annu Rev Pharmacol Toxicol 2011; 51: 45-73.

Schinkel AH. P-glycoprotein, a gatekeeper in the blood-brain barrier. Adv Drug Del Rev 1999; 36: 179-194.

Sheiner LB, Stanski DR, Vozeh S, Miller RD, Ham J. Simultaneous modeling of pharmacokinetics and pharmacodynamics: application to d-tubocurarine. Clin Pharmacol Ther 1979; 25: 358-371.

Shen DD, Artru AA, Adkison KK. Principles and applicability of CSF sampling for the assessment of CNS drug delivery and pharmacodynamics. Adv Drug Del Rev 2004; 56: 1825-1857.

Stevens J, Ploeger BA, Hammarlund-Udenaes M, Osswald G, van der Graaf PH, Danhof M, de Lange ECM. Mechanism-based PK-PD model for the prolactin biological system response following an acute dopamine inhibition challenge: quantitative extrapolation to humans. J Pharmacokinet Pharmacodyn 2012; 39: 463-477.

Van Montfoort JE, Müller M, Groothuis GMM, Meijer DKF, Koepsell H, Meier PJ. Comparison of “type I” and “type II” organic cation transport by organic cation transporters and organic anion-transporting polypeptides. J Pharmacol Exp Ther 2001; 298: 110-115.

Watson J, Wright S, Lucas A, Clarke KL, Viggers J, Cheetham S, Jeffrey P, Porter R, Read KD. Receptor occupancy and brain free fraction. Drug Metab Dispos 2009; 37: 753-60.

Appendix

Nederlandse samenvatting

Factoren die de farmacokinetiek in de hersenen bepalen

De ontwikkeling van geneesmiddelen voor aandoeningen aan het centrale zenuwstelsel (CZS), waaronder de ziekte van Alzheimer, de ziekte van Parkinson, multiple sclerose, schizofrenie, migraine, slapeloosheid, depressie en "attention deficit hyperactivity disorder" (ADHD) verloopt veelal moeizaam, omdat het moeilijk is om de concentratie van het geneesmiddel op de plaats van werking in de hersenen te meten of voorspellen. Veel potentiële CZS geneesmiddelen in ontwikkeling falen doordat deze onvoldoende de bloed-hersen barrière (BHB) weten te passeren. De BHB beschermt de hersenen tegen blootstelling aan lichaamsvreemde stoffen (waaronder geneesmiddelen) die zich in de bloedbaan bevinden door de aanwezigheid van "tight junction" eiwitten, welke de endotheelcellen van bloedvaten in de hersenen met elkaar verbinden. Daarnaast zijn er ook nog verschillende actieve transportsystemen en enzymen aanwezig op de BHB die de concentratie van geneesmiddelen in de hersenen laag houden. Echter is de BHB niet de enige oorzaak van het lage slagingspercentage van geneesmiddelonderzoek voor CZS aandoeningen.

Naast de plasma farmacokinetiek (PK), plasma eiwitbinding, passieve en actieve transportsystemen op de bloed-hersen barrières (de BHB en de bloed-cerebrospinale vloeistof barrière (BCSFB)) zijn er ook processen binnen de hersenen die een rol kunnen spelen. Binnen de hersenen heb je te maken met verschillende vloeistofstromen, diffusie en extracellulaire-intracellulaire uitwisseling. Dit geeft aan dat er ook nog andere processen zijn die een belangrijke rol spelen om het geneesmiddel op de *juiste plek,* de *juiste tijd* en met de *juiste concentratie* te krijgen.

Veel (potentiële) CZS geneesmiddelen hebben hun plaats van werking aan de buitenzijde van de hersencellen. Doelconcentraties zijn daarmee in veel gevallen gelijk aan de ongebonden concentraties in de extracellulaire vloeistof van de hersenen ($hersen_{ECF}$). Echter is het meten van concentraties in $hersen_{ECF}$ zeer beperkt mogelijk in de mens, dus als alternatief worden vaak ongebonden concentraties in CSF gebruikt. Vaak wordt aangenomen dat CSF concentraties goed vergelijkbaar zijn met $hersen_{ECF}$ concentraties vanwege het gebrek aan een

fysieke barrière tussen de twee vloeistoffen. De hersenen zijn echter een dynamisch, complex orgaan, waarbij alle processen van opname, diffusie, metabolisme, binding en eliminatie de lokale hersenconcentraties bepalen. Door kwalitatieve en kwantitatieve verschillen in de processen die de PK van de geneesmiddelen in de hersenen bepalen bestaat er geen algemeen toepasbare relatie tussen CSF concentraties en hersen$_{ECF}$ concentraties (**Hoofdstuk 1**). Dit geeft aan dat er de behoefte is aan mechanistisch onderzoek naar de bijdrage van de verschillende processen die de uiteindelijke doelconcentraties bepalen.

In de preklinische fase van geneesmiddelonderzoek kunnen de snelheid en mate van distributie naar de hersenen met verschillende *in vitro*, *ex vivo* en *in vivo* technieken bestudeerd worden, zoals beschreven staat in **Hoofdstuk 1**. Vaak worden totale hersenconcentraties in proefdieren bepaald met behulp van technieken zoals de hersenperfusie techniek. Ongebonden hersen$_{ECF}$ concentraties worden dan vervolgens berekend door de mate van binding te bepalen met hersen homogenaat monsters. Het nadeel van het homogeniseren van de hersenen is echter dat de cellulaire structuur van de hersenen verloren gaat, waardoor mogelijk andere bindingsplaatsen beschikbaar komen die bij intacte hersenen niet toegankelijk zijn. Hierdoor kan er een vertekend beeld ontstaan van de mate van binding, waardoor de berekening van de ongebonden concentraties onjuist zal zijn. Bovendien is deze techniek niet toepasbaar in de mens, dus dat maakt het lastig om de resultaten te extrapoleren. Het nemen van CSF monsters wordt veelal gezien als zeer waardevolle techniek omdat het toepasbaar is in zowel proefdieren als de mens. De intracerebrale microdialyse techniek is echter het meest bruikbaar, omdat met deze techniek de ongebonden concentraties op meerdere plaatsen in de hersenen (bijvoorbeeld CSF en hersen$_{ECF}$) gemeten kunnen worden. Aangezien de microdialyse techniek een invasieve techniek is wordt deze slechts zeer beperkt in de mens toegepast. Het toepassen van deze techniek in proefdieren stelt ons echter in staat om mechanistische informatie te verzamelen over de verschillende processen die de relatie bepalen tussen hersen$_{ECF}$ en CSF PK. In combinatie met farmacodynamische (PD) parameters kan de informatie zeer bruikbaar zijn om de processen in de mens beter te begrijpen en voorspellen.

Parallelle intracerebrale microdialyse

In **Hoofdstuk 3** hebben we een experimentele methode ontwikkeld waarbij simultaan de ongebonden concentraties van paracetamol in bloed (plasma), $hersen_{ECF}$ en CSF kon worden bepaald. De implantatie van meerdere microdialyse probes in $hersen_{ECF}$, CSF in de laterale ventrikel (CSF_{LV}) of CSF in de cisterna magna (CSF_{CM}) van een enkel dier stelde ons in staat om de relatie tussen $hersen_{ECF}$ en CSF concentraties te bepalen. Het toepassen van de intracerebrale microdialyse techniek vereist echter wel dat de relatieve opbrengst wordt bepaald. Aangezien de microdialyse probe constant geperfuseerd wordt zal de concentratie in het dialysaat lager zijn dan de concentratie in de omliggende $hersen_{ECF}$ of CSF. Dit geeft aan dat de relatieve opbrengst bij voorkeur *in vivo* voor elke probe locatie dient te worden bepaald om de dialysaat concentraties om te kunnen rekenen naar $hersen_{ECF}$ en CSF concentraties.

Het doel van het onderzoek waar dit proefschrift over gaat was het opstellen van een preklinisch hersendistributiemodel waarmee de vrije concentraties op de plaats van werking in de hersenen van de mens kan worden voorspeld op basis van preklinische data. Om dit model te kunnen opstellen is het essentieel om te begrijpen hoe de kinetiek van het ongebonden geneesmiddel afhankelijk is van de tijd en waarbij de concentraties niet met elkaar in evenwicht zijn. Hiervoor hebben we een aantal studies uitgevoerd in de rat, waarbij we op een systematische manier hebben gekeken naar de onderlinge verhouding tussen plasma PK, BHB transport, BCSFB transport en distributie binnen de hersenen. Om dit te kunnen doen hebben we in elke rat op meerdere plaatsen in de hersenen een microdialyse probe geïmplanteerd. Voor de studies hebben we drie stoffen geselecteerd met verschillende fysisch-chemische eigenschappen.

Paracetamol (**Hoofdstuk 3**) was geselecteerd als modelstof voor passief transport van, naar en in de hersenen, met een logP van 0.46 en geen lading bij fysiologische pH. Aangezien in het geval van passieve diffusie de snelheid waarmee het evenwicht tussen CSF en $hersen_{ECF}$ concentraties zich instelt wordt bepaald door de lipofiliciteit en het molecuulgewicht gingen wij er van uit dat de concentraties in het CSF en $hersen_{ECF}$ vergelijkbaar zouden zijn. Wij hebben echter gevonden dat de concentraties in CSF ongeveer een factor 4 lager zijn

dan $hersen_{ECF}$ concentraties. Mogelijk wordt dit veroorzaakt door de relatief hoge verversingssnelheid van CSF, waarbij het CSF als afvoer kan dienen.

Quinidine (**Hoofdstuk 4**) was geselecteerd als modelstof met een hoge logP van 3.44, indicatief van een hoge mate van passief transport over de BHB, en een positieve lading bij fysiologische pH. Daarnaast is quinidine een bekend substraat voor actief transport uit de hersenen door P-glycoproteïne (P-gp). Om de bijdrage van P-gp-gemedieerd transport te kunnen bepalen is een selectieve inhibitor van P-gp, tariquidar, toegediend. Voor quinidine hadden we verwacht dat er significante verschillen zouden zijn tussen $hersen_{ECF}$ concentraties en CSF concentraties, aangezien van P-gp bekend is dat deze functioneert als afvoer transporter op de BHB, terwijl deze mogelijk als opname transporter zou functioneren op de BCSFB. Gek genoeg vonden wij slechts kleine verschillen tussen $hersen_{ECF}$ concentraties en CSF concentraties. De $hersen_{ECF}$-CSF concentratieratio was 0.72 ± 0.20 zonder inhibitie van P-gp en 2.22 ± 0.57 met de inhibitie van P-gp.

Op basis van de algemeen geaccepteerde foutmarge van factor 3 zou dit betekenen dat deze resultaten als niet significant kunnen worden beschouwd. Wij zijn er echter van overtuigd dat zelfs een klein verschil in de PK van een stof drastische gevolgen kan hebben voor de PD van de stof als er een sterke relatie is tussen de concentratie en het effect van de stof. Zodoende vinden wij dat zelfs de kleinste verschillen als potentieel relevant moeten worden beschouwd. Deze resultaten geven aan dat de variatie in P-gp functionaliteit een grote invloed hebben op de $hersen_{ECF}$-CSF concentratieratio en mogelijk ook op de extrapolatie van de rat naar de mens.

Voor quinidine hadden we verwacht dat de ongebonden concentraties in de hersenen lager zouden zijn dan de ongebonden concentraties in plasma. Tot onze verbazing waren de ongebonden concentraties in de hersenen echter significant hoger dan die in plasma. Aangezien quinidine actief uit de hersenen wordt getransporteerd door P-gp geven deze resultaten aan dat quinidine mogelijk ook door andere transportsystemen, zoals organische cation transporters, op de BHB en BCSFB in de richting van de hersenen wordt getransporteerd. Dit geeft aan dat er een belangrijke samenwerking kan zijn tussen de verschillende transportsystemen op de BHB en BCSFB. Om de bijdrage van een enkele transporter te kunnen bestuderen is het essentieel om inhibitoren te hebben met een hoge specificiteit voor die transporter.

Vooralsnog zijn er alleen specifieke inhibitoren voor P-gp beschikbaar, zoals tariquidar.

Tot slot was methotrexaat (**Hoofdstuk 5**) geselecteerd als modelstof met een lage logP van –1.85, indicatief van weinig passief transport over de BHB, en een negatieve lading bij fysiologische pH. Verder is methotrexaat substraat voor een breed scala aan actieve transportsystemen op de BHB en BCSFB, waaronder de "reduced folate carrier 1", "breast cancer resistance protein" (BCRP), de "multidrug resistance-associated protein" (MRP) familie, organische anion transporters (OATs) en organische anion-transporterende polypeptides (OATPs). Om de invloed van verschillende transportsystemen te kunnen bepalen werd probenecid toegediend als inhibitor van MRPs, OATs en OATPs. Op basis van de verschillen in de richting van transport en de lokalisatie van de verschillende transportsystemen op de BHB en BCSFB hadden we significant verschillende concentraties in hersen$_{ECF}$ en CSF verwacht. Deze verwachtingen bleken te kloppen, want hersen$_{ECF}$ concentraties waren meer dan 3-voud hoger dan CSF concentraties, ook na de toediening van probenecid. Dit geeft aan dat actief transport van methotrexaat door Mrps, Oats en Oatps geen invloed heeft op de relatie tussen hersen$_{ECF}$ en CSF concentraties. De inhibitie van Mrps, Oats en Oatps heeft echter wel geleid tot significant hogere concentraties in zowel hersen$_{ECF}$ als CSF.

Aangezien methotrexaat wordt getransporteerd door meerdere transporters die niet individueel geblokkeerd kunnen worden is het lastig om de bijdrage van elke transporter afzonderlijk te bepalen. Om dit toch te kunnen bestuderen is het efficiënter om op een systematische manier te werk te gaan, waarbij telkens een aantal variabelen kunnen worden gevarieerd, bijvoorbeeld door een andere inhibitor te gebruiken waarbij alleen de Oats en Oatps geblokkeerd worden. Ook zouden andere stoffen gekozen kunnen worden die in meer of mindere mate affiniteit hebben voor één of meerdere transporters. Op deze manier kunnen we de betekenis van de veranderingen van het transport naar en distributie in de hersenen ontrafelen.

Systeem-gebaseerd farmacokinetisch modeleren

Om de effecten van geneesmiddelen in de hersenen van de mens te kunnen voorpellen zijn verschillende farmacokinetische modellen toepasbaar. Vaak wordt een compartimenteel model gebruikt waarbij de hersenen als effectcompartiment worden beschreven. Bij deze aanpak is de ongebonden plasmaconcentratie de belangrijkste drijfkracht voor de concentraties in de hersenen, waarbij de opname in de hersenen of eliminatie uit de hersenen geen invloed hebben op de concentraties in bloed. Extrapolatie van PK parameters die zijn bepaald in dieren gaat in sommige gevallen best goed door allometrische schaling op basis van lichaamsgewicht of lichaamsoppervlak.

In fysiologisch-gebaseerde farmacokinetische (PBPK) modellen staat de fysiologie van het organisme centraal. In ieder PBPK model wordt het onderscheid gemaakt tussen systeem-specifieke parameters en stof-specifieke parameters. De systeem-specifieke fysiologische parameters van het PBPK model kunnen aangepast worden aan het organisme waar naar gekeken wordt, dus op deze manier is het schalen tussen diersoorten beter onderbouwd dan bij de allometrische schaling. Het gebruik van een andere stof, met zijn eigen stof-specifieke eigenschappen, stelt ons in staat om de bijdrage van de verschillende eigenschappen op het transport naar en distributie in de hersenen te ontrafelen. Het toevoegen van mechanistische informatie over bijvoorbeeld het transport over de BHB en BCSFB resulteert in een meer systeem-gebaseerd farmacokinetisch (SBPK) model.

Informatie over de verschillen in de dichtheid en activiteit van verschillende actieve transportsystemen en enzymen op de BHB en BCSFB, maar ook in de lever en nier, onder gezonde en zieke omstandigheden, is essentieel voor de extrapolatie van dier naar mens. Door gebruik te maken van specifieke SBPK modellen kunnen individuele mechanismen in dieren geïdentificeerd worden die ons veel kunnen leren over de processen in de mens. In principe zouden de beste voorspellingen gedaan kunnen worden met een SBPK model waarbij het hele organisme in alle detail is beschreven. Dit vergt echter een enorme hoeveelheid informatie, tijd en geld om de bijdrage van specifieke parameters te kunnen identificeren. Daarom hebben wij ervoor gekozen om alleen de hersenen te beschrijven met een SBPK model, waarbij de plasmakinetiek beschreven kon worden met een compartimenteel model. Met de gemeten

ongebonden concentraties in plasma, $hersen_{ECF}$, CSF_{LV} en CSF_{CM} zijn de tijdsafhankelijke parameters voor de uitwisseling tussen de verschillende hersencompartimenten bepaald. De hersencompartimenten zijn hierbij beschreven op basis van hun anatomie, met een bepaald volume en oppervlakte, onderling verbonden door middel van diffusie, vloeistofstromen en actieve transportsystemen. Voor deze aanpak hebben we gebruik gemaakt van non-lineaire gemengde effecten modellen, waarbij NONMEM als software is gebruikt. Hierbij hebben we de onderlinge relatie tussen $hersen_{ECF}$ concentraties en CSF concentraties bepaald.

Door gebruik te maken van hetzelfde structurele SBPK model voor de drie modelstoffen kan de bijdrage van de verschillende stof-specifieke eigenschappen op de PK in de hersenen en de $hersen_{ECF}$-CSF concentratierelatie bestudeerd worden op een mechanistische manier. Deze aanpak zal bijdragen aan de voorspelbaarheid van doelconcentraties in de mens op basis van preklinische data.

Extrapolatie naar de mens

Aangezien CSF concentraties beschouwd worden als best beschikbare alternatief voor $hersen_{ECF}$ concentraties hebben we in **Hoofdstuk 3** geprobeerd om $hersen_{ECF}$ concentraties van paracetamol in de mens te voorspellen om deze te kunnen vergelijken met gemeten CSF concentraties. Hiervoor hebben we eerst de verschillende fysiologische parameters van de rat veranderd in de waarden van de mens en is de uitwisseling tussen plasma en de hersenen geëxtrapoleerd op basis van de fysiologie. Door vervolgens de humane plasma data te fitten met ons SBPK model, konden lumbale CSF concentraties, zoals gepresenteerd in de literatuur, goed worden voorspeld. Op basis van ons model is voorspeld dat $hersen_{ECF}$ concentraties ongeveer een factor 2 hoger zijn dan ongebonden plasmaconcentraties. De $hersen_{ECF}$-CSF (in de subarachnoïdale ruimte) concentratieratio was erg afhankelijk van de tijd na doseren. Ondanks dat we deze voorspelling niet kunnen valideren geeft de juiste voorspelling van de lumbale CSF concentraties wel aan dat we vertrouwen kunnen hebben in het nut van ons model.

Voor quinidine (**Hoofdstuk 4**) hebben we de invloed van het actieve transport door P-gp op beide hersenbarrières toegevoegd aan het model. We

hebben gezien dat de functionaliteit van P-gp een belangrijke rol speelt in de relatie tussen hersen$_{ECF}$ en CSF concentraties. Helaas is er geen data beschikbaar van quinidine concentraties in CSF van de mens, dus het is nog niet mogelijk om deze observatie te valideren.

Voor methotrexaat (**Hoofdstuk 5**) was er aardig wat literatuur beschikbaar waarin CSF concentraties in zowel kinderen als volwassenen zijn gemeten. In een enkel geval zijn zelfs hersen$_{ECF}$ concentraties gemeten met behulp van de intracerebrale microdialyse techniek. We moeten er echter wel rekening mee houden dat deze data is verkregen uit patiënten met verschillende ziektebeelden. Het was dan ook niet te verwachten dat de voorspelling van hersenconcentraties in de zieke mens goed zou gaan met het model dat is gebaseerd op data verkregen uit de gezonde rat. Het is namelijk bekend dat ziekte in het algemeen een invloed kan hebben op de relatieve bijdrage van de verschillende processen die de doelconcentraties van (niet-)CZS actieve stoffen bepalen. Het is daarom van belang om te bepalen op welke PK parameters een ziekte effect heeft, aangezien hiermee ook het potentiële effect op de PD bepaald kan worden. Op basis van de aanname dat het preklinische SBPK model de situatie voor de gezonde mens goed voorspelt is het mogelijk om "verdachte" parameters te identificeren die afwijkende hersenconcentraties bepalen.

In **Hoofdstuk** 5 hebben we het SBPK model toegepast op literatuurdata (plasma en hersen$_{ECF}$ concentraties) van gezonde ratten en van ratten die een tumor geïmplanteerd hadden gekregen in de hersenen. Door dezelfde PK parameters te gebruiken die wij op basis van onze data hadden bepaald konden de plasma en hersen$_{ECF}$ concentraties in de gezonde rat goed worden voorspeld. Voor de ratten met een hersentumor bleek de voorspelling van de plasmaconcentraties nog goed te kloppen, maar er was een onderschatting van de hersen$_{ECF}$ concentraties nabij de hersentumor. Dit geeft aan dat er een toename is in de distributie van methotrexaat naar de hersentumor. Daarna werd het SBPK model toegepast op plasma en CSF concentraties gemeten in gezonde honden. Met de voorkennis dat de klaring van methotrexaat in honden door de lever slechts een fractie is van de klaring door de nieren, terwijl de hepatische klaring in de rat juist meer dan 5 keer hoger is dan de renale klaring, konden plasma en CSF concentraties redelijk goed voorspeld worden.

Als de status van de ziekte gebruikt wordt als variabele in een kruislings-vergelijkende studie dan is het mogelijk om de parameters te identificeren die

worden beïnvloed in het SBPK hersendistributiemodel. Deze parameters zouden bijvoorbeeld de eliminatie vanuit plasma of het transport tussen bloed en de hersenen kunnen zijn. In de veronderstelling dat het SBPK model de processen onder gezonde omstandigheden goed beschrijft kan de relatieve bijdrage van de veranderingen van de verschillende parameters inzichtelijk gemaakt worden aan de hand van simulaties.

In de mens is er een substantiële enterohepatische circulatie van methotrexaat, waardoor de hepatische eliminatiesnelheid effectief gereduceerd wordt tot ongeveer de renale eliminatiesnelheid. Met deze voorkennis is de voorspelling van ongebonden plasmaconcentraties in de mens redelijk. De gemeten concentraties in hersen$_{ECF}$ en CSF waren echter significant hoger dan wat was voorspeld op basis van gezonde omstandigheden. Simulaties hebben aangegeven dat zowel een gereduceerde afvoer vanuit hersen$_{ECF}$ als een gereduceerde CSF vloeistofstroom hier mogelijk de oorzaken van kunnen zijn. De mogelijke invloed van een gereduceerde CSF vloeistofstroom komt overeen met bevindingen in de literatuur.

Interessant genoeg is het niet alleen het transport van en naar de hersenen die een belangrijke rol speelt in de relatie tussen hersen$_{ECF}$ concentraties en CSF concentraties. De vloeistofstroom van CSF mag hierin niet onderschat worden. Voor paracetamol en methotrexaat ziet het er naar uit dat CSF als afvoer kan dienen, wat resulteert in lagere concentraties in CSF in vergelijking tot hersen$_{ECF}$ concentraties. Aangezien de relatieve CSF vloeistofstroom in ratten veel hoger is dan die in de mens zou het kunnen betekenen dat de afvoer in de mens veel minder is. Daarnaast kan het zo zijn dat een geneesmiddel of ziekte een effect kan hebben op de productie van CSF. Dit geeft aan dat er rekening moet worden gehouden met de verversingssnelheid van CSF bij het bepalen van de relatie tussen hersen$_{ECF}$ concentraties en CSF concentraties.

Toekomstperspectieven

Om het effect van CZS geneesmiddelen in de mens te kunnen voorspellen op basis van preklinische data is het essentieel om de onderliggende processen en mechanismen te bestuderen die uiteindelijk de concentratie-effect relatie bepalen. Het is daarom belangrijk om de onderlinge relatie tussen plasma PK, BHB en BCSFB transport, distributie in de hersenen, binding aan het doeleiwit,

activatie van het doeleiwit, transductie, homeostatische terugkoppeling en ziekteprocessen te bestuderen. Het preklinische hersendistributiemodel dat wij hebben opgesteld is een stap in de goede richting en stelt ons in staat om de onderlinge relatie tussen plasma PK, BHB en BCSFB transport en distributie in de hersenen te kunnen bepalen.

Door op een systematische manier één of meerdere parameters (bijvoorbeeld de functionaliteit van P-gp) te variëren kan de relatieve bijdrage van die variatie op de hersendistributie in kaart worden gebracht. Om deze informatie te kunnen bevatten is het essentieel om vooruitstrevende wiskundige modellen te gebruiken die de bijdragen van individuele mechanismen van elkaar kunnen onderscheiden. Dit is namelijk essentieel voor de extrapolatie van de ene situatie naar de andere. Ons huidige preklinische SBPK hersendistributiemodel volgt deze aanpak en dient nog verder ontwikkeld en verfijnd te worden door data toe te voegen van andere stoffen met hun eigen fysisch-chemische eigenschappen. Hiermee kunnen we de invloed van specifieke eigenschappen op de kinetiek en distributie in de hersenen inzichtelijk maken. Daarnaast is het van belang om de PK van het geneesmiddel op meerdere plaatsen in de hersenen te koppelen aan (biomarkers van) het effect om te kunnen ontrafelen welke concentraties als doelconcentraties kunnen worden beschouwd.

Het SBPK hersendistributiemodel kan nog verder aangevuld worden met informatie over de doeleiwit-gemedieerde dispositie en de kinetiek van doeleiwit associatie en dissociatie. Als een geneesmiddel in hoge mate (ten opzichte van de dosis) sterk bindt aan een doeleiwit kan het zijn dat het geneesmiddel langer het doeleiwit kan activeren dan wat je op basis van de plasma eliminatiesnelheid zou verwachten. Dit maakt het lastig om de PK-PD relatie vast te stellen. De doeleiwit-gemedieerde dispositie speelt een belangrijke rol in de PD van bijvoorbeeld risperidon en paliperidon, met de dopamine D_2 en seretonine 5-HT_{2A} receptor als doeleiwit. Naast informatie over de regionale distributie van de geneesmiddelen in de hersenen geeft de toevoeging van informatie over de receptordichtheid en de kinetiek van associatie en dissociatie een beter beeld van de processen die de PK-PD relatie bepalen.

Naast informatie over de transportprocessen tussen bloed en de hersenen en binnen de hersenen biedt informatie over doeleiwit-gemedieerde dispositie een toegevoegde waarde ten opzichte van alleen plasma PK om doelconcentraties te

kunnen voorspellen. Dit geeft aan dat er meer informatie nodig is over de PK in de nabijheid van het doeleiwit, aangezien dit de PK-PD relatie bepaalt. Omdat deze informatie niet verkregen kan worden in de mens is het het doel om de doelconcentraties en het effect in de mens op de best mogelijke manier te kunnen voorspellen, bijvoorbeeld op basis van preklinische data.

De toegevoegde waarde van de intracerebrale microdialyse techniek is eerder al bewezen. In een studie met remoxipride, een dopamine D_2/D_3-receptor antagonist, is aangetoond dat plasmaconcentraties van de biomarker prolactine direct gekoppeld konden worden aan remoxipride concentraties in hersen$_{ECF}$, gemeten met de intracerebrale microdialyse techniek in de rat. Op basis van allometrische schaling en schaling op basis van de fysiologie was het mogelijk om remoxipride hersen$_{ECF}$ concentraties in de mens te voorspellen, waarop ook de prolactine concentraties in plasma konden worden voorspeld. Deze voorspellingen kwamen goed overeen met gemeten prolactine concentraties in plasma, wat aangeeft dat de voorspelling van het effect van geneesmiddelen in de mens op basis van preklinische PK-PD data goed kan werken.

De verdere ontwikkeling van het preklinische SBPK hersendistributiemodel is vooral afhankelijk van de meetbaarheid van het effect van het geneesmiddel in de hersenen. Veelal wordt gezocht naar een enkele biomarker die het effect van het geneesmiddel in het CZS moet kunnen vertegenwoordigen. Echter, vanwege de complexiteit van de verschillende aandoeningen aan het CZS, is het zeer onwaarschijnlijk dat er een enkele biomarker kan worden geïdentificeerd die het onderscheid kan maken tussen gezondheid en ziekte. Dit maakt het lastig om het effect van geneesmiddelen op de status van de ziekte te kunnen volgen. Eigenlijk kunnen we niet echt spreken van “het” effect, maar gaat het meer om een samenstelling van meerdere effecten. Daarom zouden we beter kunnen zoeken op de tijdsafhankelijke “vingerafdruk” van meerdere biomarkers, om zo het brede scala aan effecten te kunnen bestuderen. Met de opkomende techniek van de metabolomics zijn we in staat om veel meer stoffen in de hersenvloeistoffen en plasma in parallel te meten in de tijd. Daarnaast moet de aandacht uit gaan naar de metingen die zowel preklinisch als klinisch verricht kunnen worden, om zo onze inzichten in de vertaling tussen dier en mens te vergroten en de voorspellende waarde van preklinische data te verhogen.

Samenvattend kunnen we zeggen dat de toekomst ligt in het combineren van stof-specifieke informatie, systeem-specifieke informatie over de distributie

naar het doeleiwit en mechanistische informatie over het concentratie-effect spectrum (en de variatie daarin, afhankelijk van de diersoort, de leeftijd en de status van de ziekte, maar ook de variatie tussen individuen en binnen individuen). De combinatie van deze informatie zal uiteindelijk leiden naar een systeem-gebaseerd PK-PD model, waarvan wij verwachten dat deze het effect van geneesmiddelen in de hersenen van de mens op basis van preklinische data goed kan voorspellen.

Nawoord

Het onderzoek dat ik heb gedaan heb ik natuurlijk niet in mijn eentje gedaan, dus daarvoor wil ik graag een aantal mensen bedanken.

In de eerste plaats wil ik graag Liesbeth bedanken voor alle kennis die ik heb mogen opdoen tijdens de verschillende studies en discussies. Daarnaast wil ik je bedanken voor het vertrouwen en geduld.

Ook wil ik Meindert bedanken voor de kans die ik heb gekregen om dit mooie onderzoek te kunnen uitvoeren.

Jasper, wat had ik toch zonder jou moeten beginnen? Je hebt mij op gang geholpen met alle verschillende onderdelen van mijn onderzoek, van dierexperiment tot analyse en modeleerwerk. Je was een geweldige kamergenoot en naast de wetenschappelijke discussies hebben we ook op persoonlijk vlak veel met elkaar mogen delen.

Robin, met jou heb ik vele dagen samen operaties en experimenten uit mogen voeren. Niet alleen op dierkundig gebied, maar ook op muzikaal gebied heb ik veel van jou mogen leren.

Dirk-Jan, zonder jou was het niet mogelijk geweest om tot deze resultaten te komen. Niet alleen de analyse van duizenden monsters, maar ook het verwerken van de data heeft mij veel werk gescheeld.

Verder ben ik Bart, Jean en Henk-Jan, werkzaam bij LAP&P consultants, zeer dankbaar voor de kennis en middelen die zij mij hebben gegeven bij het modeleren van de data. Zonder jullie hulp had ik het niet voor elkaar gekregen.

Ook wil ik Maarten en Stina bedanken. Onze experimenten hadden enige overeenkomsten, dus de discussies die we hierover hebben gevoerd waren zeer nuttig en leerzaam.

Daarnaast wil ik natuurlijk alle overige (oud-)collega's bij Farmacologie bedanken voor de geweldige tijd die ik daar heb beleefd.

Tot slot wil ik graag mijn familie, schoonfamilie en vrienden bedanken voor de oneindige steun die ik heb gekregen tijdens dit hele proces.

Jeroen wil ik graag bedanken voor de hulp bij het maken van de verschillende figuren voor de artikelen en voor de hulp bij de lay-out en controle van dit proefschrift. Daarnaast is het wel handig geweest dat jij dit proces al eens hebt doorlopen.

Roos, Lucas en Lotte wil ik graag bedanken voor de rust die ik (af en toe) heb gekregen terwijl ik achter de computer zat. Nu mijn proefschrift af is kan ik weer ongestoord papa zijn.

Lieve Caroline, mijn dank voor jou is het grootst! De avonduren die ik eenzaam achter de computer heb doorgebracht betekende voor jou eenzame avonden op de bank. Je hebt het volgehouden omdat het einde in zicht was, maar soms leek dat einde slechts een stipje op de horizon. Desalniettemin heb je mij onvoorwaardelijk gesteund met al je liefde. Zonder jou had ik het niet gered.

Curriculum vitae

Joost Westerhout werd geboren op 24 oktober 1982 te IJsselstein. Na het behalen van het diploma VWO in 2000 aan het Oosterlicht College te Nieuwegein begon hij aan de studie Bio-Farmaceutische Wetenschappen aan de Universiteit van Leiden. Tijdens deze studie heeft hij stage gelopen bij de vakgroep Farmacochemie van het Leiden Academic Centre for Drug Research waar hij onderzoek heeft gedaan naar de synthese en activiteit van verschillende adenosine A_1 receptor antagonisten. Bij de afdeling Neurofysiologie van het Leiden Universitair Medisch Centrum heeft hij onderzoek gedaan naar de verschuiving van de circadiane ritmiek in migraine muizen.

Na het behalen van het doctoraal diploma in september 2006 begon hij in februari 2007 als assistent in opleiding bij de vakgroep Farmacologie van het Leiden Academic Centre for Drug Research onder begeleiding van dr. E.C.M. de Lange en Prof. dr. M. Danhof waar hij het in dit proefschrift beschreven onderzoek heeft uitgevoerd.

Sinds augustus 2011 is Joost werkzaam bij TNO in Zeist als PBPK modeling scientist voor de extrapolatie van *in vitro* toxiciteit data naar de mens en voor de extrapolatie van absorptiedata van *ex vivo* varkensdarm naar de mens. Daarnaast doet hij onderzoek naar de optische detectie van biomarkers in CSF voor de diagnose van de ziekte van Alzheimer en de ziekte van Parkinson.

Joost Westerhout was born on October 24th, 1982 in IJsselstein, the Netherlands. After obtaining his ‘VWO diploma’ in 2000 at the Oosterlicht College in Nieuwegein he started the study Bio-Pharmaceutical Sciences at Leiden University. During his studies he performed an internship at the department of Medicinal Chemistry of the Leiden Academic Centre for Drug Research investigating the synthesis and activity of several different adenosine A_1 receptor antagonists. At the department of Neurophysiology of the Leiden University Medical Center he investigated the shift in the circadian rhythm of migraine mice.

After obtaining his master’s degree in September 2006 he started his PhD research at the division of Pharmacology at the Leiden Academic Centre for

Drug Research in February 2007 under supervision of dr. E.C.M. de Lange and Prof. dr. M. Danhof, which resulted in this thesis.

Since August 2011 Joost is working as a PBPK modeling scientist at TNO in Zeist to extrapolate *in vitro* toxicity data to the human situation and for the extrapolation of absorption data of *ex vivo* porcine intestinal tissue to the human situation. He is also investigating the optical detection of biomarkers in CSF for the diagnosis of Alzheimer's disease or Parkinson's disease.

List of publications

Westerhout J, Danhof M, de Lange ECM. Preclinical prediction of human brain target site concentrations: considerations in extrapolating to the clinical setting. J Pharm Sci 2011; 100: 3577-3593.

Westerhout J, Ploeger B, Smeets J, Danhof M, de Lange ECM. Physiologically based pharmacokinetic modeling to investigate regional brain distribution kinetics in rats. AAPS J 2012; 14: 543-553.

Westerhout J, Smeets J, Danhof M, de Lange ECM. The impact of P-gp functionality on non-steady state relationships between CSF and brain extracellular fluid. J Pharmacokinet Pharmacodyn 2013; 40: 327-342.

Westerhout J, van den Berg D-J, Hartman R, Danhof M, de Lange ECM. Prediction of methotrexate CNS distribution in different species – influence of disease conditions. Eur J Pharm Sci 2014, accepted for publication.